Parallel Genetic Algorithm based Thresholding Schemes for Image Segmentation

A thesis submitted in partial fulfillment of
the requirements for the degree of

Doctor of Philosophy

by

Priyadarshi Kanungo
(Roll No. 50402002)

Under the guidance of
Prof. Pradipta Ku. Nanda

DEPARTMENT OF ELECTRICAL ENGINEERING
NATIONAL INSTITUTE OF TECHNOLOGY–ROURKELA
2009

To

my parent Dr. Rabinarayan Kanungo & Mrs. Ashalata Kanungo,

my wife Mrs. Leena Kanungo and my son Yash.

Thesis Approval

The thesis entitled

Parallel Genetic Algorithm based Thresholding Schemes for Image Segmentation

by

Priyadarshi Kanungo
(Roll No. 50402002)

is approved for the degree of

Doctor of Philosophy

Examiner	Examiner
Guide	Chairman

Date: _____

Place: _____

Certificate

This is to certify that the thesis entitled "**Parallel Genetic Algorithm based Thresholding Schemes for Image Segmentation**", being submitted to the National Institute of Technology, Rourkela, India by **Priyadarshi Kanungo** for the award of the degree of **Doctor of Philosophy** is a bonafide research work carried out by him under my supervision and guidance. To the best of my knowledge this work has not been submitted in part or full to any other University or Institution for the award of any degree.

Rourkela
Date:

Dr. P. K. Nanda
Professor (Retd.)
Department of Electrical Engineering.
National Institute of Technology
ROURKELA

Abstract

In this thesis, the problem of image segmentation has been addressed using the notion of thresholding. Since the focus of this work is primarily on object/objects background classification and fault detection in a given scene, the segmentation problem is viewed as a classification problem. In this regard, the notion of thresholding has been used to classify the range of gray values and hence classifies the image. The gray level distributions of the original image or the proposed feature image have been used to obtain the optimal threshold.

Initially, PGA based class models have been developed to classify different classes of a nonlinear multimodal function. This problem is formulated where the nonlinear multimodal function is viewed as consisting of multiple class distributions. Each class could be represented by the niche or peaks of that class. Hence, the problem has been formulated to detect the peaks of the functions. PGA based clustering algorithm has been proposed to maintain stable sub-populations in the niches and hence the peaks could be detected. A new interconnection model has been proposed for PGA to accelerate the rate of convergence to the optimal solution. Convergence analysis of the proposed PGA based algorithm has been carried out and is shown to converge to the solution. The proposed PGA based clustering algorithm could successfully be tested for different classes and is found to converge much faster than that of GA based clustering algorithm.

Two thresholding schemes namely Feature Less (FL) and Feature Based (FB) thresholding have been proposed using the PGA based clustering algorithm and PGA based optimization strategy. Both the approaches have been tested with images of different classes and it has been found that FB approach proved to be better than FL approach. The performance of the proposed approaches are found to be better than Otsu's and Kwon's methods in many cases.

A Minimum Mean Square Error (MMSE) based FL and FB schemes have been proposed to deal with fault detection in a given scene whose histogram does not exhibit clear bi-modality and almost becomes unimodal. These schemes also employ the proposed PGA based clustering

algorithm. The schemes could successfully be tested with images of earth surface cracks and performance of the proposed method proved to be better than Fuang's fault detection method. The scheme could also be validated with general images and the efficacy has been demonstrated especially with image for colour-blindness.

Adaptive thresholding based schemes have been proposed to separate object and background in images with nonuniform lighting conditions. The methods are based on the notion of window merging and window growing. Three new window selection criteria have been proposed to adaptively fix the size of windows for segmentation. The selected windows have been segmented by Otsu's, Kwon's, the proposed PGA, and MMSE based schemes. Sizes of the windows have also been fixed based on the window growing approach where, selection of windows is based on notion of entropy and feature entropy. The windows, thus fixed, have been segmented by Otsu's, Kwon's, and MMSE based approaches. The results obtained by window merging and window growing are found to be better than that of results obtained by Huang's approach. The efficacy of the proposed schemes has been demonstrated with different images of having nonuniform lighting condition.

Contents

Abstract **iii**

List of Tables **ix**

List of Figures **xi**

Nomenclature **xx**

List of Symbols **xxii**

1 Introduction **1**

1.1 Non-parametric shape based methods 2

1.2 Evaluation method 5

1.3 Parametric shape based methods 6

1.4 Entropy based thresholding methods 6

1.5 Multi-thresholding approach 9

1.6 Thresholding for fault detection 10

1.7 Adaptive thresholding 11

1.8 Summary of the thesis 13

1.9 Organization of thesis 18

2 Background on Genetic Algorithm and Parallel Genetic Algorithm **20**

2.1 Genetic Algorithm 20

2.1.1 Definitions 22

2.1.2 Description of the Operators 23

2.1.3 Working of Genetic Algorithm 25

2.1.4 Steps of the basic Genetic Algorithm 26

2.2 Parallel Genetic Algorithm 27
2.2.1 Coarse-grained PGAs 28
2.2.2 Fine grained PGAs 29
2.2.3 Migration policy 29
2.2.4 Steps of the Parallel Genetic Algorithm 30

3 Parallel Genetic Algorithm based Class Models for Clustering 32
3.1 Introduction 32
3.2 GA based class models 33
3.2.1 Crowding method 35
3.2.2 Tournament selection 36
3.2.3 Generalized crossover 37
3.3 PGA based class model 39
3.3.1 Island model 40
3.3.2 Island model with inter-deme migration 40
3.3.3 Island model with intra-deme migration 40
3.4 Island model with neighbourhood structure 41
3.4.1 Convergence Analysis 43
3.5 Results and discussions 45
3.5.1 Clustering for two classes 45
3.5.2 Clustering for four classes 48
3.5.3 Clustering for eight classes 49
3.5.4 Effect of parameters of PGA 51
3.6 Conclusions 54

4 Feature Less and Feature Based Clustering Methods for Optimal Threshold 74
4.1 Introduction 74
4.2 PGA based peak and threshold determination 75
4.3 Brief review of Otsu's and Kwon's thresholding method 77
4.3.1 Otsu's approach 77
4.3.2 Kwon's approach 78
4.4 Proposed methods 79
4.4.1 Feature less method 79

4.4.2 Feature based method 79
4.4.3 PGA based algorithm 81
4.5 Results and discussions 82
4.6 Conclusions 88

5 Minimum Mean Square Error based Feature Less and Feature Based Techniques 90
5.1 Introduction 90
5.2 Brief review of Hui-Fuang's method 91
5.3 MMSE method 92
5.4 FL-MMSE 94
5.5 FB-MMSE 94
5.6 PGA based algorithm 95
5.7 Results and discussions 97
5.7.1 Real and synthetic images 97
5.7.2 Earth surface crack images 101
5.8 Conclusions 107

6 Adaptive Threshold based Segmentation 118
6.1 Introduction 118
6.2 Huang's approach 119
6.3 Implementation of Huang's approach 121
6.4 Local biased Lorentz information based window merging 124
6.5 Window merging based on weighted local and global statistics 124
6.6 Entropy based window merging 125
6.7 Adaptive window selection based on window growing 125
6.8 Implementation of proposed window merging and window growing approaches 126
6.9 Results and discussions 127
6.9.1 Window merging 129
6.9.2 Window growing 133
6.10 Conclusions 150

7 Conclusions and Future Work 151
7.1 Future work 153

Dissemination of work **169**

Acknowledgments **171**

List of Tables

4.1 Threshold values and PME for diffrent window size using the FB approach. . . 89

4.2 Performance evaluation of Otsu's, Kwon's, FL and FB approaches for two class images. 89

4.3 Performance evaluation of Otsu's, Kwon's, FL and FB approaches for three class images. 89

5.1 Threshold values obtained by Ostu's, Kwon's and MMSE approach for real and synthetic images 102

5.2 Performance evaluation of Otsu's, Kwon's, and proposed MMSE approachs. . . 102

5.3 Threshold values for different approaches 106

5.4 Performance evaluation of Otsu's, Kwon's, Hui-Fuang's, FL, FB and new proposed approaches for crack detection 107

6.1 Threshold values for Huang's Approach (Hexagon Image:400x400, initial window size 100x100) 134

6.2 Pyramid structure window merging (Biased Lorentz): Selected windows and threshold values determined by different methods (for hexagon image of size 400x400, initial window size=100x100) 139

6.3 Window overlapping (Biased Lorentz): Selected windows and threshold values determined by different methods (for hexagon image of size 400x400, initial window size=200x100) 139

6.4 Window Merging (Local & Global biased approach): Selected windows and threshold values determined by different methods (for hexagon image of size 400x400, initial window size=200x100) 140

6.5 Window Merging (Entropy based): Selected windows and threshold values determined by different methods (for hexagon image of size 400x400, initial window size=200x80) 140
6.6 Window growing approach: Selected windows and threshold values determined by different methods (for hexagon image of size 400x400, initial window size=50x10, row increment=5, col increment=1) 141
6.7 Threshold values and misclassification error (ME) for diffrent window size using the FB approach. 142

List of Figures

2.1 Single point crossover operator 24

2.2 Two point crossover operator 25

2.3 Mutation operator 26

3.1 (a) Two class function, (b) Decaying two class function, (c) Four class function, (d) Decaying four class function, (e) Eight class function, (f) Decaying eight class function 34

3.2 Generalized Crossover Operator: (a) Two strings represented parents, (b) switching function, (c) offspring generated by GC operator 38

3.3 Island Model 40

3.4 Island model with inter-deme migration 41

3.5 Island model with intra-deme migration 41

3.6 Net topology with different order neighbourhood structure(a)1st order, (b) 2nd order, (c) 3rd order, and (d) connected to all 42

3.7 GA based Crowding for 2-class: (a) Initial distribution (Class: A=28/192, B=41/208), (b) Distribution after 200 gen. (Class: A= 183/192, B=161/208), (c) Final distribution after 6000 gen.(Class: A=192/192, B=208/208), (d) Convergence rate 55

3.8 PGA based Crowding for 2-class: (a) Initial distribution (Class: A=22/207, B=25/193),(b) Distribution after 10 gen. (Class: A=100/207, B=120/193), (c) Final distribution after 100 gen.(Class: A=207/207, B=193/193), (d) Convergence rate with GB migration policy 56

3.9 GA based Crowding for 2-class decaying function: (a) Initial distribution (Class: A=36/292, B=9/108), (b) Distribution after 500 gen. (Class: A=183/292, B=58/108), (c) Final distribution after 3000 gen.(Class: A=292/292, B=108/108), (d) Convergence rate 57

3.10 PGA based Crowding for 2-class decaying function: (a) Initial distribution (Class: A=28/266, B=41/134), (b) Distribution after 20 gen. (Class: A=170/266, B=65/134), (c) Final distribution after 100 gen. (Class: A=266/266, B=134/134), (d) Convergence rate with GB migration policy 58
3.11 GA based Crowding for 4-class: (a) Initial distribution (Class: A=17/98, B=12/88, C=23/122, D=16/92), (b) Distribution after 500 gen. (Class: A=89/98, B=70/88, C=91/122, D=60/92), (c) Final distribution after 4000 gen.(Class: A=98/98, B=88/88, C=122/122, D=92/92), (d) Convergence rate 59
3.12 PGA based Crowding for 4-class: (a) Initial distribution (Class: A=12/103, B=19/91, C=15/97, D=16/109), (b) Distribution after 10 gen. (Class: A=56/103, B=58/91, C=51/97, D=54/109), (c) Final distribution after 40 gen.(Class: A=103/103, B=91/91, C=97/97, D=109/109), (d) Convergence rate with GB migration policy 60
3.13 GA based Crowding for 4-class decaying function: (a) Initial distribution (Class: A=12/147, B=17/97, C=14/113, D=14/43), (b) Distribution after 100 gen. (Class: A=132/147, B=94/97, C=94/113, D=15/43), (c) Final distribution after 800 gen.(Class: A=147/147, B=97/97, C=113/113, D=43/43), (d) Convergence rate 61
3.14 PGA based Crowding for 4-class decaying function: (a) Initial distribution (Class: A=10/104, B=13/94, C=14/100, D=12/102), (b) Distribution after 20 gen. (Class: A=79/104, B=67/94, C=75/100, D=56/102), (c) Final distribution after 80 gen.(Class: A=104/104, B=94/94, C=100/100, D=102/102), (d) Convergence rate 62
3.15 GA based Crowding for 8-class: (a) Initial distribution (Class: A=6/139, B=2/49, C=4/14, D=1/55, E=3/16, F=10/17, G=10/59, H=4/51), (b) Distribution after 400 gen. (Class: A=54/139, B=30/49, C=12/14, D=38/55, E=14/16, F=12/17, G=47/59, H=42/51), (c) Final distribution after 1000 gen. (Class: A=139/139, B=49/49, C=14/14, D=55/55, E=16/16, F=17/17, G=59/59, H=51/51), (d) Convergence rate. 63

3.16 PGA based Crowding for 8-class: (a) Initial distribution (Class: A=6/139, B=2/49, C=4/14, D=1/55, E=3/16, F=10/17, G=10/59, H=4/51), (b) Distribution after 10 gen. (Class: A=112/139, B=46/49, C=13/14, D=34/55, E=13/16, F=11/17, G=45/59, H=46/51), (c) Final distribution after 40 gen. (Class: A=139/139, B=49/49, C=14/14, D=55/55, E=16/16, F=17/17, G=59/59, H=51/51), (d) Convergence rate with GB migration policy. 64

3.17 GA based Crowding for 8-class decaying function: (a) Initial distribution (Class: A=10/107, B=7/49, C=9/30, D=12/55, E=10/32, F=8/26, G=13/50, H=4/51), (b) Distribution after 500 gen. (Class: A=107/107, B=47/49, C=29/30, D=46/55, E=24/32, F=17/26, G=29/50, H=27/51), (c) Final distribution after 4000 gen. (Class: A=107/107, B=49/49, C=30/30, D=55/55, E=32/32, F=26/26, G=50/50, H=51/51), (d) Convergence rate 65

3.18 PGA based Crowding for 8-class decaying function: (a) Initial distribution (Class: A=11/107, B=9/49, C=6/30, D=10/55, E=15/32, F=11/26, G=13/50, H=5/51), (b) Distribution after 20 gen. (Class: A=107/107, B=42/49, C=23/30, D=45/55, E=28/32, F=20/26, G=42/50, H=43/51), (c) Final distribution after 40 gen. (Class: A=107/107, B=49/49, C=30/30, D=55/55, E=32/32, F=26/26, G=50/50, H=51/51), (d) Convergence rate with GB migration policy 66

3.19 PGA based Crowding for 4-class: (a) Comparision of different Migration policies GB, RB and GR, (b) RR migration policy 67

3.20 Comparision of Migration Policies GB, RB, GR and RR in Decaying 4-class: (a) Class-A, (b) Class-B, (c) Class-C, (d) Class-D. 68

3.21 PGA based Crowding for 8-class: (a) Comparision of different Migration policies GB, RB and GR, (b) RR migration policy 69

3.22 PGA based Crowding for 4-class:(Comparision of migration rate) (a) GB Migration policy, (b) GR Migration policy, (c) RB Migration policy, (d) RR Migration policy 70

3.23 Comparison of different neighbourhood structures for 4-class: (a) Without self loop and 16% migration rate, (b) With self loop and 16% migration rate, (c) Without self loop and 25% migration rate (d) With self loop and 25% migration rate 71

3.24 Avg. Fitness vs Generation (4-Class)(a) TPC-SL vs TPC-WSL with GB migration (b) TPC-SL vs TPC-WSL with RB migration (c) TPC-SL vs TPC-WSL with GR migration 72
3.25 Avg. Fitness vs Generation (4-Class)(a) GC-SL vs GC-WSL with GB migration (b) GC-SL vs GC-WSL with RB migration (c) GC-SL vs GC-WSL with GR migration 72
3.26 Avg. Fitness vs Generation (a) GC and TPC with GB for 2-class, (b) GC and TPC with GB for 4-class, (c) GC and TPC with GB for 8-class 72
3.27 Avg. Fitness vs Generation (4-Class)(a) TPC-SL vs GC-SL with GB migration (b) TPC-SL vs GC-SL with RB migration (c) TPC-SL vs GC-SL with GR migration 73

4.1 (a) Normalized histogram of the image; (b) Normalized histogram of the feature image. 80
4.2 (a) Image 1; (b) Histogram with detected peaks and valley; (c) Average fitness versus generation of class “A” PGA and GA; (d) Average fitness versus generation of class “B” PGA and GA; (e) Class “A” with SL and WSL; (f) Class “B” with SL and WSL; (g) Segmented image using FL; (h) Segmented image using Otsu’s approach. 83
4.3 Percentage of misclassification error verses window size (images 1, 2 & 3 correspond to Fig. 4.4(a), 4.5(a) & 4.6(a)) 84
4.4 (a) Image 1,(b) Histogram; (c) Featured histogram; (d) Detected peaks and valley; (e) Average fitness versus generations of class “A” PGA and GA; (f) Average fitness versus generations of class “B” PGA and GA; (g) Class “A” with SL and WSL; (h) Class “B” with SL and WSL; (i) Segmented image using the FB approach; (j) Segmented image using Otsu’s approach; (k) Segmented image using Kwon’s approach. 85
4.5 (a) Image 2; (b) Noisy version of image 2 with SNR 22dB; (c) Histogram of (b) with detected peaks and valley; (d) Featured histogram of (b) with detected peaks and valley; (e) Segmented image using FL; (f) Segmented image using FB approach; (g) Segmented image using the Otsu’s approach; (h) Segmented image using the Kwon’s approach. 86

4.6 (a) Image 3; (b) Noisy version of image 3 with SNR 22dB; (c) Histogram of (b) with detected peaks and valley; (d) Featured histogram of (b) with detected peaks and valley; (e) Segmented image using FL; (f) Segmented image using FB approach; (g) Segmented image using the Otsu's approach; (h) Segmented image using the Kwon's approach. 86
4.7 (a) Image 4; (b) Histogram with detected peaks and valleys; (c) Featured histogram with peaks and valleys; (d) Segmented image using FL; (e) Segmented image using FB; (f) Segmented image using Otsu's approach; (g)Segmented image using Kwon's approach. 87
4.8 (a) Image 5; (b) Histogram with detected Peaks and valleys; (c) Featured histogram with Peaks and Valleys; (d) Segmented image using the FL; (e) Segmented image using FB; (f) Segmented image using Otsu's approach; (g) Segmented image using Kwon's approach. 87

5.1 Bimodal distribution with the peaks representing the dominant gray value of object and background 92
5.2 (a) Image 1; (b) Image 2; (c) Image 3; (d) Image 4; (e) Ground trouth (GT) of image 1; (f) GT of image 2; (g) GT of image 3; (h) GT of image 4. 101
5.3 (a) Original Image 1; (b) Histogram of original image with detected peaks and threshold; (c) Avg. fitness vs generations of class "A" PGA and GA; (d) Avg. fitness vs generations of class "B" PGA and GA; (e) Avg. fitness vs generations of class "A" with self loop (SL) and without self loop(WSL); (f) Avg. fitness vs generations of class "B" with self loop (SL) and without self loop(WSL); (g),(h) and (i) shows segmented image using Otsu's, Kwon's and proposed MMSE method respectively 108
5.4 (a) Image 2; (b) Featured histogram with detected peaks and threshold; (c) Avg. fitness vs generations of class "A" PGA and GA; (d) Avg. fitness vs generations of class "B" PGA and GA; (e) Avg. fitness vs generations of class "A" with SL and WSL; (f) Avg. fitness vs generations of class "B" SL and WSL; (g),(h), and (i) shows segmented image using Otsu's, Kwon's, and proposed MMSE method respectively 109

5.5 (a) Image 3; (b) Featured histogram with detected peaks and threshold; (c) Avg. fitness vs generations of class “A” PGA and GA; (d) Avg. fitness vs generations of class “B” PGA and GA; (e) Avg. fitness vs generations of class “A” with SL and WSL; (f) Avg. fitness vs generations of class “B” with SL and WSL; (g), (h), and (i) shows segmented image using Otsu’s, Kwon’s, and proposed MMSE method respectively 110

5.6 (a) Image 4; (b) Original histogram with detected peaks and valley; (c) Featured histogram with detected peaks and valley; (d) Avg. fitness vs generations of class “A” PGA and GA; (e) Avg. fitness vs generations of class “B” PGA and GA; (f) Avg. fitness vs generations of class “A” with SL and WSL; (g) Avg. fitness vs generations of class “B” with SL and WSL; (h), (i), (j), and (k) shows segmented images using , Otsu’s, Kwon’s, FL-MMSE, and FB-MMSE method respectively 111

5.7 (a) Origina image 1; (b) Original image 2; (c) Original image 3; (d) Original image 4; (e) Detected peaks and threshold in the histogram for image 1; (f) Detected peaks and threshold in the histogram for image 2; (g) Detected peaks and threshold in the histogram for image 3; (h) Detected peaks and threshold in the histogram for image 4; (i) Segmented image of image 1 using MMSE method; (j) Segmented image of image 2 using MMSE method; (k) Segmented image of image 3 using MMSE method; (l) Segmented image of image 4 using the proposedMMSE method. 112

5.8 (a), (b), (c) and (d) shows the ground trouth image of image 1, image 2, image 3 and image 4; (e), (f), (g) and (h) shows the segmented image of image 1, image 2, image 3 and image 4 using the Otsu’s method; (i), (j), (k) and (l) shows the segmented image of image 1, image 2, image 3 and image 4 using the Kwon’s method; (m), (n), (o) and (p) shows the segmented image of image 1, image 2, image 3 and image 4 using the proposed MMSE method. 113

5.9 (a) Image 1; (b) Histogram with detected Peaks and valleys; (c) Avg. fitness vs generation of class “A” PGA and GA; (d) Avg. fitness vs generation of class “B” PGA and GA; (e) Class “A” with SL and WSL; (f) Class “B” with SL and WSL; (g),(h),(i), and (j) segmented images using FL, Otsu’s, Kwon’s, and Hui-Huang Method 114

5.10 (a) Image 1; (b) Histogram; (c) Featured histogram; (d) Detected peaks and valley; (e) Avg. fitness vs generations of class “A” PGA and GA; (f) Avg. fitnee vs generations of class “B” PGA and GA; (g) Avg. fitness vs generations of class “A” with SL and WSL; (h) Avg. fitness vs generations of class “B” with SL and WSL; (i), (j), (k) and (l) segmented images using FB, Otsu’s, Kwon’s and Hui-Huang’s method respectively 115

5.11 (a), (b), (c) and (d) are original crack images; (e), (f), (g) and (h) shows the detected peaks and threshold in the histogram of corresponding images using FL-MMSE; (i), (j), (k) and (l) segmented images using FL-MMSE; (m), (n), (o) and (p) shows detected peaks and threshold in the feature histogram of the original images using FB-MMSE; (q), (r), (s) and (t) segmented images using FB-MMSE. 116

5.12 Row-1: Original crack Images (Image 1, 2, 3 and 4); Row-2: Ground Truth, Row-3:Otsu’s method; Row-4: Kwon’s method; Row-5: Hui’s method; Row-6: Feature Less method; Row-7: Feature Based Method; Row-8: Feature Less MMSE; Row-9: Feature Based MMSE 117

6.1 Schematic diagram of the proposed adaptive thresholding methods 119

6.2 Example of Lorentz information curve (G=3) 121

6.3 Pyramid structure of window merging 122

6.4 Window Merging using Pyramid structure 123

6.5 Window overlapping concept with LIM criterion:(a) Image is devided into 16 subimages (Windows), (b) w1, w3, w4, w8, w13,w16 are satisfied the criterion, (c) w2 is merged with w3, w6 and w7 to form a window w2w3w6w7 after satisfying the criterion, (d) w5 is merged with w6, w9 and w10 to form a window w5w6w9w10 after satisfying the criterion, (e) w11 is merged with w12, w15 and w16 to form a window w11w12w15w16 after satisfying the criterion, (f) w14 is merged with w15, w11, w10, w16, w12, w8, w7 and w6 to form a window w6w7w8w10w11w12w14w15w16 after satisfying the criterion 128

6.6 Pyramid structure Window Merging Concept: (a) Image is partitioned into 16 sub-images (windows); (b) corresponding histograms of the sub-images; (c) 4 sub-images after window merging; (d) corresponding histograms of the sub-images. 135

6.7 Pyramid structure Window Merging Concept with Huang's criterion:(a) Histograms of the subimages with the selected windows are tick marked for segmentation, (b) histograms of the subimages after merging and the selected windows are tick marked for segmentation. 136
6.8 Pyramid structure Window Merging Concept with biased LIM: (a) Histograms of the sub-images with the selected windows are tick marked for segmentation; (b) histograms of the sub-images after merging and the selected windows are tick marked for segmentation. 136
6.9 Window overlapping concept with LIM criterion: (a) Image is divided into 8 sub-images (Windows); (b) corresponding histograms with tick marked windows are satisfied the criterion for segmentation; (c) Window 1 is overlapped with window 2, 5, & 6 and window 3 is overlapped with window 4, 7 & 8; (d) corresponding histograms with tick marked windows are satisfied the criterion . 137
6.10 Window Growing Concept 138
6.11 Nonuniform lighting images (a) Hexagon (400x400); (b) Crow (400x512); (c) Rabbit (300x500); (d) Rice (256x256) 143
6.12 Corresponding histogram of the (a) Hexagon; (b) Crow; (c) Rabbit; (d) Rice . . 143
6.13 Segmented images using Ostu's Global Thresholding approach 143
6.14 Corresponding ground truth images manually constructed 143
6.15 Nonuniform lighting images (a) Hexagon; (b) Crow; (c) Rabbit; and (d) Rice . 144
6.16 Segmented images using Huang's Approach with Pyramid window merging. Initial window size: (a) 100x100; (b) 50x64; (c) 75x125; and (d) 32x32 144
6.17 Adaptive window merging with Biased Lorentz Pyramid structre and segmentaion of windows using Otsu's and proposed method1, method2, and method 3 145
6.18 Adaptive thresholded images using Biased Lorentz Window Overlapping approach 146
6.19 Adaptive window merging in pyramid structure using the local global information and segmentaion of windows using Otsu's and proposed method1, method2, and method 3 147

6.20 Adaptive window growing method (Window overlapping) with entropy based criterion and segmentaion of windows using Otsu's and proposed method1, method2, and method 3 148
6.21 Adaptive window growing with entropy based criterion and segmentaion of windows using Otsu's and proposed method1, method2, and method 3 149

Nomenclature

FL	Feature Less.
FB	Feature based.
$FL-MMSE$	Feature less minimum mean square error.
$FB-MMSE$	Feature based minimum mean square error.
$FLPGA$	Feature less PGA.
$FBPGA$	Feature based PGA.
GAs	Genetic Algorithms.
GB	Good Bad migration policy.
GC	Generalized crossover.
G	Maximum value of Gray levels.
GR	Good Random migration policy.
GT	Ground Truth.
LIM	Lorentz information measure.
$MMSE$	Minimum Mean Square Error.
ME	Misclassification error.
$NIPM(x)$	Normalized picture information measure of image X.
PGA	Parallel Genetic Algorithm.

PIM	Picture information measure.
RB	Random Bad Migration policy.
RR	Random Random Migration policy.
SL	Self-loop in the intra-deme migration.
WSL	Without self-loop (Inter-deme migration model only).

List of Symbols

D_1	Deme1 (Sub-population 1)
D_2	Deme2 (Sub-population 2)
D_3	Deme3 (Sub-population 3)
D_4	Deme4 (Sub-population 4)
$fit(x)$	Fitness of the candidate solution “x”.
$\hat{\mu}_{w_{ij}}$	First order moment of a window ”w” with center pixel coordinate i, j.
$\hat{\sigma}^2_{w_{ij}}$	Second order moment of a window ”w” with center pixel coordinate i, j.
$\hat{\mu}_{w_{ij}}$	First order moment of a window ”w” with center pixel coordinate i, j.
$\hat{\sigma}^2_{w_{ij}}$	Second order moment of a window ”w” with center pixel coordinate i, j.
$h(i)$	Histogram of image.
H	Entropy (Average Information).
H_w	Entropy in a window “w”.
k	Positive constant where $k \in \{0, 1, ..., G\}$
K	Positive constant bounded between 1 to 10.
n	Number of generations
N	Population size
N_w	Number of pixels in the window “w”.

N_v	Population size for valley detection.
$N(x)$	Total number of pixels in image X.
Q_0	Initial proportion of bad individuals in a deme (sub-population)
Q_n	Proportion of bad individuals in a deme (sub-population) after n^{th} generation
P_c	Crossover probability
P_m	Mutation probability
P_{mig}	Migration probability
P_{smig}	Self-migration probability
$P(t)$	Population elements after selection process at time "t"
P_{k-1}	Proportion of good individuals after $(k-1)^{th}$ migration
P_0	Initial proportion of good individuals in a deme (sub-population)
P_n	Proportion of good individuals in a deme (Sub-population) after n^{th} generation
$PIM(x)$	Picture information measure of image X.
p_i	Probability of i^{th} gray value in image X.
q	Tournament size
q_1	Weights (positive constant)
q_2	Weights (positive constant)
R_{mig}	Rate of migration.
R_{smig}	Rate of self-migration.
S_k	$NIPM_{G-k}(x)$
T	Threshold value (Constant).
T_h	Total entropy of the image.

T_h Total entropy of the feature image

T_{fOtsu} Threshold determined using Otsu's method from the featured gray level distibution.

$x_{i_{th}}$ i_{th} feature of the feature histogram.

x_{ij} Gray value of the pixel at the coordinate (i, j).

λ Constant

δ_k population of good individuals taking part in k^{th} migration.

$\%age$ Percentage

ΔW Incremental size of window.

$X(m, n)$ Representation of an image.

$f(x, y)$ Representation of an image.

$\Theta(k)$ k highest value of histogram $h(i)$.

σ_{wh} Standard deviation of the gray level distribution in a window considered for mearging.

$\sigma_{fh(LIM)}$ Standard deviation of the feature gray level distribution.

Chapter 1

Introduction

Image segmentation is one of the basic early vision problems in computer vision paradigm. Detection and tracking of moving objects in a given scene serves as the front end of an automated vision system. Often, in many applications the gray levels of pixels belonging to object are substantially different from the gray levels of pixels belonging to background. In some cases, the scene could be with multiple objects and background. In such situations, thresholding has been a simple but effective tool to separate objects from background. Thresholding operation segments the image into regions which may subsequently be analyzed based on their shapes, sizes, relative positions, and other characteristics. Thresholded image requires less storage space than the original one and hence more suitable for transmission. Since object detection and tracking has to be accomplished in real-time for visual surveillance and monitoring, thresholding being a simple and efficient strategy provides a viable solution for many real-time applications such as fault diagnosis, tracking, monitoring, crack detection, and bio-medical image analysis etc. [1, 2, 3, 4]. Thresholding, in its simplest form, means to classify the pixels of a given image into two groups for example, object and background, one including those pixels with their gray values above a certain threshold and the other including those with gray values equal to or below the threshold. This is called bi-level thresholding. Generally one can select more than one threshold and use them to divide the whole range of gray values into several sub-ranges.

Since, each range of gray value will correspond to one object class, multiple ranges will correspond to multiple objects and background and hence multiple classes. This process is known as multilevel thresholding. There has been consistent effort for more than three decades to devise novel strategies based thresholding schemes for image segmentation. The proposed methods can be broadly categorised as; (i) global thresholding techniques, and (ii) adaptive

thresholding techniques. Global thresholding methods can further be classified as; (a) bi-level thresholding, and (b) multilevel thresholding. In this regard, a good number of techniques have been reported in the literature [1, 2, 3, 4]. The schemes and strategies proposed in the literature for global thresholding may be broadly viewed as; (i) histogram shape based methods, (ii) Entropy based methods, (iii) clustering based methods, (iv) higher order statistics based methods, and (v) local characteristics based methods. In order to deal with the real world environment, where images could have been acquired under non-uniform lighting conditions, many adaptive methods have been proposed. In a wide variety of techniques, the problem has been formulated as an optimization problem and therefore stochastic optimization methods such as Genetic algorithm, Particle Swarm optimization, etc. have been used to determine the optimal threshold. By and large, the techniques used are either based on the shape information of the histogram or on any derivative of shape information. These methods can further be categorized as parametric and non-parametric methods. In the following, the proposed methods based on different approaches have briefly been described.

1.1 Non-parametric shape based methods

One of the landmark work on non parametric method is Otsu's [5] method where the shape information of the histogram has been exploited to find optimal threshold. In this work, an optimal threshold has been obtained so as to maximize the separability of the resultant classes in gray levels. This method [5] determines the optimal threshold while maximizing the inter-class variance and in turn minimizing the intra-class variance. Otsu's method produced promising results with two class problems and could also be extended to multiclass problems. But Otsu's method for multiclass problems is found to be computationally expensive. This method produced good results when the histogram distribution exhibited clear bi-modality. A fast search scheme has been presented by Reddi *et al*. [6] to determine the single or multiple thresholds that maximize the interclass variance between dark and bright regions. Lee *et al*. [7] have investigated the issue of convergence of a fast Otsu's method suggested by Reddi *et al*. [6]. They have also pointed out that if the object area is small compared with the background area, the histogram no longer exhibits bi-modality, and in such situation Otsu's method produced optimal threshold that results in poor segmentation. If the image has been corrupted by additive noise, the histogram looses clear bi-modality and hence Otsu's scheme results in segmentation error.

The limitations of Otsu's method has been partially overcome by an automatic image segmentation method presented by Boukharouba *et al*. [8], where the method does not depend on the existence of modes of the histogram rather based on the intrinsic properties of the distribution function of the image. Since the method exploits the subtle variations in the form of the histogram, the method could successfully deal with almost flat histograms. A correlation based optimal threshold detection technique has been proposed by Brink [9] and the optimal threshold has been obtained by maximizing the correlation between the original image and the thresholded bi-level image. Subsequently, it has been pointed out by Cseke *et al*. [10] that the function to be maximized by Brinks's method [9] is same as that Otsu's [5] method. Dong *et al*. [11] have proposed a fast efficient iterative search procedure to determine optimal threshold from single and two dimensional histogram distributions. Most of the thresholding approaches are based on the notion of variance and in this regard, Hou *et al*. [12] have shown that the bias for Otsu's method may be attributed to the differences in class variances and the resulting threshold is biased towards the component with larger class variance. Thus, they have proved that the minimum class variance thresholding (MCVT) method is similar to the methods based on minimum error thresholding. Recently, Liu *et al*. [13] have shown that the objective function of Otsu's method is equivalent to that of the K-means method in multilevel thresholding and both of them are based on the same criterion that minimizes the within-class variance. Saha *et al*. [14] have proposed a novel thresholding method which is based on the combination of intensity based class uncertainty, histogram based property, region homogeneity, and image morphology based property. They have formulated a new threshold energy criterion exploiting the above mentioned attributes.

Since, an automatic threshold detection still remains a challenging task due to poor contrast, low signal to noise ratio, and complex patterns of the images, optimum threshold detection by phase correlation between gray level image and its binary counter part has been proposed by Belkasim *et al*. [15] and this method is found to be better than many other methods. Segmentation of colour blind images is another hard problem because the histogram distribution is very typical, neither it exhibits clear class distribution nor a distinct valley. For such cases, Kwon [16] has proposed an optimal threshold detection technique based on cluster analysis. His technique could segment the colour blind images properly. It has already been pointed out that Otsu's method exhibits poor performance when the object size in a given scene is much smaller than that of background. In order to address such issues, a thresholding criterion has

been suggested by Qiao *et al*. [17] to specifically segment small objects. This criterion exploits the knowledge about the intensity contrast and the formulation is based on the weighted sum of within-class variance and intensity contrast between the objects and background. The proposed algorithm could successfully segment synthetic as well as real images with small objects.

Besides using the shape information of the histogram, optimal threshold detection scheme based on the spatial features of the histogram has been proposed by Zhang *et al*. [18]. They have employed Fisher criterion and mutual information to measure discriminability and feature correlation of spatial histogram features. A new discriminant criterion emphasizing the homogeneity of the object gray level distribution while de-emphasizing the heterogeneity of the background has been proposed by Chen *et al*. [19], where some of the shortcomings of the Otsu's method have been overcome. A novel thresholding approach has been proposed by Hu *et al*. [20], where the proposed thresholding scheme exploits the region of interest and the threshold is determined by minimizing the classification error within the constrained variable background range. This could successfully be tested with Magnetic Resonance (MR) and CT images. Segmentation of small objects in a given scene is a challenging problem and in this regard, a new thresholding criterion has been formulated by Qiao *et al*. [17] by exploring the knowledge about intensity contrast. Their thresholding criterion is based on the weighted sum of within-class variance and intensity contrast between the object and background. Subsequently, Wang *et al*. [21] has proposed a new criterion function that is obtained by integrating the histogram and the Parzen window technique. Global optimal threshold is obtained by optimizing the criterion function and this method proved to be better than Otsu's minimum error threshold method and maximum cross entropy method. Another histogram modification technique is proposed by Sen *et al*. [22], where histogram is modified based on the beam theory and the ambiguity in the over all information is minimized to obtain the optimal threshold. Dong *et al*. [23] have proposed an iterative algorithm based on minimizing a weighed sum of square errors of objective function. They have also proved that their proposed algorithm is equivalent to the Otsu's method but incurs less computational burden. Besides finding out the optimal threshold for segmentation, a thresholding method for detection of edges has been proposed by Carnicer *et al*. [24] to deal with unimodal histogram. This algorithm performed satisfactorily on different images with unimodal histogram. A transition region based thresholding algorithm has been proposed by Hu *et al*. [25] and the algorithm is robust and easy to implement. Instead of determining a threshold for the whole histogram, Chen [26] has developed an automatic volumetric segmenta-

tion scheme by partitioning the histogram into intervals followed by thresholding the intervals. The efficacy of this algorithm could successfully be demonstrated for volumetric breast tissue segmentation. Besides Otsu's method, a new thresholding strategy based on standard deviation has been proposed by Li *et al*. [27] and the method could successfully be tested for wide variety of images. Further, a thresholding strategy based on the notion of fractional differentiation has also been proposed by Nakib *et al*. [28] and it could segment well many real world images. The thresholding schemes discussed so far have been implemented off-line. Attempts have been made to implement the thresholding scheme in real-time to build automatic machine vision system. A thresholding algorithm has been implemented in real time by Maria *et al*. [29] and in this scheme, histogram has been generated in real time and thereafter FPGA based controller has been developed. Recently, Jianlai *et al*. [30] has implemented Otsu's method in real time on FPGA using Altera's Cyclone II chip and they could successfully segment the images in real-time environment. An enhanced histogram based thresholding method has also been suggested by Cristo *et al*. [31] to automatically detect stars in astronomical images.

1.2 Evaluation method

Over the last three decades many thresholding algorithms have been proposed to achieve proper classification and hence there has been a necessity of quantitatively evaluating the performance. Lie [32] has proposed evaluation methods for thresholding algorithm, where the performance has been analysed and efficient computing of block measures has been presented. Towards this end, Zhang [33] has categorised the proposed methods as; (i) analytical, (ii) the empirical goodness, and (iii) empirical discrepancy. In this work, he has provided a rank of the algorithm's evaluation capability. The algorithms have been evaluated based on goodness and discrepancy criteria. Zhang [34] has in his subsequent work reviewed the evaluation methods based on goodness and discrepancy. He has also highlighted some of the criteria such as intra-region uniformity, inter-region contrast, region shape, number of mis-segmented pixels, position of mis-segmented, number of objects in the image, and feature values of segmented objects. Sezgin *et al*. [4] have surveyed 40 thresholding methods and they are evaluated based on non-destructive testing applications.

1.3 Parametric shape based methods

Analogous to Otsu's [5] method, another landmark parametric thresholding strategy has been proposed by kittler *et al*. [35]. In this method, the gray level distribution of object and background pixels are assumed to be known or estimated and the optimal threshold is obtained while minimizing the average pixel classification error rate. Besides, Kittler's [35] model based approach, Mardia *et al*. [36] have proposed several model based approaches that use spatial information. A thresholding method insensitive to shading or gradually varying interference has been proposed by Chow *et al*. [37], where each local region of the image is modelled by a mixture of normal distributions. A common framework has also been devised for eleven thresholding algorithms by Glasbey [38] and it has been shown that the iterated version of Kittler's [35] algorithm is the best among all the eleven algorithms. In addition to Kittler's criterion, two automatic thresholding algorithm based on minimizing sum of square errors and the variance of the approximated histogram has been proposed by Ramesh *et al*. [39]. The efficacy of the algorithm has been compared with the entropy based and moment based approaches. All the above proposed approaches have dealt with images free from noises and the performance is found to deteriorate with noisy images. In this regard, Caglioti *et al*. [40] have proposed a mode detection algorithm for noisy images and the method proved to work satisfactorily for highly noisy cases. Analogous to Kittler's [35] method, a peak detection algorithm has been proposed by Lui *et al*. [41] while minimizing the classification error and maximizing the Mahalonobis distance besides statistical decision criterion an all pole model histogram based thresholding algorithm has been presented by Cai *et al*. [42] and it has been advocated that the algorithm can be used both for binarization and multilevel thresholding.

1.4 Entropy based thresholding methods

Parallel to the notion of non-parametric use of the shape of the histogram, a new notion of the entropy of the gray level histogram has been introduced by Pun [43] to the research domain of histogram based thresholding. Thresholds have been determined by an *apriori* maximization of entropy determined *aposteriori*. Successively, Pun [44] also suggested an automatic threshold selection related to the asymmetry of the gray level histogram that facilitated the derivation of entropy based thresholding. Pun [44] in his work has also advocated the use of this method for multi-thresholding applications. The fundamental notion of Pun [43, 44] has been analysed by

Kapur *et al.* [45] and a new algorithm based on entropy has been proposed for real and artificially generated histograms. The entropy based notion has been exploited by many researchers and in this regard Pal *et al.* [46] has presented a new definition of entropy which could be viewed as modification of Shannon's entropy but suitable for thresholding. This proved to be effective in many cases. The concept of entropy was further extended by Li *et al.* [47], Brink *et al.* [48], and Pal [49], where the optimal threshold has been selected while minimizing the cross entropy between the image and its segmented versions. The first cross entropy based thresholding has been introduced by Li *et al.* [47] and the proposed method provides an unbiased estimate of binarized version of the image in an information theoretic sense. Li *et al.*'s [47] cross entropy method has been analysed by Pal [49] and towards this end a new cross entropy based method is presented overcoming the limitation of Li *et al.*'s [47] method. Besides entropy and cross entropy, relative entropy based thresholding has been proposed by Chang *et al.* [50], where the entropy of the co-occurrence matrix of one image has been used. Extension of this work is carried out by Althouse [51], where local entropy and local relative entropy thresholding methods have been described and compared with Otsu's [5] and Kittler's [35] method. An iterative method for cross entropy based thresholding has been proposed by Li *et al.* [52] and could successfully be tested for many real images further extension of this entropy based thresholding has been carried out by Sahoo *et al.* [53] and this thresholding is based on Renyi's entropy.

By and large, the definition of image entropy has been associated with the probability distribution of the gray levels. This entropy measured has been modified by Brink [54], where the spatial information of image has been incorporated into the entropy measure to devise the criterion function that improved the result substantially. Jinsong *et al.* [55] have implemented the methods proposed by Kapur *et al.* [45] and Sahoo *et al.* [53] using Genetic algorithm. Both single and multi-thresholding methods have been dealt using Genetic algorithm. All the entropy based methods described above are more or less based on Shannon's entropy. Pavesic *et al.* [56] have devised thresholding criterion based on the sum of Havrda and Charvat entropy and have shown that this entropy based scheme results in better segmentation than that of using Shannon's entropy. The computational burden of maximum entropy based thresholding has been reduced using Q-learning algorithm in the Reinforced Learning (RL) paradigm proposed by Yin [57]. In Yin's method [57], it has also been shown that the algorithm is suitable for multilevel thresholding applications.

Besides, a thresholding algorithm using Tsallis entropy has also been proposed by Albu-

querque *et al.* [58] and local entropy based method for extraction of transition region has been proposed by Yan *et al*. [59]. In the sequel, local entropy based algorithm for blood vessel detection has been devised by Chanwimaluang *et al*. [60] and the method produced promising results in case of many examples. Relative entropy based thresholding algorithm has also been proposed by Zhu *et al*. [61], where two dimensional histogram instead of single dimensional histogram of the image has been used to obtain optimal threshold. Yang *et al*. [62] have proposed a fast threshold selecting algorithm based on one-dimensional entropy. Recently, texture Renyi entropy has been proposed by Shareha *et al*. [63] for determining accurate threshold and minimum cross entropy based thresholding [64] has been proposed for thresholding SAR images. A non-extensive relative entropy also known as Tsallis entropy has been employed to develop optimal threshold detection strategy [65] and the Tsallis entropy has been applied as a generalized entropy formalism for information theory. Entropy based thresholding algorithms have also been validated for biomedical images specifically ultrasound images [66].

It has been found out that the spatial correlation among the pixels do influence the underlying notion of separation of object from the background. In order to take into account the spatial correlation of the pixels together with the gray level distribution of images, two dimensional entropy based thresholding method was first introduced by Abutaleb [67]. The proposed 2-D entropy based approach produced appreciable result even when signal to noise ratio (SNR) is decreased. Subsequently, Chen *et al*. [68] have suggested a fast two-dimensional entropy based thresholding algorithm to reduce the computational burden. It has been shown that the processing time reduced drastically. Besides, a wavelet transform based fast 2D entropic thresholding algorithm also been proposed by Wang *et al*. [69]. Specifically for ultrasound images, a two-dimensional minimum cross entropy based algorithm has been developed by Zimmer *et al*. [70] and the algorithm could successfully be tested for ovarian cysts. The two-dimensional entropy based algorithm has also been extended [71] further to incorporate Tsallis-Havrda-Charvat entropy while devising optimal threshold algorithm. Recently, thresholding strategy has further been reinforced using 2D Tsallis entropy [72] and the resulting algorithm produced better segmentation result than the previously proposed two dimensional thresholding methods. Recently, Tian *et al*. [73] has proposed a Tsallis-entropy image thresholding method using two-dimension histogram obque segmentation. The superiority of this method has also been shown to other methods.

1.5 Multi-thresholding approach

There was considerable research effort to separate object and background in a given scene and hence the focus was on bi-level classification. This requires a single optimal threshold to be determined. It has been argued in many cases that the proposed single thresholding methods could be extended to multi-thresholding paradigm for multiclass problems. In this regard, a recursive technique for multiple threshold has been proposed by Wang *et al.* [74] and this algorithm could successfully detect multiple thresholds from the histogram. The multiple thresholds by and large, have been obtained from the histogram by segmenting the histogram itself. A three stage multi-thresholding algorithm has been proposed by Papamarkos *et al.* [75], where the scheme consists of the notion of; (i) hill clustering, (ii) histogram segmentation, and (iii) Golden search minimization technique. The algorithm could successfully determine more than two peaks. In multimodal histogram case, a Gaussian kernel smoothing method has been proposed by Tsai [76] to detect multiple thresholds for a multiclass problems. The performance of the algorithm could be compared with methods based on the notion of between-class variance and entropy. In order to accelerate the convergence of multi-thresholding schemes, three fast multi-thresholding schemes [77, 78, 79] have been proposed. One of the schemes [77] is iterative in nature and hence starts with a bi-level thresholding and thereafter, using this as the initial result, higher order thresholds have been obtained. The proposed algorithm could be automatic and could save a significant amount of computing time. In the sequel, Yin [78] has proposed a fast multi-thresholding scheme using Genetic Algorithm (GA) and the Genetic algorithm has been used to make the optimal thresholding technique more practical. The third fast multi-thresholding is based on maximum entropy theorem [79] and this technique is computationally less expensive and hence computes the threshold quickly. Besides GA, another soft-computing based multi-thresholding technique has been proposed by Papamarkos *et al.* [80], where the proposed technique is implemented by principal component analysis (PCA) and a Kohonene Self-Organized Feature Map (SOFM) neural network. Chen *et al.* [81] have proposed a multi thresholding algorithm that obtains the multiple thresholds from the support vectors that fits the histogram. This method does not require prior assumption about the image. A new dichotomization technique has been proposed by Sezgin *et al.* [82] and the technique is based on selection of the consistent peak location function as the threshold value over the interested histogram region. This algorithm has specifically been designed for automated inspection ap-

plication. A hybrid optimization technique based on Otsu's minimum within group variance and Gaussian function fitting has been proposed by Zahara *et al.* [83] and the method could expedite Otsu's method in the context of determining multiple thresholds. Arora *et al*. [84] have proposed a multi-thresholding technique using its mean and variance. Recently, Maitra *et al*. [85] have developed a particle swarm optimization based multi-thresholding algorithm. This approach employs both cooperative learning and comprehensive learning. The algorithm could be found to be quite effective to determine multiple thresholds and out perform many other GA based algorithms. GA, when applied as an optimization technique to determine the threshold, is found to be computationally intensive and in this regard Cao *et al*. [86] have proposed a strongest schema based GA which could be successfully applied to multi-thresholding. A biological inspired computing based multi-thresholding algorithm has been proposed by Liou *et al*. [87], where the algorithm is based on honey bee mating optimization. The performance of the algorithm is found to be superior to PSO based algorithm. It has been observed that the landmark work of Otsu's thresholding when extended to multi-class problems is very time consuming. In order to reduce the computational burden, very recently Huang *et al*. [88] have proposed a two stage multi-threshold Otsu's method, which is less time consuming than Otsu's method. The method is found to be more efficient with an accuracy equivalent to Otsu's method.

1.6 Thresholding for fault detection

Thresholding is a simple and computationally efficient technique and therefore, it is suitable for real-time applications. Bi-level thresholding has been employed for automatic fault detection in many real world environment. Suitability for specific applications has been a decisive task quantitatively. Towards this end, Sezgin *et al*. [89] have carried out quantitative evaluation of several algorithms for non-destructive (NDT) testing application. A robust automatic threshold selection technique based on the notion of moving window has been developed by Wilkinson *et al*. [90] and the technique has been found to achieve fast segmentation of blood vessels against a varying background. Hui-Fuang Ng [91] has proposed an automatic thresholding method that deals with both unimodal and bimodal histograms and has successfully tested for detecting small or large size defects in a given scene. Recently, Lievers *et al*. [92] have proposed a thresholding technique to segment images of micro-structures of three automotive aluminium alloys. The defects in the welding process has been detected by a thresholding technique proposed by

Mahmoudi *et al*. [93]. This method produced comparable results with other methods, but the proposed method is quite simple. Very recently, Otsu's [5] method, minimum error based approach of Kittler have been applied to detect cracks in a painting [94] and this method could successfully be applied to detect cracks.

1.7 Adaptive thresholding

Although several bi-level thresholding and multi-level thresholding strategies have been proposed to achieve proper classification, there are many challenges to handle noisy images and images acquired under non-uniform lighting conditions. The fixed thresholding methods, both bi-level and multi-level, produce poor results in such situations. Therefore, attempts have been made over past two and half decades to devise adaptive thresholding methods to segment images under above conditions. By and large, adaptive thresholding methods are based on the notion of local thresholding. In late seventies, Nakagawa *et al*. [95] have proposed an adaptive quantization scheme based on histogram peak sharpening and the application of this produced better results than that of variational thresholding of Chow and Kaneko [37]. Subsequently, Yang *et al*. [96] have suggested an adaptive raster-scan thresholding algorithm to deal with images under imperfect illumination. This algorithm is based on the notion called Largest Static State Difference (LSSD) and it has been argued that hardware implementation of this algorithm can be realized in real-time. Adaptive thresholding based schemes have also been proposed by Ribaric *et al*. [97] to deal with video image or sequence of image frames. This algorithm is spatially and temporally adaptive and it has been advocated for real-time segmentation. Adaptive thresholding has also been applied to detect specific objects. Jhang *et al*. [98] have devised an adaptive thresholding algorithm based on multi-resolution analysis. They have carried out the performance analysis based on Gaussian distribution model and have shown that the adaptive threshold thus determined is closed to the Baye's threshold. The algorithm is robust even when the image distribution is unknown.

Followed by this, another adaptive thresholding algorithm have been proposed to detect targets with precision [99]. This algorithm determines the threshold by learning the characteristics of the background from the given images. The algorithm has been found to exhibit superior performance to the optimal laying algorithm in target detection and tracking. Kim *et al*. [100] has also suggested a motion estimation and tracking scheme using adaptive thresholding and

K-means clustering. In this algorithm, the motion mask region in a scene is indicated using an adaptive thresholding method, which is a histogram based approach to discard temporal variation due to illumination. In order to track objects, specially missile tracking, Haker *et al*. [101] proposed an adaptive thresholding technique to separate the object and background and hence track the missile in a video frames. A local adaptive thresholding algorithm has been developed by Herman *et al*. [102] to allow segmentation of television images at video rates. They have tested the scheme with grass and sky detection. An adaptive threshold algorithm based on Mumford-Shah and Chan-Vise functionsal has been proposed by Feigin *et al*. [103], where they have proposed a functional build upon an adaptive threshold surface coupled with the smoothed image. This method produced good smoothing results even in cases, where the images can not be segmented using other adaptive thresholding techniques.

In order to deal with images under uneven lighting condition, Huang *et al*. [104] has proposed an adaptive window selection based technique to determine optimal threshold. The method is based on window merging approach, where the image is partitioned into small windows and each window is tested with a criterion based on Lorentz information measure. If the window satisfies the criterion, then the window is fixed to be segmented by Otsu's method and if the window fixing criterion is not satisfied, then windows are merged based on pyramid structure. The algorithm produced satisfactory results for many poorly illuminated images but, the accuracy of segmentation of this method greatly depends upon the proper choice of initial window size. Each window is segmented by Otsu's method and segmentation of whole image is the union of segmentation over all the windows.

Adaptive thresholding has also been applied to the detection of vessels in retinal image [105]. The proposed adaptive local thresholding is based on verification based multi-threshold probing scheme. The approach is a knowledge guided adaptive thresholding. The algorithm produced satisfactory results for a wide variety of images. Adaptive thresholding techniques have also been applied for classification of ultrasound images [106] and in-situ microscopy [107]. Filho *et al*.'s [106] adaptive thresholding method is based on Otsu's [5] method to detect classification regions in intra-vascular ultrasound images. For in-situ microscopy, Espinoza *et al*. [107] have proposed local thresholding based technique to segment images captured by in-situ microscopy. Adaptive thresholding has also been applied to segment digital subtraction of angiography images [108]. The algorithm introduces the vessel existence measure to determine whether each sub-image contains vessels. The overall segmentation of the whole image is

achieved by combining the thresholded images. This algorithm has produced better results than global thresholding methods and other local thresholding methods. Recently, Jiang *et al*. [109] have proposed an adaptive thresholding based technique to detect infestation in fruit by X-ray images. The algorithm also has been implemented in real-time and tested with X-ray image of several fruits such as citrus, peach, guava etc..

The problem of detection of particles in an image has been addressed by Pi *et al*. [110] and their technique consists of combination of thresholding and watershed transforms. This could successfully used for oil-sand size analysis and the algorithm also speed up the size estimation of fine particles. The gray level co-occurrence has been used to develop an adaptive thresholding technique [111] that handles images with fuzzy boundaries. The co-occurrence matrix contains information on the distribution of gray level transition frequency and edge information. The algorithm could successfully be tested with star fruit defect images.

Recently, Saha *et al*. [112] have proposed an adaptive thresholding technique via minmax optimization of a novel energy functional that consists of a non-linear convex combination of an edge sensitive data fidelity term and a regularization term. The efficacy of the proposed method has been demonstrated for delineating lung's boundaries from Magnetic Resonance Imaging (MRI). Tsai [113] has developed an adaptive thresholding based approach to deal with non-uniform illuminations. The optimal threshold has been selected based on Simulated Annealing (SA) algorithm. The algorithm has successfully been tested for many real images. Shafait *et al*. [114] have suggested a local adaptive thresholding technique for document images and proved to be effective for many documented images. Recently, a projection distance minimization based adaptive thresholding technique has been proposed by Batenburg *et al*. [115] and the proposed method demonstrated more accurate segmentation results than other local thresholding based approaches.

1.8 Summary of the thesis

In this thesis, the problems addressed are; (i) the separation of object and background, and (ii) fault detection in a given scene. The problem has also been extended to separation of multiple objects and background. This problem is a segmentation problem and is viewed as the classification problem in a given scene. Separation of an object and the background in a given scene reduces to a two class problem, where object belongs to one class and the background as

another class. There could be multiple objects in a given scene and separating multiple objects and the background reduces to a multiclass problem. Since it has been intended to devise novel schemes for real-time object detection and tracking, the notion of thresholding which is simple and efficient, has been used to address the problem of classification. The issue of thresholding based image segmentation and classification has been addressed for more than three decades, but reducing the misclassification error, in case of overlapping class distributions still remains an open problem. This research has attempted to address this issue in a novel framework of Genetic Algorithm (GA) and Parallel Genetic Algorithm (PGA) based Clustering.

Separation of object and background has been viewed as a classification problem with two classes. The gray level distributions i.e. histogram has been used to determine the threshold for dividing the range of gray values into two classes. We have used the shape information of the histogram to determine the threshold. The discrete histogram of a two class image consists of two class distributions, one belonging to the object class and the other belongs to the background class. In other words, the problem of separating the two classes is to determine a threshold that will separate the range of values into two sets. We have devised GA and PGA based clustering schemes to determine the threshold. The problem is simple when two class distributions in the histogram landscape is well separated and becomes challenging when the two class distributions in the histogram landscape overlap each other. In case of overlapping, few pixels that would have belonged to the object class would belong to the background class, thus resulting in classification error. In a two class case, the problem reduces to determining optimal threshold that minimizes the misclassification error. Each class distribution in a two class problem has a niche or peak and hence there will be two peaks and a valley point in between these two peaks. In order to separate the two classes with distinct separability, the valley point that corresponds to the threshold needs to be determined. Thus, for a two class problem determination of the valley point that mostly corresponds to the minimum point between the two peaks of class distribution needs to be found out. A simple iterative search for the whole range of gray values would often mislead many other gray values as the minimum one. In order to ameliorate such cases, we have adopted the following GA and PGA based clustering strategy. Since, this valley point is assumed to exist in between the two niches or peaks corresponding to the two classes, it is necessary to detect the two peaks first followed by detection of the valley point. We have proposed GA based class models to determine the peaks and thereafter, the valley point that corresponds to the threshold.

We have viewed the histogram landscape as a non-linear multi-modal function and each mode of a class distribution represents a class. Hence, GA and PGA based class models have been proposed to determine the peaks and thereafter, the valley point. The thesis work can be summarized as follows.

- First GA and PGA based class models have been proposed to detect the peaks. For a non-linear multi-modal function, there could be several global optima and many local optima. This classification problem is formulated to determine all the optima in the non-linear multi-modal function landscape. We have considered sinusoidal functions with multiple global optima and also with one global optima and many local optima. GA based crowding algorithm has been used to maintain stable sub-populations at respective niches and in turn determine all the optima. It has been observed that GA based crowding although maintains stable sub-populations in different niches, it is found to converge after large number of generations and hence incurs high computational burden. Hence, a PGA based crowding scheme has been proposed to maintain sub-population in the niches thus determining all the optima. PGA based scheme is based on Island model and a new interconnection model has been proposed to accelerate convergence. This interconnection model is based on the Island model, where a new notion of intra-deme migration has been introduced besides the existing inter-deme migration. This interconnection model is found to accelerate the rate of convergence as compared to GA based clustering. The proposed PGA based algorithm is found to maintain stable sub-populations at different niches, thus detecting the respective classes. The PGA based clustering scheme could successfully be tested with two, four, and eight class models. This PGA based scheme could detect successfully the different optima in case of decaying and non-decaying sinusoidal functions of two, four, and eight class models. The effect of different parameters of PGA based scheme such as network topology, migration policy, rate of migration, and interconnection model on the rate of convergence has been investigated in detail and the optimum parameters thus found are used for the PGA based scheme. Convergence analysis of PGA based scheme has been carried out and it is shown to converge to the optimal solution with a bound.

- The PGA based algorithm thus developed has been used to determine optimal threshold for image segmentation. Two schemes namely Feature Less (FL) scheme and Feature

Based (FB) scheme have been proposed to determine optimal threshold. In FL scheme, the histogram of the original image is considered and the peaks corresponding to different classes have been found out using the PGA based clustering schemes and the valley points in-between the peaks have also been found out using PGA. It has been observed that this scheme proved to be effective when the histogram exhibited clear bi-modality condition. The results deteriorated with increase in the overlapping of the class distributions in the histogram landscape. In order to circumvent this problem, a feature based scheme is proposed. In this scheme, threshold is determined in the feature plane instead of the gray level plane. Hence, a feature pixel corresponding to each pixel of the original image is found out and thus a feature image is created. It has been observed that the degree of overlapping of the class distributions in the feature histogram reduced substantially. Threshold of the feature histogram has been found out by the PGA based scheme. The threshold thus determined in the feature plane has been used to segment the original image. It has been found that feature based scheme often produced better results than the featureless scheme. The results have also been compared with Otsu's [5] and Kwon's [16] method and the proposed feature based (FB) scheme outperformed the above two methods and proposed featureless scheme.

- PGA based thresholding schemes have been proposed to detect cracks in the images of earth surface cracks. It has been observed that our previously proposed FL and FB based schemes and many existing schemes fail to detect cracks with different size of granules. The histogram in case of crack images have lost the bimodal property and have many misleading modes or almost appearing unimodal. In this piece of work, feature less minimum mean square error (FL-MMSE) and feature based minimum mean square error (FB-MMSE) scheme have been proposed to detect cracks of different size. This also produced better results than Otsu's [5], Kwon's [16], Hui-Fuang's [91], and of earlier proposed schemes. This also produced satisfactory results in case of general two class images.

- Adaptive thresholding based segmentation scheme has been proposed to segment images acquired under uneven lighting conditions. The proposed approaches can be categorised as window merging and window growing. In both the cases, the window size is adopted to make it suitable for segmentation with low misclassification error. In window merging

approach, the approaches can further be divided into pyramid approach and overlapping windowing approach. The three proposed window merging criteria are based on; (i) locally biased Lorentz information measure (LIM), (ii) weighted local and global statistics, and (iii) entropy measure. Adaptive thresholding based on the proposed window merging criterion proved to be better than Huang *et al.*'s [104] approach. But the efficacy of the proposed scheme is found to greatly depend on the proper choice of initial window size. In order to overcome this bottleneck, a window growing approach based adaptive thresholding scheme has been proposed. In window growing approach, the window size is fixed based upon entropy and feature entropy based criterion. Window growing based scheme is found to be more efficient than that of the window merging approach. In both window merging and window growing approach, the proposed thresholding schemes and Otsu's method have been used to segment different windows and the overall segmentation is the union of all the segmentation over all the windows.

The major contribution of the thesis can be summarized as follows:

1. *A Parallel Genetic Algorithm (PGA) based clustering scheme is developed to determine the niches of the nonlinear multimodal function by maintaining stable sub-populations at each niche.*

2. *The PGA based algorithm is shown to converge to the optimal solution with probability. For PGA based scheme, new interconnection model is proposed to accelerate convergence.*

3. *PGA based clustering is used to develop a feature less and feature based global thresholding scheme for segmentation.*

4. *A new thresholding scheme based on Minimum Mean Square Error (MMSE) has been proposed. Two thresholding schemes such as Feature based MMSE and Feature Less MMSE have been proposed.*

5. *Segmentation of images under non-uniform lighting condition has been achieved using adaptive thresholding. Adaptive thresholding schemes are developed based on information theoretic approach. They are based on adaptively fixing the window size. The proposed adaptive thresholding schemes are based on both window merging and window growing concept.*

1.9 Organization of thesis

Chapter 2 provides the basic background on GA and PGA. The working principle of GA and PGA has been described in this chapter.

In chapter 3, the classification problem, in case of nonlinear multimodal function, has been developed using GA and PGA based clustering. Sinusoidal nonlinear multimodal functions of different classes have been considered and PGA based crowding algorithm has been proposed to determine the peaks of the nonlinear functions and hence, classes. The PGA based crowding algorithm has been tested on two, four, and eight class models with decaying sinusoids and non-decaying sinusoids. The proposed new interconnection PGA model has been developed in this chapter. Convergence analysis of the proposed PGA algorithm has been carried out and is shown to converge to the optimal solution with a bound. The proposed algorithm has been tested with two, four, and eight class models and the effect of different parameters on the rate of convergence has also been studied. Results pertaining to all the different class models have been presented and discussion on results obtained has been presented.

Chapter 4 provides the segmentation of a given image using PGA based thresholding scheme. Segmentation problem is viewed as a classification problem and thresholds for these segmentation have been obtained by PGA based algorithm. In this regard, *Feature Less* (FL) and *Feature Based* (FB) scheme have been proposed to determine thresholds from the histogram of the original image and from the feature histogram corresponding to the feature image. Results and discussion on two and three class images have been presented. The performance of the proposed schemes has also been compared with that of the Otsu [5], and Kwon's [16] approaches. A brief review on Otsu's and Kwon's algorithm has also been presented.

Minimum Mean square Error MMSE based thresholding schemes have been developed specifically for detection of earth surface cracks in images and are presented in Chapter 5. The two schemes feature less MMSE (FL-MMSE) and feature based MMSE (FB-MMSE) have been developed in chapter 5 and have been tested with general two class images particularly images pertaining to colour blindness. Results obtained by these schemes for different crack images have also been presented. The performance of the proposed schemes has also been compared with that of the Otsu, Kwon's and Fuang's approaches. Discussion on the results obtained has been carried out. A brief review on the Fuang's [91] algorithm has also been presented.

Chapter 6 deals with the adaptive thresholding schemes for images acquired under non-

uniform lighting conditions. The window merging and window growing based adaptive thresholding schemes have been proposed. The three window merging schemes and one window growing scheme have been presented in this chapter. The efficacy of these schemes has been demonstrated with different two class real images acquired under non-uniform lighting conditions. The performance of the proposed schemes has been compared with Huang's [104] approach. Therefore, Huang's adaptive window selection based thresholding scheme has been described. Results and discussion on different images have also been presented.

Conclusions drawn on different works of this thesis have been provided in chapter 7. The scope of future work have been highlighted.

Chapter 2

Background on Genetic Algorithm and Parallel Genetic Algorithm

2.1 Genetic Algorithm

Most classical methods of optimisation generate a deterministic sequence of trial solutions, based on the gradient or higher order statistics of the cost function. Under regularity conditions on this function, this technique can be shown to generate sequence that asymptotically converges to local optimal solution. In certain cases they converge exponentially fast. Variations in these procedures are often applied to training neural networks, or estimating parameters in system identification, pattern recognition, machine learning, adaptive image processing, expert system and adaptive control application. But the method often fails to perform adequately when random perturbations are imposed on the cost function. Also local optimal solution proves insufficient for real world engineering problem.

Genetic algorithm (GAs) has recently emerged from a study of the mechanics of evolution. They are stochastic optimisation techniques that can often outperform classical methods of optimisation when applied to difficult real world problems. Genetic Algorithms are searching strategies suitable for finding the globally optimal solutions. The main advantage of using GAs is that they can find global optima without being stuck at local optima [116, 117, 118, 119, 120] in the solution space. The power of GA comes from the fact that the technique is robust and can deal successfully on a wide range of problem areas. GAs and its variance have been extensively used in the past. GA researchers have been aware that there are multiple solutions for a given problem but the traditional GA proves to be quite efficient, which converges to one of the best

possible solution.

In GA, the candidate solutions are represented by chromosomes, which are nothing but binary coded strings carrying information regarding solutions. GAs are capable of forming niches for the purpose of multi-modal function optimisation. Mostly previous GA models have been slightly complex and typically based on Markov chains. Several studies have been carried out on proportional solutions, mutation using Markov chains analysis, where it is assumed that the population size is infinite or very large.

Genetic algorithms are randomized search algorithms based on the mechanics of natural selection and genetics. They implement survival of the fittest among the string structures. The behavior of genetic algorithm can be subtle, but their basic construction and execution cycle is straight forward. GA is an iterative procedure maintaining a population of structures that are candidate solutions to specific domain challenges. During each generation, the structures in the current population are rated for their effectiveness as domain solutions. On the basis of these evaluations, a new population of candidate solutions is formed using specific genetic operators such as reproduction, crossover, and mutation.

The natural law of evolution is derived from Darwins theory of evolution. According to this theory, reproduction and mutation play major part. While reproduction leads to intermingling of different chromosomes and hence, creation of individuals having hybrid characteristics with genetic properties derived from both parents by inheritance, mutation is a factor that causes changes in the basic chromosomes structure itself, and thus leads to diversity of the population. GAs are based on the above mentioned phenomena and can be used for optimization of the given problems by mimicking the natural processes of reproduction and mutation.

The power of GAs comes from the fact that the technique is robust and can deal successfully with a wide range of problems areas, including those, which are difficult for other methods to solve. GAs are not guaranteed to find the global optimum solutions to a problem, but they are generally good at finding acceptably good solutions to a problem, acceptably quickly. Where specialized techniques exist for solving particular problems, they are likely to out- perform GAs in both speed and accuracy of the final result. The main ground for GAs are in difficult areas, where no such technique exists. Even where existing techniques work well, improvements have been made hybridizing them with GA.

2.1.1 Definitions

Chromosomes

It is a binary coded string containing information regarding the variable to be optimized. It is a string of real values or as an individual.

Gene

It is the smallest unit of information carrying block of chromosomes. Multiple genes are present in the chromosomes, when more than one unit of information about the variables have to be coded.

Bit

Since, the information is coded as a binary string, the smallest unit of string is a digital bit, with only two states: 0 and 1. a number of bits together give a practical method of storing coded information.

Population

A population is composed of a number of individuals and basic data set on which GA operates. A population is said to be diverse, when the chromosomes are sufficiently different from each other and the candidate solutions (that encoded into chromosomes) are spaced over the entire solution space. In GA, population size affects both global performance and efficiency. Genetic algorithm with small population usually performs insufficient convergence of the problem space. A large population is more likely to be representative of the entire problem domain.

Mating pool

Similar to population, it is that population on which the operators to get a new solution. The mating pool is created by the survival of the fittest, usually by fitness ranking or other appropriate selection mechanism.

Parent

Parents are the original strings on which the operators are applied. The properties of the parent strings are transferred to the resultant children strings.

Offspring

The output of the genetic operator and crossover are called children and offspring. The offspring becomes the parent of the next generation.

Operators

Simulations of the natural processes that bring about a change in the population and thus give rise to individuals that may be fitter than the parents. The operators act on the individuals of the mating pool and child population. The main operators are reproduction, crossover and mutation.

Generation

This is the number of iterations or cycles of the algorithm. It is analogous to the generation concept in the evolution. The generation gap controls the percentage of population to be replaced during each generation.

Fitness

A figure of merit of an individual, which is proportional to the utility or ability of the individual to survive in the given environment is usually a real quantity lying between 0 and 1. A fitness function must be devised for each problem to be solved. The fitness function returns a single numerical fitness.

2.1.2 Description of the Operators

A simple GA that yields good results in many practical problems is mainly composed of three operators i.e. reproduction, crossover, and mutation. It is to be noted that crossover and mutation are not only two operators in use, various other operators do also exist.

Reproduction

Reproduction is a process in which individual strings are copied according to their objective function values. It is actually a copy operator in the sense that it merely copies the parent chromosome into the mating pool without actually changing the chromosome structure. However, the copying is done probabilistically, with higher fit strings having more chance of being transferred to the mating pool than the strings with lower fitness. This characteristic simulates the

survival of the fittest. This operation results in a progressive increase of the number of high fitness string over the less fitness strings with each successive generation. This operator, of course, is an artificial version of natural selection, a Darwinian survival of fittest among the string creatures.

Crossover

The primary exploration mechanism for GAs is crossover. Crossover randomly chooses two individuals, and cuts the individual strings at some randomly chosen position, to produce two head segments, and two tail segments. The tail segments then swapped over to produce two new full-length chromosomes as shown in Fig. 2.1. The two offspring, each inherits some genes from each parent, which is known as single point crossover. However, many different crossover algorithms have been devised, often involving more than one cut point. Dejong [121] investigated the effectiveness of multiple crossover points, which reduces the performance of GA.

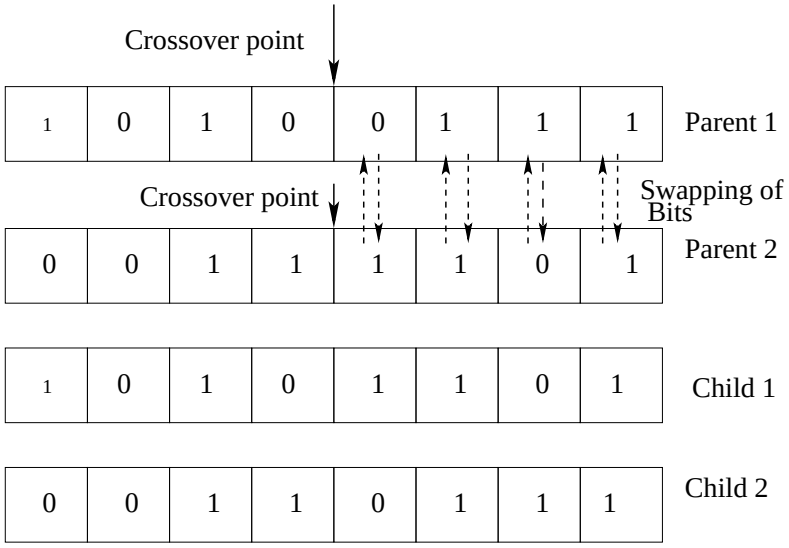

Figure 2.1: Single point crossover operator

Two point crossover

In two point crossover (and multi-point crossover, in general), rather than linear strings, chromosomes are regarded as loops by joining the ends together, to exchange a segment from one loop with that from another individuals in the population. As shown in Fig. 2.2, this two point

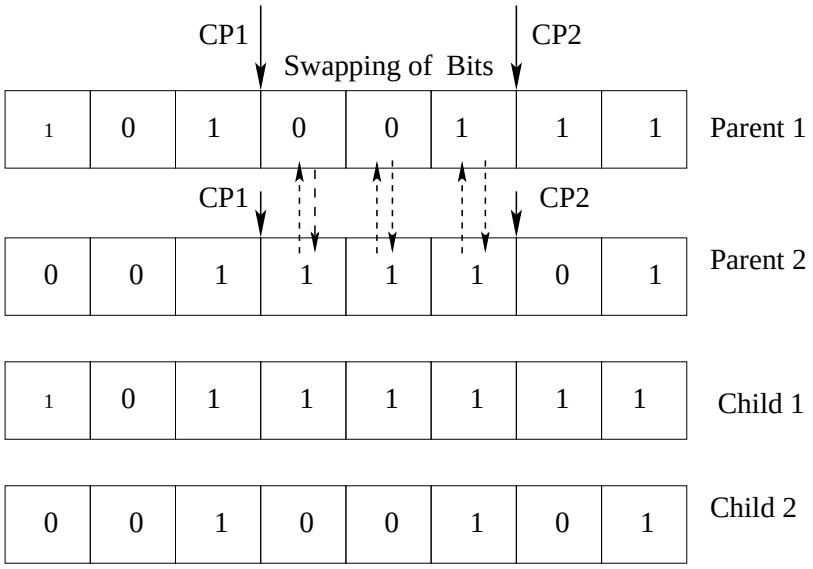

Figure 2.2: Two point crossover operator

crossover produces new individuals as offspring, which shares some features taken from each parent.

Mutation

The mutation is usually considered as a secondary operator. Mutation is applied to each child individually after crossover. This consists of the variation of a randomly chosen bit of the selected string. Mutation is analogues to the "NOT" operation in digital system and negates in the sense of bit. This is an extremely powerful operator as it can drastically change the mating pool composition by introducing new genetic material in the population. Random mutation effectively introduces new information in the knowledge base. Following example of the nature, the probability of applying the crossover operator is more than that of mutation operator. It is an useful operator, which allowed the algorithm to overcome the local extrema in the solution space and hence, leads to the global searching capability of GAs. Fig 2.3 shows the third gene (bit) of child 1 being mutated and the fifth gene (bit) of the child 2 being mutated.

2.1.3 Working of Genetic Algorithm

In the following, the working principle of GA is described as follows:

The first step consists of the codification of the variables involved in suitable binary strings. In the second step, population of strings representing initial parent population, usually randomly

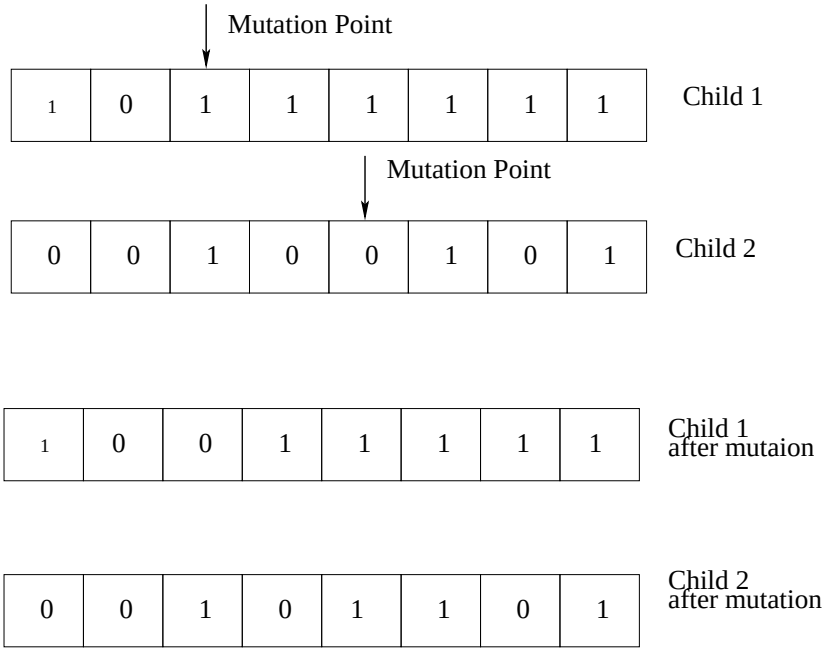

Figure 2.3: Mutation operator

selected in the entire solution space domain, is created. Random selection has advantage that this introduces diversity in the population and also avoids the problems of optimizing at local optima. The population is a dynamic entity. Iterative reproduction leads to the population of parameters towards the optimal condition. A parameter known as fitness of a string is defined and calculated at each iteration of the algorithm and the iterations are carried out until the terminal condition is reached. This corresponds to the criterion of a solution-string with the desired value. A fitness value must be devised for each problem to be solved.

2.1.4 Steps of the basic Genetic Algorithm

The step by step description of a basic GA is as follows:

Step 1: A fixed number of elements representing the initial population are randomly chosen.

Step 2: The fitness of each element is evaluated using the fitness function.

Step 3: The elements of the population are chosen probabilistically according to their fitness.

Step 4: With the respective probabilities, randomly pairs are chosen for mating through the genetic operator crossover (exchange of genetic material between two selected candidates) and selection, again possibly at random, a site where the material will be exchanged re-

sulting in the creation of offspring. Also secondary operator mutation is applied. The probability of mutation is very less i.e. between 0.003 and 0.001.

Step 5: Compute the fitness of the offspring.

Step 6: Introducing these strings into the original population discarding an equal number of randomly chosen strings.

Step 7: Repeat fixed number of generations till the maximum number of strings converges.

2.2 Parallel Genetic Algorithm

Genetic algorithms are efficient search methods based on the principle of natural selection and population genetics. They are being successfully applied to problems in business, engineering and science. GAs use randomized operators operating over a population of candidate solutions to generate new points in search space. Hard problems need a bigger population and this translates directly into higher computational cost. Though, the GA based models are able to produce the global optimal solution successfully, it has following bottlenecks: (i) It needs a very large number of population, and (ii) Increase in the computational burden.

Evolution is highly a parallel process. Each individual is selected according to its fitness value and allowed to survive and reproduce. GAs are an abstraction of the evolutionary process and is indeed very easy to parallelize. Recently, attempts have been made to devise PGA that simultaneously aims at achieving reduced computational burden and fast conergence [122, 123, 124]. The basic motivation behind PGA is to reduce the processing time to reach an acceptable solution. This was accomplished implementing GAs on different parallel architectures. In addition, it was noted that in some cases the PGAs found better solutions than comparably sized serial GAs. GAs are easy to parallelize and many variants on the basic models have been tried with good results on the different classes of problems. In the past few years, Parallel Genetic Algorithms (PGAs) have been used to solve difficult problems.

The first approach of parallelizing GAs is to do a global parallelization. In this class of parallel GAs, the evolution of individual and the application of genetic operators are explicitly parallelized. Every individual has a chance to mate with all the rest. The semantics of the operators remain unchanged. PGAs are classified into two types: -

1. Coarse Grained PGAs

2.2.1 Coarse-grained PGAs

The population is divided into few sub-populations (deme) keeping them relatively isolated from each other. The sub-populations are called demes those occasionally exchange some individuals among themselves and this process is called migration.

The important characteristics of this class of algorithms are the use of few relatively large demes and introduction of migration operation. Coarse-grained parallel GA is one of the most popular model used in PGA literature. A more sophisticated idea is used in coarse-grained parallel GAs, where the population is divided into few sub-population (deme) keeping them related and isolated from each other. This model of parallelization introduces a migration operator that is used to send some individuals from one sub-population (deme) to each other. There are two different implementation models of coarse-grained GAs: (1) The island model, and (2) The stepping stone model.

The population in the island model is partitioned into small sub-populations and individuals can migrate to any other sub-population. In the stepping stone model, the population is partitioned in the same way, but migration is restricted to neighboring sub-populations. Both models have been used in parallel GAs. Sometimes coarse-grained GAs are known as distributed GAs. Cantupaz [124] has provided a lucid survey on parallel Genetic Algorithm, where he has presented the efficacy of different models and also pointed out the limitations.

Tanese [125] proposed a parallel GA that used a 4-D hypercube topology to communicate individuals from one deme to another. In Tanese's algorithm, migration occurred at a uniform periods of time between neighboring processors along the dimensions of the hypercube. The migrations were chosen probabilistically from the best individuals in the sub-population and they replaced the worst individuals in the receiving deme. Tanese reported that the parallel GA found results as good as serial GA, with the advantage of non linear speedups.

Cohoon *et al*. [126] proposed a multi-population genetic algorithm for solving the K-partition problem on Hyper-cubes. Cohoon *et al.* [127] proposed an implementation of parallel GA based on the theory of punctuated equilibria. One aspect of this theory is that new species are likely to form quickly in relative small isolated population after some changes in the environment occur. Cohoon *et al*. noticed that the number of migrants affected the level of disruption in the demes and the new solution was found shortly after migration occured. A linear place-

ment problem was used as a benchmark and experimented using a mesh-topology. However, it is noted that the choice of topology is probably not very important in the performance of parallel GA as long as it has high connectivity and small diameter to ensure adequate mixing as time progress. They found that parallel GA with migration outperformed both parallel GA without migration and serial GA. Cohoon *et al.* [128] applied the distributed genetic algorithms for floorplan design problem to minimize the weighted sum of area and wirelength measures in the VLSI design cycle. Their method has performed better than the Simulated Annealing (SA) algorithm, both in terms of the average cost of the solutions found and the best-found solution.

Hence, it is concluded that migration is controlled by several parameters, the topology that defines the connection between the sub-populations, a migration rate that controls how many individuals migrate, and a migration interval that affects how often migrations occur. The values for these parameters are chosen using intuition rather than analysis.

2.2.2 Fine grained PGAs

Fine grained parallel GAs partition the population into a large number of very small sub-population. This model requires massive parallel computer. In case of coarse-grained parallelism, and fine-grained parallelism, selection and mating occur only within each sub-population. In biological term, the sub-population refers to deme. Deme is smaller than population, which is used by the serial GA. So we expect that the PGA will converge faster. Combination of the first three methods have been used to develop hybrid parallel GAs.

In this model, the population is divided into small demes. The demes overlap is providing a good solution across the entire population. Again selections of a mating occur only within a deme. Schleuter *et al*. [129] introduced the ASPARAGOS system. It uses a population scheme that looks like a ladder with upper and lower ends tied together. ASPARAGOS was to solve some difficult combinational optimization problems with great success.

2.2.3 Migration policy

The sub-population or demes occasionally exchange some individuals in a process called migration. Migration policy also affects the convergence time and the quality of solution. The parallelized crowding scheme is based on the course-grained approach and island model. In the island model, the following four migration policies have been used.

(i) Good migrants of one deme replacing the bad individuals of another (GB).

(ii) Good migrants of one deme replacing the random individuals of another (GR).

(iii) Random individuals of one deme replacing the bad individuals of another (RB).

(iv) Random individuals of one deme replacing random individuals of another (RR).

All these migration policies are investigated while dealing with two, four and eight class models. We have also considered multimodal functions of unequal peaks.

2.2.4 Steps of the Parallel Genetic Algorithm

The step by step description of the Parallel Genetic Algorihm (PGA) is as follows:

Step 1: Initialize randomly population elements of size N

Step 2: Divide the population space into fixed number of sub-populations (deme).

Step 3: Consider one subpopulation (deme) and go through the following steps.

Step 3.1: In the given sub-population, the fitness of each elements is evaluated.

Step 3.2: The elements of the sub-population (deme) are choosen probabilistically according to their fitness.

Step 3.3: With the respective probabilities randomly pairs are chosen for mating through two elements at random for crossover and mutation operation.

Step 3.4: Evaluate fitness of each parent.

Step 3.5: With the respective probabilities, randomly pairs are chosen for mating through the genetic operator crossover (exchange of genetic material between two selected candidates) and selection, again possibly at random, a site where the material will be exchanged resulting in the creation of offspring. Also, secondary operator mutation is applied. The probability of mutation is very less i.e. between 0.003 and 0.001.

Step 3.6: Compute the fitness of the offspring.

Step 3.7: Introducing these strings into the original population, discarding an equal number of randomly chosen strings.

Step 3.8: Repeat steps 3.1, 3.2, 3.3, 3.4, 3.5, 3.6, and 3.7 for all the elements in the given sub-population (deme).

Step 4: Repeat step 3 for fixed number of generations.

Step 5: Steps 3 and 4 are repeated for each sub-population (deme).

Step 6: Migration is allowed from each deme to every other deme. The individuals are migrated based on the selected migration policy. Number of elements to migrate are determined from the selected rate of migration R_{mig}. The elements migrate with migration probability P_{mig}.

Step 7: Repeat steps (3), (4), (5), and (6) till convergence is achieved. The migration among the sub-population is continued till convergence is achieved.

Chapter 3

Parallel Genetic Algorithm based Class Models for Clustering

3.1 Introduction

Genetic Algorithm (GA) has extensively been used to solve optimization problems in science and engineering [116, 117, 118, 119, 120]. Genetic algorithm when applied to such problems produce almost always global optimal solutions. In order to determine all the optima of a nonlinear multi-modal functions, GA based crowding method has been proposed [130, 131, 132] to determine all the solutions. If the nonlinear multi-modal function in the two dimensional landscape can be viewed as the mixture of class distributions and then each niche or peak in this distribution correspond to one class. In this class distributions, determining different classes reduces to determining the different niches of the nonlinear multi-modal functions [133, 134, 135]. This can be achieved by GA based crowding or clustering algorithm. The underlying notion behind GA based clustering is to maintain stable sub-populations at each niche. The entire population elements is divided into sub-populations and the sub-populations need to be clustered at different classes.

In this chapter, GA based crowding algorithm has been successively tested for two, four and eight class models. In one case the peak of different classes occur at same functional value (fitness) value and in another cases the peaks occur at different functional values (fitness). The first case corresponds to multiple global optima of a function while the second case correspond to both global as well as local optimal solutions. In order to accelerate the rate of convergence Paralle Genetic Algorithm (PGA) based clustering algorithm has been devised with the pro-

posed interconnection model. PGA based algorithm has also been validated for both decaying and non-decaying sinusoidal functions. The effect of different parameters of PGA based interconnection model on the rate of convergence has been investigated. Convergence analysis of the proposed PGA based algorithm has been considered out and is shown to converge to the optimal solution with a bound.

3.2 GA based class models

The proposed GA and PGA based clustering algorithms have been tested for two, four, and eight class problems. The following two, four, and eight class models have been considered in the simulation.

Two class model;

$$f(x) = |sin(2\pi x)|,\ 0 \leq x \leq 1, \tag{3.1}$$

$$f(x) = |e^{-2(x-0.125)} \times sin(2\pi x)|,\ 0 \leq x \leq 1. \tag{3.2}$$

Four class model;

$$f(x) = |sin(4\pi x)|,\ 0 \leq x \leq 1, \tag{3.3}$$

$$f(x) = |e^{-2(x-0.125)} \times sin(4\pi x)|,\ 0 \leq x \leq 1. \tag{3.4}$$

Eight Class model;

$$f(x) = |sin(8\pi x)|,\ 0 \leq x \leq 1, \tag{3.5}$$

$$f(x) = |e^{-2(x-0.125)} \times sin(8\pi x)|,\ 0 \leq x \leq 1. \tag{3.6}$$

In each class model, the function is a nonlinear function. In the two dimensional function landscape, the two modes correspond to two different classes and these classes may be represented by the peak of the respective class. For example, Fig. 3.1(a) shows the function corresponding to (3.1). As seen from Fig. 3.1(a), there are two classes and accordingly two niches/modes/peaks. It is to be noted that the two peaks occur at same value of the function i.e. unity. In other words, we say the peaks are of equal height in a nonlinear landscape. Each mode corresponds to one class and hence the sinusoidal function in (3.1) having two modes correspond to a two class model. Sometimes in two class model, two peaks corresponding to

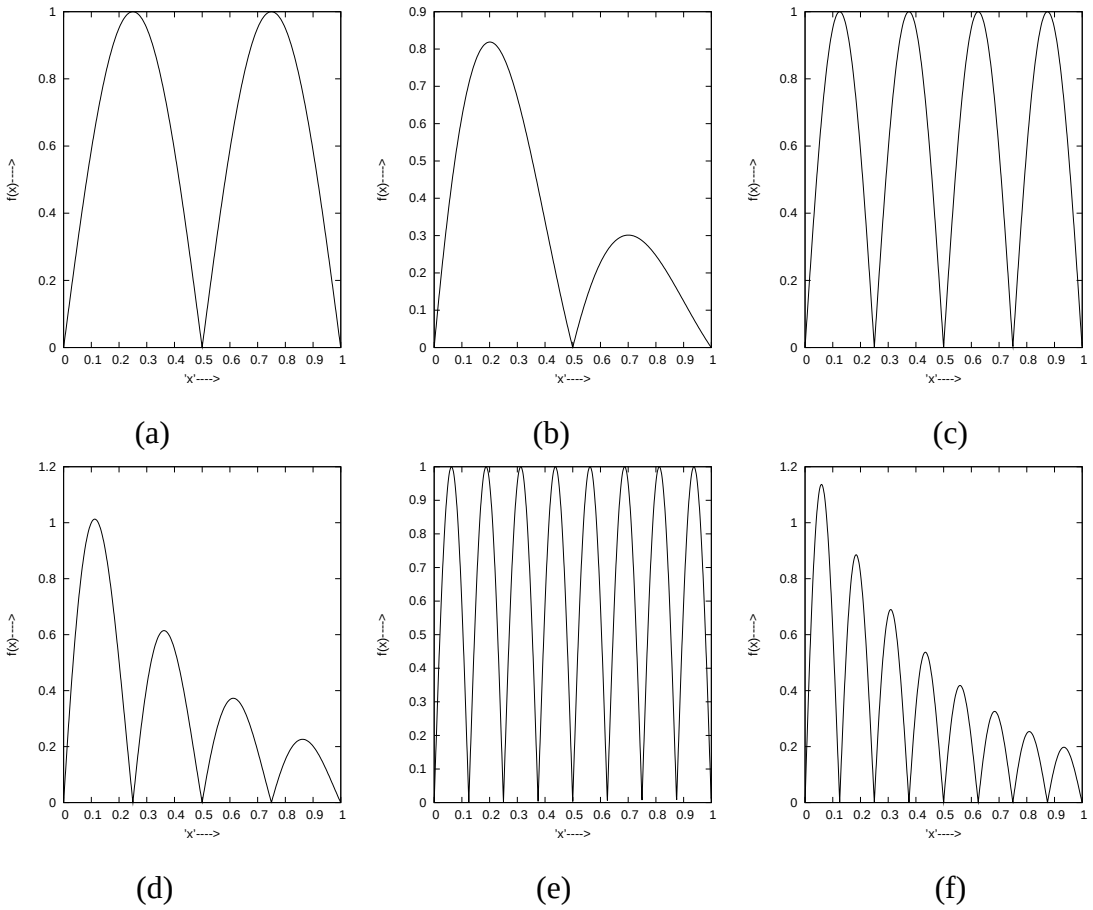

Figure 3.1: (a) Two class function, (b) Decaying two class function, (c) Four class function, (d) Decaying four class function, (e) Eight class function, (f) Decaying eight class function

two classes may not occur at the same value of the function and thus the two class distributions will be different. The decaying sinusoidal function as given by (3.2) represents a two class model with uneven class distributions. Thus, the two peaks occur at different functional values. Similarly functions given by (3.3) and (3.4) correspond to the four class model with and without decaying sinusoidal functions. Hence, there will be four niches/peaks for the 4-class models. Analogously, the eight class model given by (3.5) and (3.6) possesses eight niches/peaks corresponding to the respective class distributions. Determination of all the classes of a class model boils down to determination of all the niches or peaks of the nonlinear multi-modal function.

It is known that basic Genetic Algorithm (GA) has extensively been used for optimization of nonlinear functions and it yields a global optimal solution. The above described class models can be viewed as nonlinear multi-modal functions. Basic GA when applied to such functions will yield either a global optimum solution or one of the global optimal solutions [116, 117, 118]. Thus, in the classification paradigm, the algorithm would determine one class or one of the classes of the class model. Therefore, it is conceivable that all the classes of the class model

can be determined if all the niches/modes or all the solutions (both local and global) of the multi-modal function can be found out.

GA based class models using the notion of crowding have been proposed [130, 131, 133, 136, 137, 121] to determine all the niches of a nonlinear multi-modal functions and hence all the classes. This is achieved when GA could form stable clusters of population of elements at the niches/peaks of the nonlinear multi-modal function. In other words stable sub-populations could be maintained by GA based clustering algorithm at different niches and hence different classes could be determined. Thus, clustering has been achieved using the notion of crowding [132, 136, 137, 121] in GA. GA forms clusters at the niches of the nonlinear multi-modal functions and hence GA based class model is achieved. Stable sub-populations could also be maintained using the notion of sharing. Since, throughout the thesis we have used the notion of crowding to maintain stable sub-populations, we describe the notions of crowding in section 3.2.1

3.2.1 Crowding method

Crowding originally proposed by De Jong [121] is motivated by analogy with competition for limited resources among similar member of a natural population. Dissimilar population member often occupy different environmental niches. Older members of the niche will be replaced by the fittest of the youngest member. To maintain stable sub-population by replacing population with like individuals can be called crowding method [121]. Stochastic replacement error prevents the basic crowding algorithm from maintaining more than two peaks of multi-modal fitness.

Deterministic crowding [132, 136, 138] eliminates replacement error and maintains multiple peaks. It works by randomly pairing the population to yield n/2 pairs for n individuals in the population and each pair of parent yields two children by undergoing crossover operation. Two children compete against the parent. In partner tournament either children or both parent, the pair containing the maximally fit element, will win.

The notion of crowding is inspired by ecological phenomenon where similar individuals in a natural population compete against each other for limited resources. Dissimilar individuals tend to occupy different niches and hence typically they do not compete. Thus for a fixed size population at equilibrium, new members of a particular species replace old members of that species. Crowding method attempts to maintain diversity of the pre-existing mixtures. Deterministic crowding that we have used in our algorithms, in terms of number classes, is

explained as follows.

In deterministic crowding, sampling occurs without replacement [130, 131, 136]. We will assume that an element in a given class is closer to an element of its own class than to elements of the other classes. A crossover operation between two elements of the same class yields two elements of that class, and the crossover operation between two elements of different classes yields either: (i) one element from both the classes, (ii) one element from two hybrid classes. For example, for a four class problem, the crossover operation between two elements of class AA and BB may results in elements either belonging to the set of classes AA, BB, or AB, BA. Hence the class AB offspring will compete against the class AB parents, the class BA offspring will compete with class BA parents. Analogously for a two class problem, if two elements of class A are randomly paired, the offspring will also be of class A, and the resulting tournament will advance two class A elements to the next generation. The random pairing of two class B elements will similarly result in no net change to the distribution in the next generation. If an element of class A gets paired with an element of class B, one offspring will be from class A, and the other from class B. The class A offspring will compete against class A parent, the class B offspring against class B parent. The end results will be that one element of both the classes advances to the next generation and hence no net change.

3.2.2 Tournament selection

Selection mechanism is also a key issue that influences the convergence of Genetic Algorithms. The selection mechanism is a process that favours the selection of better individuals in the population. The selection pressure is the degree to which the better individuals are favoured. Over successive generations, this selection pressure drives the GA to improve the fitness of the population. The convergence rate of a GA is largely determined by the selection pressure with higher selection pressure resulting in higher convergence rates. The tournament selection provides selection pressure by holding tournament of “q” individuals, with “q” being the tournament size [119, 120].

In tournament selection a group of “q” individuals is randomly chosen from the population. They may be drawn from the population with or without replacement. This group takes part in a tournament where a winning individual is determined depending on its fitness value. The best individual having the highest fitness value may be chosen deterministically or through a stochastic selection process. In both the cases only the winner is selected into the next popu-

lation and the processes is repeated λ times to obtain a new population, where "λ" denotes the number of elements participating in the tournament.

When the tournament size "q" is two, this is known as binary tournament. We assume that the individuals are drawn with replacement and the winning individual is deterministically selected.

Let $P(t)$ denotes the population elements and the tournament size is denoted by $q \in 1, 2, .., \lambda$. Let $P'(t)$ denotes the population size after selection and tournament.

The following are the salient steps of the tournament selection:

(i) Select randomly the elements $(a_1, a_2, ..., a_\lambda)$ from $P(t)$ to form the tournament $q \in 1, 2, ..., \lambda$.

(ii) Select $'a_i'$, the best individual from q randomly chosen individuals $(a_1, a_2, ..., a_\lambda)$

(iii) Repeat the steps (i) and (ii) till $a_1, a_2, ..., a_\lambda$ is replaced by $a_1', a_2', ..., a_\lambda'$

3.2.3 Generalized crossover

Generalized Crossover (GC) operator proposed by Nanda *et al*. [139] when applied to two parents produces one offspring instead of two offspring as in the basic GA. The operator can be described as follows. Two parents P_1 and P_2 are selected at random and the two crossover points are also selected at random. In between the two crossover points, two bits of the respective positions of the two selected parents are now passed through a switching function to produce one output. This is shown in Fig. 3.2. If x and y are switching variables, then the possible switching functions $f(x, y)$ are 0, $x'y'$, $x'y$, x', xy', y', $x'y + xy'$, $x' + y'$, xy, $xy + x'y'$, y, $x' + y$, x, $x + y'$, $x + y$, 1. From the above sixteen functions, 0 and 1 are not used because they correspond to inconsistent functions. For a two variable case, a switching function is selected at random from the above mentioned functions and the two bits are impressed as the input. The corresponding output is stored in the same bit position as one of the parents. Analogously all other bits are generated by selecting the other respective bits from the two parents and passing them through the randomly selected switching function. Hence, a stream of bits between the two crossover points is generated that replaces one of the parents to generate one offspring. The motivation is two fold: (i) it helps to examine the diversity of solutions in solution space, (ii) this model is more plausible from the evolutionistic sense that two parents produce one offspring

at a time. Same GC operator is applied to the same two parents with the two new randomly chosen crossover points and the necessary switching function to produce one more offspring. As a result of this operation two offsprings are produced from the two parents by applying the GC operator twice. This process may be repeated to produce M offspring from N parents in order to maintain the total population of elements constant over generations M is equal to N.

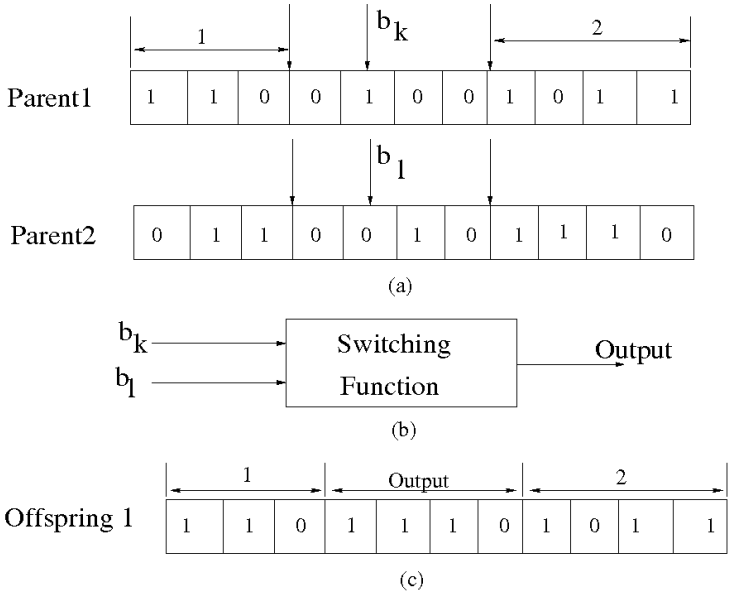

Figure 3.2: Generalized Crossover Operator: (a) Two strings represented parents, (b) switching function, (c) offspring generated by GC operator

GA based clustering Algorithm:

(i) Initialize randomly a population space of size N and their classes are determined.

(ii) Choose two parents randomly for crossover and mutation operation with crossover probability P_c and mutation probability P_m. Compute the fitness of parents and off-springs.

(iii) The offsprings generated compete with the parents based on the concept of tournament selection strategy.

(iv) After selection, the selected elements are put in their respective classes.

(v) Steps (ii), (iii), (iv) are repeated for all elements in the population.

(vi) Step (v) is repeated till the convergence is met i.e. the elements of respective classes are equally fit.

3.3 PGA based class model

The Objective of designing parallel GA [140, 124, 141] is two fold: (i) reducing the computational burden and (ii) improving the quality of the solutions. The design of PGA involves choice of multiple populations where the size of the population must be decided judiciously. These populations may remain isolated or they may communicate exchanging individuals. Parallel Genetic Algorithm (PGA) is usually based on either Coarse Grained model or Fine Grained model [140, 124, 141]. In coarse grained model the population is partitioned into a small number of sub-populations or demes and in fine grained model the population is partitioned into a large number of smaller sub-population or demes. These populations may remain isolated or they may communicate exchanging individuals. The process of communication between individual demes is known as migration. The coarse grained PGA is broadly based on the Island model and Stepping stone model. In an Island model, the population is partitioned into small sub-populations by geographic isolation and individuals can migrate to any other sub-population but in the Stepping stone model migration is restricted to neighbouring sub-populations.

The GA crowding scheme is parallelized using the Coarse grained approach. In Coarse grained approach the interconnection model considered is the Island model shown in Fig. 3.3. In this scheme the population of the size N is divided into a number of sub-populations of fixed size. The crossover and mutation operators are applied in each deme to generate candidate solution. In this regard, the Generalize Crossover (GC) operator proposed by Nanda et. al [139] and as given in section 3.2.3, has been used in our simulation. Tournament selection mechanism is applied to all the demes.In each sub-population, the crowding algorithm is applied and the migration operator is applied intermittently. The frequency of migration is governed by the average fitness of the sub-population. The migration is stopped when the individuals in all demes have grown sufficiently fit. In other words, the migration is stopped when the average fitness is above a pre-specified threshold. A new interconnection model with the notion of self migration is proposed and is shown in Fig 3.5. In this proposed model, besides the interconnection between demes, a self loop has been introduced to take care of intra-deme migration. This is intended to accelerate the convergence and also improves the quality of the solution. We have adopted the good-bad(GB) based migration policy. In our problem we have considered four demes D1, D2, D3 and D4 and the interaction network model is shown in Fig 3.5.

3.3.1 Island model

Island model is an interconnection model used in coarse grained approach [140, 124, 141]. In this approach, the entire population of elements is divided into a number of sub-populations called demes. The demes are interconnected to each other for exchanging individuals.

3.3.2 Island model with inter-deme migration

A typical Island model is shown in Fig. 3.3, where it can be observed that a deme D_{ij} is connected to eight other demes for migration. In each deme the basic GA based crowding scheme is applied and after a few generations individuals of D_{ij} migrates to other demes using a migration policy. For example, in Good-Bad (GB) migration policy, certain percentage of good individuals replace bad individuals of other deme. The process of exchanging the individuals is bi-directional. After migration among different demes, GA based crowding is again applied. Since, before migration, GA based crowding notion can be independently applied. Operation in each deme can be submitted to individual processor. This exchange process together with the rate of migration plays a vital role in determining the solution and the quality of the solution. In this thesis, the network model consists of four demes as shown in Fig. 3.4.

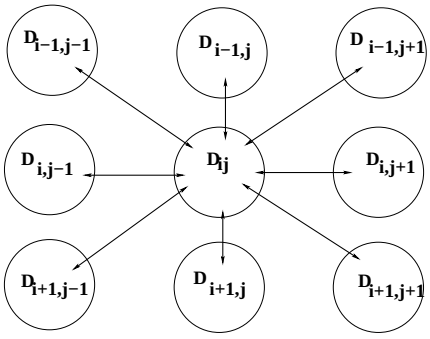

Figure 3.3: Island Model

3.3.3 Island model with intra-deme migration

PGA with Island model is found to converge to the solution much faster than that of the GA based algorithm. In order to further accelerate the rate of convergence, we have introduced the notion of self migration called intra-deme migration. In this migration, the best fit individuals of a deme will replace the worst fit individuals of the same deme. This notion is akin to the notion of reproduction. In this process, depending upon the rate of self migration, the number of best

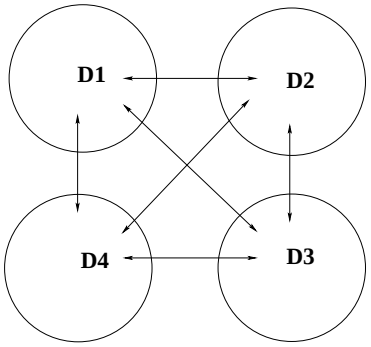

Figure 3.4: Island model with inter-deme migration

fit individuals increases. Thus, together with the inter-deme migration the percentage of good individuals in a deme increases. Therefore the inter-deme migration accelerates the process of convergence.

Fig. 3.5 shows an Island model with four demes and it can be observed from this figure that each deme is connected to every other deme bidirectionally. This is known as inter-deme migration. As observed from Fig. 3.5, besides inter-deme migration a self-loop has been introduced in each deme, making the model a fully connected one. This proposed interconnection model accelerates the convergence.

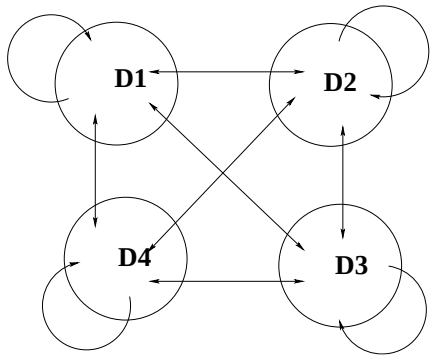

Figure 3.5: Island model with intra-deme migration

3.4 Island model with neighbourhood structure

Our parallelization of crowding scheme is based on the coarse grain approach, where the migration is allowed among all the demes. In other words communication is allowed between a deme and every other deme of the network. This yields appreciable results but the computational burden is horrendous. Hence, we introduced the notion of neighbourhood and thus various network

structure evolves. In the neighbourhood scheme, population elements of a deme need not migrate to all other demes rather migrate to the neighbouring demes. Towards this end, we define the order of the neighbourhood. The closest ones of a deme belong to the first order neighbourhood as shown in Fig. 3.6(a). Similarly, the second and third order neighbourhood structures are shown in Fig. 3.6(b) and (c) respectively. Increase in the order of neighbourhood structure, incorporates more number of demes for the migration. Thus, different network structures are evolved for PGA based clustering. If the order of neighbourhood is increased further, eventually a fully connected network is obtained. Thus, the fully connected network can be viewed as a network of special neighbourhood structure as shown in Fig. 3.6(d). We have studied all the three neighbourhood structure based network together with fully connected network.

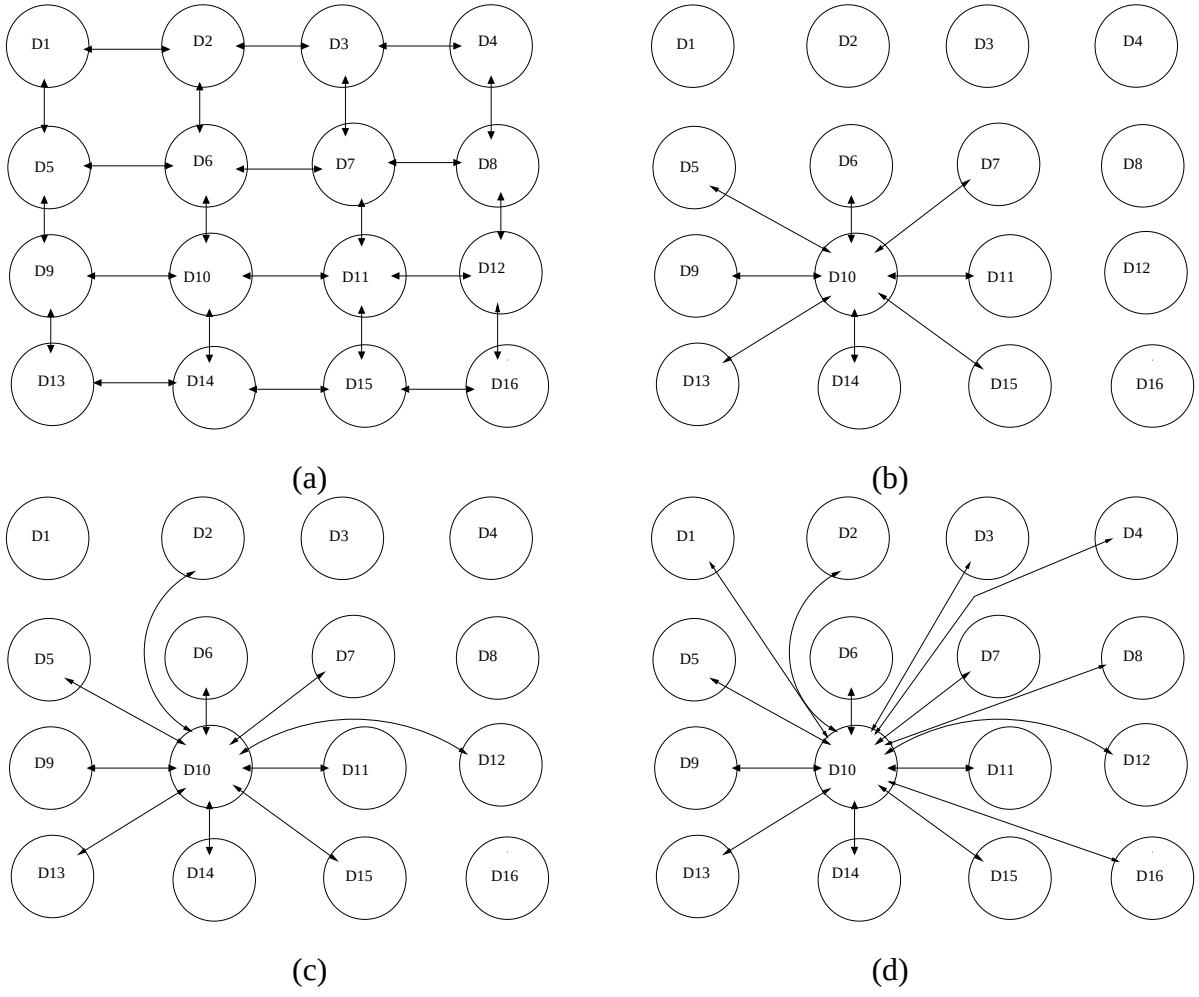

Figure 3.6: Net topology with different order neighbourhood structure(a)1st order, (b) 2nd order, (c) 3rd order, and (d) connected to all

3.4.1 Convergence Analysis

Even though we present simulation results for one migration policy, the convergence analysis is valid for all schemes. In all the type of net structures, there is a finite proportion of good individuals after a certain number of migrations. Thus, the following theorem provides a bound on the proportion of good individuals taking part in migration among the demes.

Theorem 1 *Assume P_{k-1} to be the proportion of good individuals after $(k-1)^{th}$ migration, then for any arbitrary initial condition with P_0, the algorithm converge for*

$$P_{k-1} = (1 - \delta_k)^{\frac{1}{N}}$$

where, $N = s^n$, s=Tournament size of tournament selection method, n=Number of generations between two consecutive migrations and, δ_k = Proportion of good individuals taking part in k^{th} migration.

Proof:

In the whole population of mixed fitness, we assume an element to be a *good* individual if its fitness is above a threshold and *bad* if the fitness is below a threshold. Thus, in the whole population each individual may be either good or bad. Let the individuals be selected to the next generation using tournament selection. In tournament selection a random sample of *s* individuals is selected and out of these *s* participants one best individual is selected. If all the *s* participants are bad and since one individual is to be selected, then the selected individual is a bad individual. Thus a bad individual will survive only if all the *s* individuals are bad. If the initial proportion of good and bad individuals are P_0 and Q_0 respectively, then the proportion of bad individuals in the next generation is:

$$Q_1 = Q_0^s. \tag{3.7}$$

Equation (3.7) implies that $Q_2 = (Q_1)^s = ({Q_0}^s)^s = {Q_0}^{s^2}$. Therefore, at the n_{th} generation, ${Q_n} = {Q_0}^{s^n}$. Let the first migration be allowed after *n* generations. Then the proportion of bad individuals after first migration or in other words after n generations can be expressed as ${Q_{1n}} = {Q_0}^{s^n} - \delta_1$; where δ_1 = proportion of bad individuals replaced by good migrated individuals after first migration. It can be shown that the proportion of bad individuals after k^{th} migration or kn generations.

$$Q_{kn} = Q_{k-1}^{s^n} - \delta_k; \tag{3.8}$$

where $\delta_k =$ proportion of bad individuals replaced by good migrated individuals by k^{th} migration. Since there are only two types of individuals i.e. good and bad, the sum of proportion of good and bad individuals is always unity. The algorithm will converge to the desired solution when all individuals are good individuals or the proportion of good individuals P_{kn} is unity. This implies that the proportion of bad individuals is zero. Thus for convergence $Q_{kn} = 0$. Since, δ_k is the proportion of good individuals taking part in k^{th} generation,

$$\delta_k \geq 0 \tag{3.9}$$

Substituting (3.9) in (3.8),we have

$$Q_{kn} \leq Q_{k-1}^{s^n} \tag{3.10}$$

Since Q_{k-1} is a proportion, from (3.10) it is evident that the population of bad individuals has a monotonically decreasing trend. This implies that the population of good individuals will have an increasing trend. From (3.8), we have $Q_{k-1}^{s^n} = \delta_k$. This implies that $P_{k-1}^{s^n} = 1 - \delta_k$ or $P_{k-1} = (1 - \delta_k)^{\frac{1}{N}}$. Hence, proved. The theorem provides a bound on the proportion of good individuals taking part in migration among the demes to achieve convergence.

PGA based clustering algorithm:

1 Initialize randomly population elements of size N.

2 Divide the population space into fixed number of sub-populations and determine the class of individual in each sub-population.

3 Select a sub-population (deme) and go through the following steps:

3.1 In the given sub-population (deme), choose two elements at random for Generalized Crossover (GC) and mutation operation.

3.2 Evaluate fitness of each parents and offspring.

3.3 The tournament selection mechanism is applied to select two individuals among the two parents and offspring to be parents for the next generation.

3.4 Repeat steps 3.1, 3.2, and 3.3 for all the elements in the sub-population (deme).

3.5 Repeat steps 3.1, 3.2, 3.3 and 3.4 for a fixed number of generation.

4 Step (3) is repeated for each sub-population (deme).

5 Migration is allowed from each sub-population (deme) to every other sub-population (deme). The individuals are migrated based on the selected migration policy. Number of elements to migrate are determined from the selected rate of migration. The elements migrate with migration probability P_{mig}. At last some percentage of individuals of one deme replace the same percentage of individuals of the same deme based on the selected migration policy. This self migration is valid for all demes with a probability of migration P_{mig}.

6 Repeat steps 3, 4, and 5 till convergence is achieved. (The inter-deme migration and intra-deme migration is continued till convergence is achieved.)

3.5 Results and discussions

We have considered two, four and eight class models in simulation

3.5.1 Clustering for two classes

Non-decaying functions

The functions given in (3.1) and (3.2) have been considered to test the schemes for a two class model. Both the functions produce two classes but different types of functions as seen from Fig. 3.1(a) and 3.1(b). The first one given by (3.1) produced two class model with peaks occurring at same functional value where as (3.2) produced a function with peaks occurring at different functional values. These two functions are shown in Fig. 3.7 and Fig 3.9 respectively.

In order to implement the GA and PGA based clustering, the fitness function considered is same as the function of two class model that is $fit(x) = f(x)$ of (3.1) and (3.2). Thus, the problem reduces to determining all the niches of the fitness function. The corresponding function is shown in Fig 3.7 (a) where the two niches/peaks corresponding to two different classes need to be determined. Fig. 3.7(a) shows the initial distribution of population in the functional landscape. It can be seen that the whole population is distributed over the fitness landscape. GA based clustering algorithm has been applied to determine the peaks. The parameters chosen for GA are; population size N=400, crossover probability $P_c = 0.8$ and mutation probability $P_m = 0.001$.

With progress in generation, the population elements of respective classes are pulled up to form clusters at the two niches. This effect is observed in Fig. 3.7(b) which is obtained after 200 generations. As observed from Fig. 3.7(b), the fitness values of the population elements of respective classes have been enhanced and hence it appears that they are pulled up towards the respective niches. At 200 generations, out of 400 number of elements, 183 elements have clustered at the first niche that corresponds to class 'A' and 161 elements clustered at the second niche i.e. class 'B'. As seen from Fig. 3.7(b) 192 elements are distributed over class A and 208 elements are distributed over class 'B'. Eventually, all these elements have been pulled up to form clusters at the two niches. As seen from Fig. 3.7(c) after 2000 generations, 192 nos of elements clustered at the 1st niche corresponding to class 'A' and 208 nos of elements clustered in the 2nd niche corresponding to class B. These sub-populations have been found to be stable at the respective niches even after 6000 generations. This implies that the GA based crowding scheme could successfully maintain sub-populations at different niches thus detecting the two classes. The rate of convergence is shown in Fig. 3.7(d), where it may be seen that the algorithm converges to form the clusters after 2000 generations. As observed from Fig. 3.7(d) GA based clustering takes large number of generations to converge and hence a computationally intensive algorithm. In order to reduce computational burden, PGA based clustering algorithm has been proposed. PGA based algorithm, when applied to the two class problem, yields results as shown in Fig. 3.8. The parameters used in the PGA algorithm are; population size N=400, crossover probability $P_c = 0.8$, mutation probability $P_m = 0.001$, number of demes = 4, migration rate $R_{mig} = 8\%$, self migration rate $R_{smig} = 4\%$, probability of migration $P_{mig} = 0.1$ and probability of self-migration $P_{smig} = 0.1$.

The PGA interconnection model considered is shown in Fig. 3.6(a) and this model is the first order neighbourhood structure with inter-deme migration only. Two point crossover operator has been used in PGA algorithm. Fig. 3.8(a) shows the initial distribution of the population elements. Fig. 3.8(b) shows the distribution of population over the class distributions after 10 generation. As observed from Fig. 3.8(b), most of the population elements have been pulled up towards the niche of the class distributions and hence all the population elements are above fitness value of 0.6. The population of elements have clustered at two niches/peaks after 100 generations in case of Parallel Genetic algorithm. The rate of convergence is shown in Fig. 3.8(d) where it is observed that after 40 generations the average fitness values is close to unity thus implying that the algorithm has converged to the desired solutions. Thus, the PGA is almost

20 times faster than that of GA. Thus the PGA based algorithm could successfully maintain sub-populations at the respective niches of the distribution and therefore the two different classes could be determined.

Decaying functions

We have also considered two class models where the area of each class in the fitness landscape has unequal and hence the peaks corresponding to classes are at different fitness values. Equation (3.2) corresponds to such a case and the fitness function is shown in Fig. 3.9(a). There are two classes: (i) peak of one class occurs at the functional value of 0.85, and (ii) the peak of the second class occurs at around 0.34. In this case, application of basic GA would have converged to the highest niche i.e. 0.85. In the view point of nonlinear multi-modal functions, the small peak corresponds to the local solution and the large peak corresponds to the global optimal solution. In the clustering approach, all the peaks must be determined. Fig 3.9(a) shows the initial distribution of population elements where 36 population elements converged at peak A and 9 population elements converged at class B. As generation progresses, the population elements are pulled up and after 500 generations, 183 elements converged at peak A and 58 elements converged at peak B. This effect is shown in Fig. 3.9(b). After 3000 generations, 292 elements converged at peak A and 108 elements converged at peak B. Thus two stable sub-populations could be maintained at the two peaks and hence two classes could be determined as shown in Fig. 3.9(c). The rate of convergence is shown in Fig. 3.9(d) where it may be observed that the two classes converged at two different fitness values. However it can be observed that GA converges after 3000 generations. In order to accelerate the rate of convergence, PGA based algorithm has been used and the results are shown in Fig. 3.10. Fig. 3.10(a) shows the initial distribution and as seen from Fig. 3.10(b), after 20 generations, most of the population elements have been pulled up towards the respective niches. The parameters of PGA is same as that of the case of non-decaying sinusoidal function. In Fig. 3.10(b), 170 population elements have converged at peak A and 65 elements have clustered at B. All the population elements converged at the respective peaks after 100 generations thus identifying the clusters. Fig 3.10(e) shows the final converged stable sub-populations. The rate of convergence is shown in Fig. 3.10(d). Thus the two classes could be identified properly.

3.5.2 Clustering for four classes

Non-decaying functions

The functions in equation (3.3) and (3.4) have been considered for validating the proposed approaches for four class model. The functions given by (3.3) and (3.4) produce four class models with peaks occurring at same fitness value and different fitness values respectively. One corresponds to four niches occurring at same fitness value and the other one is a decaying sinusoidal function where peaks occur at different functional values.

Fig. 3.11(a) shows the functional landscape of four class model with four distinct peaks corresponding to four classes. The initial distribution of population elements have been presented in Fig. 3.11(a). The parameters chosen for GA based clustering algorithm are, population size N=400, crossover probability $P_c = 0.8$ and mutation probability $P_m = 0.001$. It may be seen from Fig. 3.11(b) that after 500 generations, most of the population elements have been pulled up to the different niches and have formed clusters. This is also reflected from the number of population elements those have clustered around class-A, B, C and D. The population elements are A=89, B=70, C=91 and D=60 which indicate that they are close to forming clusters. The converged population of elements after 4000 generations as shown in Fig. 3.11(c), where it can be seen that stable population could be maintained at four different niches thus detecting four classes of the four class model. The rate of convergence is shown in Fig. 3.11(d) and it is seen that the algorithm converges after 1000 generations and remains stable even after 4000 generations. Since GA based crowding is found to be computationally intensive, PGA based crowding algorithm is also applied.

Fig 3.12(a) shows the initial distribution of population of elements and after 10 generations the distribution is shown in Fig. 3.12(b). It may be observed that most of the population elements in the respective classes have been pulled up to form clusters around the respective peaks. It is found that the algorithm converged after 20 generations as seen from Fig. 3.12(d) and the stable population elements formed the clusters around each peak thus detecting four peaks. The rate of convergence is much faster than that of GA and as observed from Fig. 3.12(d), where the average fitness is close to unity after 10 generations and converges after 20 generations which is 20 times faster than that of convergence of GA shown in Fig. 3.12(d). Thus the PGA based clustering algorithm could detect eight peaks within 20 generations.

Decaying function

Fig. 3.13(a) shows the function for four class model where each class has different area and hence the peaks occur at different values. Since it is a decaying sinusoidal function, the first mode occurs at a fitness value of unity and the subsequent modes occur at fitness value with decreasing order. As seen from Fig. 3.13(b) with progress in generation, the population elements have been pulled up and finally after 800 generations the population elements clustered at four different classes. This is shown in Fig. 3.13(c) and the rate of convergence is shown in Fig. 3.13(d) where it may be seen that the population of elements converged to four different fitness values. The parameters used for GA and PGA are same as the non-decaying case. Fig. 3.14(a) shows the initial distribution of elements for PGA based class model and with progress in generation the population elements are pulled up towards the cluster and after 80 generations the population elements converged to the respective peaks identifying respective classes. Thus with peaks at different hights, stable sub-populations could be identified. As observed from Fig. 3.14(d), the algorithm converged around 20 generations which is around 40 times faster than that of using GA.

3.5.3 Clustering for eight classes

Non-decaying functions

Eight class models as given by (3.5) and (3.6) have also been considered in simulation. First, we consider a nonlinear multi-modal function given in (3.5) where there are eight classes and hence there are eight corresponding peaks. The function is shown in Fig 3.1(e), where it is seen that there are eight peaks occurring at same functional value. We have applied GA and PGA based crowding to determine the eight peaks and hence eight classes. The parameters for GA and PGA are same as two class and four class models. In PGA based scheme the number of demes considered is 4 with both intra-deme and inter-deme migration.

Analogous to previous cases, the fitness function is same as the function itself that is $f(x)$ as in (3.5) and (3.6) respectively. The initial distribution of 400 population elements is shown in Fig. 3.15(a) and after 400 generations the distribution is shown in Fig. 3.15(b), the population element in the respective classes have been pulled up towards the respective niches. Fig. 3.15(c) shows that stable sub-population have been clustered around eight different peaks thus detecting eight classes. As observed from Fig. 3.15(d) the algorithm converged after 600

generations but the sub-populations at respective peaks remained stable even after 1000 generations. Thus the same network model with four demes could detect eight peaks corresponding to eight classes. Since GA based crowding is found to be computationally intensive, PGA based crowding algorithm is also applied.

Fig 3.16(a) shows the initial distribution of population of elements and after 10 generations the distribution is shown in Fig. 3.16(b). It may be observed that most of the population elements in the respective classes have been pulled up to form clusters around the respective peaks. It is found that the algorithm converged after 20 generations as seen from Fig. 3.16(d) and the stable population elements formed the clusters around each peak thus detecting eight peaks as shown in Fig. 3.16(c). The rate of convergence is much faster than that of GA and as observed from Fig. 16(d) the average fitness is close to unity after 10 generations and converges after 20 generations which is 20 times faster than that of convergence of GA shown in Fig. 3.16(d). Thus the PGA based clustering algorithm could detect eight peaks within 20 generations.

Decaying function

Eight class model with uneven distribution of classes have also been studied. Fig 3.17(a) correspond to (3.6) of a decaying sinusoids. As observed from Fig. 3.17(a) that there are eight different peaks occurring at different values of the fitness landscape. Fig. 3.17(a) shows the initial distribution of the population elements. Fig. 3.17(b) shows the intermediate distribution of elements after 500 generations and it is observed that the most of the elements have clustered around different peaks. Fig. 3.17(c) shows that stable populations have been maintained after 4000 generations. The rate of convergence is shown in Fig. 3.17(d), where it may be seen that the algorithm converged to eight different peaks, thus successfully identifying eight different classes. The parameters are same as that of the non-decaying cases. The rate of convergence has been accelerated using PGA algorithm. The parameters used in this case are same as that of non-decaying case. Fig. 3.18(a) shows the initial distribution and intermediate distribution after 20 generations is shown in Fig. 3.18(b). It may be seen from Fig. 3.18(b) that most of the population elements have clustered around the respective peaks and after 40 generations the population elements converged at the respective peaks. The rate of convergence is shown in Fig. 3.18(d) and this is 20 times faster than that of GA. PGA based algorithm could maintain stable sub-population at different niches and hence eight different classes could be detected.

3.5.4 Effect of parameters of PGA

PGA based scheme has several parameters and the parameters do influence significantly the rate of convergence. The effect of parameters such as, migration policy, rate of migration, topology of the interconnection model, and crossover operation on the convergence of the algorithm has been investigated. In the following we discuss the effect of individual parameters on the issue of convergence.

Migration policy

There are four migration policies namely Good-Bad (GB), Good-Random (GR), Random-Bad (RB) and Random-Random (RR) migration policies. The effects of different policies on the rate of convergence has been analysed for a four class model problem. Fig. 3.19(a) shows the rate of convergence for a four class model. As seen from Fig. 3.19(a) the PGA algorithm using GB migration policy converges after 20 generations while RB policy closely follows the GB policy. Use of GR migration policy makes the algorithm to converge after 200 generations. As observed from Fig. 3.19(b), the PGA with RR migration policy converges after 2000 generations. Fig. 3.19(a), shows that PGA with GB migration policy converges at around 20 generations but after 10 generations the algorithm is very close to convergence.

Similar observations have also been made for four class decaying functions. Convergence of different classes with different migration policies are shown in Fig. 3.20. Since this corresponds to decaying sinusoidal four class model, the population elements in different classes converge at different fitness values as shown in Fig 3.20(a), (b), (c) and (d). Fig. 3.20(a) shows the convergence for class A and it is observed that GB policy converges fastest among all the four policies. PGA with RB policy follows GB policy and algorithm with GB policy converges around 10 generations, while RB policy converges around 15 generations. GR and RR policies converge after 200 generations. Similar observations have also been made in case of other three classes except in case of class B, the algorithm for RR policy converges around 350 generations.

The effects of different policies on the rate of convergence has been analysed for a eight class model problem. Fig. 3.21(a) and (b) shows the rate of convergence for a eight class model. As seen from Fig. 3.21(a) the PGA algorithm using GB migration policy converges after 20 generations while RB policy closely follows the GB policy. Use of GR migration policy makes the algorithm to converge after 80 generations. As observed from Fig. 3.21(b), the PGA with

RR migration policy converges after 1000 generations. Fig. 3.21(a) shows that PGA with GB migration policy converges at around 20 generations but after 10 generations the algorithm is very close to convergence. Thus, it has been observed that the proposed PGA algorithm with GB migration policies converges fast among all other policies. Therefore, we have considered GB policy throughout the thesis.

Rate of migration

The effect of rate of migration on the solution has also been studied. This effect has been investigated for four class problem. Fig. 3.22 show the rate of convergence at different rates of migration with different migration policies. Fig. 3.22(a) shows the convergence of PGA with GB migration policy. Here, migration rates are varied from 8% to 80% and 8% migration means eight percentage good individual of one deme replaces 8% bad individuals of another deme. As observed from Fig. 3.22(a), with increase in the rate of migration from 8% to 28% the rate of convergence increases i.e. the average fitness increases from 0.91 to 0.97. Further increase in the rate of migrations that is with 40% and 60% the rate of convergence increases but deteriorates with further increase in rate of migration. Hence, with 80% of migration rate, the rate of convergence slows down. This is also intuitively expected because the high rate of migration not only migrate the good but also the low fit individuals to other deme. This makes the overall process slow. Similar observations are also made for GR and RB migration policies. This effect can be observed from Fig. 3.22(b) and 3.22(c). Specifically for GR migration policy of Fig. 3.22(b) with increase in rate of migration the enhancement in the rate of convergence is appreciable. For RR migration policy increase in the rate of migration hardly produce any effect on the rate of convergence. This can be observed from Fig. 3.22(d).

Neighbourhood

The effect of network topology on the rate of convergence has also been investigated. The net topology with different orders are shown in Fig. 3.6. Fig. 3.6(a) shows a topology with 16 demes and each deme is interconnected with its 1st order neighbours. For example, deme D_6 is connected to D_2, D_5, D_{10}, and D_7, the first order neighbours. Similarly, Fig. 3.6(b) indicates that the migration takes place among the 2nd order neighbours i.e eight demes. Analogously, the third order neighbourhood based net topology is shown in Fig. 3.6(c) and the all connected net topology is shown in Fig 3.6(d). Migration takes place among the connected demes in a net

topology.

The effect of network topology on the rate of convergence has been studied. We have introduced the notion of intra-deme migration besides the inter-deme migration. This topology is shown in Fig. 3.5, where the intra-deme migration is achieved by introducing a self-loop in each deme. Fig 3.23(a) shows the rate of convergence without self loop structure and with different network topologies. As seen from Fig 3.23(a), the all connected network converges fastest among all the topologies. The all connected network converges at around 10 generations while the 1st, 2nd and 3rd order convergesd at 40 generations. The rate of convergence up to 0.9 fitness value remains almost same and thereafter 3rd order converged faster than that of 1st and 2nd order neighbourhood based topology. This effect has changed with the self loop model and the rate of convergence is shown in Fig. 3.23(b) that with self loop structure, the rate of convergence increased and the all connected structure converges around 10 generations while the rest structures converge at around 30 generations. Fig. 3.23(a) and 3.23(b) are achieved with a 16% migration rate. With increase in the neighbourhood structure the number of demes participating in migration increases and hence will computationally be more expensive. There is marginal improvement by switching from 1st order neighbourhood structure to all connected network. Similar observations are also made with increase in the rate of migration from 16% to26%. It may be observed from Fig. 3.23(c) and 3.23(d) that with self loop the all connected network has marginal improvement over the 1st order neighbourhood structure. Since all connected network incurs more computational burden with marginal improvement on the rate of convergence, we have adhered to the 1st order neighbourhood structure all through our thesis work.

Network model

In PGA models, the interconnection structure takes care of only the inter-deme migration. We have introduced a notion of intra deme migration and hence the effect of self-loop has been investigated. Fig. 3.24(a), (b), and (c) show results with two point crossover (TPC) and with different migration policies. It is evident from the above three figures that the self-loop based model enhanced the convergence to some extent even though not radical. Similar observations have also been made with Generalized Crossover operation. The rate of convergence has been enhanced with self loop structure as opposed to without self loop structure. Similar observations have also been made for the use of generalized crossover operator with the proposed

interconnection model. As seen from Fig 3.25(a), GB migration policy with self-loop based interconnection model converges faster than that of without self-loop model. Similar observations are also made for the RB migration policy as shown in Fig. 3.25(b). But in case of GR migration policy, as evident from Fig. 3.25(c), that introduction of intra-deme migration did not improve and the rate of convergence remained same for both the models.

Crossover operator

We have employed two crossover operators namely GC and TPC and the performance of the two operators have been compared for two, four and eight class models. Fig. 3.26 (a) shows the rate of convergence for TPC and GC operator, and it may be observed that although the initial rate of rise remains same, after 0.88 fitness, GC operator based algorithm rises faster than that of TPC operator. The algorithm with GC converges to the final solution faster than that of TPC operator. In case of 4 class problem, even the initial rate of rise with GC operator is faster than that of using TPC operator. This effect can be observed from Fig. 3.26(b). As seen from Fig 3.26(c), for eight class model, GC operator based algorithm converges faster than that of TPC operator. This GC operator in all the cases outperformed the TPC operator.

We have compared the performance of crossover operation on the rate of convergence. The performance of GC and TPC have been compared with self-loop interconnection structure and different migration policies. Fig. 3.27 shows the results with different migration policies. Considering Fig. 3.27(a), it may be observed that use of GC operator enhances the rate of convergence as compared to that of TPC operator and also GC based system converged earlier than that of TPC based system. This observation is made with the Good-Bad (GB) migration policy. Similar observations are also made with migration policies as shown in Fig. 3.27(b) and 3.27(c). Hence, it is inferred that GC-GB-SL based scheme outperforms all other schemes.

3.6 Conclusions

In this chapter we have developed the PGA based class models and compared the performance with GA based class models. Two, four and eight class models have been studied and specifically the sinusoidal functions have been considered as the multi-modal nonlinear functions. Both decaying and non-decaying sinusoidal functions have been considered and it has been found out that GA based crowding and the PGA based crowding could successfully maintain

stable sub-populations at each cluster and thus could identify different classes. The notion of intra-deme has been introduced to develop a fully connected network model. This fully connected network model is found to enhance the rate of convergence. Besides the effect of neighbourhood structure, migration policy, migration rate and crossover operation on the rate of convergence has been investigated and it has been found that judicious choice of the parameters significantly influence the rate of convergence.

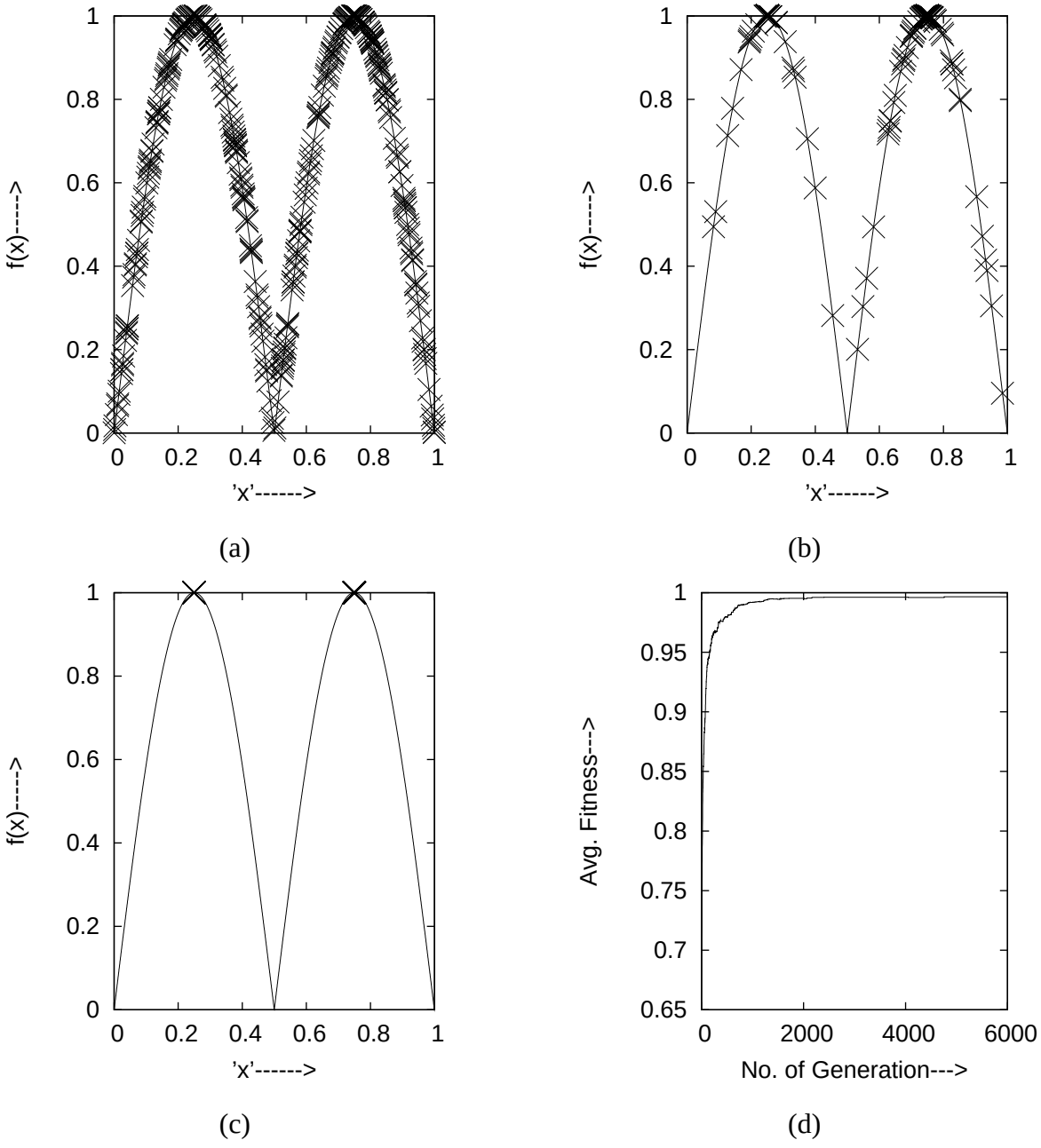

Figure 3.7: GA based Crowding for 2-class: (a) Initial distribution (Class: A=28/192, B=41/208), (b) Distribution after 200 gen. (Class: A= 183/192, B=161/208), (c) Final distribution after 6000 gen.(Class: A=192/192, B=208/208), (d) Convergence rate

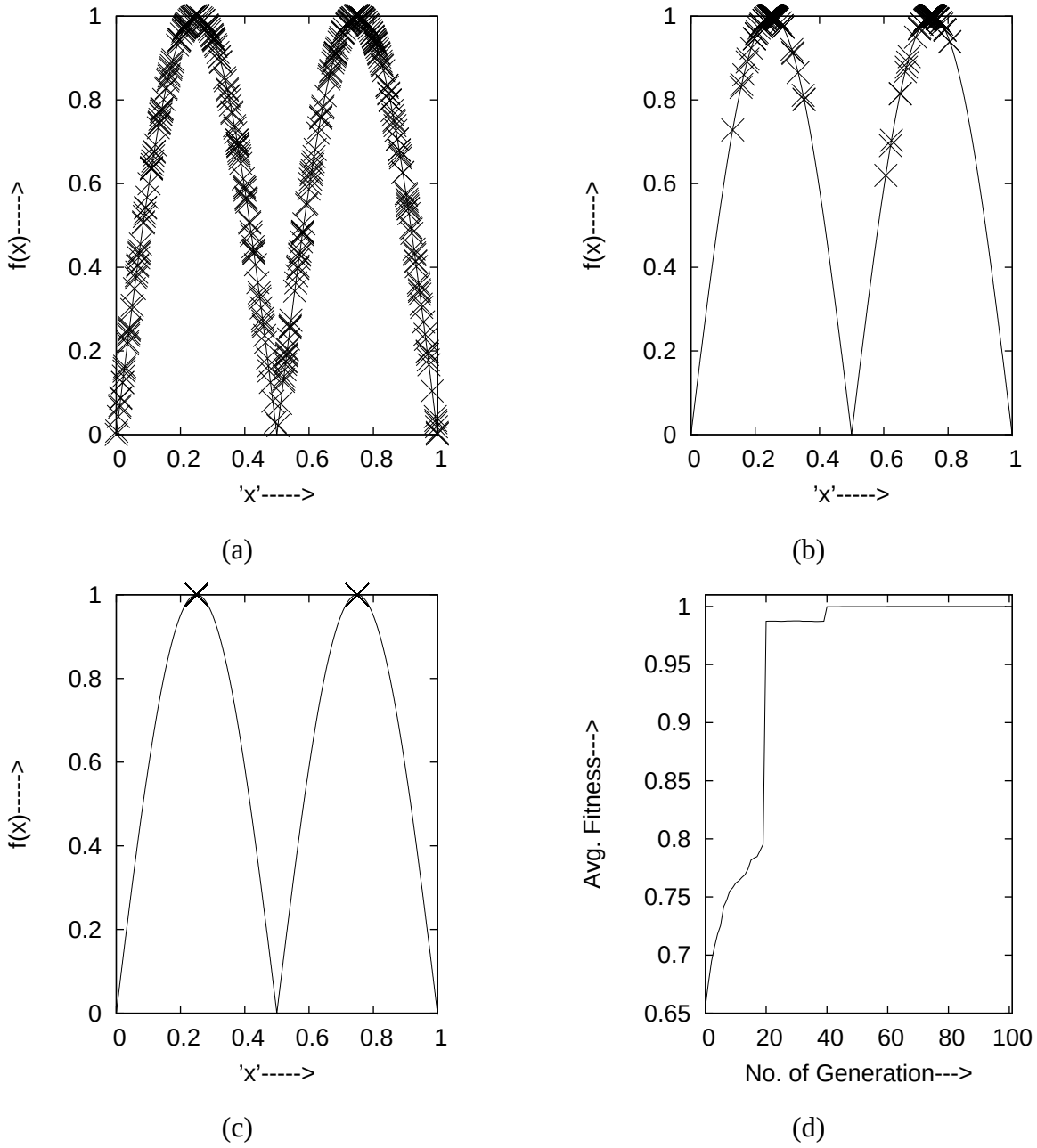

Figure 3.8: PGA based Crowding for 2-class: (a) Initial distribution (Class: A=22/207, B=25/193),(b) Distribution after 10 gen. (Class: A=100/207, B=120/193), (c) Final distribution after 100 gen.(Class: A=207/207, B=193/193), (d) Convergence rate with GB migration policy

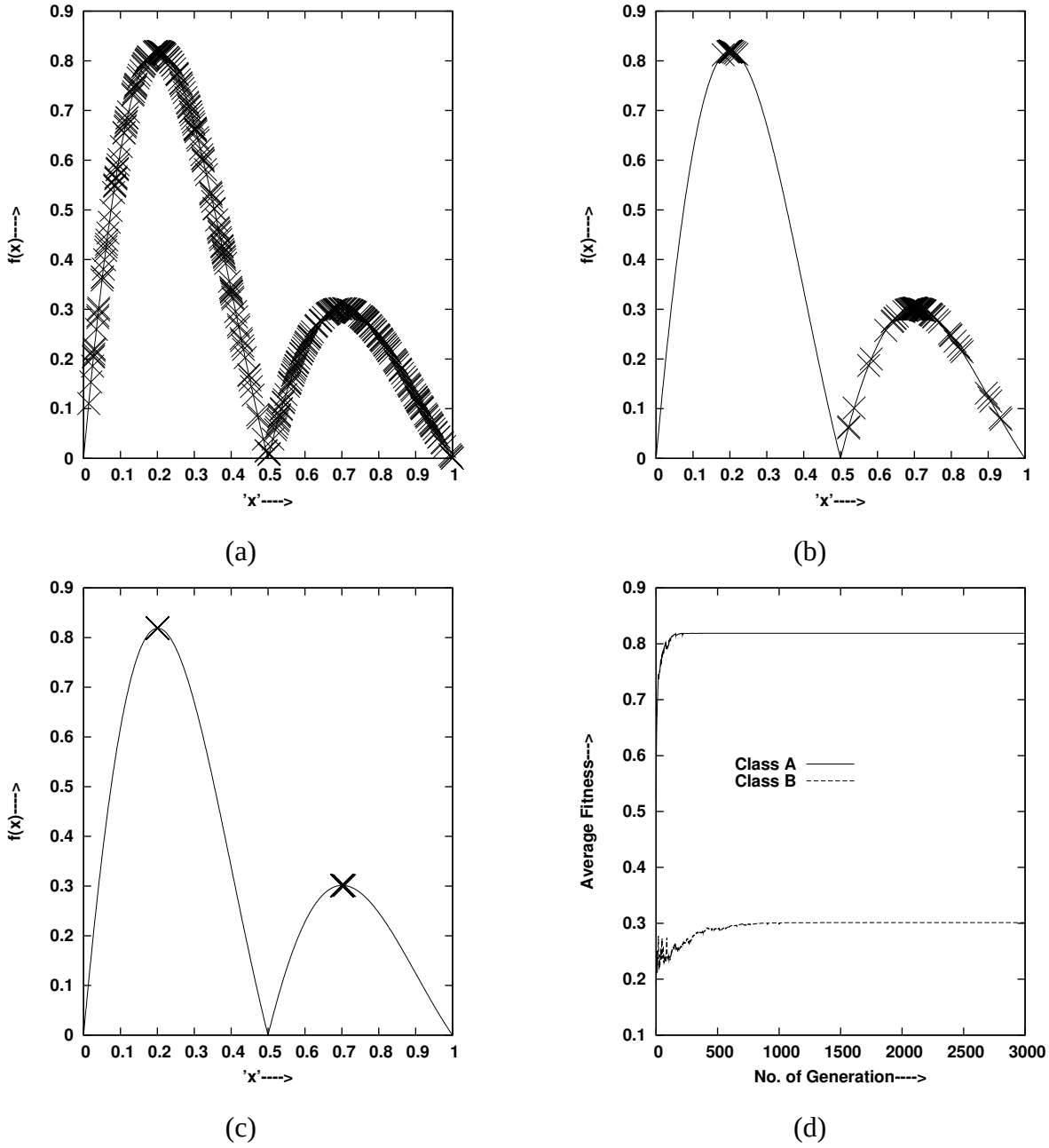

Figure 3.9: GA based Crowding for 2-class decaying function: (a) Initial distribution (Class: A=36/292, B=9/108), (b) Distribution after 500 gen. (Class: A=183/292, B=58/108), (c) Final distribution after 3000 gen.(Class: A=292/292, B=108/108), (d) Convergence rate

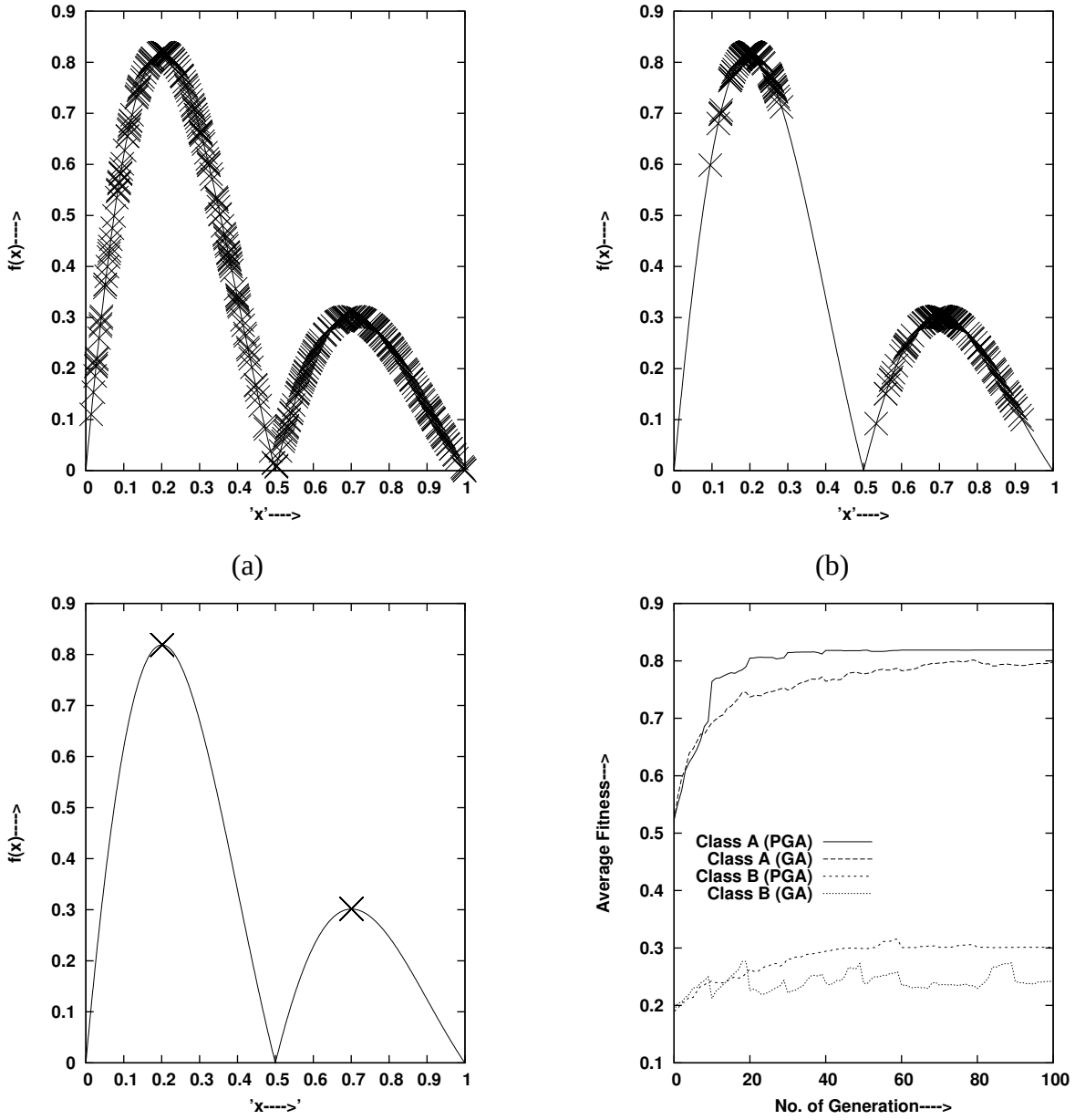

Figure 3.10: PGA based Crowding for 2-class decaying function: (a) Initial distribution (Class: A=28/266, B=41/134), (b) Distribution after 20 gen. (Class: A=170/266, B=65/134), (c) Final distribution after 100 gen. (Class: A=266/266, B=134/134), (d) Convergence rate with GB migration policy

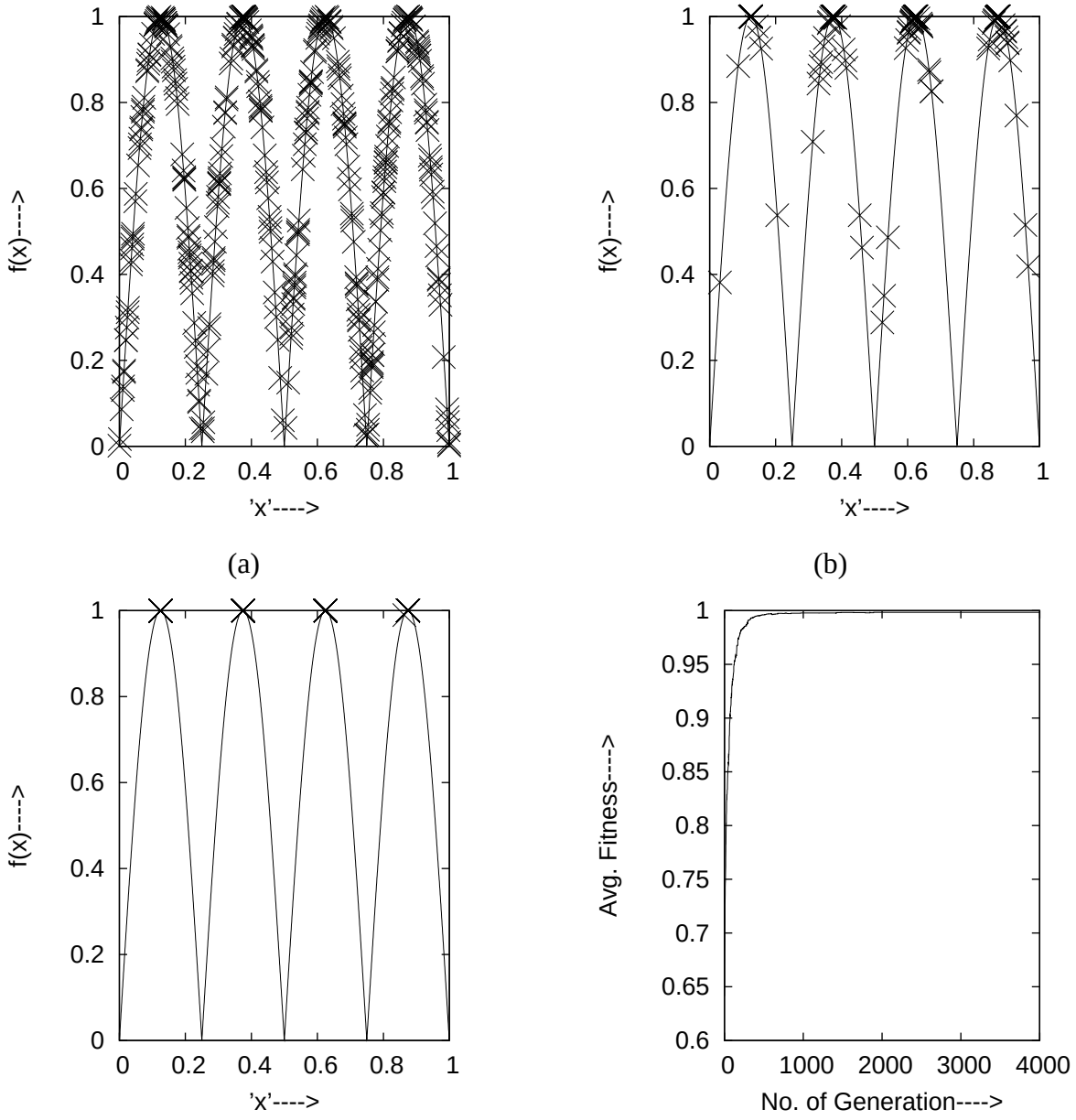

Figure 3.11: GA based Crowding for 4-class: (a) Initial distribution (Class: A=17/98, B=12/88, C=23/122, D=16/92), (b) Distribution after 500 gen. (Class: A=89/98, B=70/88, C=91/122, D=60/92), (c) Final distribution after 4000 gen.(Class: A=98/98, B=88/88, C=122/122, D=92/92), (d) Convergence rate

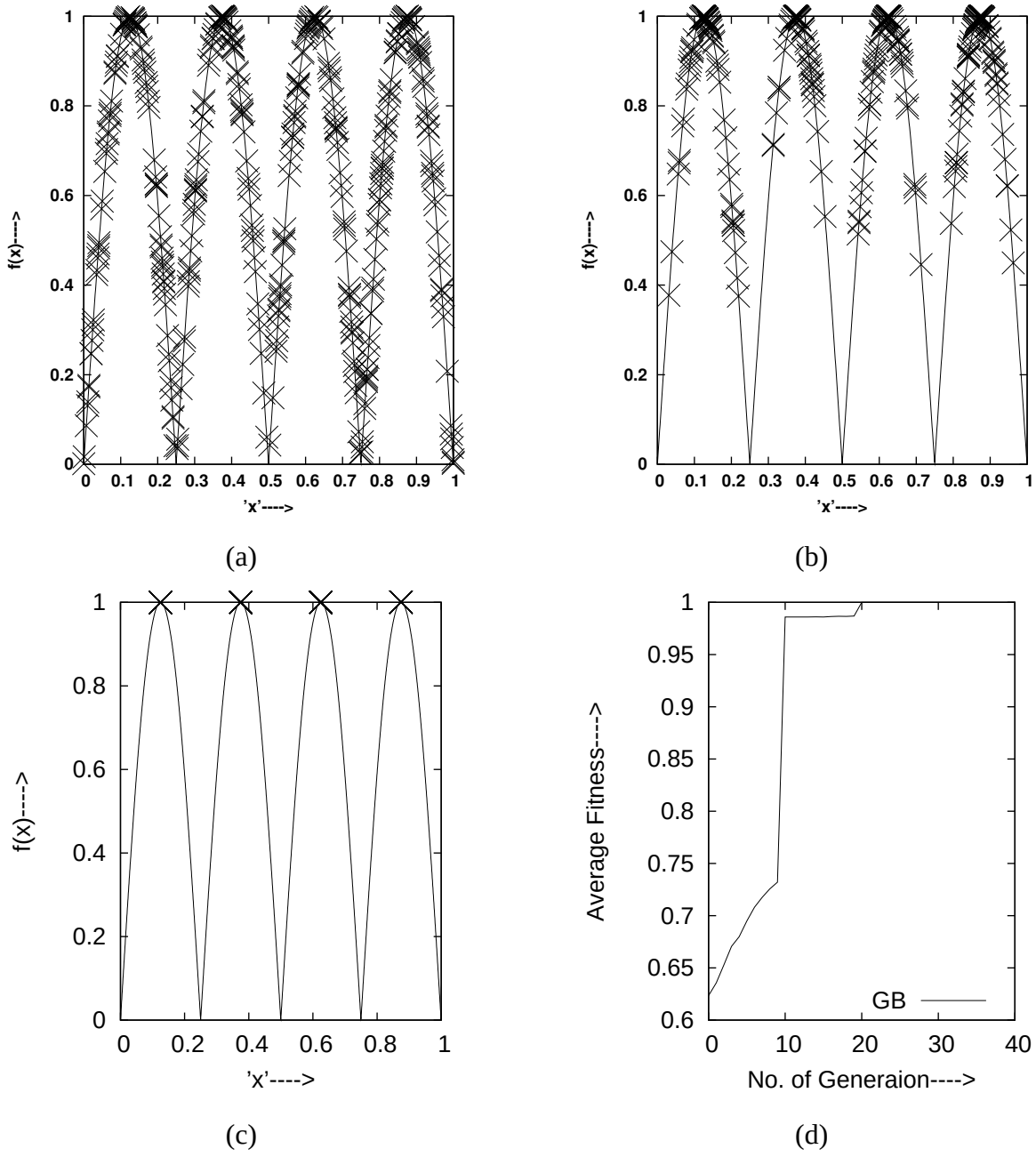

Figure 3.12: PGA based Crowding for 4-class: (a) Initial distribution (Class: A=12/103, B=19/91, C=15/97, D=16/109), (b) Distribution after 10 gen. (Class: A=56/103, B=58/91, C=51/97, D=54/109), (c) Final distribution after 40 gen.(Class: A=103/103, B=91/91, C=97/97, D=109/109), (d) Convergence rate with GB migration policy

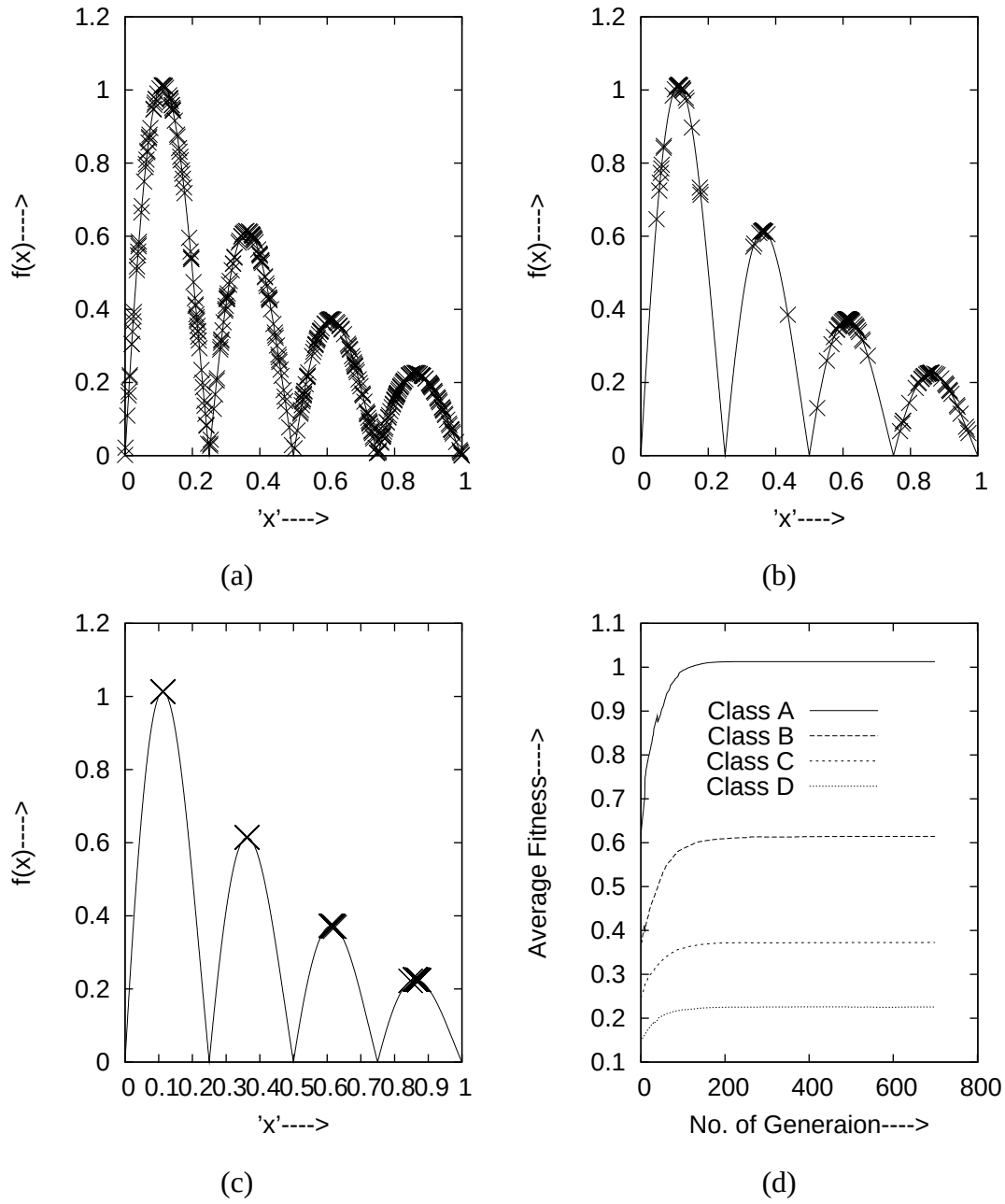

Figure 3.13: GA based Crowding for 4-class decaying function: (a) Initial distribution (Class: A=12/147, B=17/97, C=14/113, D=14/43), (b) Distribution after 100 gen. (Class: A=132/147, B=94/97, C=94/113, D=15/43), (c) Final distribution after 800 gen.(Class: A=147/147, B=97/97, C=113/113, D=43/43), (d) Convergence rate

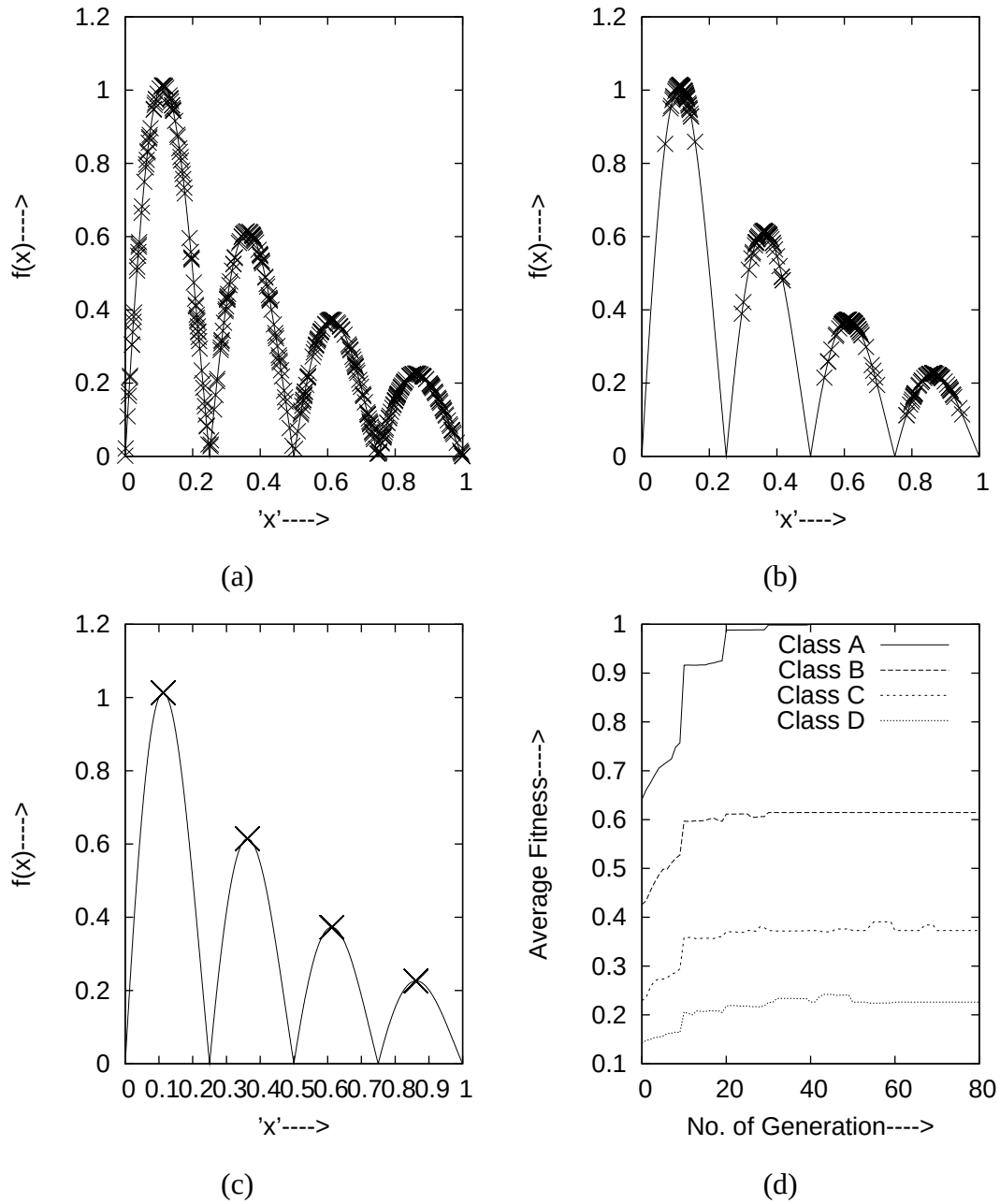

Figure 3.14: PGA based Crowding for 4-class decaying function: (a) Initial distribution (Class: A=10/104, B=13/94, C=14/100, D=12/102), (b) Distribution after 20 gen. (Class: A=79/104, B=67/94, C=75/100, D=56/102), (c) Final distribution after 80 gen.(Class: A=104/104, B=94/94, C=100/100, D=102/102), (d) Convergence rate

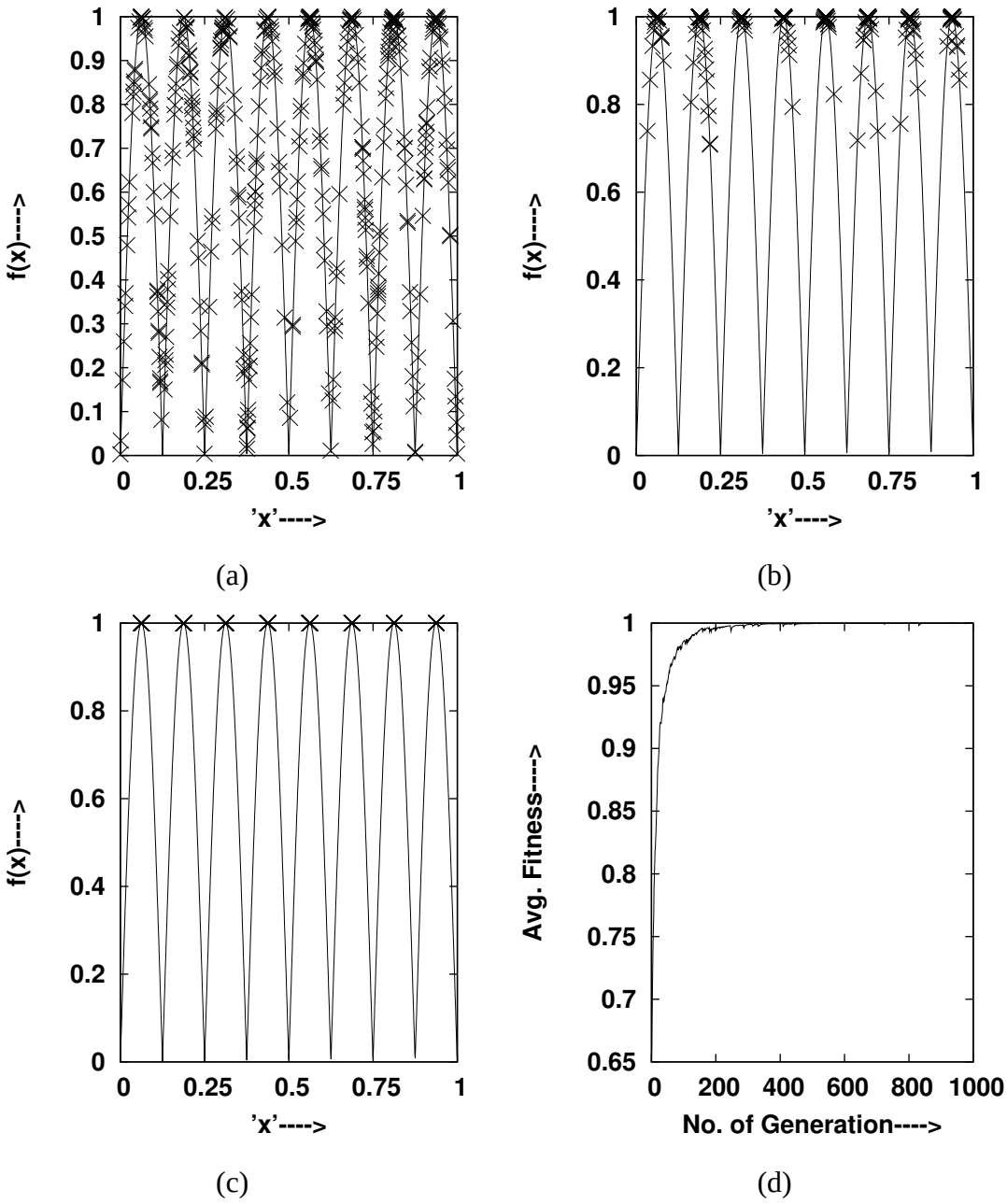

Figure 3.15: GA based Crowding for 8-class: (a) Initial distribution (Class: A=6/139, B=2/49, C=4/14, D=1/55, E=3/16, F=10/17, G=10/59, H=4/51), (b) Distribution after 400 gen. (Class: A=54/139, B=30/49, C=12/14, D=38/55, E=14/16, F=12/17, G=47/59, H=42/51), (c) Final distribution after 1000 gen. (Class: A=139/139, B=49/49, C=14/14, D=55/55, E=16/16, F=17/17, G=59/59, H=51/51), (d) Convergence rate.

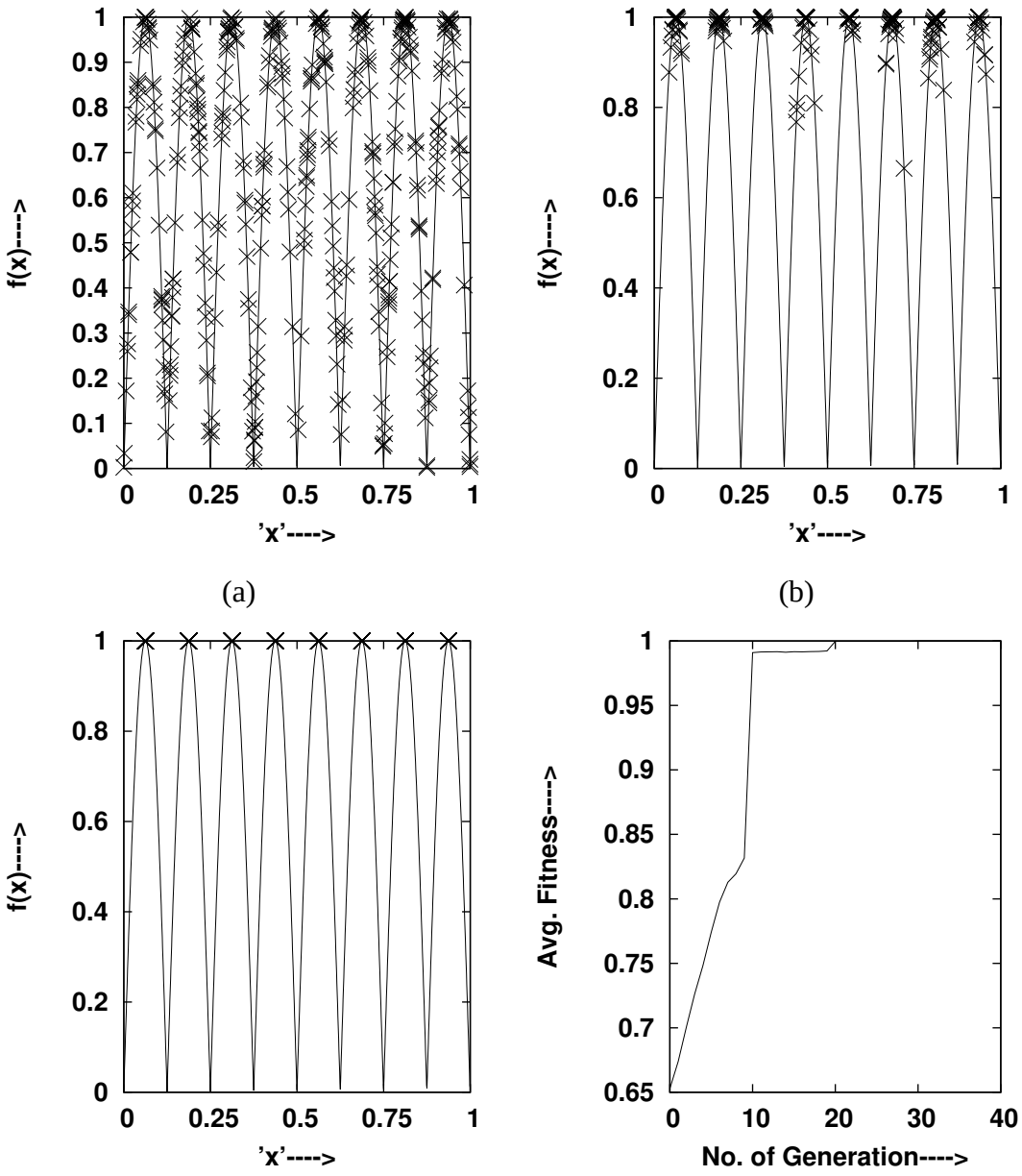

Figure 3.16: PGA based Crowding for 8-class: (a) Initial distribution (Class: A=6/139, B=2/49, C=4/14, D=1/55, E=3/16, F=10/17, G=10/59, H=4/51), (b) Distribution after 10 gen. (Class: A=112/139, B=46/49, C=13/14, D=34/55, E=13/16, F=11/17, G=45/59, H=46/51), (c) Final distribution after 40 gen. (Class: A=139/139, B=49/49, C=14/14, D=55/55, E=16/16, F=17/17, G=59/59, H=51/51), (d) Convergence rate with GB migration policy.

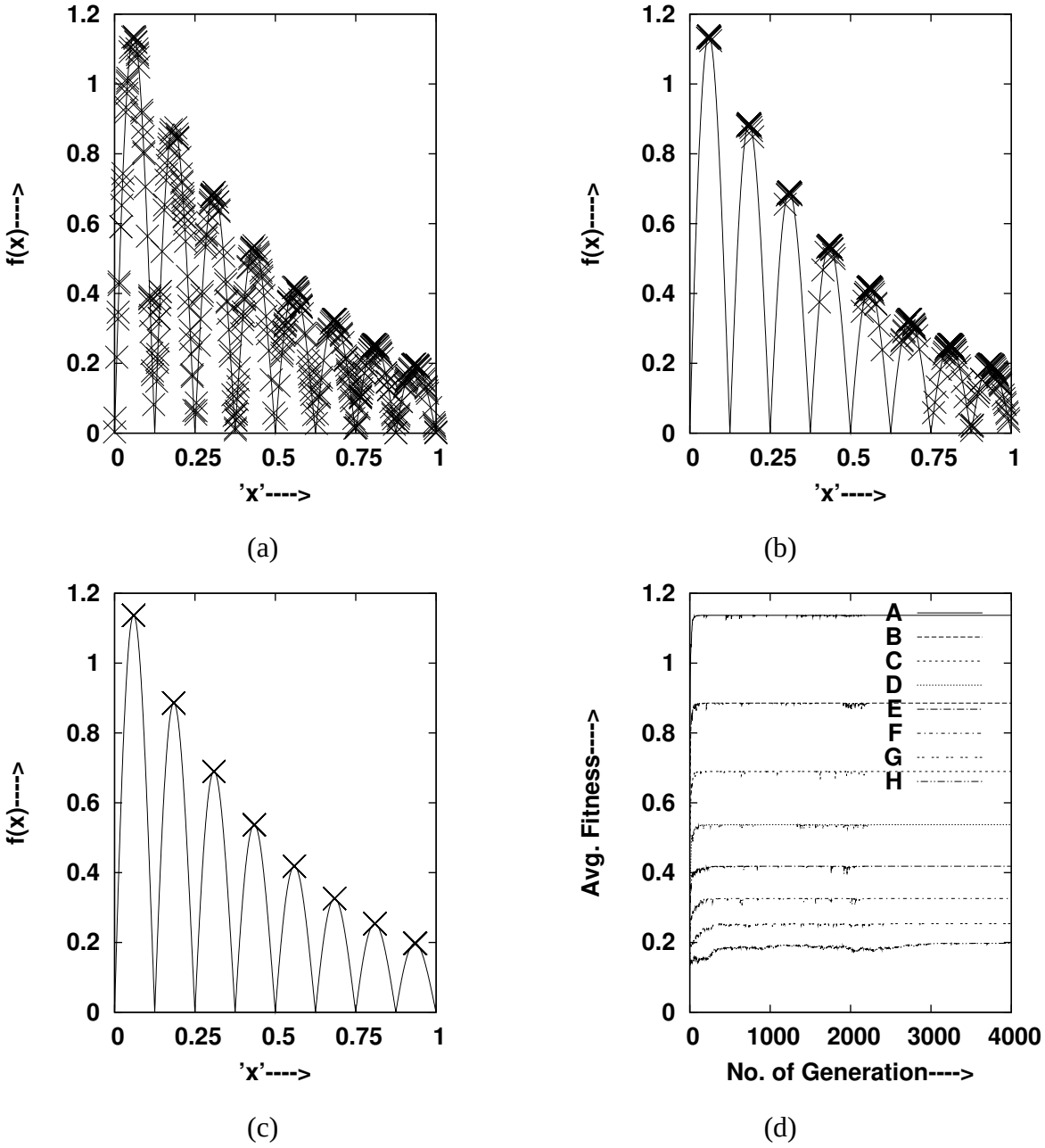

Figure 3.17: GA based Crowding for 8-class decaying function: (a) Initial distribution (Class: A=10/107, B=7/49, C=9/30, D=12/55, E=10/32, F=8/26, G=13/50, H=4/51), (b) Distribution after 500 gen. (Class: A=107/107, B=47/49, C=29/30, D=46/55, E=24/32, F=17/26, G=29/50, H=27/51), (c) Final distribution after 4000 gen. (Class: A=107/107, B=49/49, C=30/30, D=55/55, E=32/32, F=26/26, G=50/50, H=51/51), (d) Convergence rate

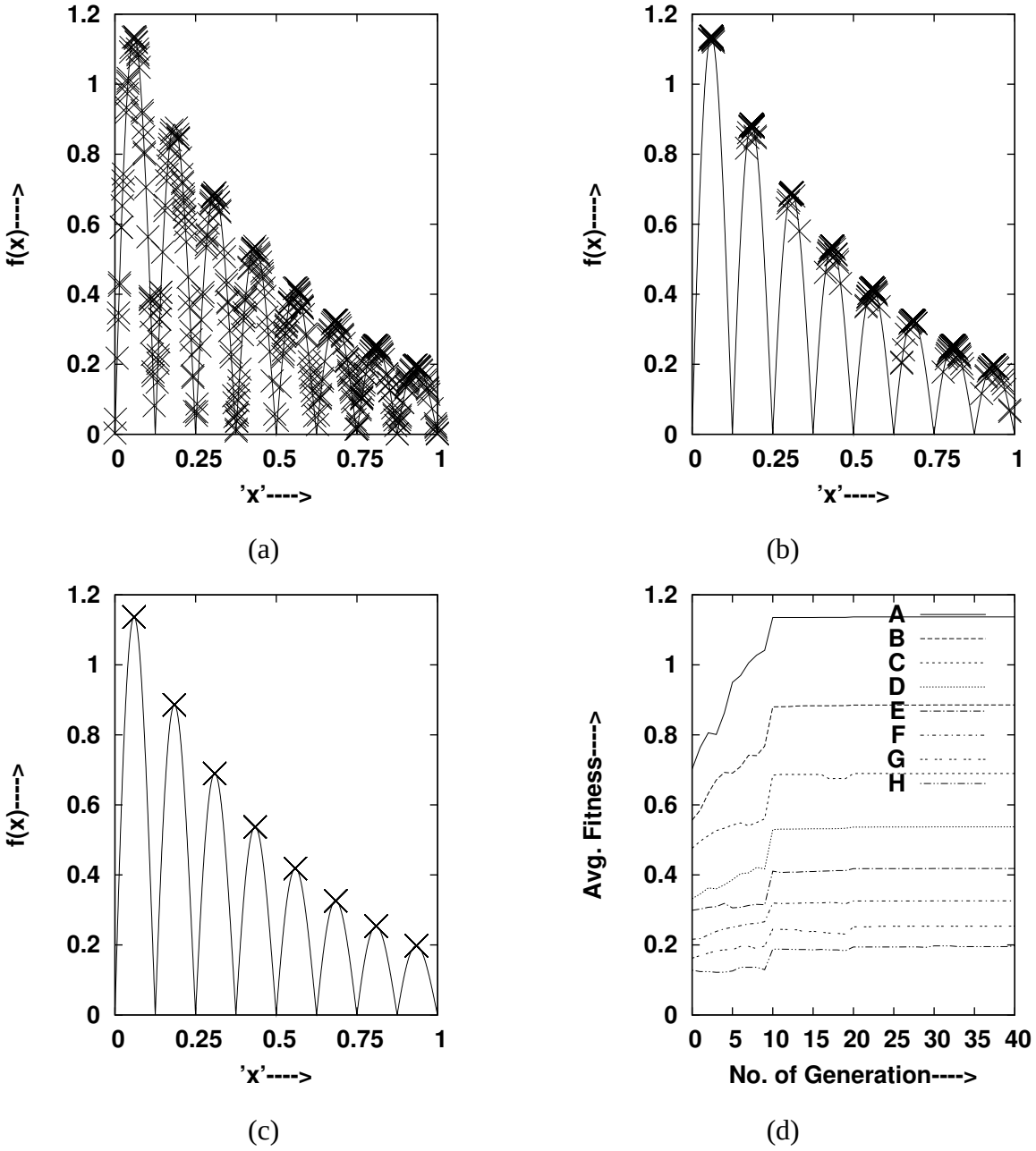

Figure 3.18: PGA based Crowding for 8-class decaying function: (a) Initial distribution (Class: A=11/107, B=9/49, C=6/30, D=10/55, E=15/32, F=11/26, G=13/50, H=5/51), (b) Distribution after 20 gen. (Class: A=107/107, B=42/49, C=23/30, D=45/55, E=28/32, F=20/26, G=42/50, H=43/51), (c) Final distribution after 40 gen. (Class: A=107/107, B=49/49, C=30/30, D=55/55, E=32/32, F=26/26, G=50/50, H=51/51), (d) Convergence rate with GB migration policy

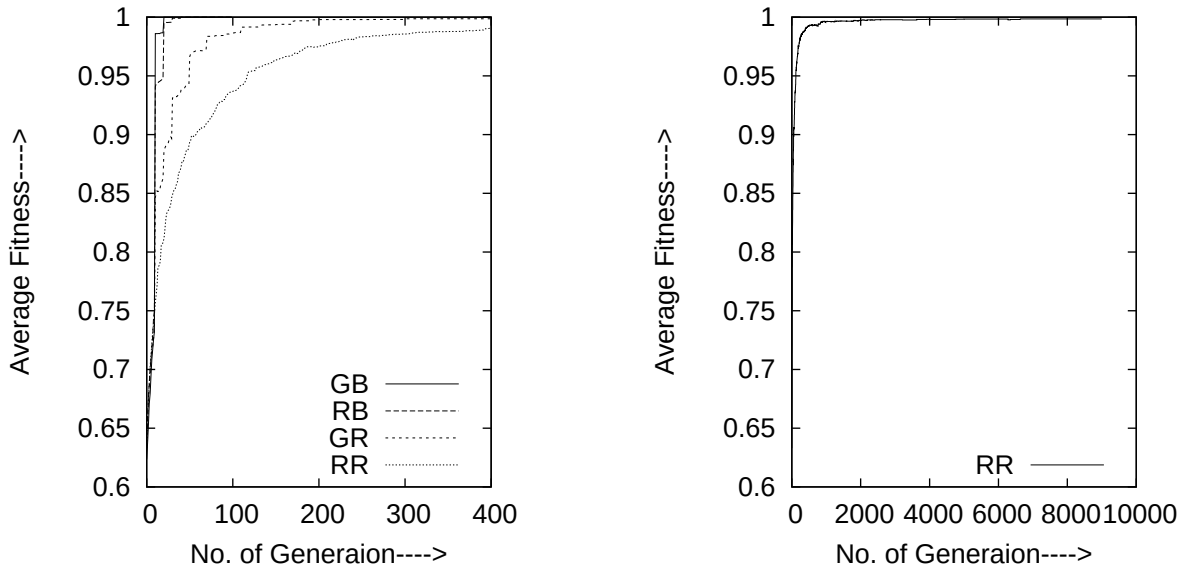

(a) (b)

Figure 3.19: PGA based Crowding for 4-class: (a) Comparision of different Migration policies GB, RB and GR, (b) RR migration policy

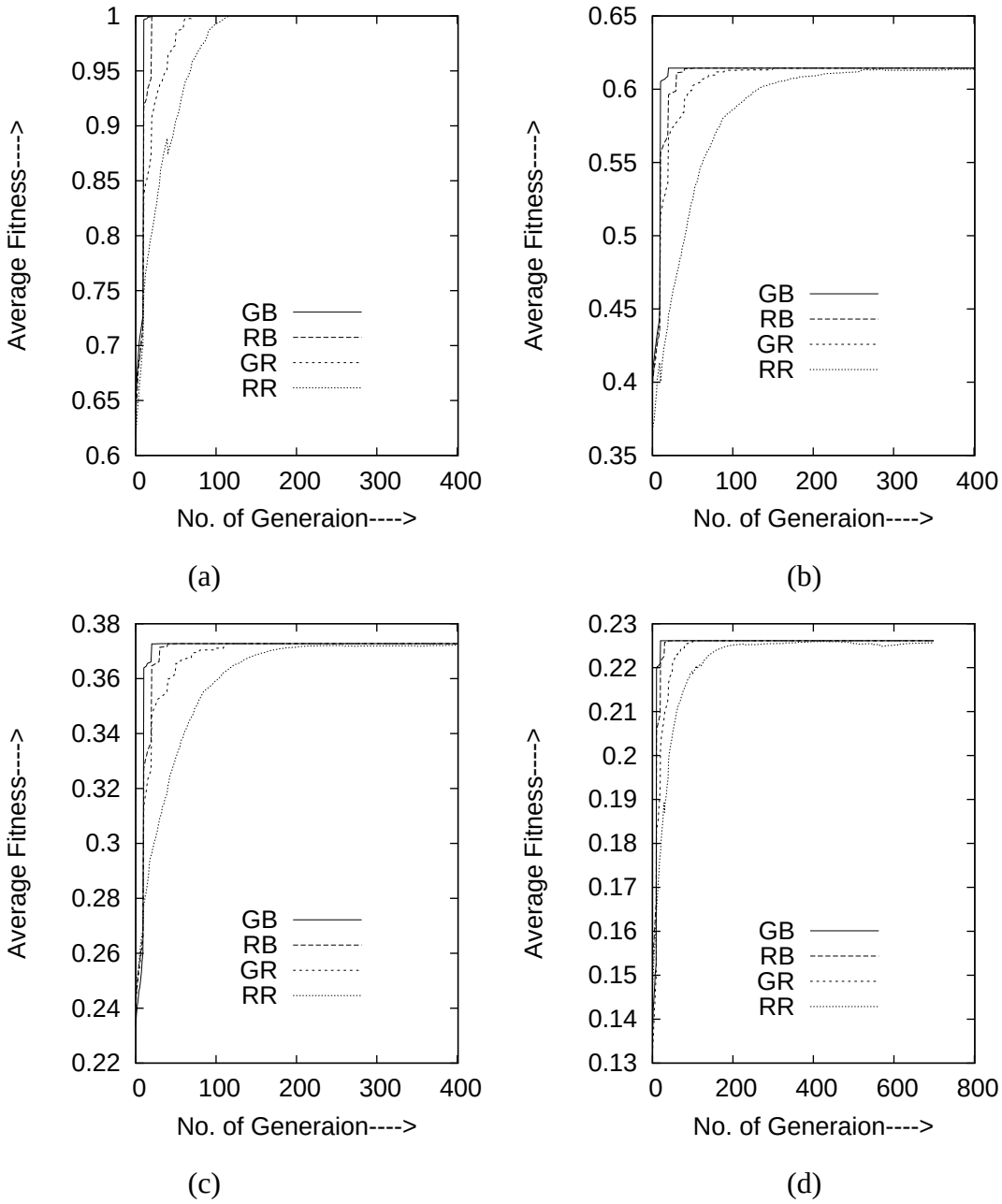

Figure 3.20: Comparision of Migration Policies GB, RB, GR and RR in Decaying 4-class: (a) Class-A, (b) Class-B, (c) Class-C, (d) Class-D.

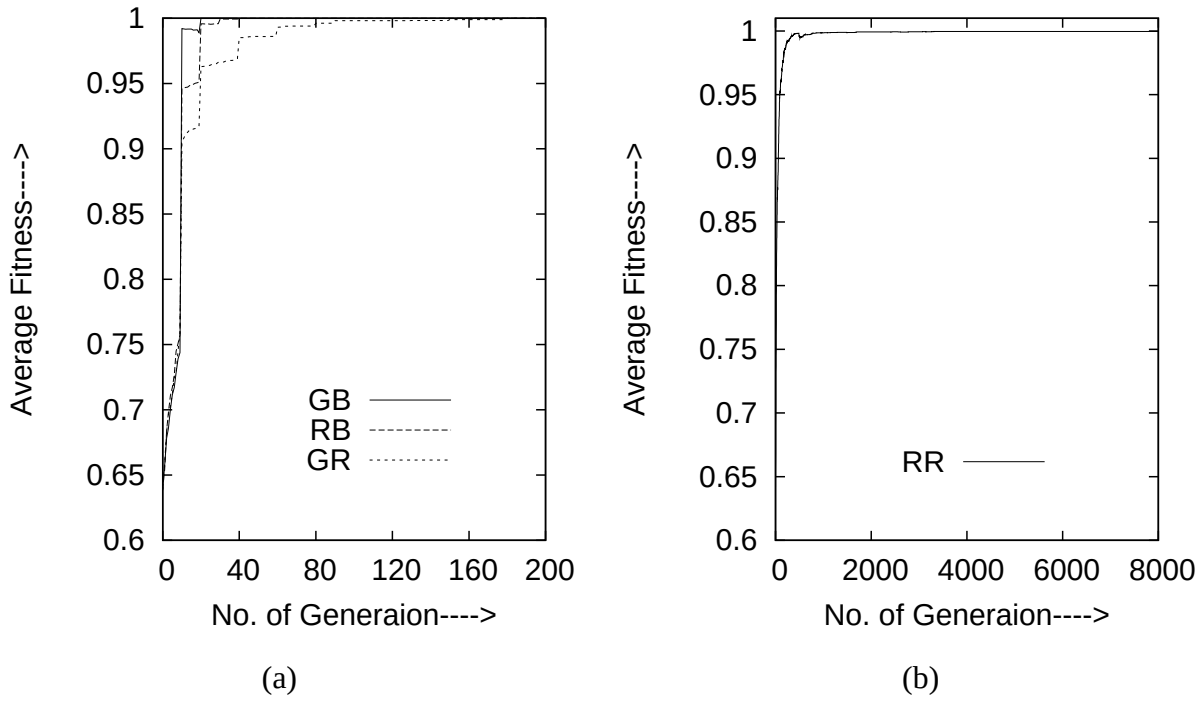

Figure 3.21: PGA based Crowding for 8-class: (a) Comparision of different Migration policies GB, RB and GR, (b) RR migration policy

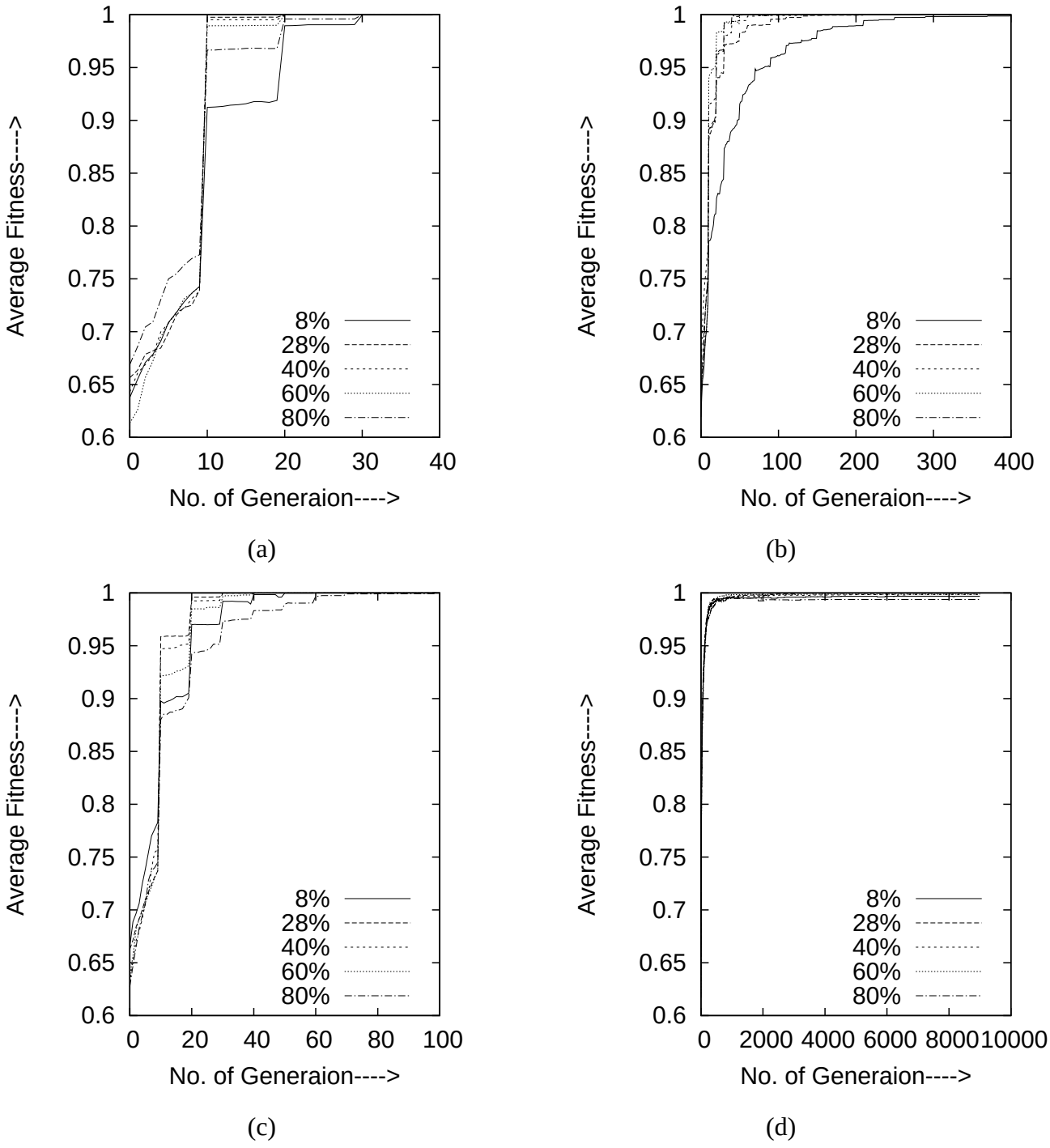

Figure 3.22: PGA based Crowding for 4-class:(Comparision of migration rate) (a) GB Migration policy, (b) GR Migration policy, (c) RB Migration policy, (d) RR Migration policy

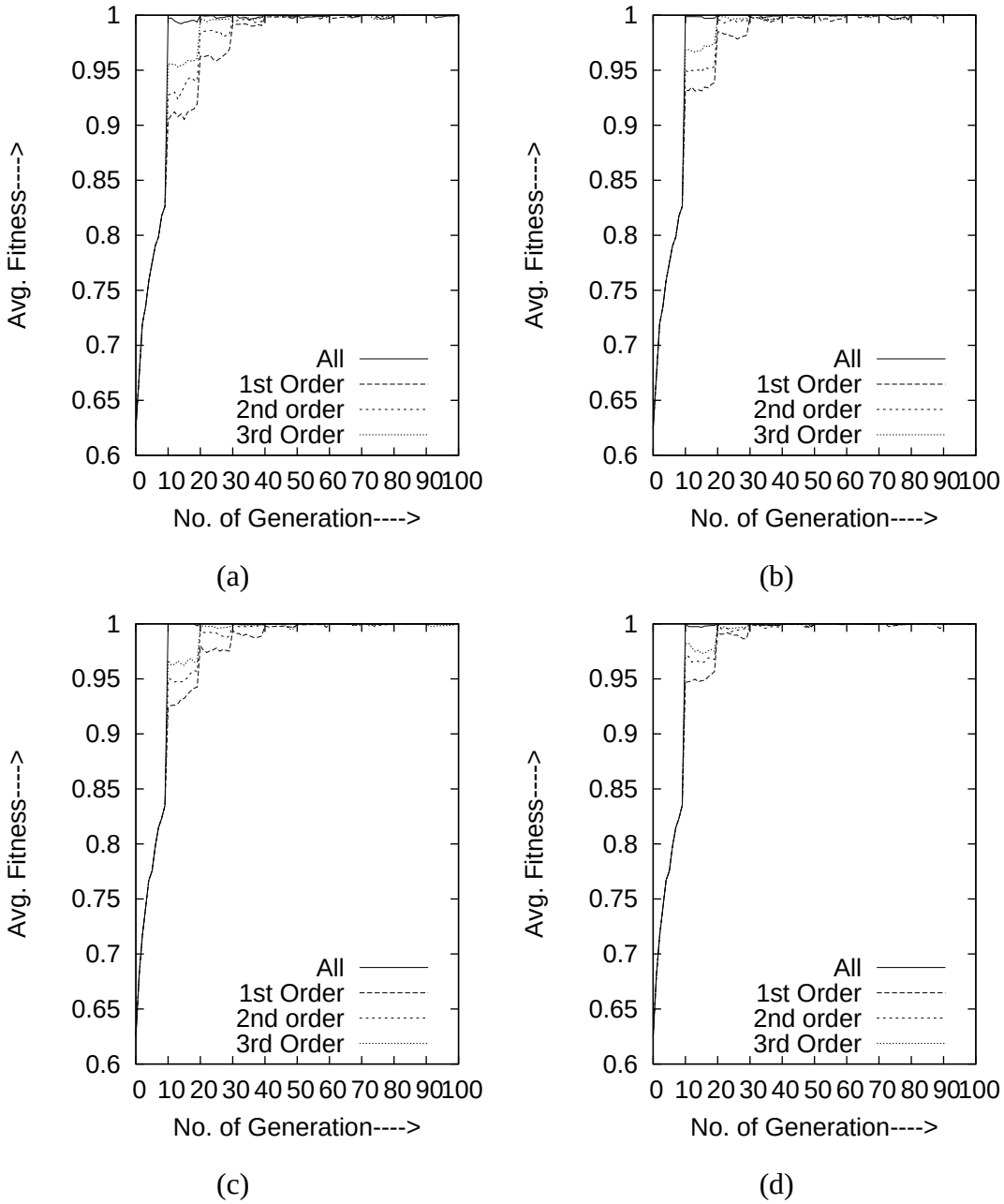

Figure 3.23: Comparison of different neighbourhood structures for 4-class: (a) Without self loop and 16% migration rate, (b) With self loop and 16% migration rate, (c) Without self loop and 25% migration rate (d) With self loop and 25% migration rate

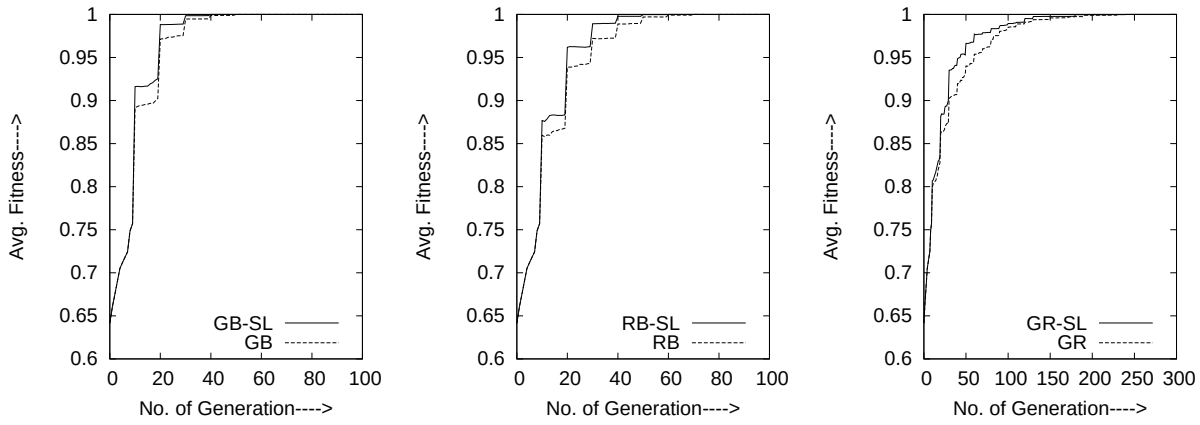

(a) (b) (c)

Figure 3.24: Avg. Fitness vs Generation (4-Class)(a) TPC-SL vs TPC-WSL with GB migration (b) TPC-SL vs TPC-WSL with RB migration (c) TPC-SL vs TPC-WSL with GR migration

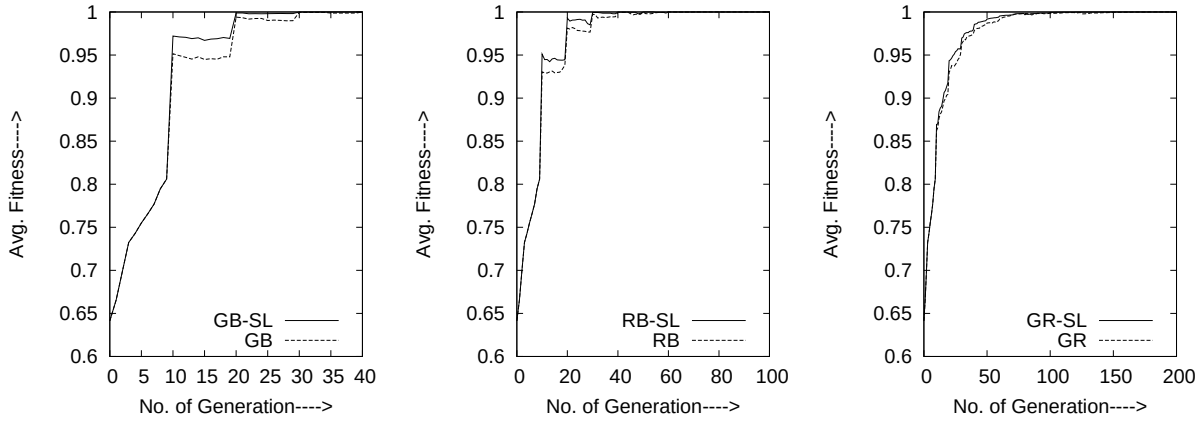

(a) (b) (c)

Figure 3.25: Avg. Fitness vs Generation (4-Class)(a) GC-SL vs GC-WSL with GB migration (b) GC-SL vs GC-WSL with RB migration (c) GC-SL vs GC-WSL with GR migration

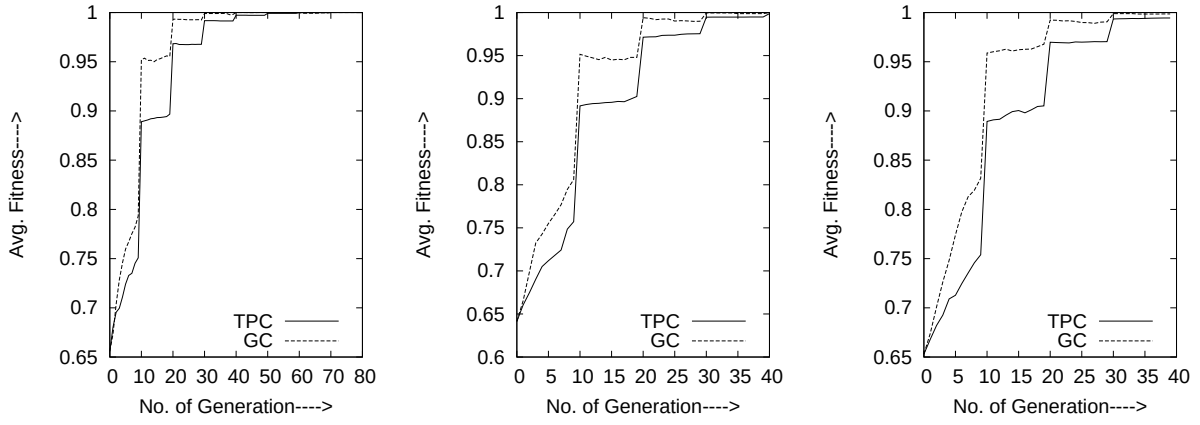

(a) (b) (c)

Figure 3.26: Avg. Fitness vs Generation (a) GC and TPC with GB for 2-class, (b) GC and TPC with GB for 4-class, (c) GC and TPC with GB for 8-class

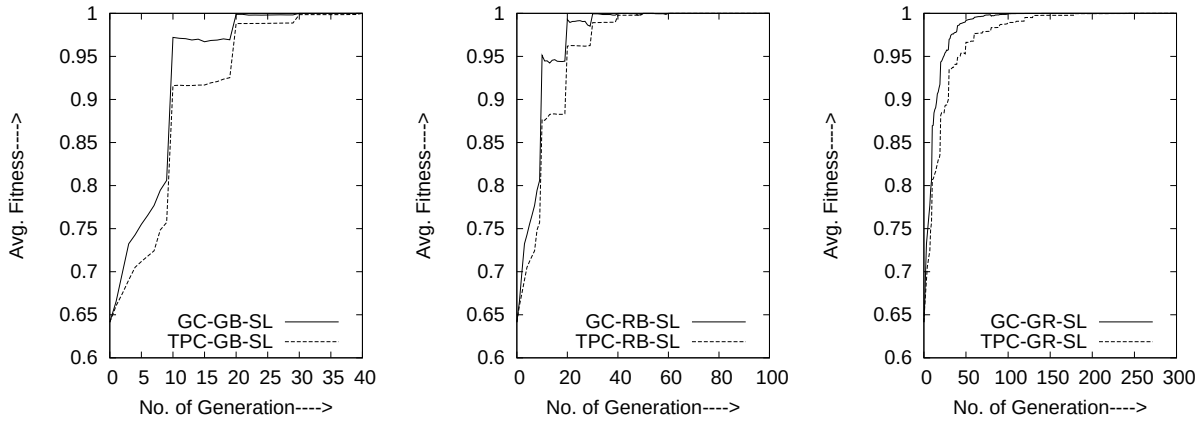

(a) (b) (c)

Figure 3.27: Avg. Fitness vs Generation (4-Class)(a) TPC-SL vs GC-SL with GB migration (b) TPC-SL vs GC-SL with RB migration (c) TPC-SL vs GC-SL with GR migration

Chapter 4

Feature Less and Feature Based Clustering Methods for Optimal Threshold

4.1 Introduction

By and large, histogram based thresholding techniques are based on the shape information of the histogram distribution on the shape information of the histogram distribution [1, 2, 3, 4, 142]. In the paradigm, a threshold is detected to separate the range of gray levels into different segments in the histogram. The corresponding thresholds are used to segment the image into different segments [1, 2, 3, 4, 142]. Such segmentation problem is viewed as a classification problem and the thresholding approaches are extensively used for two class or multiclass problem. A two class problem typically consists of separating the object class from the background whereas in a multiclass problem the problem reduces to separating multiple objects and background. The problem is more challenging when the object size is much smaller than that of the background. In such cases, the histogram distribution exhibits unequal distribution corresponding to the object and background. In thresholding research, the landmark thresholding scheme has been used to determine a threshold based on maximizing the inter-class distance while minimizing the intra-class distance. Otsu's [5] approach produces promising results when the histogram exhibits clear bi-modality as a clear valley to be determined. Otsu's method could also be extended to multiclass problem. Over the years, good number of thresholding schemes have been proposed and these schemes by and large, can be viewed as either analogous to the Otsu's notion or derivative of Otsu's scheme. Over the years, attempts have been made to minimize the classification error when the histogram looses the bi-modality or multi-modality property and

the respective classes have appreciable amount of overlapping.

In this chapter, two thresholding schemes have been proposed. The first one is based on the shape information of the histogram of the original image called feature less (FL) scheme and the second one is based on the feature plane (feature based (FB))as opposed to the gray level plane. In both the proposed schemes, the histogram distribution has been viewed as a nonlinear multimodal function and hence, the peaks could be determined by the proposed PGA based clustering scheme of chapter 3 and therefore, the valley is determined by PGA. The threshold thus determined is used to segment the images. It has been found that performance of the feature less (FL) schemes deteriorates when the overlapping of the class distribution increases. A feature based (FB) scheme has been proposed, where feature pixels have been generated and the corresponding feature histogram has been found out. The PGA based clustering algorithm has been used to determine the peaks of the feature histogram and the valley of the feature histogram. This valley point is used as threshold to segment the original images. Both the FL and FB schemes have been tested for a wide variety of class and have been compared with Otsu's [5] and Kwon's [16] method and it has been found that the proposed FB method outperforms Otsu's and Kwon's method.

4.2 PGA based peak and threshold determination

Histogram distribution provides some first hand information about the image. Selection of threshold from histogram often depends upon the shape of the distribution. If the histogram distribution exhibits clear bi-modality separated by a distinct valley, the determination of threshold selection reduces to determination of valley point. Different methods have been proposed[2, 3, 4, 142] to determine the valley point. Nevertheless, accurate determination of valley points is not a trivial task because of noise, nonuniform lighting etc. In the following, we describe about the two methods that we propose to determine the valley even in case of noisy as well as overlapping classes of histogram distribution.

We have proposed two methods to determine the optimal threshold for classification. The first one, called Feature Less (FL) approach, exploits the shape information of the discrete histogram distribution of the original image to determine the optimal threshold. This optimal threshold corresponds to the valley of the histogram landscape. In the histogram landscape, each mode is assumed to correspond to one of the classes of the image. For example, histogram

having two modes (two peaks and one valley) as shown in Fig. 4.1(a) corresponds to two classes in the given image. Therefore, the problem is cast as a classification problem.

Often, because of the non-smooth nature of discrete histogram distribution, the conventional exhaustive method may obtain incorrect threshold leading to poor classification. In case of discrete histogram distribution, exhaustive search for the minimum gray value may lead to pseudo thresholds because the exhaustive search may obtain minimum value at either the initial portion or the final portion of the histogram distribution. Hence, we propose a clustering technique to detect peaks corresponding to different modes of the histogram. Irregularity in the distribution, for example, could be due to the presence of a small kink in one of the peaks of the distribution, thereby misleading one peak as two peaks. In our work, a Parallel Genetic Algorithm (PGA) based clustering technique is proposed to detect the peaks and, in the sequel, the valley between the successive peaks is obtained by exhaustive search method. The peaks or niches are determined by maintaining stable sub-population at each peaks. This is achieved by the proposed GA and PGA based crowding method that maintains stable sub-population or clusters of population elements at different peaks. Maintenance of stable sub-population could be attributed to the maintenance of diversity among the population elements. Thus, the peaks can be determined. The proposed FL approach yields satisfactory results, but the performance is found to deteriorate with overlapping class distributions that results from either the nature of the image or the presence of noise. In such situations, FL approach found incorrect thresholds and hence, poor classification. In order to ameliorate the situation, a Feature Based (FB) approach is proposed. In this approach, a feature of the image is determined and the histogram corresponding to the feature is considered as opposed to the histogram of the original image. This feature histogram is used for determination of optimal threshold for the original image. The process of determination of optimal threshold, or in other words valley of the featured histogram, is same as that of the FL approach. PGA based clustering algorithm is used to determine the peaks and thereafter the valley is obtained by the exhaustive search method. The valley, thus obtained, is used as the threshold for the original image. FL and FB methods are validated for two as well as three class images. FB approach is compared with FL, Otsu's [5] and Kwon's [16] approaches and it is found that the FB approach is the best among these four methods.

4.3 Brief review of Otsu's and Kwon's thresholding method

4.3.1 Otsu's approach

Otsu's [5] method is a non-parametric and unsupervised method of automatic threshold selection for image segmentation. In this method, the selection is based on the discriminant criterion that maximizes the inter-class variance while minimizing the intra-class variance. The threshold is determined using gray level distribution. For two class problem, one needs to determine one threshold. Otsu's method can also be extended to multi-threshold problems. Otsu's method for a two class problem is briefly summarized below.

For a two class problem, thresholding operation is regarded as the partitioning of pixels of an image into two classes namely object class C_o and background class C_b. Let the object class C_0 denotes the pixels with gray values $\{0, 1, ..., t\}$ and background class C_b denotes the pixels with gray values $\{t+1, t+2, ..., L-1\}$, where L is the total number of gray levels of the image. Let the the threshold be at level of "t", and thus the class probabilities are $q_1(t) = \sum_{i=1}^{i=t} p(i)$ and $q_2(t) = \sum_{i=t+1}^{i=L-1} p(i)$. The class mean gray values are $\mu_1(t) = \sum_{i=1}^{i=t} \frac{ip(i)}{q_1(t)}$ and $\mu_2(t) = \sum_{i=t+1}^{i=L-1} \frac{ip(i)}{q_2(t)}$, where p(i) is the probability of i^{th} gray value in the image. The class variance at threshold t is also defined as $\sigma_1(t) = \sum_{i=1}^{i=t}(i-\mu_1(t))^2 \frac{p(i)}{q_1(t)}$ and $\sigma_2(t) = \sum_{i=t+1}^{i=L-1}(i-\mu_2(t))^2 \frac{p(i)}{q_2(t)}$.

Using the class probabilities, the class means and class variance are defined as follows $\sigma_W^2 = q_1(t)\sigma_1^2(t) + q_2(t)\sigma_2^2(t) \quad and \quad \sigma_B^2 = q_1(t)(\mu_1(t) - \mu_T)^2 + q_2(t)(\mu_2(t) - \mu_T)^2$, where $\mu_T = q_1(t)\mu_1(t) + q_2(t)\mu_2(t)$. Replacing μ_T in σ_B^2, $\sigma_B^2(t)$ is defined as

$$\sigma_B^2(t) = q_1(t)q_2(t)(\mu_1(t) - \mu_2(t))^2$$

and $\sigma_T^2 = \sum_{i=0}^{L-1}(i - \mu_T)^2 p(i) = \sigma_W^2(t) + \sigma_B^2(t)$.

The different criteria functions defined are

$$\lambda = \sigma_B^2/\sigma_W^2, \quad \eta = \sigma_B^2/\sigma_T^2 \quad and \quad \kappa = \sigma_T^2/\sigma_W^2. \tag{4.1}$$

Maximization of the discriminant criteria λ, η, and κ for t are equivalent. Therefore, the optimal threshold is obtained by maximizing one of the criteria functions. Considering the criterion function η, the optimal threshold is as follows.

$$T_{opt} = arg \max_{0 \le t \le L-1} \eta = arg \max_{0 \le t \le L-1} \frac{\sigma_B^2}{\sigma_T^2}. \tag{4.2}$$

Since σ_T^2 is constant, maximizing (4.2) is equivalent to maximizing the following

$$T_{opt} = arg \max_{0 \leq t \leq L-1} \sigma_B^2$$

.

Maximizing the criterion function in (4.2) is equivalent to maximizing the between class variance and minimizing the within-class variance.

4.3.2 Kwon's approach

Know [16] proposed a threshold selection method using cluster analysis by modifying the Know's new cluster validation index [143]. Even though his method is valid for any number of clusters, for the sake of illustration and simplicity, he considered two class problem of images. Let the given image X be the union of two data sets X_1 and X_2, $X = X_1 \cup X_2 = \{x_1, x_2, ..., x_{M \times N} \subset R^2\}$ be a set of $M \times N$ data points (pixels), where, X_1 and X_2 denote two clusters containing pixels with gray values in $[0, t]$ and $[t+1, L-1]$, $x_k = (x_k^1, x_k^2)$ denotes the k^{th} point $(1 \leq k \leq n)$, and x_k^j denotes the j^{th} coordinate $(1 \leq j \leq 2)$ of the k^{th} point. Let $V = \{v_1, v_2\} \subset R^2$ be a set of cluster centres with $v_i = (v_i^1, v_i^2)$ for $1 \leq i \leq 2$, and $f(x_k) \in [0, L-1]$ denotes a gray level at point x_k. The clustering problem reduces to selecting an optimal gray level $T \in [0, L-1]$ which optimizes the following.

$$T^* = arg \min_{0 \leq T \leq L-1} J_k(T), \tag{4.3}$$

where

$$J_k(T) = \frac{\sum_{x_k \in X_1} p^2 \|x_k - v_1\|^2 + \sum_{x_k \in X_2} p^2 \|x_k - v_2\|^2 + \frac{1}{2} \sum_{i=1}^{2} \|v_i - \bar{v}\|^2}{\|v_1 - v_2\|^2}. \tag{4.4}$$

In (4.4), $v_1 = \frac{1}{|X_1|} \sum_{x_k \in X_1} x_k$, $v_2 = \frac{1}{|X_2|} \sum_{x_k \in X_2} x_k$, $\bar{v} = \frac{1}{|X|} \sum_{x_k \in X} x_k$, $p = \frac{1}{|X|}$ and $|\cdot|$ denotes the cardinality of a set and p is a weighting factor. The first and second terms of the numerator in (4.4) measure the intra-class similarity, that is, how compact every class is. The more similar (compact) the classes, the smaller it is. It is independent of the number of data points. The last term of the numerator in (4.4) is an ad-hoc penalty function imposed to eliminate the decreasing tendency when the number of clusters get very large and close to the number of data points. The denominator in (4.4) measures the inter-class dissimilarity. A larger value of it indicates that every cluster is well-separated.

4.4 Proposed methods

4.4.1 Feature less method

In this approach, the histogram of the original image is considered. This histogram is modelled as a nonlinear multimodal function. For a two class problem, the histogram is shown in Fig. 4.1(a), where it can be observed that there are two modes corresponding to two classes. The envelop of this distribution is viewed as a nonlinear multimodal function. Each class distribution can be represented by the dominant modes and hence, the problem reduces to determining the modes. Once the dominant modes have been determined, it is assumed that for a two class problem a valley exists in between these two peaks. For a multiclass problem, a valley has to be determined between successive peaks. The fitness function considered is same as the histogram. Hence, the PGA based scheme maintains sub-population at the peak of the histogram distributions.

Since, the histogram distribution considered is discrete, conventional iterative search would have resulted in determining the minimum at some other point. Therefore, for a two class problem, the two peaks have been determined by the PGA based crowding scheme. These two peaks correspond to a two gray levels and the valley is constrained within the two peaks. In a multiclass problem, the valley is sought between two successive peaks. The two peaks with the valley is viewed as a convex function with valley as the minimum value of the convex function.

4.4.2 Feature based method

Mostly, the histogram of noisy scenes have overlapping class distributions. In such situations, the FL approach yields approximate results with large percentage of misclassification error. This could be due to the overlapping class distributions. In order to minimize the overlapping of the class distributions, a feature based approach is proposed. This approach deals with the histogram distribution corresponding to an image dealing with features only. The feature from the original image is extracted as follows. A window of a given size is considered around a pixel and the distributions of the pixels over the window is assumed to be Gaussian. The first moment of this distribution over the window is considered as the feature and this is governed by the second moment (variance) of the distribution. With Gaussian assumption, it is known that

the likelihood estimates of the first and second moment over a window size of w is

$$\hat{\mu}_{w_{ij}} = \frac{1}{N_w}\sum_{k=1}^{N_w} x_k \quad and \quad \hat{\sigma}^2_{w_{ij}} = \frac{1}{N_w}\sum_{k=1}^{N_w}\left(x_k - \hat{\mu}_{w_{ij}}\right)^2. \tag{4.5}$$

The first moment of the pixels is considered as the feature value if the following condition is satisfied.

$$if \quad |x_{ij} - \hat{\mu}_{w_{ij}}| \leq \hat{\sigma}_{w_{ij}}/K \quad then \quad x_{ij} = \hat{\mu}_{w_{ij}} \tag{4.6}$$

where, K is a positive constant bounded between 1 to 10 to take care of smoothness and also differentiate edge and non-edge pixels. x_{ij} is the gray value of the $(i,j)^{th}$ pixel, $\hat{\mu}_{w_{ij}}$ is the mean value, $\hat{\sigma}_{w_{ij}}$ is the standard deviation, N_w denotes the number of pixels in the window. The features corresponding to pixels of the whole image are derived and histogram of the featured pixels is considered. The optimal threshold for the original image is obtained from the modified histogram shown in Fig. 4.1(b). The modified histogram either reduces the degree of overlapping or removes the overlapping between class distributions.The proposed PGA based clustering algorithm is used to determine the peaks and thereafter the valley is determined by exhaustive search.

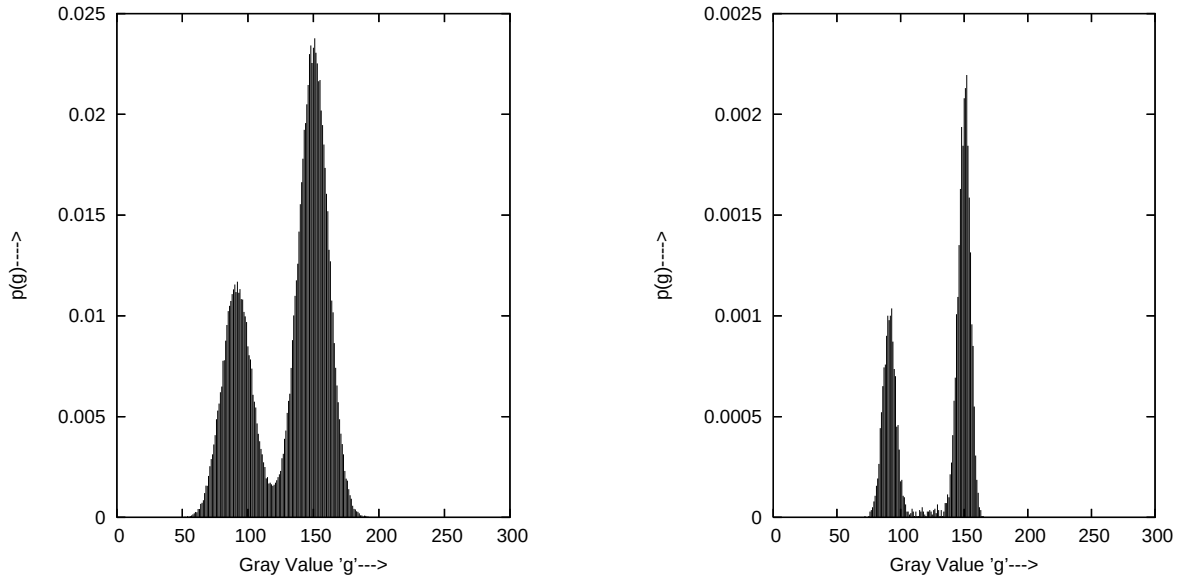

(a) (b)

Figure 4.1: (a) Normalized histogram of the image; (b) Normalized histogram of the feature image.

4.4.3 PGA based algorithm

The objective of designing parallel GA is two fold: (i) reducing the computational burden and (ii) improving the quality of the solutions. The design of PGA involves choice of multiple populations where, the size of the population must be decided judiciously. These populations may remain isolated or they may communicate exchanging individuals. In this parallel scheme, the population is divided into demes (sub-population) and the demes evolve for convergence. After some generations, migration is carried out to achieve convergence. This helps in accelerating the convergence and also improves the quality of the solution. We have adopted the good-bad (GB) based migration policy. In our problem we considered four demes D1, D2, D3 and D4 and the 1^{st} order interaction network model for interaction among the demes. Tournament selection mechanism is applied to all demes. The proposed GC operator is used in the PGA. The steps of the parallelized crowding scheme are the following.

(1) Initialize randomly a population space of size N_p (each element corresponds to a gray value between 0 and 255) and their classes are determined.

(2) Divide the population space into fixed number of sub-populations and determine the class of individuals in each sub-population.

(3) (i) In the given sub-population (deme), choose two elements at random for GC and mutation operation with crossover probability P_c and mutation probability P_m.

(ii) Evaluate fitness of each parent and offspring. The fitness function is the featured normalized histogram function $p(g)$.

(iii) Tournament selection mechanism is a binary tournament selection among the two parents and offspring, the set which contains the individual having highest fitness among the four elements is selected to the set of parents for the next generation.

(iv) Repeat steps (i), (ii) and (iii) for all the elements in the sub population.

(v) Repeat steps (i), (ii), (iii) and (iv) for a fixed number of generations.

(4) Step 3 is repeated for each sub-population (deme).

(5) Migration is allowed from each deme to every other deme. The individuals are migrated based on the selected migration policy. Number of elements to migrate are determined

from the selected rate of migrationR_{mig}. The elements migrate with migration probability P_{mig}.

(6) Self migration is allowed in each deme based on the selected migration policy and selected rate of self-migration R_{smig} with a probability P_{smig}.

(7) Repeat Steps 3, 4, 5, and 6 till convergence is achieved. The algorithm stops when the average fitness of the total population is above pre-selected threshold.

(8) Peaks are detected from the converged classes of Step 7.

(9) Go for the iterative search to find the valley point or go for the following steps for PGA (without crowding method) based optimization (minimization in this problem) for valley detection between two peaks. For PGA based valley detection go to step 10.

(10) Initialize randomly a population space of size N_v between the two peaks (i.e between the two corresponding gray levels of the peaks).

(11) Divide the population space into fixed number of sub-populations (demes).

(12) Follow the steps 3 to 7 (without tournament selection) till the convergence is achieved. If the population is converged, then the converged solution is the valley point.

(13) If all the elements of the population is converged then use the solution as threshold to segment the given image.

4.5 Results and discussions

Images exhibiting bi-modality and tri-modality in the histogram distribution are considered. Histograms with bi-modality and tri-modality features correspond to two and three class images respectively. The two proposed schemes have been successfully tested with two and three class images. In the FL approach, the histogram distribution of the original image is used. The image considered is shown in Fig. 4.2(a) and the corresponding discrete histogram is shown in Fig. 4.2(b). The PGA based crowding and search scheme is used to detect the peaks followed by determination of the valley point that corresponds to the threshold. The parameters used for GA are: Generation=1000, Probability of Crossover $P_c = 0.8$, Probability of Mutation $P_m = 0.001$, population size $N_p = 400$ and $N_v = 100$. The parameters used for PGA are: Generation=1000,

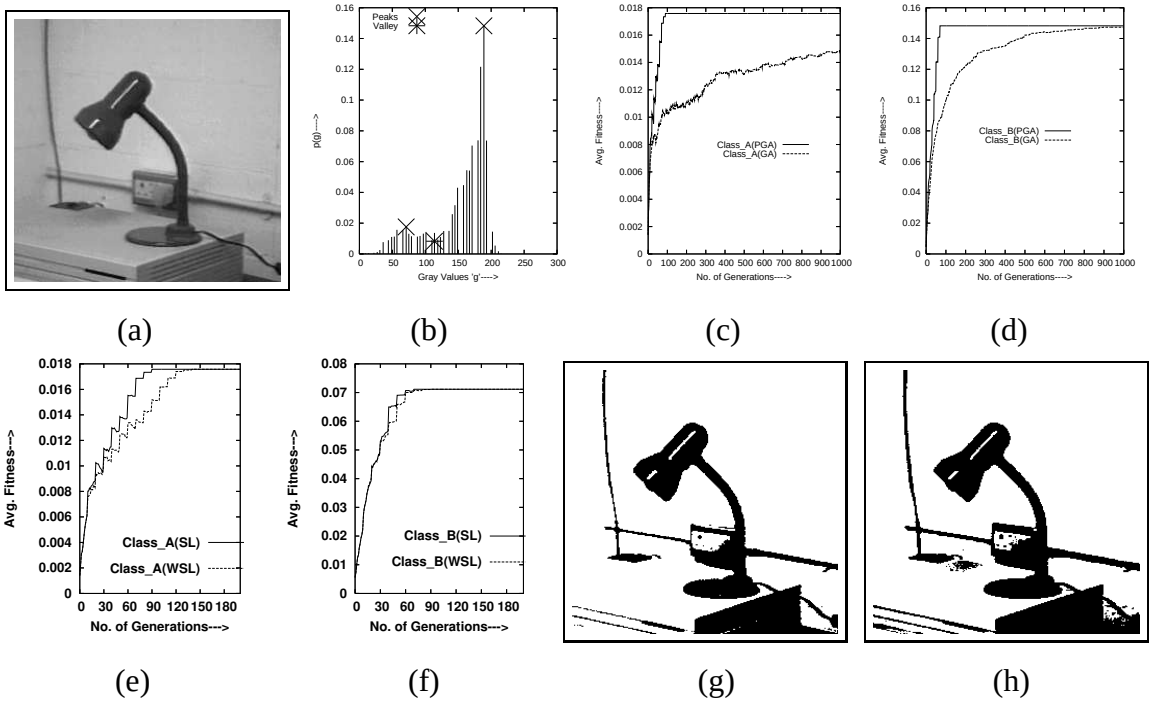

Figure 4.2: (a) Image 1; (b) Histogram with detected peaks and valley; (c) Average fitness versus generation of class "A" PGA and GA; (d) Average fitness versus generation of class "B" PGA and GA; (e) Class "A" with SL and WSL; (f) Class "B" with SL and WSL; (g) Segmented image using FL; (h) Segmented image using Otsu's approach.

Migration period is 10 generations, Number of demes is 4, Probability of Crossover $P_c = 0.8$, Probability of Mutation $P_m = 0.001$, population size $N_p = 400$ and $N_v = 100$, Probability of migration $P_{mig} = 0.8$, Migration rate $R_{mig} = 4\%$,, Probability of self migration $P_{smig} = 0.8$ and Self migration rate $R_{smig} = 2\%$. The peaks detected by PGA are at 71 and 189 and the corresponding threshold T=114. GA and PGA based algorithms are compared and it is observed that PGA converges much faster than that of GA. This phenomenon is evident from Fig. 4.2(c) and (d) that corresponds to class A and class B respectively. For example, for class A, PGA converges around 100 generations while GA takes around 1000 generations. In PGA, we have used the island model with interconnection and we have proposed a fully interconnected model by introducing a new notion of self migration(SL). The proposed interconnection model is found to converge faster than that of the model without self migration(WOSL). This may be observed from Fig. 4.2(e) and (f) for both the classes. The threshold value thus obtained is used to segment the image and the segmented image is shown in Fig. 4.2(g). Our result is compared with that of Otsu's in Fig. 4.2(h) and it can be observed from Fig. 4.2(h) that there are misclassified pixels near the rod and also at the back of the table of the image. This misclassification is absent in case of result obtained by the proposed FL method in Fig. 4.2(g).

The percentage of misclassification is determined as follows

$$PME = 1 - \frac{\mid B_O \cap B_T \mid + \mid F_O \cap F_T \mid}{\mid B_O \mid + \mid F_O \mid} \tag{4.7}$$

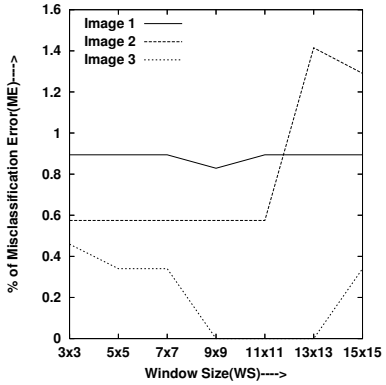

Figure 4.3: Percentage of misclassification error verses window size (images 1, 2 & 3 correspond to Fig. 4.4(a), 4.5(a) & 4.6(a))

Where background and foreground are denoted by B_O and F_O for the original image, and by B_T and F_T for the test image. The threshold and the Percentage of Misclassification Error(PME) are tabulated in Table 4.1 for different size of windows. The FB approach is also validated with two and three class images. The feature pixels are generated as follows; a window of a given size is considered around the pixel x_{ij} and the first moment i.e. average value of the pixels is considered as the feature of the pixel. The distribution of the pixels over a window is assumed to be Gaussian and the selection of the feature is governed by the variance of the distributions as given by (4.6). Since, the feature depends on window size, initially the selection of optimum window size is considered based on the PME. The PME for three images is shown in Fig. 4.3. It is found from simulation that the PME is minimum with a window size of 9x9. The corresponding results are also tabulated in Table 1. The optimum size, thus found empirically is used as the window size in case of the images. The featured pixels are generated and thus feature image is created. In this approach, the histogram of the featured pixels is used. The image considered in FB approach is shown in Fig. 4.4(a) and the histogram is shown in Fig. 4.4(b). The histogram of featured pixels is shown in Fig. 4.4(c). This featured histogram exhibits clear modes and the almost all gray levels are present. The proposed PGA based crowding algorithm is used to detect the peaks and the peaks are at 73 and 188 and the valley at 116. The detected peaks and valleys are shown in Fig. 4.4(d). The parameters of the PGA is same as that of the FL approach. The convergence of PGA based scheme predominantly

depends on the proper choice of the migration policy and the rate of migration. The effect of these two parameters is also studied. The segmented result obtained using the FB approach, Otsu's approach, and Kwon's approach are shown in Fig. 4.4(i), (j) and (k) respectively. It is observed that there are misclassified pixels near base of the rod and back of the table. These are absent in image obtained by the FB approach. This phenomenon is also reflected from the percentage of misclassification error tabulated in Table 2.

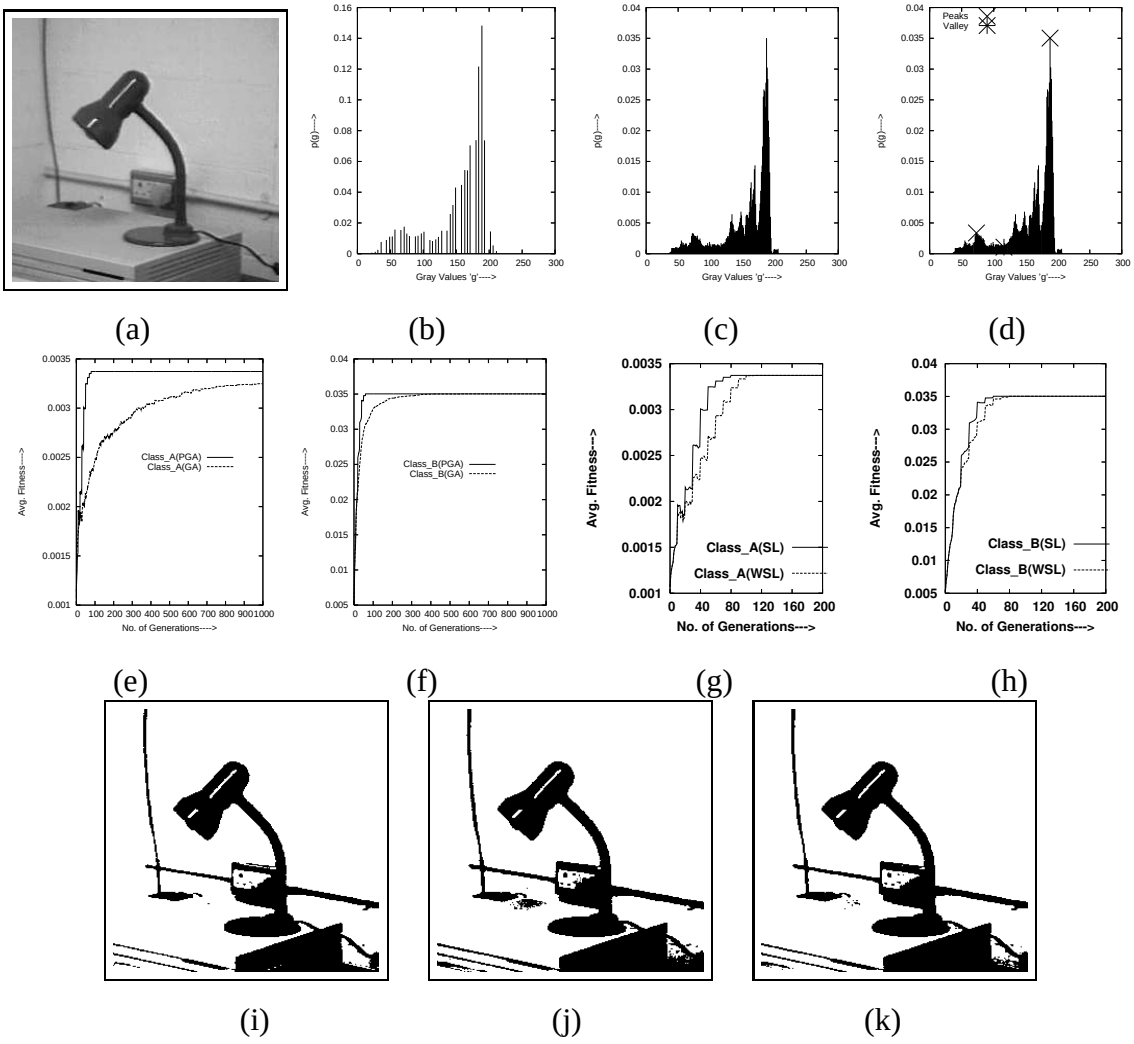

Figure 4.4: (a) Image 1,(b) Histogram; (c) Featured histogram; (d) Detected peaks and valley; (e) Average fitness versus generations of class "A" PGA and GA; (f) Average fitness versus generations of class "B" PGA and GA; (g) Class "A" with SL and WSL; (h) Class "B" with SL and WSL; (i) Segmented image using the FB approach; (j) Segmented image using Otsu's approach; (k) Segmented image using Kwon's approach.

The FB approach has also been tested with noisy images as shown in Fig. 4.5(a) and Fig. 4.6(a). Fig. 4.5(a) is a clearly bimodal image. The noisy version of image of Fig. 4.5(a) having signal to noise ratio (SNR) 22dB is shown in Fig. 4.5(b). We define SNR as $SNR_{dB} =$

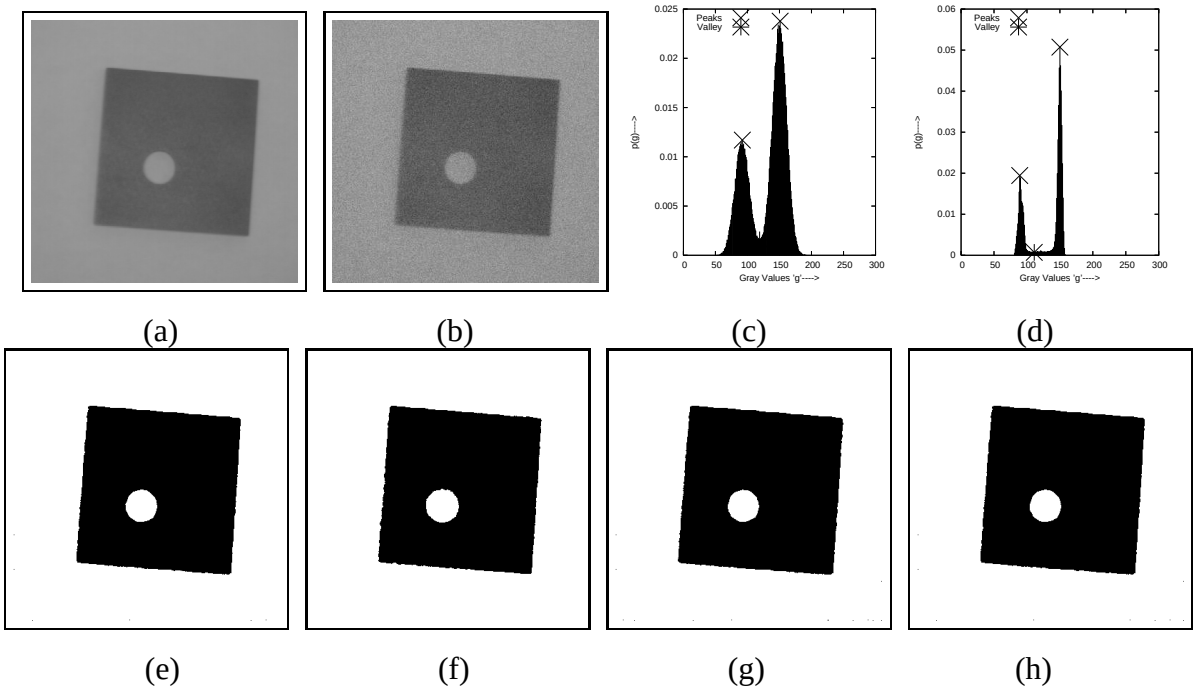

Figure 4.5: (a) Image 2; (b) Noisy version of image 2 with SNR 22dB; (c) Histogram of (b) with detected peaks and valley; (d) Featured histogram of (b) with detected peaks and valley; (e) Segmented image using FL; (f) Segmented image using FB approach; (g) Segmented image using the Otsu's approach; (h) Segmented image using the Kwon's approach.

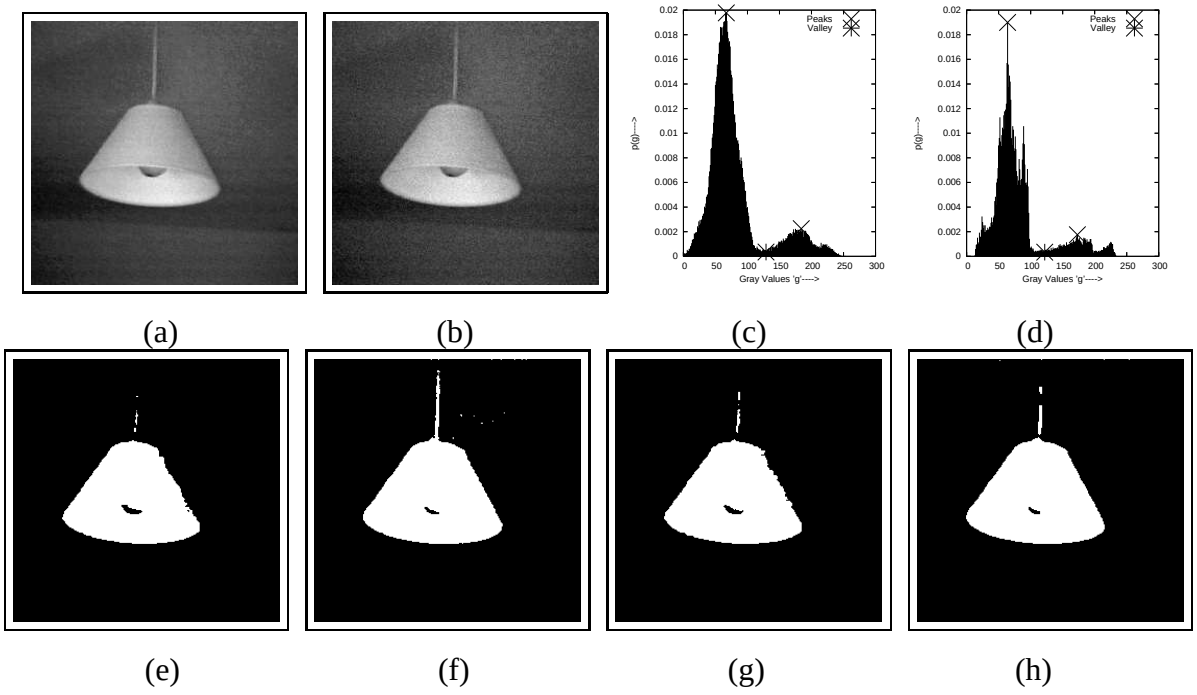

Figure 4.6: (a) Image 3; (b) Noisy version of image 3 with SNR 22dB; (c) Histogram of (b) with detected peaks and valley; (d) Featured histogram of (b) with detected peaks and valley; (e) Segmented image using FL; (f) Segmented image using FB approach; (g) Segmented image using the Otsu's approach; (h) Segmented image using the Kwon's approach.

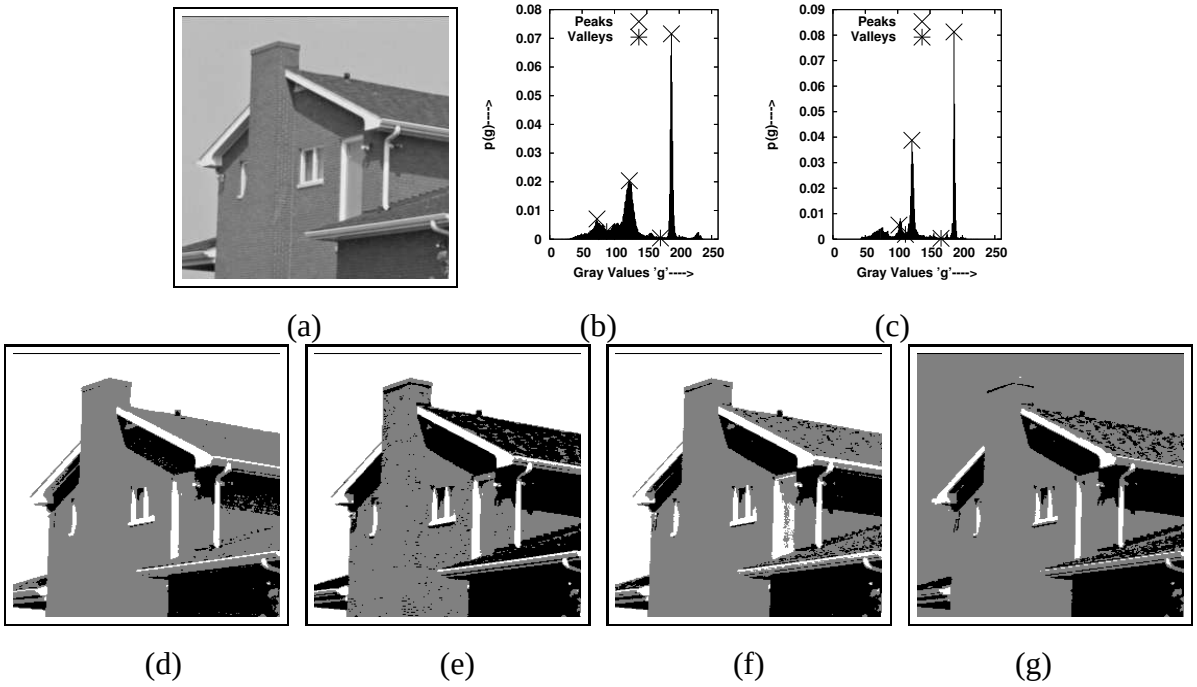

Figure 4.7: (a) Image 4; (b) Histogram with detected peaks and valleys; (c) Featured histogram with peaks and valleys; (d) Segmented image using FL; (e) Segmented image using FB; (f) Segmented image using Otsu's approach; (g)Segmented image using Kwon's approach.

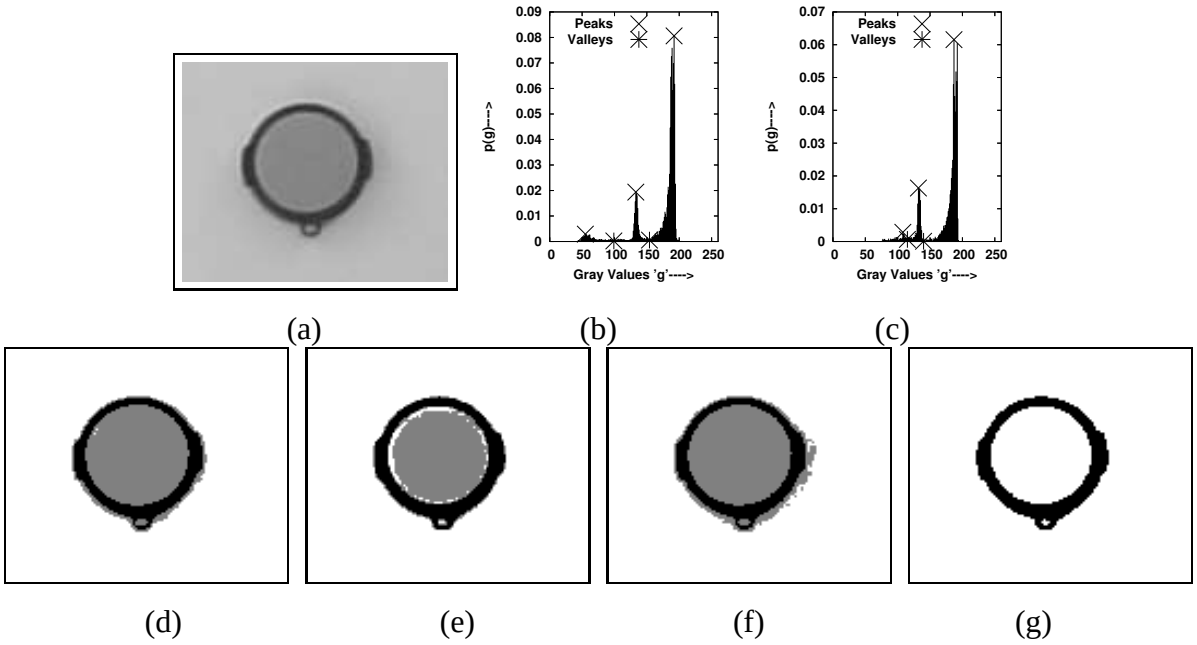

Figure 4.8: (a) Image 5; (b) Histogram with detected Peaks and valleys; (c) Featured histogram with Peaks and Valleys; (d) Segmented image using the FL; (e) Segmented image using FB; (f) Segmented image using Otsu's approach; (g) Segmented image using Kwon's approach.

$10\log_{10}\left(\sum_{ij} x_{ij}^2 / \sum_{ij} n_{ij}^2\right)$. The histogram of the noisy image, as shown in Fig. 4.5(c), shows overlapping of the object and background distributions. The peaks are detected at 92 and 151 and the corresponding threshold is at 119. It is clearly observed from Fig. 4.5(d) that the histogram of the featured pixels shows bi-modality. The peaks and valley are detected at 89, 150, and 111 respectively. The segmented images are shown in Fig. 4.5(e), (f), (g), and (h) that corresponds to FL, FB, Otsu's and Kwon's approach. From Table 2, it is found that the misclassification error is more in case of Otsu's method. Hence, the FB approach performs better than that of FL, Otus's and Kwon's approach. The efficacy of the FB approach is more evident in the third example as shown in Fig. 4.6. It is observed from the segmented results shown in Fig. 4.6(e), (f), (g) and (h) that FB approach could preserve edges and reduced the number of misclassified pixels. In case of Otsu's approach from Table 2, it is observed that the PME is more than two times of that of the FB approach. Thus, the FB approach is more suitable for noisy as well as images having overlapping class distributions.

We have also validated the proposed FL and FB scheme in case of three class images as shown in Fig. 4.7 and 4.8. The percentage of misclassification is presented in Table 3. It may be observed from the segmented results of Fig. 4.7. and 4.8 that FB outperforms the FL, Otsu's and Kwon's approach. It is also evident from Table 3 that the PME is minimum in case of FB approach. Thus, in all the cases the proposed FB approach yielded better results than the FL, Otsu's and Kwon's approach.

4.6 Conclusions

In this chapter, optimal threshold is obtained using the discrete histogram of the original image. For a two class problem, the two dominant modes have been determined and the valley is assumed to exist in between the two peaks. The valley that corresponds to the threshold is found out by PGA based minimization. This scheme produced satisfactory results when the histogram exhibited clear bi-modality with a prominent valley point. When there was overlapping of the class distributions, this method found out a valley point that resulted in increased PME. Therefore, the feature based scheme was proposed, where the threshold is found out in the feature plane that is threshold is determined from the feature histogram. The feature histogram reduces the amount of overlapping of two class distribution as compared to the original histogram. This feature based scheme, could successfully handle overlapping class distribution cases.

Table 4.1: Threshold values and PME for diffrent window size using the FB approach.

Window Size (WS)	Sample Images					
	Image1		Image2		Image 3	
	T	PME	T	PME	T	PME
3x3	107	0.8942	126	0.5748	106	0.4593
5x5	107	0.8942	129	0.5748	119	0.3403
7x7	110	0.8942	127	0.5748	121	0.3403
9x9	116	0.8286	130	0.5748	112	0.0000
11x11	107	0.8942	129	0.5748	114	0.0000
13x13	104	0.8942	108	1.4148	114	0.0000
15x15	110	0.8942	110	1.2904	118	0.3403

Table 4.2: Performance evaluation of Otsu's, Kwon's, FL and FB approaches for two class images.

Sample images	Threshold Selection Methods							
	Otsu's Approach		Kwon's Approach		FL Approach		FB Approach	
	T	PME	T	PME	T	PME	T	PME
Image 1	123	2.8595	122	1.762	114	0.0	116	0.8286
Image 2(SNR 22dB)	121	0.705	119	0.759	119	0.759	111	0.5748
Image 3(SNR 22dB)	126	0.6165	109	0.162	129	0.8240	106	0.2472

Table 4.3: Performance evaluation of Otsu's, Kwon's, FL and FB approaches for three class images.

Sample images	Threshold Selection Methods											
	Otsu's Approach			Kwon's Approach			FL Approach			FB Approach		
	T_1	T_2	PME	T_1	T_2	PME	T_1	T_2	PME	T_1	T_2	PME
Image 4	96	155	11.2503	101	197	76.6708	88	171	13.0600	112	167	5.5298
Image 5	100	160	2.3787	125	127	14.9711	99	154	1.5349	115	140	2.9010

Chapter 5

Minimum Mean Square Error based Feature Less and Feature Based Techniques

5.1 Introduction

Automatic fault detection system has a wide application domain. Specifically, in machine vision system for hazardous situation detection of faults in real-time is indispensable and also challenging. In faulty condition, the detection problem reduces to classification of pixels to healthy pixels or unhealthy pixels corresponding to the fault situations. In this chapter, attempts have been made specifically to develop schemes that would detect earth surfaces cracks in a real image with cracks. A novel scheme has been formulated while minimizing the mean square error (MMSE) of class distributions. Since, the faults could be of small or big size, the histogram distribution becomes complex and loses clear bi-modality without trace of valley. Therefore, the scheme is based on considering the peaks to represent classes and hence need to be detected. The PGA based algorithm of chapter 4 has been used to detect peaks followed by the algorithm to detect the valley to minimize the class distribution error. In this regard, feature less MMSE (FL-MMSE) and feature based MMSE (FB-MMSE) have been proposed to deal with the typical histograms corresponding to the crack images. The proposed algorithms could satisfactory segment different crack images. The proposed MMSE based algorithm have also been tested with other real world images and a typical image for colour blindness. The performance of the proposed algorithms has been found to be superior to that of Otsu and Kwon's method in case

of crack images and the performance is comparable to Kwon's method in case of other real images.

5.2 Brief review of Hui-Fuang's method

The objective of automatic thresholding proposed by Hui-Fuang [91] is to find the valley in the histogram that separates the foreground from the background. For the case of single thresholding, the threshold value exists at the valley of the two peaks (bimodal), or at the bottom rim of a single peak (unimodal). It is observed that the probability of occurrence of the threshold value (p_t) is too small. With this observation Hui-Fuang [91] proposed an improvement to the Otsu's [5] method for selecting threshold values and named it as *valley-emphasis* method. The idea of the valley-emphasis method is to select a threshold value that has a small probability of occurrence (valley in the gray-level histogram), and also maximize the between group variance, as in the Otsu's [5] method. The formulation for the valley-emphasis method is:

$$t^* = Arg \max_{0 \le t \le L-1} (1 - p_t)(w_1(t)\mu_1^2(t) + w_2(t)\mu_2^2(t)). \tag{5.1}$$

Where, $p_i = \frac{n_i}{n}$ represents the probability of occurrence of gray-level i, n_i is the number of pixels with gray-level i, n is the total number of pixels in a given image, $w_1(t) = \sum_{i=0}^{t} p_i$ and $w_2(t) = \sum_{i=t+1}^{L-1} p_i$ are the probabilities of the classes respectively and $\mu_1(t) = \sum_{i=0}^{t} \frac{ip_i}{w_1(t)}$ and $\mu_2(t) = \sum_{i=t+1}^{L-1} \frac{ip_i}{w_2(t)}$ are the mean gray-level values of the two classes.

The key to valley-emphasis formulation made by Hui-Fuang [91] is the application of a weight, $(1 - p_t)$, to the Otsu's [5] criterion function for threshold calculation. The smaller the p_t value, the larger the weight will be. This weight ensures that the result threshold will always be a value that resides at the valley or bottom rim of the gray-level distribution. The valley-emphasis method does not attempt to split a peak in unimodal distribution as the Otsu's method does. A peak in the histogram normally corresponds to a single entity in the image.

Hui-Fuang [91] extended the valley-emphasis method to handle multi-level thresholding. For M-1 level threshold (M class), the optimal thresholds $\{t_1^*, \quad t_2^*, ... \quad t_{M-1}^*\}$ are given as:

$$\{t_1^*, \quad t_2^*, ... \quad t_{M-1}^*\} = Arg \max_{0 \le t_1 < .... < t_{M-1} \le L-1} \left\{ \left(1 - \sum_{j=1}^{M-1} p_{tj}\right) \left(\sum_{k=1}^{M} w_k \mu_k^2\right) \right\}. \tag{5.2}$$

Where, the first term in (5.2) corresponds to the weight.

5.3 MMSE method

In this scheme, we assume object to be one class and rest of the classes (one or more) are assumed to be background. In case of a two class problem, the object and background have distinct class distributions as shown in Fig. 5.1 that depicts two class distributions corresponding to object and background. It is assumed that the two peaks correspond to the mean of the class distributions. Let T denote the threshold selected to distinguish the object and background classes. Because of threshold T, the distribution as shown in Fig. 5.1 is divided into two classes, one to the left of T and the other to the right of T. The class distribution to the left of T may either correspond to object or background and analogously the distribution to the right of T may correspond to either background or object. Let m_{o_T} and m_{b_T} denote the mean value of the object and background class distribution respectively. Let e_o denotes the error in the object class

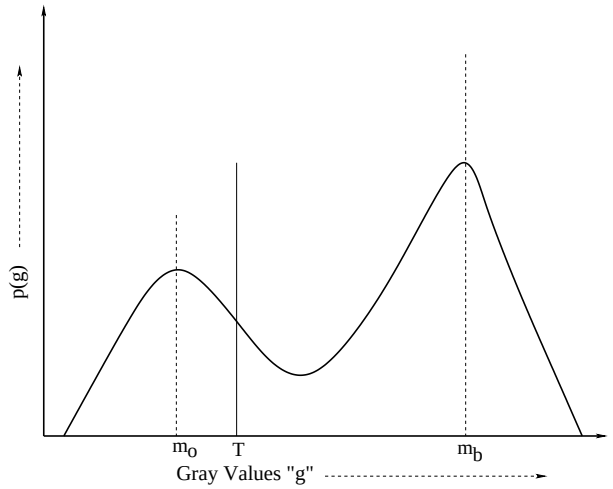

Figure 5.1: Bimodal distribution with the peaks representing the dominant gray value of object and background

occurring due to the selection of threshold T and is defined as $e_o = |(m_{o_T} - m_o)|$. Analogously e_b denotes the error in the background class occurring due to the selection of threshold T and is defined as $e_b = |(m_{b_T} - m_b)|$. Since, the threshold is varried from 0 to maximum gray value G_{max}, the errors are modeled as random variables.

Let e_o and e_b denote the instantaneous values of the random variables $\mathbf{e_o}$ and $\mathbf{e_b}$ respectively. We assume e_o and e_b to be uncorrelated. The total error for both the class distribution at a given time instant k is

$$E[\xi] = E[\mathbf{e_o}(k)] + E[\mathbf{e_b}(k)] \tag{5.3}$$

In order to achieve the optimum threshold, T_{opt}, in the minimum mean square error (MMSE)

sense, the following function needs to be minimized. Assuming $e_o(k)$ and $e_b(k)$ to be uncorrelated

$$\xi(k) = e_o(k) + e_b(k)$$

$$\xi^2(k) = \mathbf{e_o}^2(k) + \mathbf{e_b}^2(k) + 2\mathbf{e_o}(\mathbf{k})\mathbf{e_b}(\mathbf{k}) \tag{5.4}$$

Taking expectation of both sides

$$E[\xi^2(k)] = E[\mathbf{e_o}^2(k)] + E[\mathbf{e_b}^2(k)] + 2E[\mathbf{e_o}(\mathbf{k})\mathbf{e_b}(\mathbf{k})] \tag{5.5}$$

Since $e_o(k)$ and $e_b(k)$ are uncorrelated, $2E[e_o(k)e_b(k)] = 0$

$$E[\xi^2(k)] = E[{e_o}^2(k)] + E[{e_b}^2(k)] \tag{5.6}$$

which can be expressed as

$$E[\xi^2(k)] = E[\mathbf{e_o}^2(k)] + E[\mathbf{e_b}^2(k)]. \tag{5.7}$$

In (5.7), evaluation of the expectation of the individual term is difficult because at k^{th} instant, all possible values of the errors are not available. We consider only the available instantaneous value and hence

$$E[\mathbf{e_o}^2(k)] = \mathbf{e_o}^2(k) \quad and \quad E[\mathbf{e_b}^2(k)] = \mathbf{e_b}^2(k). \tag{5.8}$$

Therefore, (5.7) can be expressed as

$$E[\xi^2(k)] = \mathbf{e_o}^2(k) + \mathbf{e_b}^2(k). \tag{5.9}$$

The optimum threshold value is obtained by minimizing (5.9) with respect to T. Hence, the optimum threshold T_{opt} can be determined as

$$T_{opt} = arg\min_{T} E[\xi^2(k)] \tag{5.10}$$

$$or \quad T_{opt} = arg\min_{T} (\mathbf{e_o}^2 + \mathbf{e_b}^2). \tag{5.11}$$

Substituting ${e_o}^2$ and ${e_b}^2$ in (5.11), it can be written as

$$T_{opt} = arg\min_{T} \{(m_{b_T} - m_b)^2 + (m_{o_T} - m_o)^2\}. \tag{5.12}$$

The optimum value is obtained by the proposed iterative algorithm. The salient steps of the algorithm is as follows.

Iterative algorithm

Step 1 Select m_o and m_b from the PGA based algorithm.

Step 2 Choose an arbitrary initial threshold T. Initialize the error $e^2_{min}$to a large value.

At each time step k, compute the following:

Step 3 Compute $m_{oT}(k)$ and $m_{bT}(k)$ corresponding to the chosen T_k.

Step 4 Compute $e^2_T(k) = \{(m_{oT}(k) - m_o)^2 + (m_{bT}(k) - m_b)^2\}$ or $e^2_T(k) = (e^2_o(k) + e^2_b(k))$.

Step 5 If $e^2_T(k) < e^2_{min}$, then $e^2_{min} = e^2_T(k)$, $T = T_k$; k=k+1; $T_k = T_k + \Delta T$;

else k=k+1, $T_k = T_k + \Delta T$

Step 6 Check if all gray values are exhausted. If "No" Go to Step 3 or If "YES" go to Step 7

Step 7 T denotes the optimum threshold corresponding to the minimum error.

5.4 FL-MMSE

We consider the histogram of the given image. The histogram, depending on the nature of the image, exhibits two dominant niches or modes corresponding to two classes besides other less dominant modes. The distribution thus can be viewed as a nonlinear multimodal function, where each dominant mode corresponds to one class. The PGA based clustering algorithm is used to determine the two modes. This is achieved when the PGA based clustering algorithm maintains stable sub-populations at the respective modes thus forming clusters around the node. The gray value of the histogram corresponding to these clusters are assumed to be the respective means of the two classes. The MMSE based algorithm considers these dominant modes as the means and determines the valley or threshold that minimizes the intra-class classification error.

5.5 FB-MMSE

By and large, the gray level distribution in histogram of noisy scenes have overlapping class distribution. In such situations, the feature less (FL) [144] approach yields approximate results with large percentage of misclassification error. This could be precisely attributed to the error due to the overlapping class distributions. Hence, in this scheme, the feature based histogram

distribution is considered. The feature image is generated as follows. A window of a given size is considered around a pixel and the distributions of the gray values over the window is assumed to be Gaussian. The first moment of this distribution over the window is used as the feature and this is governed by the second moment (variance) of the distribution. With Gaussian assumption it is known that the likelihood estimates of the first and second moment becomes

$$\hat{\mu}_{w_{ij}} = \frac{1}{N_w}\sum_{k=1}^{N_w} x_k \quad and \quad \hat{\sigma}_{w_{ij}} = \frac{1}{N_w}\sum_{k=1}^{N_w}\left(x_k - \hat{\mu}_{w_{ij}}\right)^2. \tag{5.13}$$

The first moment of the pixels is considered as the feature value if the following condition is satisfied.

$$if \quad |x_{ij} - \hat{\mu}_{w_{ij}}| \leq \hat{\sigma}_{w_{ij}}/K \quad then \quad x_{ij} = \hat{\mu}_{w_{ij}}; \tag{5.14}$$

where, K is any positive constant, x_{ij} is the gray value corresponding to the $(i,j)^{th}$ pixel, $\hat{\mu}_{w_{ij}}$ and $\hat{\sigma}_{w_{ij}}$ are the average value and standard deviation of the Gaussian distributed pixels over the window centered at $(i,j)^{th}$ pixel, and N_w is the number of pixels in the window. Thus, another image, consisting of featured pixels is generated. Fig.1(a) shows the histogram of a two class image. It is seen from Fig.1(a) that there are distinct overlapping of the class distributions. The histogram of the featured image, generated using (5.13) and (5.14) is shown in Fig.1(b) that exhibits clear bi-modality with minimum overlapping. Hence, optimal threshold can be determined using Fig.1(b).

The two dominant peaks of the feature histogram are determined by the PGA based crowding algorithm. Using these dominant modes as the means of different classes, in the feature plane, the MMSE based iterative algorithm is used to obtain the valley or threshold in the feature plane. The threshold thus obtained in the feature planes is used to segment the image.

5.6 PGA based algorithm

The steps of the parallelized crowding scheme are the following.

Algorithm

(1) Initialize randomly a population space of size N_p (each element corresponds to a gray value between 0 and 255) and their classes are determined.

(2) Divide the population space into fixed number of sub-populations and determine the class of individuals in each sub-population.

(3) Go through the following steps:

(3.1) In the given sub-population, choose two elements at random for Generalized Crossover (GC) and Mutation operation with crossover probability P_c and mutation probability P_m.

(3.2) Evaluate fitness of each parent and offspring. The fitness function is the featured normalized histogram function $p(g)$ in (3).

(3.3) The tournament selection mechanism is a binary tournament selection among the two parents and two offspring, the set which contains the individual having highest fitness among the four elements is selected to the set of parents for the next generation.

(3.4) Repeat steps 3.1, 3.2 and 3.3 for all the elements in the sub population.

(3.5) Repeat steps 3.1, 3.2, 3.3 and 3.4 for a fixed number of generations

(4) Step 3 is repeated for each sub-population.

(5) Migration is allowed from each deme to every other deme. The individuals are migrated based on the selected migration policy. Numbers of elements to migrate are determined from the selected rate of migrationR_{mig}. The elements migrate with migration probability P_{mig}.

(6) Self Migration is allowed in each deme based on the selected migration policy and selected rate of self-migration R_{smig} with a probability P_{smig}

(7) Repeat Steps 3,4,5 and 6 till convergence is achieved. The algorithm stops when the average fitness of the total population is above pre-selected threshold.

(8) The peaks will be determined from the converged classes of Step 7.

(9) Select the two peaks (for a two class problem) as m_o and m_b.

(10) Consider the normalized histogram of the image. Choose an arbitrary initial threshold T. Initialize the error $e^2_{min}$to a large value.

At each time step k compute the following:

(11) Compute $m_{oT}(k)$ and $m_{bT}(k)$ corresponding to the chosen T_k.

(12) Compute $e_T^2(k) = \{(m_{oT}(k) - m_o)^2 + (m_{bT}(k) - m_b)^2\}$ or $e_T^2(k) = (e_o^2(k) + e_b^2(k))$.

(13) If $e_T^2(k) < e_{min}^2$, then $e_{min}^2 = e_T^2(k)$, $T = T_k$; k=k+1; $T_k = T_k + \Delta T$;

else k=k+1, $T_k = T_k + \Delta T$

(14) Check, if all gray values are exhausted. If "No" Go to Step 3 or If "YES" go to Step 7

(15) T denotes the optimum threshold corresponding to the minimum error.

5.7 Results and discussions

The proposed MMSE based methods such as FL-MMSE and FB-MMSE have been validated with real images having typical histograms. The potentiality of the proposed MMSE based method has been tested with images of earth surface cracks and the corresponding histograms possess either unimodal trend or have many misleading modes. Firstly, in this section the results corresponding to general images have been analysed followed by the next section that deals with specifically crack images. Besides, in this section we test with a typical colour image.

5.7.1 Real and synthetic images

The real and synthetic images considered for this section are shown in Fig. 5.2(a), (b), (c), and (d) and the corresponding manually constructed ground truth images are shown in Fig. 5.2(e), (f), (g), and (h) respectively. All these images belong to two class problem, for example, the first image is a plate image having to class, the second image is a table lamp image exhibits two class, the third image which is a hanging light (ceiling light) image is also a two class image. The last image is a typical synthetic image used for detection of colour blindness. This image has been selected because of the typical nature of its histogram distribution. The first image considered is the plate image as shown in Fig. 5.3(a) and the corresponding histogram is shown in Fig. 5.3(b). In this case, the histogram has a flat valley and unequal size of object and background distribution. We have employed the FL-MMSE scheme to test this image. The two peaks of the histogram has been detected by the PGA based algorithm. This is tested for, both the without self-loop based and self-loop based interconnection models. The performance of the PGA is also compared with that of GA. The parameters of GA are: Generation=1000,

Probability of Crossover $P_c = 0.8$, Probability of Mutation $P_m = 0.001$, population size $N_p = 400$. The chosen parameters of PGA are: Generation=1000, Migration period is 10 generations, Number of demes is 4, Probability of Crossover $P_c = 0.8$, Probability of Mutation $P_m = 0.001$, population size $N_p = 400$, Probability of migration $P_{mig} = 0.8$, Migration rate $R_{mig} = 4\%$,, Probability of self migration $P_{smig} = 0.8$ and Self migration rate $R_{smig} = 2\%$.

The two peaks of the histogram of Fig. 5.3(b) have been detected by PGA/ GA based peak detection method of chapter 4. The population of elements clustered around the peaks have been shown by "X" in Fig 5.2(b). The proposed MMSE based methods have been used to detect the threshold and the threshold has been found to 108. The threshold values determined by Otsu and Kwon method are 121 and 122 respectively. These threshold values are tabulated in Table 5.1. The segmented images obtained by FL-MMSE method is shown in Fig. 5.2(i) where it can be observed that the edge of the white circle could not be preserved properly and hence the percentage of misclassification error (PME) is found to be 1.3. As seen from Fig 5.3 (g) and (h) the edge pixels of the inner white circle has been preserved properly and hence, the PME is 0.6 in both the cases. The two classes have been classified properly. Hence, Otsu and Kwon method classified the plate image properly and the performance of the proposed MMSE based approach is close to that of Kwon and Otsu's method. For the two classes, the convergence of GA and PGA has been analysed. Fig. 5.3(c) and 5.3(d) show the convergence of class-A and class-B respectively and from Fig. 5.3(c) it can be seen that the PGA converged around 50 generations, whereas GA converged at 1000 iterations. Similarly, for class-B, PGA converged at around 70 generations while GA converged at 400 generations. Thus, in both the case, PGA converged much faster than that of GA.

The second image considered is the Table lamp image as shown in Fig. 5.4(a). In this case, the feature image has been generated and corresponding histogram is shown in Fig. 5.4(b), where it can be observed that there are many small misleading modes and the valley is not precisely defined. The PGA based scheme could detect the peaks as shown by "X". The corresponding valley point is detected by MMSE method and is shown as dotted line in Fig. 5.4(b). The threshold, thus found by MMSE method is 122 where as the thresholds found by Otsu and Kwon method are 123 and 122 respectively. Since, the threshold are found to be either same or very close to each other, the segmented results are also almost close to each other. The segmented results for Otsu, Kwon and MMSE methods are shown in Fig. 5.4(g), (h) and (i) respectively. As observed from these figures, there are some misclassified pixels near the right

corner edge of the table. The misclassification is observed in all these three cases and in case of Fig. 5.4(g), there are additional misclassified pixels near the base of the rod on the table. Because of this additional pixels, PME for Otsu is 2.9 which is higher than that of Kwon and MMSE, which is 1.8. Analogous to the previous case also, PGA for class A and B converges faster than that of GA. This phenomenon may be observed in Fig. 5.4(c) and (d) respectively. The effect of self-loop model on the rate of convergence has been demonstrated in Fig. 5.4(e) and (f), where it can be observed that use of self-loop (SL) model made the algorithm converge faster than that of use of without self-loop (WSL) model. Of course, there is no radical change in the rate of convergence but there is some improvement in the final convergence of the algorithm.

Similar observations have also been made for the hanging light (ceiling lamp) image as shown in Fig. 5.5(a). This FB-MMSE based algorithm has been applied to this image. The feature image has been generated using the feature pixels and the corresponding histogram is shown in Fig. 5.5(b). Since, the background occupies more portions of the image and the light portion is small corresponding to background, is more prominent than that of the foreground portion. The proposed PGA based scheme could detect the peaks shown as "X" and the MMSE based scheme detected the valley point shown as dotted line. The corresponding threshold is 107, where as the thresholds found by Otsu's and Kwon's method are 116 and 107 respectively. These thresholds have been used for segmentation. The segmented results are shown in Fig. 5.5(g), (h), and (i) and it may be observed from Fig. 5.5(g) that the portion of the rod joining the lamp has been missing because of misclassification and also the portion of rod joining the wall is also missing. The right edge of the reflector has been distorted. But in case of Kwon and MMSE method, the portion of the rod joining the reflector has been properly segmented the sharpness of the edges in case of the MMSE method is better than that of Kwon's method. This effect has also been reflected in the PME values tabulated in Table 5.2. PME in case of Otsu's method is higher than that of Kwon's and MMSE method. As far as the convergence of the algorithm is concerned, PGA for class-A is found to converge around 70 iterations while GA converges at around 1000 generations and for class-B also PGA converges at around 70 iterations. Thus PGA converges much faster than that of GA. Furthermore, it has also been found that use of self-loop based interconnection model made the algorithm to accelerate faster towards the converged solution than that of the without self-loop case. This effect may be observed from Fig. 5.5(e) and 5.5(f). Thus, in this example also FB-MMSE produced result

close to that of Kwon's method.

The next image considered is a synthetic image shown in Fig. 5.6, which is used for detection of colour blindness. It has been found out that both Otsu and Kwon's methods produce very poor results while FL-MMSE, and FB-MMSE methods produce very promising result. This example clearly demonstrates the efficacy of the proposed FB-MMSE based method. The histogram of the colour blind image is shown in Fig. 5.6(b), where it may be observed that there is very small mode with very small area of distribution, and the other one is not very prominent. There is hardly any valley observed between these two modes. The feature histogram shown in Fig. 5.6(c), where the modes have been enhanced. The peaks detected by PGA are shown and the valley is found to be at 37 and FL-MMSE method determined the same threshold. The peaks are at different positions as shown in Fig. 5.6(c). The threshold found by Otsu and Kwon's method are 169 and 148 and are tabulated in Table 5.1. The segmentation obtained by these thresholds are shown in Fig. 5.6(j), (k) and (l) and it is clearly observed that the image could not be segmented and the object, that is "12", could not be detected. The PME for Otsu's and Kwon's cases are also high i.e. 17.4, 22.6. Fig. 5.7(j) and 5.7(k) show the segmented image obtained by FL-MMSE and FB-MMSE approach and it can be observed that the image could be segmented properly and accordingly the PME for both the cases and FB-MMSE is 0.2. Thus FL-MMSE method could segment the image properly while FB-MMSE, Otsu and Kwon's method failed to segment this image. The effect of PGA over GA has been demonstrated in Fig. 5.6(d) and (e). Analogous to previous cases, the self-loop model converged faster than that of without self-loop model. This is demonstrated in Fig. 5.6(f) and 5.6(g). This effect of FL-MMSE and FB-MMSE on these four images have been shown in Fig. 5.7. Fig. 5.7(a) and Fig. 5.7(d) have been segmented by FL-MMSE, while Fig. 5.7(b) and (c) have been segmented by FB-MMSE method. The corresponding histograms with detected peaks and valleys are shown in Fig. 5.7(e), (f), (g), and (h). The segmented images are shown in Fig. 5.7(i), (j), (k), and (l) and it can be seen from these figures that the images could be properly segmented by MMSE method. Thus, MMSE based scheme proved to be more effective than that of other proposed schemes. Moreover, MMSE based method, besides segmenting real world two class images, could also segment the typical image for colour blindness. This demonstrates clearly the efficacy of the proposed MMSE based schemes.

The performance of MMSE based scheme has also been compared with that of Otsu and Kwon's method for all these images shown in Fig. 5.8. The ground truth images have been

provided for ease of reference. Fig. 5.8(a), (b), (c), and (d) show the ground truth images. Fig. 5.8(e), (f), (g), and (h) show the results by Otsu's method and Fig. 5.8(i), (j), (k), and (l) show the results by Kwon's method and Fig. 5.8(m), (n),(o), and (p) show the results by MMSE method. It may be observed from these figures that for the first image, Otsu's method could produce result comparable to that of Kwon's and MMSE method. For the table lamp and ceiling light image, Kwon's and MMSE method produced results superior to that of Otsu's method. But in case of colour blindness image, only FL-MMSE method could segment properly while Otsu's and Kwon's method and FB-MMSE failed to produce satisfactory results.

Thus, it has been demonstrated with different examples that the proposed MMSE method could prove to be effective for real world image and also typical synthetic images, where other methods failed to segment the image.

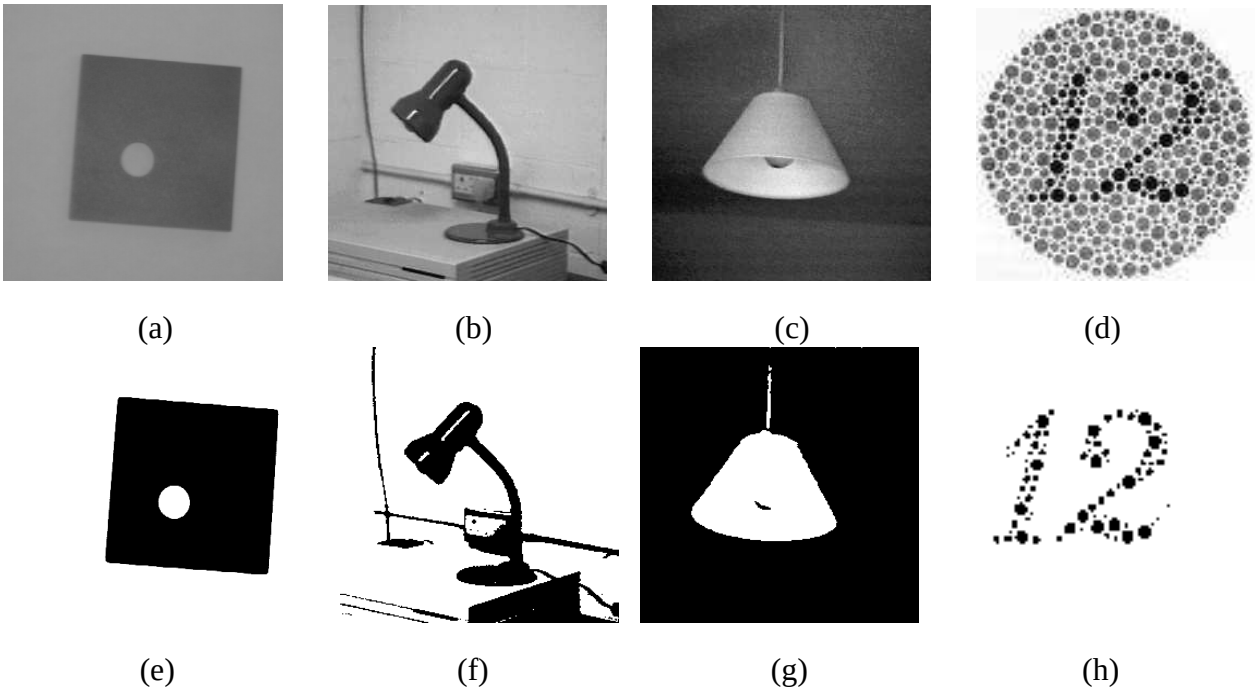

Figure 5.2: (a) Image 1; (b) Image 2; (c) Image 3; (d) Image 4; (e) Ground trouth (GT) of image 1; (f) GT of image 2; (g) GT of image 3; (h) GT of image 4.

5.7.2 Earth surface crack images

In simulation, we have considered a wide variety of cracks, whose gray level histograms exhibit misleading modes that would have been classified as classes by classical thresholding approaches. Specifically, four typical images have been considered with the following attributes, (i) fine and coarse cracks with edges, (ii) cracks partitioning the image with apparent granules

Table 5.1: Threshold values obtained by Ostu's, Kwon's and MMSE approach for real and synthetic images

Sample Images	Peaks and Threshold values using the MMSE method		
	Ostu	Kwon	MMSE
Image 1	121	122	108
Image 2	123	122	122
Image 3	116	107	107
Image 4	169	148	37

Table 5.2: Performance evaluation of Otsu's, Kwon's, and proposed MMSE approachs.

Sample Images	Threshold Selection Methods		
	Otsu's	Kwon's	MMSE
	PME	PME	PME
Image 1	0.6	0.6	1.3
Image 2	2.9	1.8	1.8
Image 3	0.4	0.2	0.2
Image 4	17.4	22.6	0.2

of different sizes, (iii) cracks creating very small and large granules, and (iv) large size granules with shades apparent to be cracks.

Feature less approach

Fig. 5.9(a) shows the crack surfaces with fine and coarse cracks. The corresponding gray level histogram is shown in Fig. 5.9(b), where two modes are prominent and a third mode is present with less prominence. A classical peak search mechanism would have identified three peaks and accordingly two valleys corresponding to two thresholds. This in turn would have segmented the image into three classes as opposed to the existing two classes. The histogram of Fig. 5.9(b) is discrete in nature and hence, we have devised the PGA based clustering to detect the peaks. The parameters of PGA are: number of demes=4, population size=400, probability of migration P_{mig}= 0.1, probability of self-migration P_{smig}= 0.1, probability of crossover P_c= 0.8, and probability of mutation P_{mut}= 0.001. Migration from deme to deme takes place after every 10 generations, and the percentage of migration R_{mig} is 4% and the percentage of

self-migrationR_{smig} is 4%. With increase in the number of generations, the proposed PGA converged to two peaks as shown by 'X' that indicates the point of convergence of population of elements. The number of population of elements that converged in the first and second peak are 25 and 155 respectively. Thus, stable sub-populations are maintained resulting in different classes. In this case, as observed from Fig. 5.9(b), 'X' denotes the convergence of stable sub-population at peaks corresponding to two classes denoted as 'A' and 'B'. Thereafter, PGA is used to search the valley point and hence, the '*' corresponds to the convergence of the total number of population elements. The threshold is found to be at a gray value of 56. The convergence of the population of elements of PGA for class A and Class B is shown in Fig. 5.9(c) and 5.9(d). As expected, the PGA based algorithm converges much faster than GA. It is also observed that the self loop PGA model accelerates the convergence as opposed to that without self-loop PGA model. This phenomenon is evident from Fig. 5.9(e) and 5.9(f). The segmented image, as obtained using the threshold of 56, is shown in Fig. 5.9(g), where it can be observed that the fine cracks could be obtained together with the coarse cracks. The fine cracks are detected as thin dark lines, whereas the coarse cracks of right side have been detected with dark patch. However, the cracks appear as black while the non-crack portion appears as white. The left portion of the image has no cracks and hence, assumed one class appearing as "white" as shown in Fig. 5.9(g). The result obtained by FL method is compared with that of Otsu's, Kwon's and Hui-Fuang's method. The threshold obtained by Otsu's method is 114 while the threshold by Kwon's method is 79. The segmented image by Otsu's method is shown in Fig. 5.9(h), where it is observed that the fine cracks in the mid portion could be detected while the left portion has been misclassified as crack pixels. It is to be noted that the left side of the original image contains no cracks but edges. A ground truth image has been constructed manually and the misclassification error is computed based on this ground truth image. The misclassification error by Otsu's method is 18.45$\%$ while the error due to FL is 1.52$\%$. Fig. 5.9(i) shows the segmented results obtained by Kwon's method and the percentage of misclassification error (PME) is 0.781$\%$. As observed, Kwon's method in this case yielded good results. Fig. 5.9(j) shows the results obtained by Hui-Fuang method, and the threshold is 84 and this method produced appreciable result with 1.54$\%$ of misclassification error. Thus, PGA based FL approach produced better results than that of Otsu's but comparable to Kwon's approach but the result by Hui-Fuang's method is comparable to FL approach.

Feature based approach

The proposed Feature Based(FB) approach is tested with the same crack image as shown in Fig. 5.10(a). Gray level histogram is shown in Fig. 5.10(b). A window size of 3x3 has been used to determine the features and value of K in (6) is selected to be 3. The feature histogram is shown in Fig. 5.10(c) and the peaks detected are shown as ”x”. The valley corresponding to the threshold is found to be at 58, which is very close to 56 as determined by FL method. It may be observed from the feature histogram that the second mode, which was less prominent in Fig. 5.10(b) becomes predominant and, however, the 1st mode, which was less prominent as compared to the third mode become more prominent because of the feature selection. This first mode corresponds roughly to the cracks of the images. Therefore, the feature helps the modes to be more prominent to be detected by the clustering algorithm. In the FB approach also, for both class A and Class B, PGA converged faster than of GA. This is shown in Fig. 5.10(e) and Fig. 5.10(f). The self-loop introduced in the PGA model has intra-deme migration besides inter-deme migration. This employs good-bad migration policy and hence, accelerates convergence. This phenomenon is evident from Fig. 5.10(g) and (h). Thus, the proposed interconnected PGA model converges faster than that of PGA model without self-loop. The segmented image obtained using the threshold is shown in Fig. 5.10(i), where both fine as well as coarse cracks could be detected. Here, the black edges corresponds to fine cracks and the black portion on the right hand side correspond to the coarse cracks. The left side in the original image has no cracks but edges and hence, the FB approach could detect the cracks as opposed to the edges. The results obtained by Otsu’s, Kwon’s and Hui-Fuang’s method are produced in Figs. 5.10(j), 5.10(k) and 5.10(l) for the case of comparison. In case of Otsu’s method, edges have been misclassified as crack pixels.

FL-MMSE and FB-MMSE approach

It has been observed from the previous examples that the proposed FL and FB methods could detect the cracks but need further improvement in performance. In order to improve the performance, threshold is detected by the proposed MMSE approach rather than the earlier GA based approach. The four different crack images as shown in Figs. 5.11(a), (b), (c) and (d) are considered to test the MMSE approach. The 2nd image is different from the first one in the sense that all the edges are cracks only, whereas in Fig. 5.11(a) there are edge pixels those are not cracks

but edges. The third image as shown in Fig. 5.11(c) has very fine cracks and some fine edge pixels. This inturn results in small and large granular appearance in the surface. The fourth image considered is shown in Fig. 5.11(d). As observed, this image has fine as well as coarse cracks and a shaded portion that appears like cracks and hence, serves as a typical example. The corresponding histograms of these images are shown in Figs. 5.11(e), (f), (g) and (h). As seen from these histograms, there are misleading modes in case of the first image and the fourth image. The detected peaks for these images are shown as 'X'. The valley corresponding to the thresholds are determined by the proposed MMSE approach. The thresholds obtained by this method are 60, 12, 37 and 51. As observed from Table. 5.3, threshold for image 1 is 60, which is close to that of the FL and FB methods using PGA based search for minimum value. Fig. 5.11(f), the histogram of the second image, exhibits two modes, which are unevenly distributed in the histogram. The PGA based valley seeking algorithm yielded a threshold of 60 while the MMSE based approach yielded a threshold of 12. The segmented image using this threshold could detect cracks precisely. Similar observations are also made for the third and fourth image as shown in Figs. 5.11(g) and 5.11(h). In case of the fourth image with large granules, the threshold obtained by MMSE approach is 51 as opposed to 72 in case of PGA based minimum search. The segmented images are shown in Figs. 5.11(i), (j), (k) and (l). As seen, the fine as well as coarse cracks could be detected in case of images 1, 2 and 3. But for image 4, the coarse and fine cracks could be detected with the shades appearing as crack, which may be observed in Fig. 5.11(e).

The above problem in case of fourth image could be ameliorated by the proposed FB based MMSE approach. In order to obtain feature image and in turn feature histogram, the window size for the first image was considered as 3x3. The corresponding feature histogram, as shown in Fig. 5.11(m) shows prominent modes and the peaks detected are same as FL approach. The MMSE approach determined the threshold to be at 52 and the corresponding segmented image is shown in Fig. 5.11(q). Since, the threshold value is close to that of FL approach, the segmented image is almost close to that of FL approach and hence, the percentage of misclassification is 1.74 as given in Table 5.4. The feature histograms for 2nd and 3rd images are shown in Figs. 5.11(n) and (o) and in these cases also the modes corresponding to different classes are prominent. The window size used to generate the feature image and histogram for 2nd and 3rd images is 31x31 and K is 4. The thresholds determined are different from that of FL approach but they are close to each other. The segmented images obtained could detect the thin cracks

as shown in Figs. 5.11(r) and 5.11(s). In case of the fourth image, the modes in the feature histogram are predominant and the MMSE based approach detected the threshold to be 46. Here the window size used to generate the feature image and histogram is 3x3 and K is 4. The segmented image obtained using this threshold, could eliminate the shades partially and in turn reduced the misclassification error from 2.5% to 0.83%. Thus, FB-MMSE approach has been found to produce better results than that of FL-MMSE. For the sake of comparison, Fig. 9 shows all the segmented images obtained by different methods. As observed from these figures, Otsu's and Know's method failed to detect the cracks in 2nd, 3rd and 4th image. As seen from 3rd and 4th row, there are many misclassified pixels and the shades appear like cracks. In case of the fourth image with large granules and shades, the shades are falsely detected as crack pixels. The results presented in the fifth row correspond to the results obtained by Hui-Fuang's [91] approach for fault detection. For the first image, the result obtained is appreciable but for 2nd, 3rd and 4th image, there are many misclassified pixels. As seen in the 2nd image, many background pixels have been misclassified while in 3rd image many crack pixels as well as background pixels have been misclassified. In case of 4th image, besides cracks, there are shades in the background of the image. As seen from Table 5.4, the misclassification errors for 2nd, 3rd and 4th images are much higher as compared to our proposed methods of FL-MMSE and FB-MMSE. Even though FL and FB approach could detect the cracks in case of 2nd and 3rd image, the shaded part was present. FB-MMSE approach could detect the cracks properly while eliminating the shaded portion in the image. This is also reflected in the percentage of misclassification error as given in 5.4. Thus, FB-MMSE approach could be the best choice among Ostu's, Kwon's, Hui-Fuang's and other proposed methods.

Table 5.3: Threshold values for different approaches

Sample Images	Threshold Selection Methods						
	Otsu's	Kwon's	Hui-Fuang's	FL	FB	FL-MMSE	FB-MMSE
	T	T	T	T	T	T	T
Image 1	114	79	84	56	58	60	52
Image 2	110	125	104	60	60	12	15
Image 3	108	117	102	31	58	37	32
Image 4	114	120	106	72	73	51	46

Table 5.4: Performance evaluation of Otsu's, Kwon's, Hui-Fuang's, FL, FB and new proposed approaches for crack detection

Sample Images	Threshold Selection Methods						
	Otsu's	Kwon's	Hui-Fuang's	FL	FB	FL-MMSE	FB-MMSE
	PME	PME	PME	PME	PME	PME	PME
Image 1	18.45	0.781	1.54	1.52	1.302	1.16	1.74
Image 2	22.932	30.7881	14.11	8.232	8.232	4.5	3.5
Image 3	17.51	22.6	15.0	28	4.5	3.1	2.8
Image 4	14.44	16.11	12.51	6.964	7.1	2.5	0.83

5.8 Conclusions

In this chapter, two schemes namely FL-MMSE and FB-MMSE have been proposed for classifying object and background. Specifically, the schemes have been proposed to detect cracks of earth surfaces. In the crack images, the pixels have to be classified as either unhealthy pixels corresponding to cracks and others are healthy pixels. Often, the edge pixels of images appear like cracks and have been classified as healthy pixels. The histogram of such crack images either tends to uni-modal or almost uni-modal. Under such circumstances methods such as Otsu's, Kwon's and the proposed methods of chapter 4 produced unsatisfactory results, where as MMSE based method could segment the images properly. Similarly, for typical image of colour blind image, MMSE method could produce promising result where other methods fail to segment. Thus, the proposed MMSE based method yielded satisfactory results for typical images and other general real world images. This scheme can be used for detection of faults in images representing faulty conditions of environment.

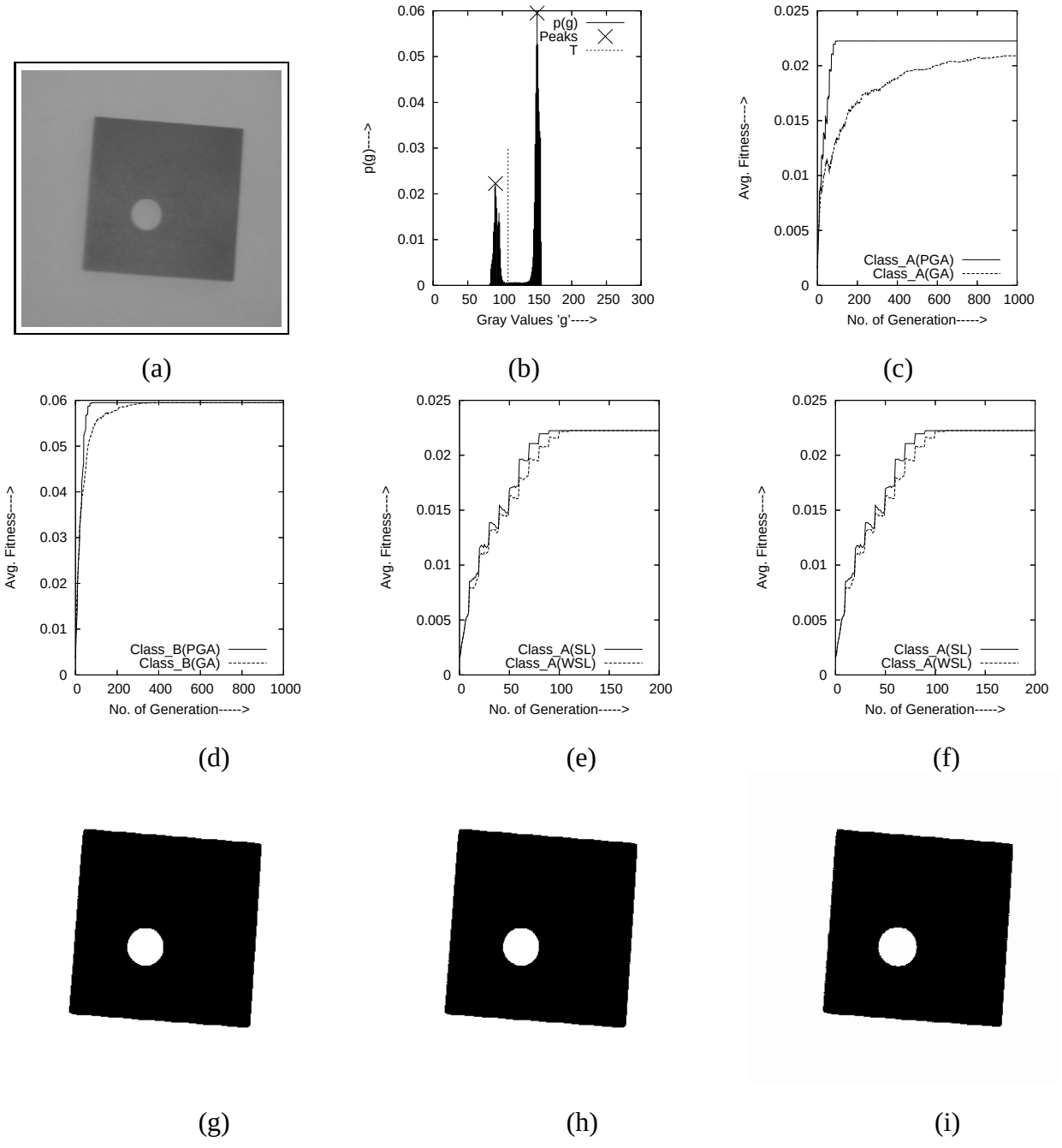

Figure 5.3: (a) Original Image 1; (b) Histogram of original image with detected peaks and threshold; (c) Avg. fitness vs generations of class “A” PGA and GA; (d) Avg. fitness vs generations of class “B” PGA and GA; (e) Avg. fitness vs generations of class “A” with self loop (SL) and without self loop(WSL); (f) Avg. fitness vs generations of class “B” with self loop (SL) and without self loop(WSL); (g),(h) and (i) shows segmented image using Otsu’s, Kwon’s and proposed MMSE method respectively

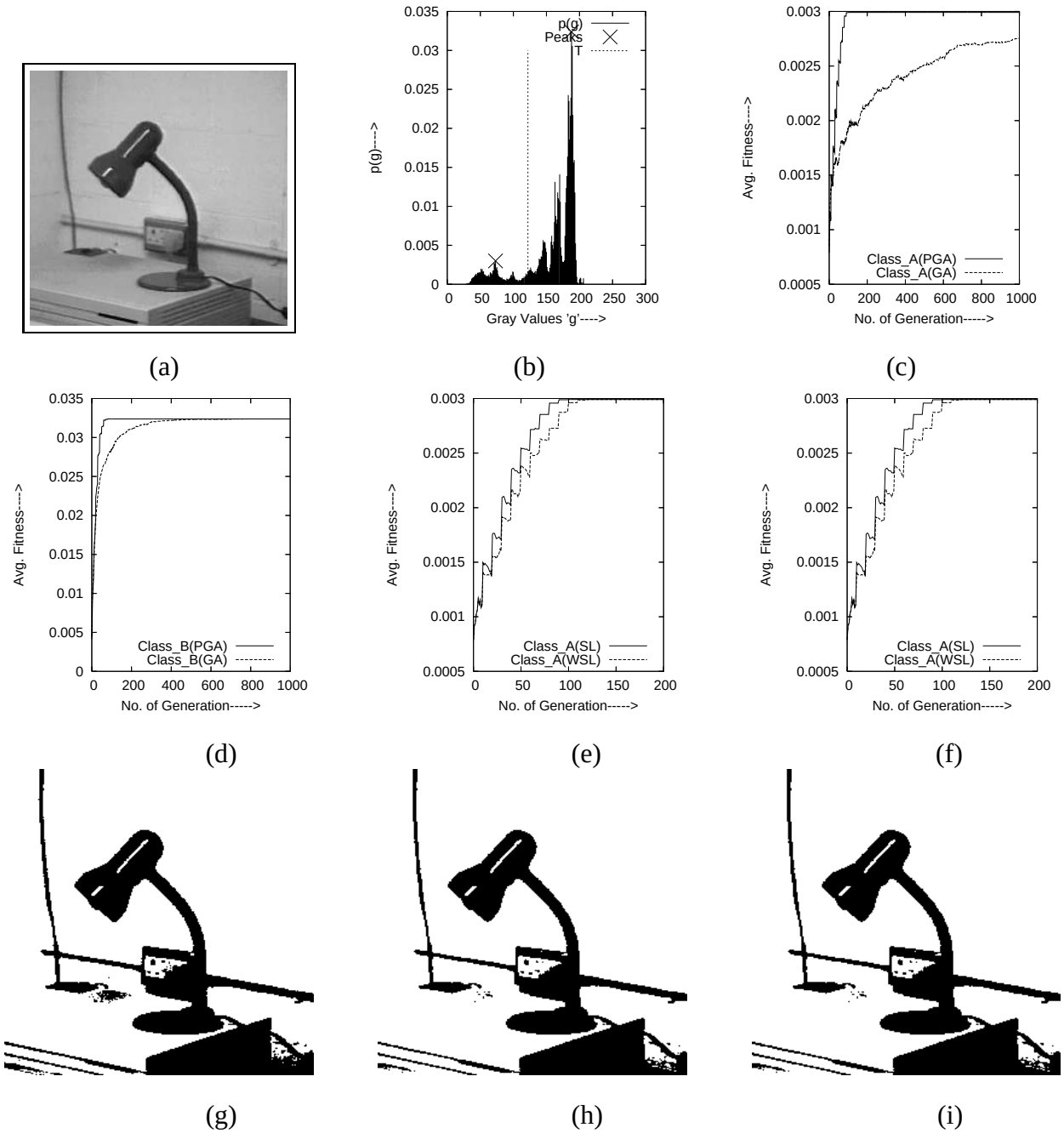

Figure 5.4: (a) Image 2; (b) Featured histogram with detected peaks and threshold; (c) Avg. fitness vs generations of class “A” PGA and GA; (d) Avg. fitness vs generations of class “B” PGA and GA; (e) Avg. fitness vs generations of class “A” with SL and WSL; (f) Avg. fitness vs generations of class “B” SL and WSL; (g),(h), and (i) shows segmented image using Otsu’s, Kwon’s, and proposed MMSE method respectively

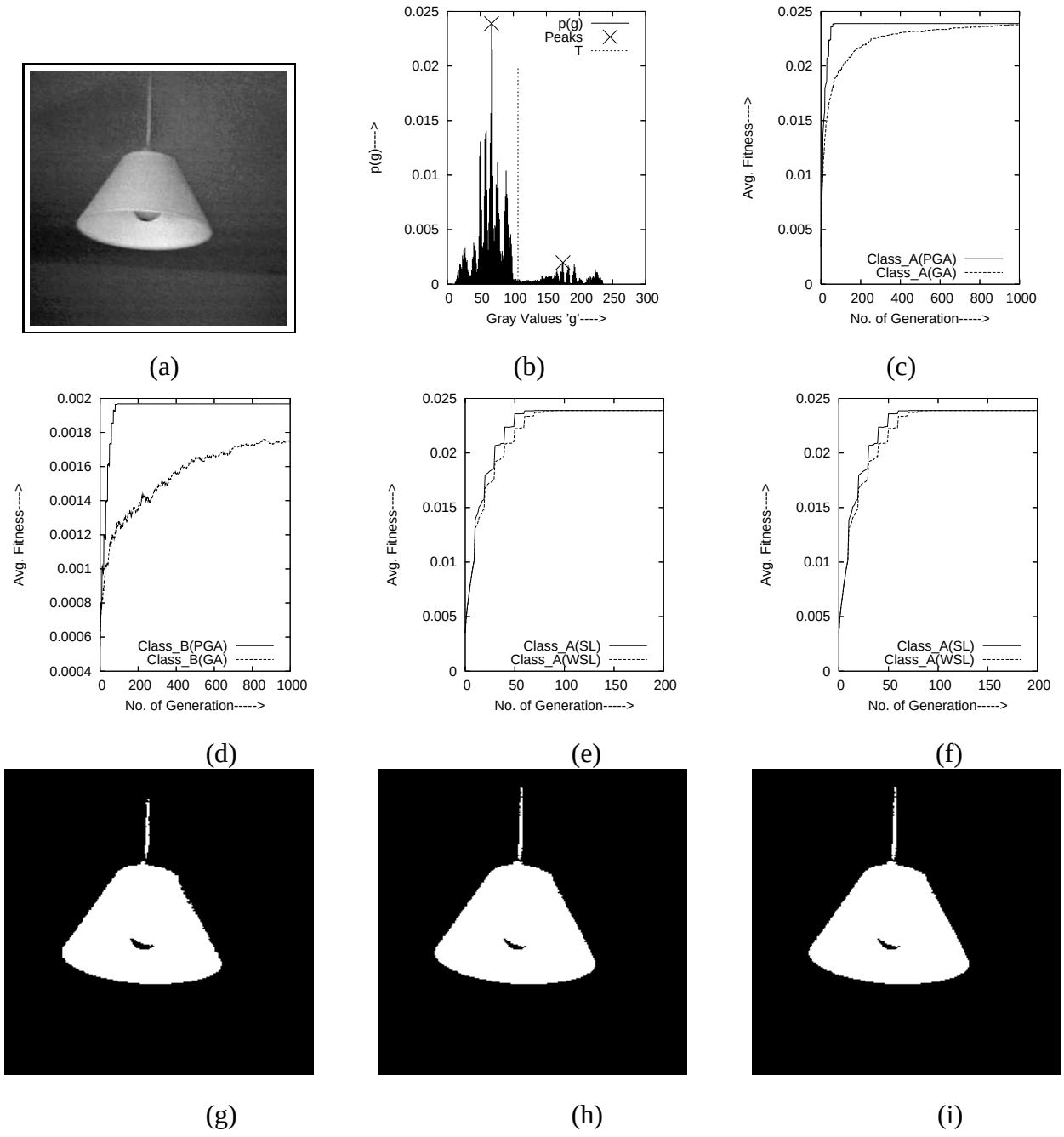

Figure 5.5: (a) Image 3; (b) Featured histogram with detected peaks and threshold; (c) Avg. fitness vs generations of class “A” PGA and GA; (d) Avg. fitness vs generations of class “B” PGA and GA; (e) Avg. fitness vs generations of class “A” with SL and WSL; (f) Avg. fitness vs generations of class “B” with SL and WSL; (g), (h), and (i) shows segmented image using Otsu’s, Kwon’s, and proposed MMSE method respectively

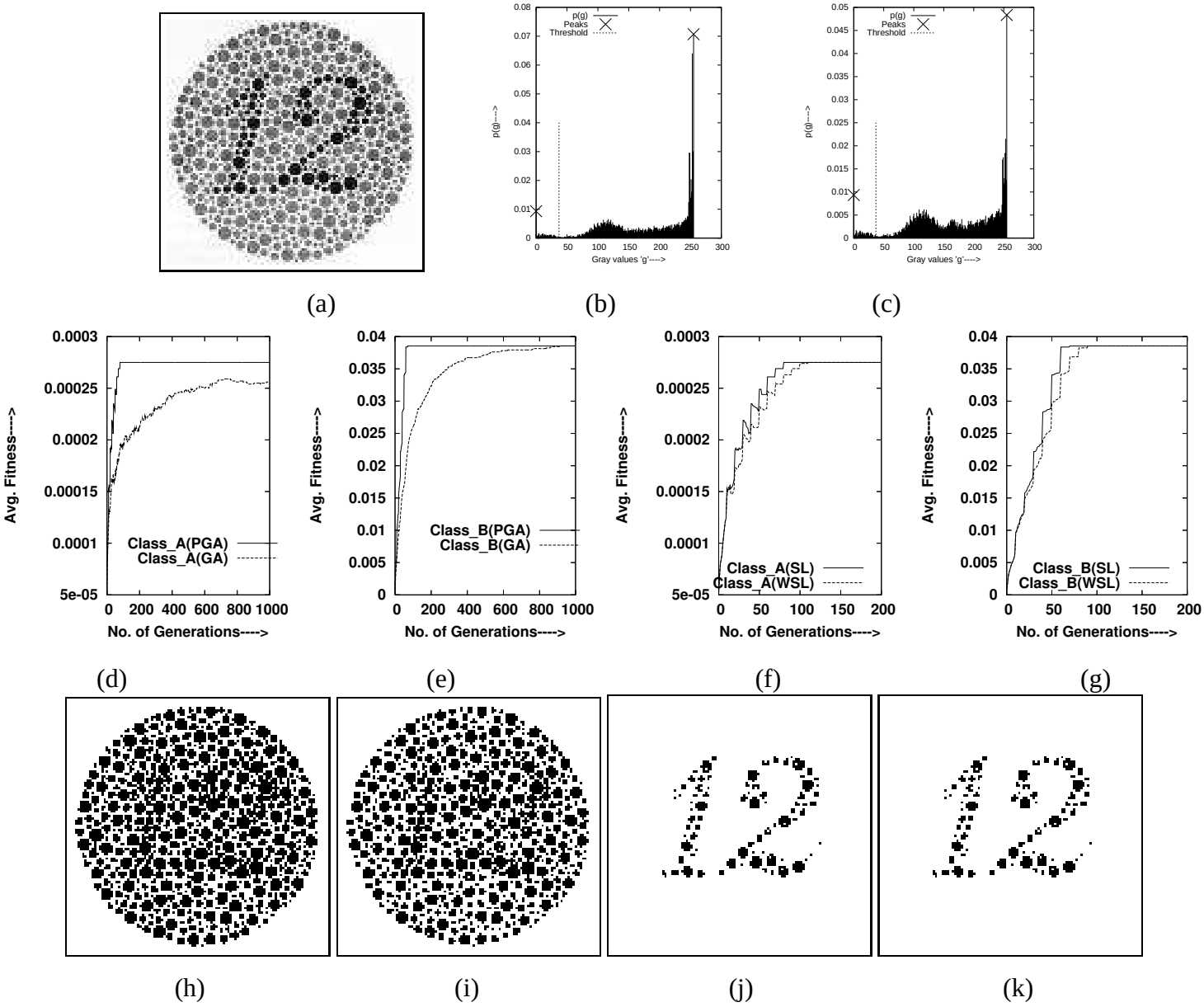

Figure 5.6: (a) Image 4; (b) Original histogram with detected peaks and valley; (c) Featured histogram with detected peaks and valley; (d) Avg. fitness vs generations of class “A” PGA and GA; (e) Avg. fitness vs generations of class “B” PGA and GA; (f) Avg. fitness vs generations of class “A” with SL and WSL; (g) Avg. fitness vs generations of class “B” with SL and WSL; (h), (i), (j), and (k) shows segmented images using , Otsu’s, Kwon’s, FL-MMSE, and FB-MMSE method respectively

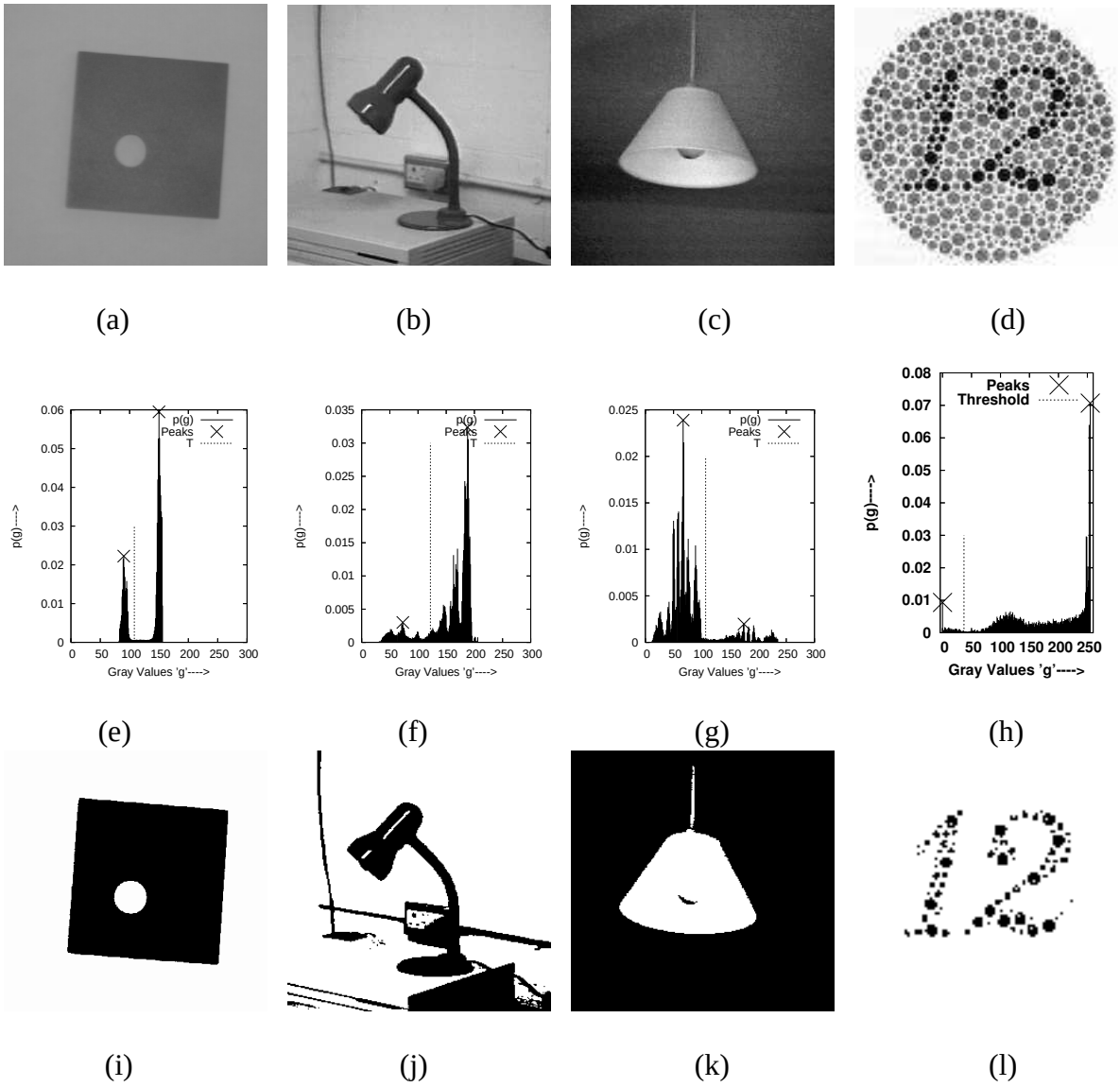

Figure 5.7: (a) Origina image 1; (b) Original image 2; (c) Original image 3; (d) Original image 4; (e) Detected peaks and threshold in the histogram for image 1; (f) Detected peaks and threshold in the histogram for image 2; (g) Detected peaks and threshold in the histogram for image 3; (h) Detected peaks and threshold in the histogram for image 4; (i) Segmented image of image 1 using MMSE method; (j) Segmented image of image 2 using MMSE method; (k) Segmented image of image 3 using MMSE method; (l) Segmented image of image 4 using the proposedMMSE method.

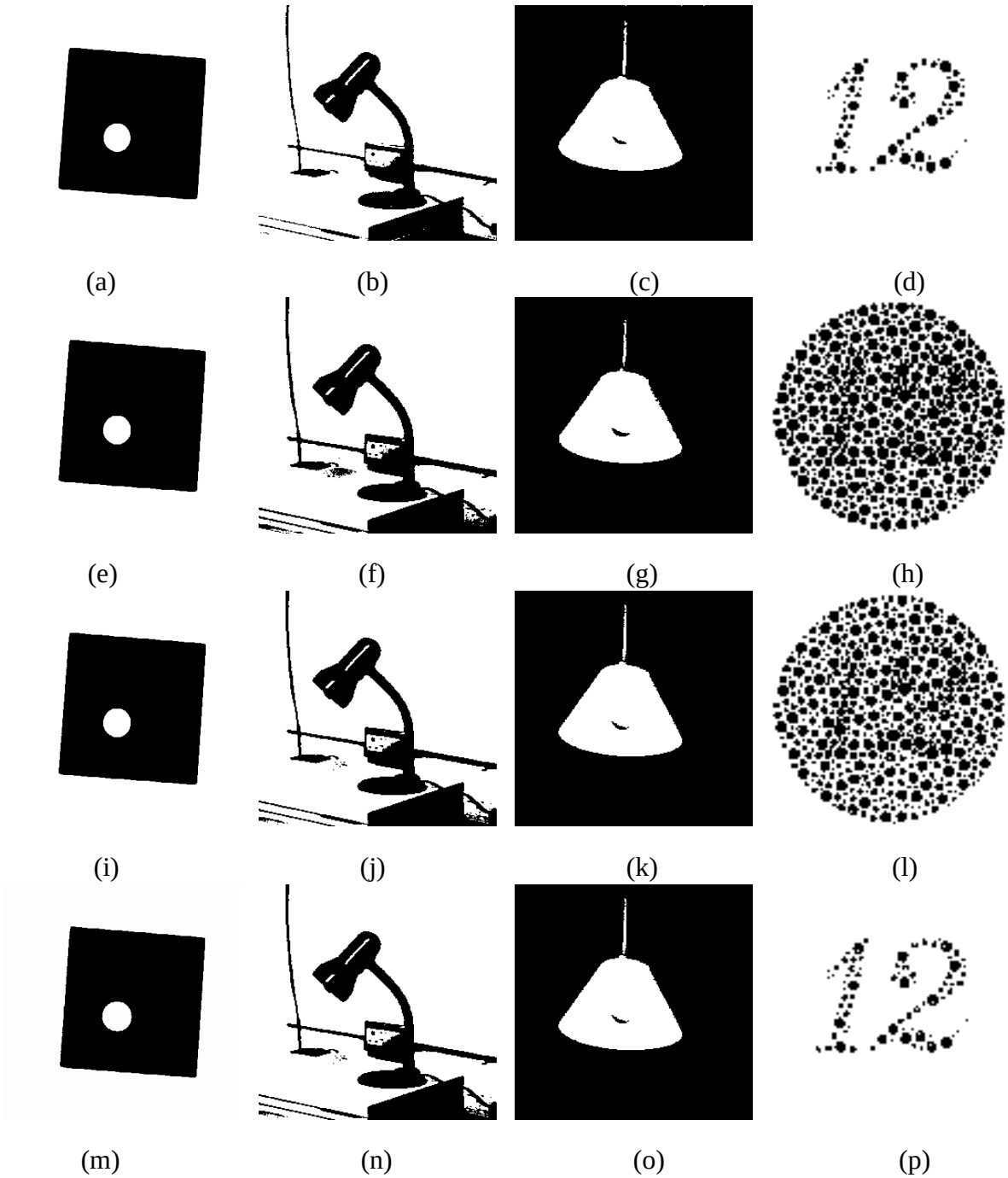

Figure 5.8: (a), (b), (c) and (d) shows the ground trouth image of image 1, image 2, image 3 and image 4; (e), (f), (g) and (h) shows the segmented image of image 1, image 2, image 3 and image 4 using the Otsu's method; (i), (j), (k) and (l) shows the segmented image of image 1, image 2, image 3 and image 4 using the Kwon's method; (m), (n), (o) and (p) shows the segmented image of image 1, image 2, image 3 and image 4 using the proposed MMSE method.

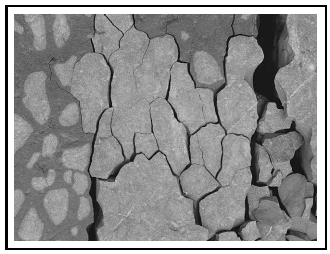

(a)

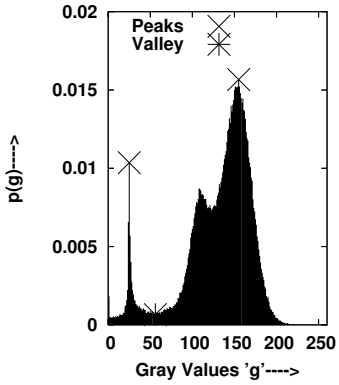

(b)

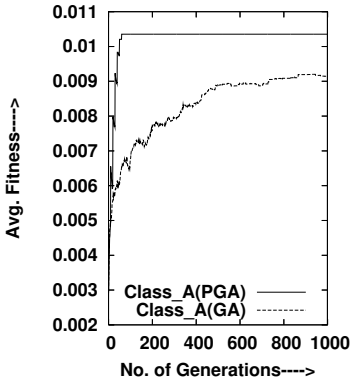

(c)

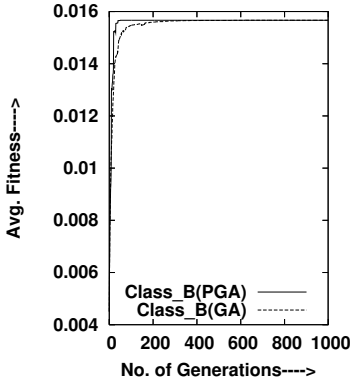

(d)

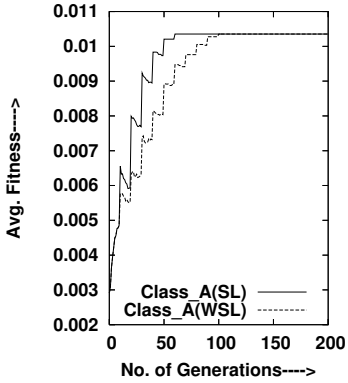

(e)

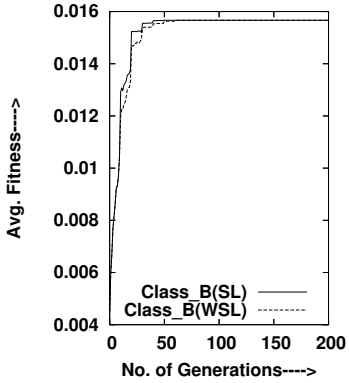

(f)

(g)

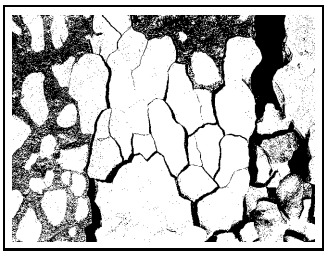

(h)

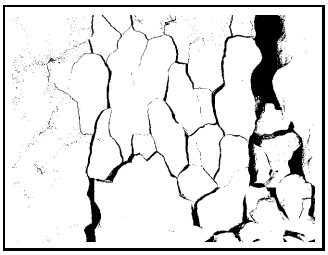

(i)

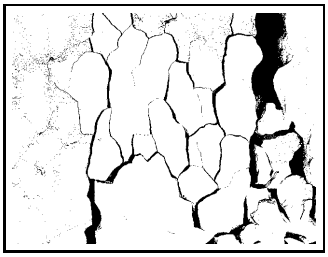

(j)

Figure 5.9: (a) Image 1; (b) Histogram with detected Peaks and valleys; (c) Avg. fitness vs generation of class "A" PGA and GA; (d) Avg. fitness vs generation of class "B" PGA and GA; (e) Class "A" with SL and WSL; (f) Class "B" with SL and WSL; (g),(h),(i), and (j) segmented images using FL, Otsu's, Kwon's, and Hui-Huang Method

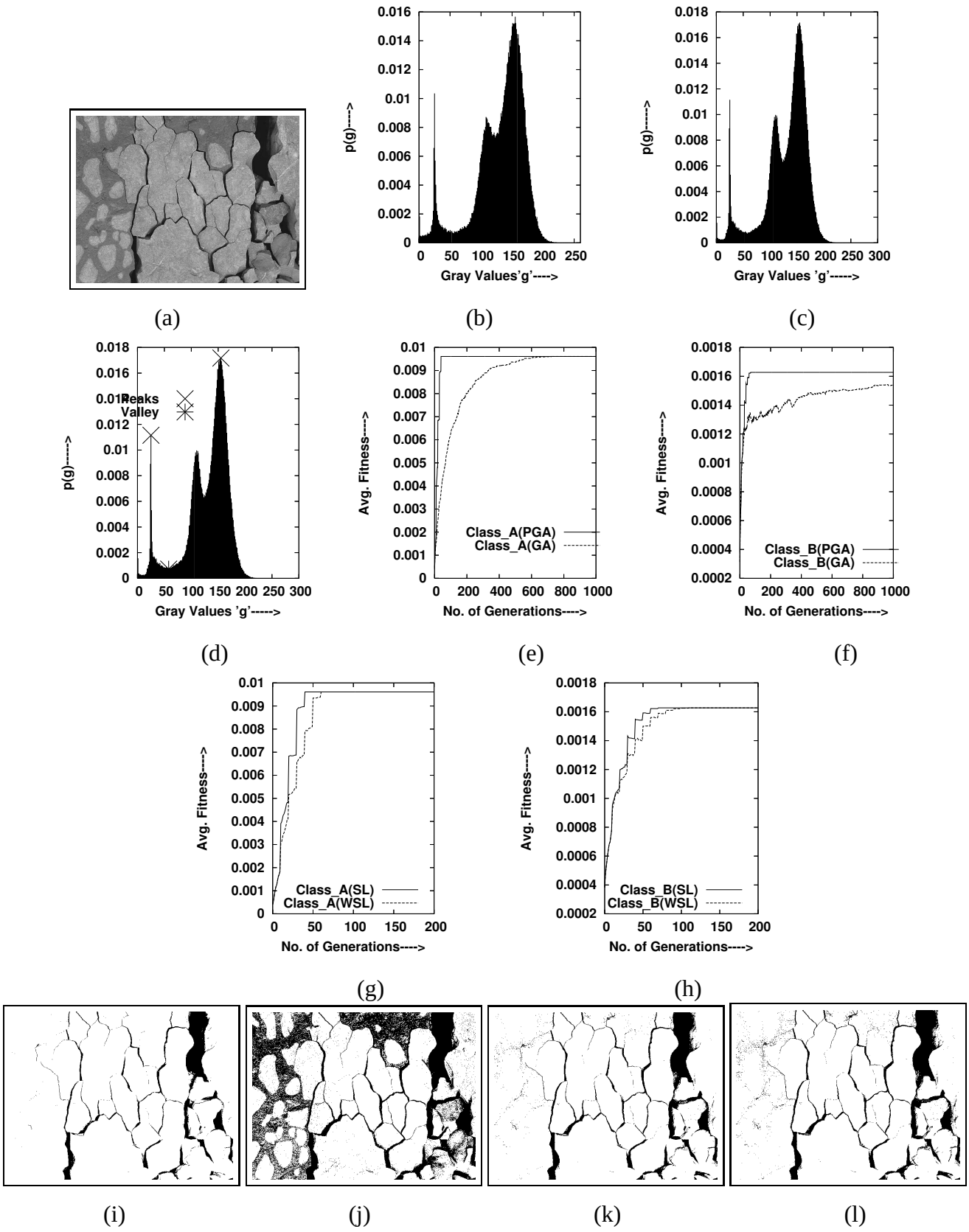

Figure 5.10: (a) Image 1; (b) Histogram; (c) Featured histogram; (d) Detected peaks and valley; (e) Avg. fitness vs generations of class "A" PGA and GA; (f) Avg. fitnee vs generations of class "B" PGA and GA; (g) Avg. fitness vs generations of class "A" with SL and WSL; (h) Avg. fitness vs generations of class "B" with SL and WSL; (i), (j), (k) and (l) segmented images using FB, Otsu's, Kwon's and Hui-Huang's method respectively

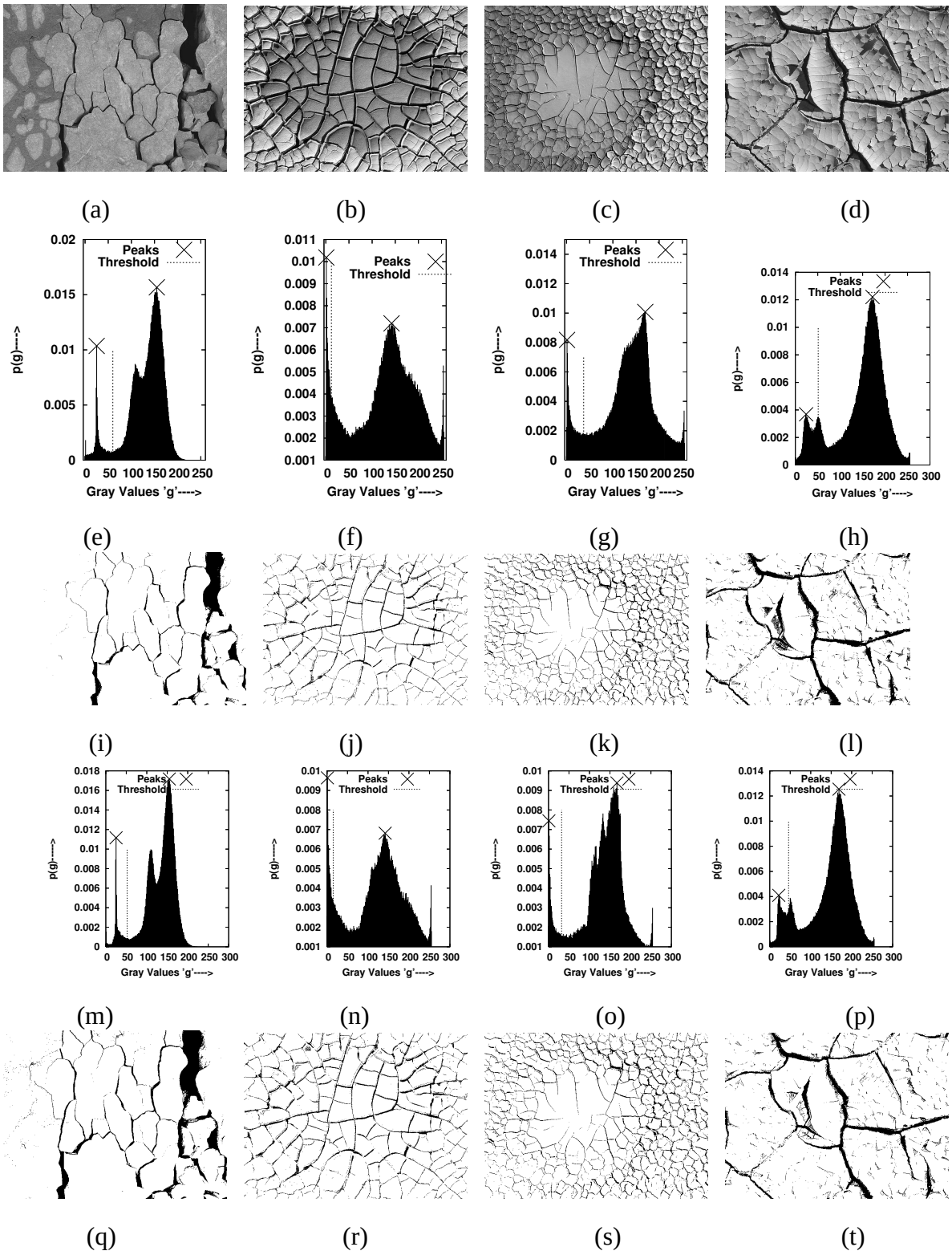

Figure 5.11: (a), (b), (c) and (d) are original crack images; (e), (f), (g) and (h) shows the detected peaks and threshold in the histogram of corresponding images using FL-MMSE; (i), (j), (k) and (l) segmented images using FL-MMSE; (m), (n), (o) and (p) shows detected peaks and threshold in the feature histogram of the original images using FB-MMSE; (q), (r), (s) and (t) segmented images using FB-MMSE.

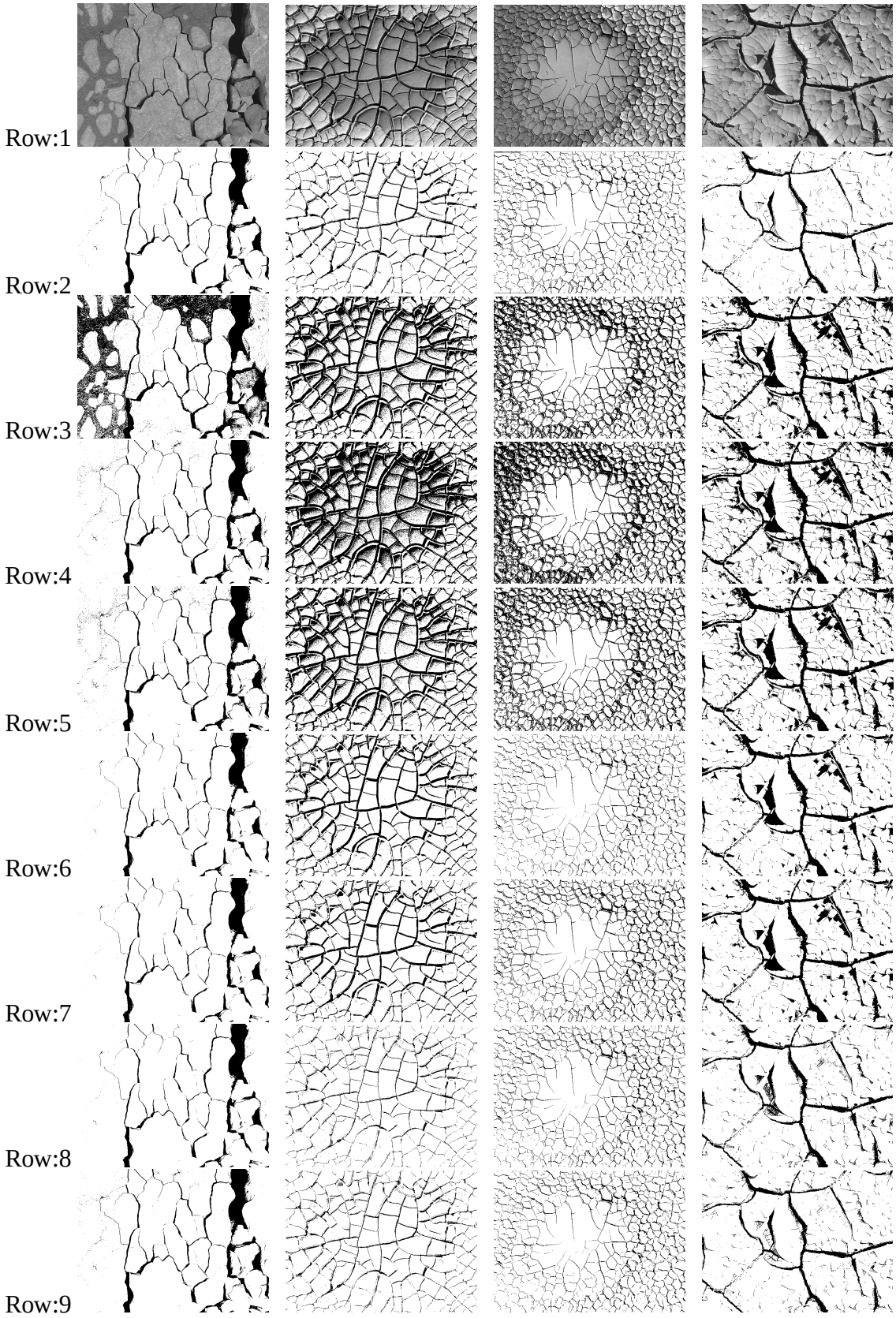

Figure 5.12: Row-1: Original crack Images (Image 1, 2, 3 and 4); Row-2: Ground Truth, Row-3:Otsu's method; Row-4: Kwon's method; Row-5: Hui's method; Row-6: Feature Less method; Row-7: Feature Based Method; Row-8: Feature Less MMSE; Row-9: Feature Based MMSE

Chapter 6

Adaptive Threshold based Segmentation

6.1 Introduction

In this chapter, the problem of segmentation of images acquired under uneven lighting condition has been addressed. It has been found that the existing global thresholding methods and the proposed global thresholding methods proved to be quite inefficient and hence, it has been necessary to devise adaptive thresholding methods. Many adaptive methods have been proposed in the literature for quite some time [95, 37, 96, 97, 98, 99, 100, 101, 102, 103, 104] and these methods are based on different approaches. Recently, Huang *et al.* [104] have proposed an adaptive thresholding method based on the window merging approach. The basic notion is to adaptively select the window size for local thresholding. His approach uses Lorentz Information Measure (LIM) as criterion for selection of windows. The window merging is based on the pyramid approach. Even though it provided satisfactory results for many cases, it produced poor results in case of different uneven lighting conditions. The method although proved to be quite effective, the efficacy of this method is found to greatly depend upon the poor selection of initial window size. This motivated to develop adaptive window selection criteria for determining local thresholds. In this regard, two strategies namely window merging and window growing have been proposed.

In window merging approach, three new criteria have been proposed to select the window for segmentation. An overlapping window merging approach has been proposed and the performance of this approach has been compared with that of Huang *et al.*'s approach. The proposed approaches have been found to have a proper choice of initial window size for accurate segmentation. Therefore, a window growing approach has been proposed to adaptively select

windows. This overcomes the problem of initial window size because this method starts from an arbitrarily small window size. The selected windows have been segmented using the proposed segmentation approaches. The schematic diagram of the proposed methods has shown in Fig. 6.1.

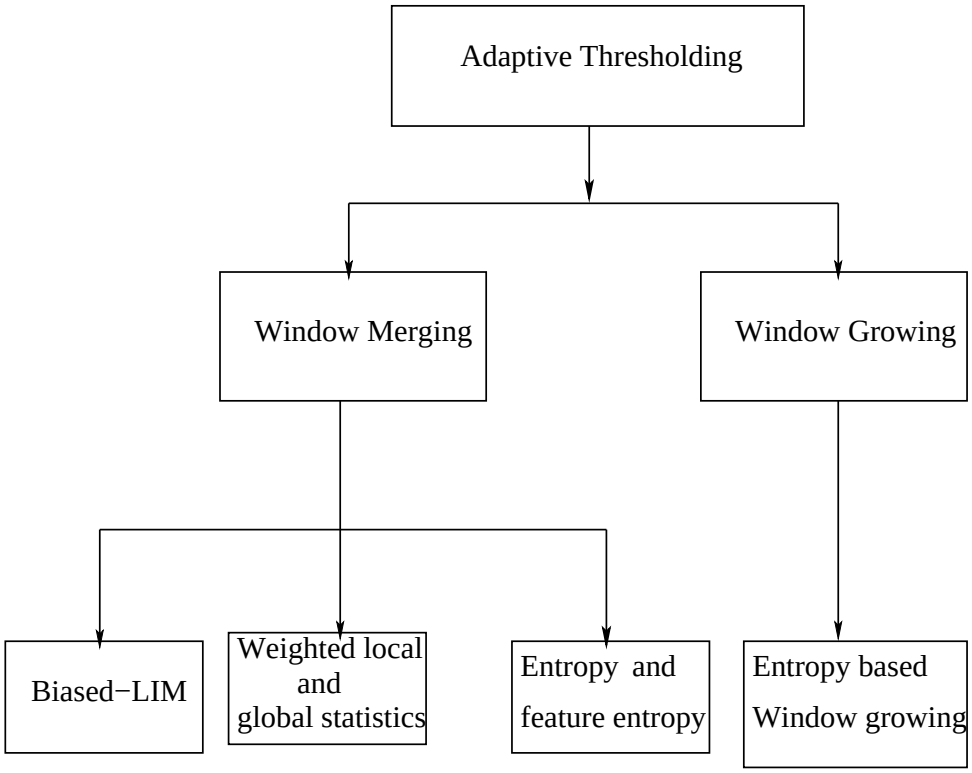

Figure 6.1: Schematic diagram of the proposed adaptive thresholding methods

6.2 Huang's approach

The window merging is based on the use of Lorentz information measure. In the following, we explain the Lorentz information measure [104] (LIM). Let us consider the image X(m,n) having G gray levels. The amount of information contained in this image is called as picture information measure (PIM) and that indicates the least gray level variation when converting the image X(m,n) to a constant gray level image and PIM can be expressed by

$$PIM(x) = \sum_{i=0}^{G-1} h(i) - max_i h(i). \tag{6.1}$$

where, h is the gray level histogram of X(m,n); h(i) represents the gray level histogram of X(m,n). PIM(x)=0, if X(m,n) consists of a constant gray value and PIM(x)= max, when the

gray level histogram h(i) is uniformly distributed. Thus, when X(m,n) has the least information, PIM(x) has its minimum value and when X(m,n) has the most information, PIM(x) has its maximum value. Assuming that total number of pixels of X(m,n) is N(x), the normalized PIM (NPIM) can be determined by

$$NPIM(x) = PIM(x)/N(x). \tag{6.2}$$

Defining the probability p_i as $h(i)/N(x)$, the NPIM(x) can also be expressed as

$$NPIM(x) = 1 - max_i p_i. \tag{6.3}$$

Thus, PIM_k can be defined as

$$PIM_k(x) = \sum_{i=0}^{G-1} h(i) - \sum_{i \in \theta(k)} h(i), \quad 0 \leq k \leq G. \tag{6.4}$$

where, k is the number of k highest values of $h(i)$ and $\theta(k)$ $=k$ highest value of $h(i)$. It indicates the minimum variation number that converts an image to the image with k gray levels. Correspondingly, normalized PIM_k is denoted as $NPIM_k$ and is obtained by

$$NPIM_k(x) = 1 - \sum_{i \in p(k)} p_i), \quad 0 \leq k \leq G. \tag{6.5}$$

where, $p(k)$=the k maximum number of p_i. Let $S_k = NPIM_{G-k}(x), \quad 0 \leq k \leq G$, then

$$S_0 = 0, \quad S_G = 1, and S_k = \sum_{i=0}^{k-1} p_i). \tag{6.6}$$

By connecting the points $(k/G, S_k)$, $k = 0, 1, ..., G$, a broken line called Lorentz information curve can be obtained. For the sake of illustration, Fig. 6.2 shows a Lorentz information curve with G=3, in which the histogram is $h : 2N/9, 3N/9, 4N/2$, with N being the total number of pixels in an image. The area defined bellow the Lorentz information curve (area of the oblique lines in the Fig. 6.2) as the Lorentz information measure LIM($p_0, p_1, ..., p_{G-1}$. When the gray level histogram of image is uniformly distributed, its Lorentz information curve becomes a line from (0,0) to (1,1) (dashed line in Fig. 6.2. Otherwise, it will be the convex broken line below the dashed line (solid line in Fig. 6.2). So when LIM ($p_0, p_1, ..., p_{G-1}$) increases, the image contains more information; as LIM($p_0, p_1, ..., p_{G-1}$) decreases, the image has less information, and vice versa.

The Lorentz information has been used as the window merging criterion by Huang *et al.* [104] and segmentation is carried out using Otsu's criterion [5].

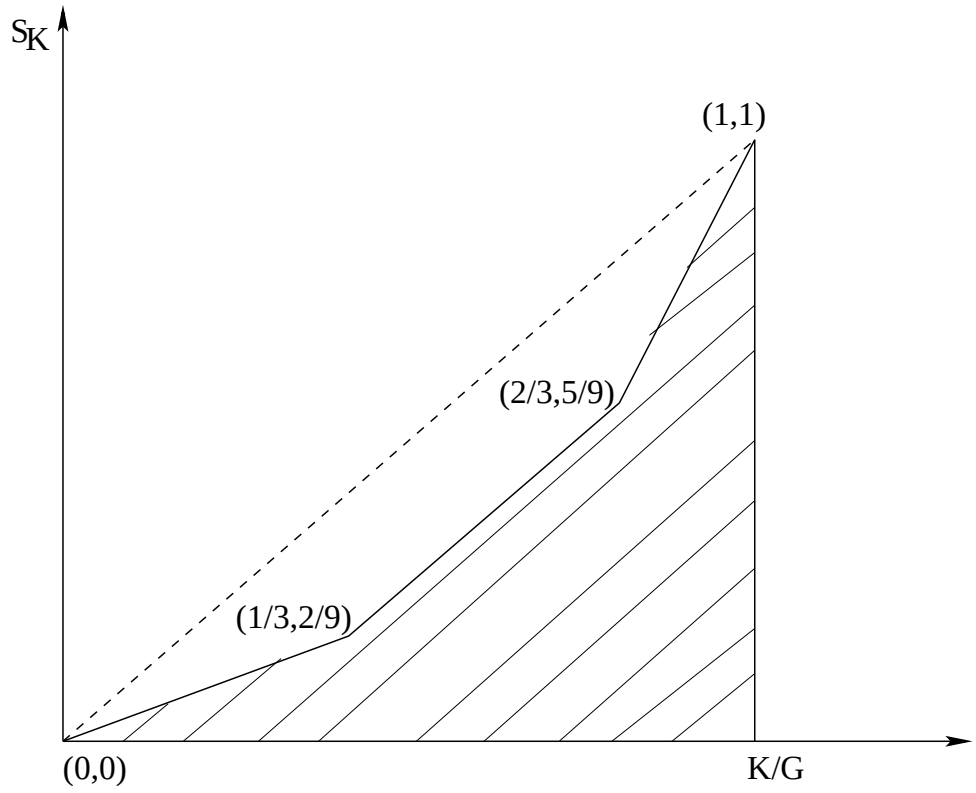

Figure 6.2: Example of Lorentz information curve (G=3)

6.3 Implementation of Huang's approach

Huang *et al.*'s [104] approach is based on the window merging approach. The image is partitioned into small windows and LIM is computed in each window. If the LIM is greater than a predefined threshold, then the window is selected for segmentation or else the window is merged based on the pyramid structure shown in Fig. 6.3. As seen from Fig. 6.3, the four windows have been merged to form a new window and the window is again tested with the criteria and if the criteria is satisfied, then this window is fixed to be segmented. This window merging procedure is also shown in Fig. 6.4. As observed from Fig. 6.4(a), the four windows have been merged to form a larger window in the next step. For example, windows w1, w2, w5, and w6 are merged to form a greater window as shown in Fig. 6.4(b). Similarly, other windows have been merged with the notion of pyramid structure. If these windows do not satisfy the criteria, then they are merged to form a single window as shown in Fig. 6.4(c).

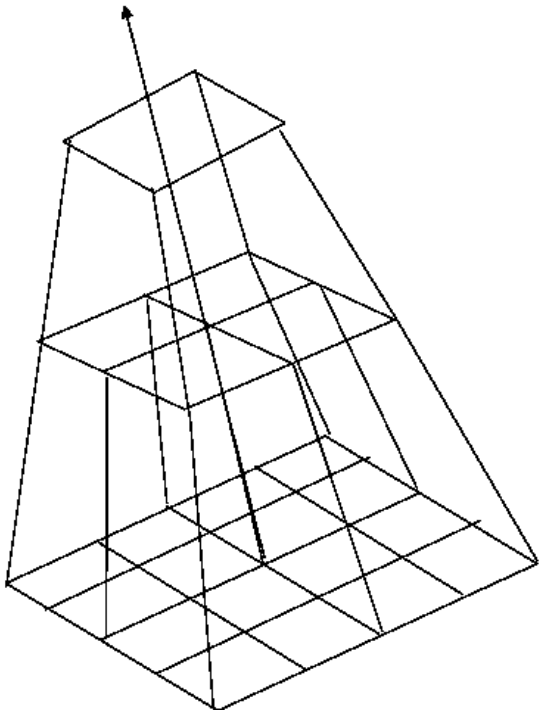

Figure 6.3: Pyramid structure of window merging

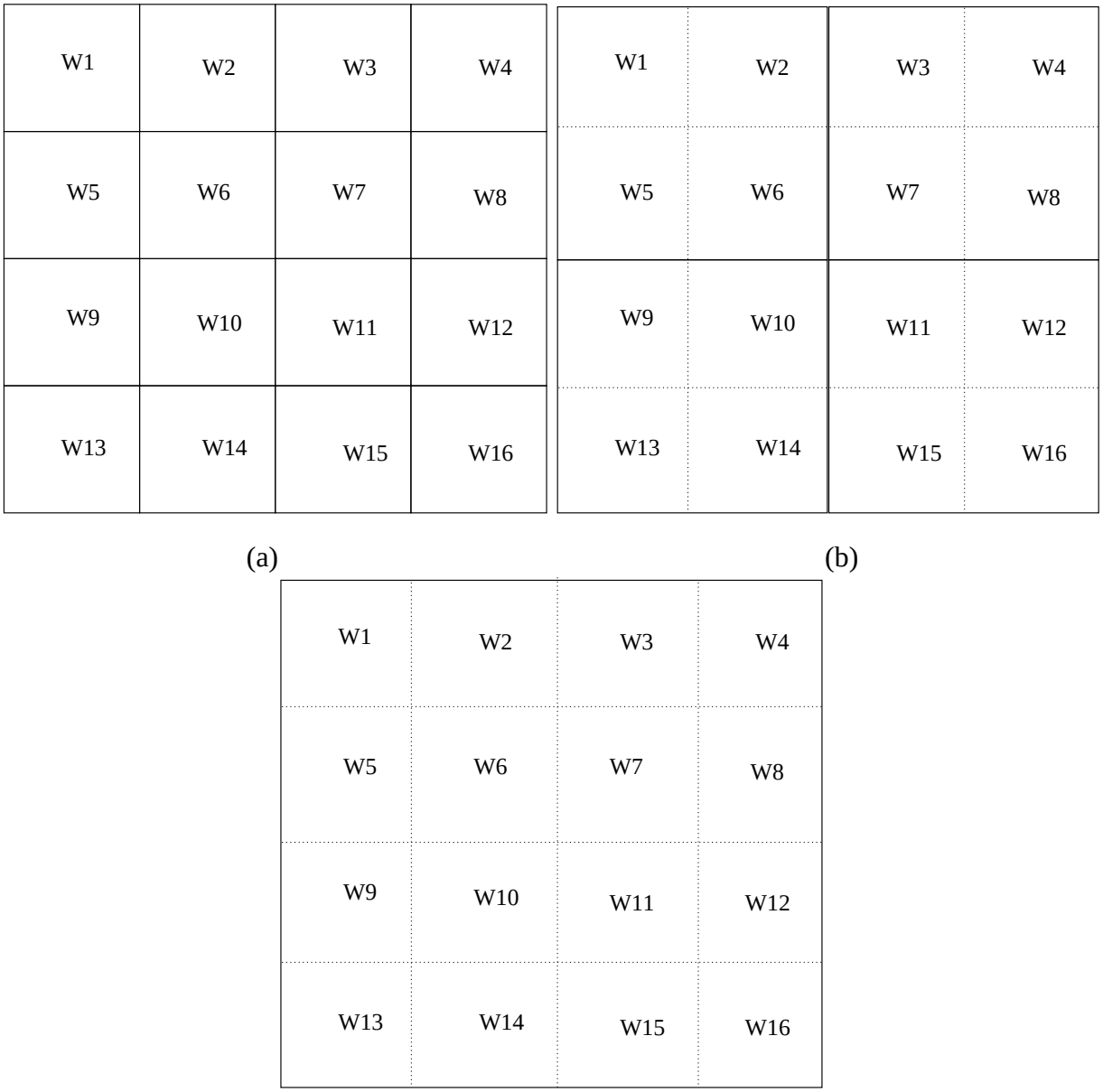

Figure 6.4: Window Merging using Pyramid structure

6.4 Local biased Lorentz information based window merging

This notion of merging is based on the comparison of local information with global information. The image is partitioned into number of windows and in each window Lorentz information measure (LIM) is computed. This LIM of each window serves as a feature of the window. The histogram of these LIM features is computed and a threshold based on Otsu's [5] approach is obtained from this feature histogram. The LIM of each window is biased by the local statistics of each window. The merging criterion becomes

$$q_1\sigma_{wh} + q_2\sigma_{LIM_w} > T_{fOtsu} \tag{6.7}$$

Where, σ_{wh} denotes the standard deviation of histogram of a given window; LIM_w denotes the Lorentz information of the window; T_{fOtsu} denotes the threshold of the feature histogram obtained by Otsu's method; q_1 and q_2 are the associated weights.

6.5 Window merging based on weighted local and global statistics

Let the image be partitioned into N sub windows. Let W_k denotes the k^{th} window and L_k denotes the Lorentz information of the k^{th} window. In each window of the image, Lorentz information measure (LIM) is computed and LIM of each window is considered as a feature of the window. The Histogram of LIM of all the windows represents the feature histogram and provides the global information. Histogram of gray values of each window provides local information. The following is the proposed window merging criterion using the linear combination of local and global statistics.

$$q_1\sigma_{wh} + q_2\sigma_{fh(LIM)} > \sqrt{\sum_{i=1}^{n_w}(x_{i_{fh}} - T_{fOtsu})^2} \tag{6.8}$$

Where, σ_{wh} denotes the standard deviation of the histogram distribution of the window considered for merging, $\sigma_{fh(LIM)}$ denotes the standard deviation of the feature histogram, q_1 and q_2 are the associated weights. $x_{i_{fh}}$ denotes the i^{th} feature of the feature histogram and the right hand side is the standard deviation of the feature histogram with the mean T_{fOtsu}, as the threshold of the feature histogram determined by Otsu's method.

6.6 Entropy based window merging

The window merging criterion is based on entropy and feature entropy of window. The image is partitioned into sub-images and in each sub-image, the entropy is computed based on the histogram. In each sub-image, the edges are considered as features and the feature entropy is computed. The entropy and the feature entropy of the total image is also computed. The window is merged with the neighbouring windows, if the following condition satisfied.

$$H_w > Th, \quad \text{subject to the constraint} \quad H_{wf} > Th_f \tag{6.9}$$

The thresholds Th and Th_f in the above inequalities are chosen based on the total entropy of the image and that of the feature image.

Based on the above decision criterion, a window is either merged or unmerged to be segmented. The windows are merged to be tested for further merging. After windows are selected to be segmented are segmented with Otsu's and our proposed methods of FLPGA, FBPGA and MMSE approaches. The windows are also segmented using Otsu's method for the sake of comparison.

6.7 Adaptive window selection based on window growing

It has been observed in the above notion of window merging that the segmentation accuracy greatly depends upon the proper choice of initial window size. In order to ameliorate the above effect, a window growing method is proposed. The initial window size considered is very small and the window selection depends on both the entropy of the gray values and the feature entropy. We consider edge as a feature and compute the entropy of the feature. If the following constraint information condition is satisfied, the window is selected to be segmented or the window size is incremented by Δw and again the selection criterion is tested. If the enhanced window satisfies the selection criterion, then a new window is considered from the rest of the image. The criterion for fixing the window is

$$H_w > Th, \quad \text{subject to the constraint} \quad H_{wf} > Th_f \tag{6.10}$$

Where, H_w represents the entropy of the window and H_{wf} represents the entropy of the feature window.

6.8 Implementation of proposed window merging and window growing approaches

Besides pyramid structure, we have proposed window overlapping technique for window merging approach. Selection of windows in these methods needs to be based on the three proposed criterion. The overlapping approach is shown in Fig. 6.5. The image is partitioned into say, for example, 16 windows and for example w1, w3, w4, w8, w13, and w16 satisfy the selection criterion and therefore, they have been selected. Since, w2, w6, and w7 do not satisfy the criteria, they are merged with w3 to form a window consisting of w2, w3, w6, and w7 and this larger window is tested with the proposed criterion. These merged windows are shown with dotted lines. Since, w5 does not satisfy the criteria, this is merged with w6, w9, and w10 to form a window to be tested with the criteria. Analogously, w11 is merged with w12, w15, and w16 to form a window to be tested with the criteria. These merged windows satisfy the criterion and hence, selected to be segmented. Finally, w14 is merged with w15, w11, w10, w16, w12, w8, w7, and w6 to form a large window as shown in Fig. 6.5(f) to satisfy the criteria. As seen from Fig. 6.5(f), all the merged blocks have been tick marked and hence, the whole image has been considered in this process.

The notion of merging affects the histogram distribution and this effect is demonstrated in Fig. 6.6. Fig 6.6(a) shows a hexagon image partitioned into 16 windows and the corresponding histograms are shown in Fig. 6.6(b). It may be observed that the histogram of most of the windows, except few ones, exhibits unimodal distribution and hence, unsuitable for segmentation. The windows have been merged based on the pyramid structure and these four windows after merging are shown in Fig. 6.6(c). The corresponding histograms are shown in Fig. 6.6(d), where it may observed that the histogram in each window exhibits bi-modality condition and hence, can be segmented by proposed approach. Thus, the notion of merging helps to add information so that the merged window can be segmented properly.

For this example of hexagon image, the histograms obtained by pyramid merging approach are shown in Fig. 6.7 (a) and (b). Fig. 6.7(a) shows the histogram before merging and after merging, the histograms are bimodal with overlapping class distribution. When the windows are tested for the proposed biased Lorentz condition, one more window that is w6 is selected as shown in Fig. 6.8(a) and after pyramid merging, histograms of the merged windows are shown in Fig. 6.7(b), where histograms are bi-modal with a lesser degree of overlapping of the class

distributions. When the windows are tested for the proposed biased Lorentz condition, two more windows that are w1 and w2 are selected as shown in Fig. 6.8(b). Hence, biased LIM method is expected to obtain more accurate thresholds and hence, better segmentation.

The effect of overlapping concept for window merging is shown in Fig. 6.9. The image is partitioned into eight windows and the corresponding windows have been merged based on the notion of overlapping as shown Fig. 6.9(c). The histograms of the merged windows are shown in Fig. 6.9 (d), where it can be observed that the histograms exhibit clear bi-modality and hence, can be segmented.

The notion of window growing is illustrated in Fig. 6.10. Fig. 6.10(a) shows that a small window has been selected initially and the window is incremented in the direction of the arrow and the window is fixed after satisfying the criterion. Once, one window has been selected for segmentation, subsequent window growing starts from other portion of the image as shown in Fig. 6.10(c). This procedure is adapted until all the portions of the image have been considered.

6.9 Results and discussions

Four different images, with non-uniform lighting conditions have been considered to validate the proposed adaptive thresholding scheme. The images are a hexagon image, crow image, rabbit image and rice image shown in Fig. 6.11(a), (b), (c) and (d) respectively. It may be observed from these figures that different portions of the image are with different lighting conditions but the images have object/ objects and background. Hence, this is a two class problem. It is apparent as if these images have been acquired under non-uniform lighting conditions. The histograms of these images have been shown in Fig. 6.12. As observed, the first one appears to be tri-modal, the second bi-modal with unequal distributions, the third is bi-modal with many misleading kinks, and fourth is almost uni-modal. It is intuitively expected that, except for Fig. 6.12(b), global thresholding method will yield poor result. The results obtained by Otsu's [5] method are shown in Fig. 6.13, where it may be observed that the method could not segment the hexagon, crow, and rice grain images but could partially segment the rabbit image. The ground truth images are shown in Fig. 6.13. This has also reflected in the percentage of misclassification error (PME). The PME is defined as

$$PME = 1 - \frac{\mid B_O \cap B_T \mid + \mid F_O \cap F_T \mid}{\mid B_O \mid + \mid F_O \mid} \tag{6.11}$$

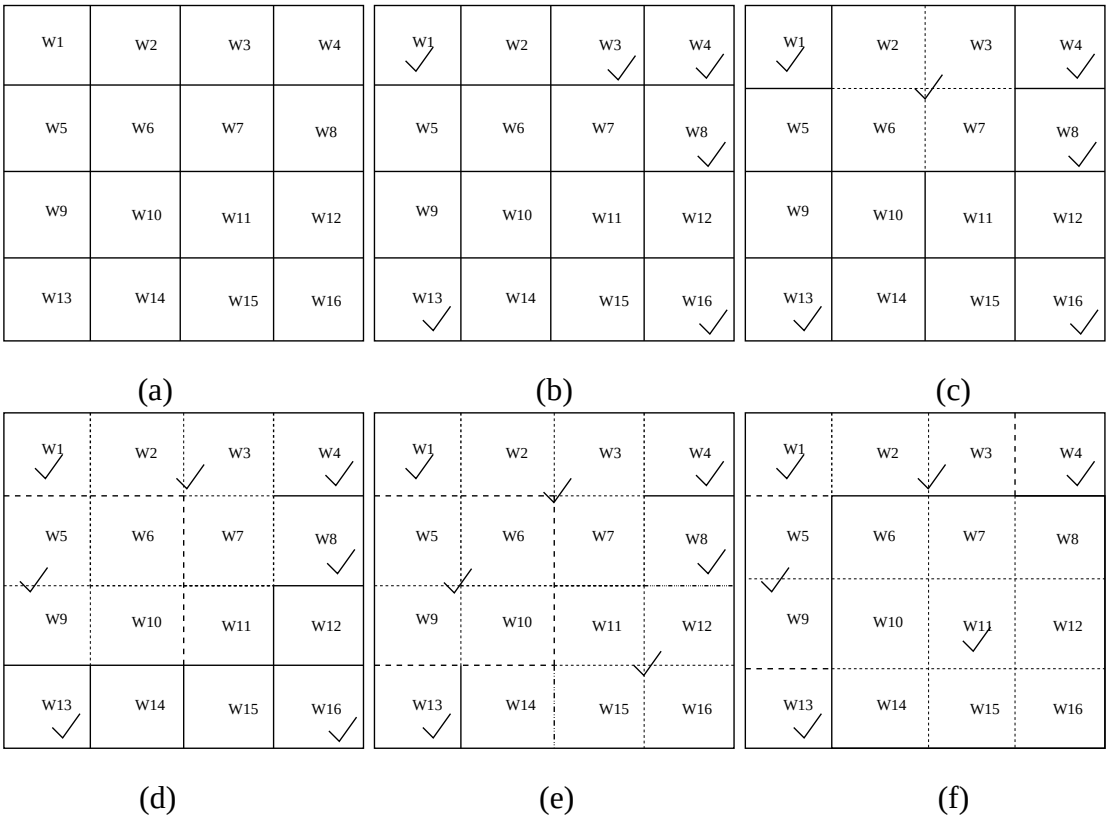

Figure 6.5: Window overlapping concept with LIM criterion:(a) Image is devided into 16 subimages (Windows), (b) w1, w3, w4, w8, w13,w16 are satisfied the criterion, (c) w2 is merged with w3, w6 and w7 to form a window w2w3w6w7 after satisfying the criterion, (d) w5 is merged with w6, w9 and w10 to form a window w5w6w9w10 after satisfying the criterion, (e) w11 is merged with w12, w15 and w16 to form a window w11w12w15w16 after satisfying the criterion, (f) w14 is merged with w15, w11, w10, w16, w12, w8, w7 and w6 to form a window w6w7w8w10w11w12w14w15w16 after satisfying the criterion

Where, background and foreground are denoted by B_O and F_O for the original image, and by B_T and F_T for the test image. The PME of the rabbit image is 2.93, which is much less as compared to that of hexagon, crow and rice grain image. Hence, it is found that global thresholding approaches are not suitable to segment images acquired under uneven lighting conditions. Fig. 6.16 shows the results obtained using Huang *et al.*'s [104] adaptive window selection approach with Lorentz information measure. The images have been partitioned into sub-images with window size 100x100 for hexagon image, 50x64 for crow image, 75x125 for rabbit image, and 32x32 for rice image. The windows that satisfied the Huang *et al.*'s [104] criteria are segmented by Otsu's approach and those do not satisfy are merged in the pyramidal structure to form a new window to be segmented. The different window sizes with the corresponding thresholds are tabulated in the Table 6.1. From Table 6.1, it may be seen that there are two merged windows, 9^{th} and 10^{th} and the corresponding thresholds have also been

given in Table 6.1. As observed four windows namely (3^{rd}, 4^{th}, 7^{th}, and 8^{th}) have been merged and (11^{th}, 12^{th}, 15^{th}, and 16^{th}) windows have also been merged and the thresholds determined are 78 and 60. As observed from Fig. 6.16, Huang's approach could not segment the image properly. In case of hexagon image, the left portion of the image, which is poorly lighted could not be segmented and also there are some black portions of the image inside the white portion as shown in Fig. 6.16(a). The corresponding PME is 8.17. The left background portion of the crow image has been merged with the foreground as shown in Fig. 6.16(b). In case of the rabbit image of Fig. 6.16(c), the background portion has been misclassified and in case of rice grain image, many grains have been merged to form a class as shown in Fig. 6.16(d), thus increasing the classification error. Accordingly the PMEs for crow, rabbit, and rice image are 5.84, 14.77, and 8.36 respectively.

It can also be observed that many pixels in the uneven lighted portions could not be segmented. We have proposed three windowing schemes and the windows are merged based on pyramid approach of Huang's method [104]. The windows are merged based on the proposed overlapping concept. Once the windows have been fixed based on the merging criterion, the windows are segmented by Otsu's [5] approach, the proposed PGA based scheme and the MMSE based scheme. The following window merging based schemes have been described.

6.9.1 Window merging

Huang *et al.* [104] method fixed the windows based on Lorentz Information Measure (LIM) criterion and after the windows have been fixed, windows are segmented using Otsu's segmentation method. We have selected the window based on following three criterion and after the windows have been selected, the windows are segmented based on the proposed PGA based FL approach and the MMSE based approach.

Biased Lorentz information measure based criterion

Pyramid approach

The image is partitioned into sub-images. In case of hexagon image of Fig. 6.17, the image is partitioned into an initial size of 100x100 and the different windows selected are tabulated in Table 6.2. As seen from the table, windows namely 1^{st}, 2^{nd}, 5^{th}, and 6^{th} have been merged in a pyramid structure and similarly 3^{rd}, 4^{th}, 7^{th}, and 8^{th} and 9^{th}, 10^{th}, 13^{th}, and 14^{th} have

been merged by pyramid structure. The thresholds obtained by Otsu's, PGA and MMSE based methods have been tabulated in Table 6.2. The overall segmentation is the union of all the segmented windows. As observed from Table 6.2, some of the threshold are different, for example, for the 4^{th} window, Otsu and PGA based methods produced same threshold 84, while MMSE method has produced 111, which is quite different from the other two. The results obtained have been presented in Fig. 6.17, where the results of Huang's approach have been given for the sake of comparison.

As observed from Row 2, the shape of the hexagon could be preserved but some mid portion of the image has been misclassified as background. Analogously, for crow image the left hand bottom corner of the background has been misclassified at foreground. The PME for this is 5.52. Some portions of the rabbit image have also been misclassified but for the rice grain image all the grains have been segmented from the background and accordingly the PME is 1.38. There is an improvement in the accuracy of the segmentation, where the selected windows have been segmented by PGA based method. As observed from Row 3 of Fig. 6.17, the hexagon has almost been classified with barely minimum number of misclassified pixel within the hexagon portion and near one edge. In case of rabbit and rice grain image, the images have been classified properly but in case of crow image there are some misclassification. Accordingly, the PME for these images have been reduced and is tabulated in Table 6.7.

As observed from Row 4 of Fig. 6.17, use of MMSE method for segmentation resulted in degraded performance as compared to that of using PGA. As observed from the results, the left portion of the hexagon and some portion of the background have been misclassified. Some background portion of the crow image has also been misclassified. There is less misclassification in case of rabbit and rice grain images. This has also been reflected in the PMEs tabulated in Table 6.7. Except for rabbit image, where PME is 1.83, the PMEs are higher than that of the PGA based segmentation. Hence, in case of local biased LIM based criterion, use of PGA based algorithm yielded satisfactory results.

Window overlapping approach

Fig. 6.18 shows the results obtained, where biased LIM criterion together with the notion of window overlapping has been used for selection of windows. Once the size of the window have been fixed, Otsu's, PGA and MMSE based segmentation methods have been used to segment over the windows. The given image is partitioned into sub-images and the windows are merged

based on the notion of overlapping of section 6.4. The windows that overlapped to form a larger window are given in Table 6.3. For example, 1^{st}, 2^{nd}, 5^{th}, and 6^{th} windows have been merged to form a new window and the threshold obtained by Otsu is 36, PGA is 37, and MMSE is 40. These four threshold values have been used to segment the images. In case of other one 3^{rd}, 4^{th}, 7^{th}, and 8^{th} are merged together to form a new window, whose threshold is determined by Otsu, PGA, and MMSE are 37,71, and 62 respectively. The threshold obtained by MMSE is quite different from Otsu and PGA approach. The selection of window by the concept of overlapping yields better results as observed from Fig. 6.18. Observing Row 2 of Fig. 6.18, it is found that some portion of hexagon has been misclassified and the background portion in case of crow image has been misclassified. The rice grain image has been classified properly where as some misclassified pixels are present in case of the rabbit image. The result improved while using the PGA approach and it can be observed that the hexagon could almost be segmented properly. Even the non-uniform lighted portion has been classified properly. Comparing the results of row 2 of Fig.6.18 with 6.17, there are visible improvements in the results obtained by window overlapping notion. The PME accordingly reduced as compared to that of using the pyramid approach. As observed for the pyramid approach case, use of MMSE based scheme did not improve the result rather deteriorated the overall segmentation. This effect can be observed from row 4 of Fig 6.18. The results obtained by the proposed approaches have been found to be better than that of Huang *et al.*'s method.

Weighted local and global statistics

In this case, the image has been partitioned and the windows have been merged using the pyramid approach of Huang *et al.*. The windows are fixed based on the criterion given by (6.8), and the windows merged and unmerged are given in Table 6.4. The thresholds obtained by these methods have also been tabulated in Table 6.4. Observing the results presented in row 2 of 6.19, Otsu's method produced results with misclassification inside the hexagon and also some misclassification in the background of crow image. The corresponding PMEs have been tabulated in Table 6.7. The results improved while using PGA based segmentation scheme. The hexagon, except very few pixels, could be segmented properly and there are some misclassified pixels in case of crow image. The result of rabbit image improved as compared to Otsu's based approach. Rice grain image also could be segmented properly. This effect has also been reflected in the values of PME tabulated in Table 6.7, which are 1.88, 4.9, 1.18, and 1.57. The segmented

results further determined with the use of MMSE approach. As seen from row 4 of 6.19, some portion of hexagon and the background portions have been misclassified. There are more misclassification in case of crow image. However, rabbit and rice grain images could be segmented properly. Thus in this case also, the PGA based approach proved superior segmentation results to Otsu's and MMSE based methods.

Entropy based criterion

In this scheme, the image is partitioned into sub-images (Windows) and the windows are merged based on the entropy based criterion given by (6.9). The windows considered have been given in Table 6.5. The initial window size is (200x80), thus there are 10 sub-images (windows). It is observed from Table 6.5 that except 1st and 6th window other windows satisfie the criterion. The 1^{st} and 6^{th} windows are merged with 2^{nd},3^{rd}, 4^{th}, 7^{th}, 8^{th} and 9^{th} windows to form a new window, which satisfied the criteria given in (6.9). Thresholds obtained for different methods also have been tabulated in Table 6.5. The results obtained by different methods have been presented in Fig. 6.20. As seen from row 2 of Fig. 6.20, the hexagon image has been segmented properly with PME 1.5619. This is due to few misclassified pixels at the left most corner of the hexagon. This criteria with Otsu's method of segmentation produced appreciable result for the rice grain image. Except few misclassified pixels, the background and rabbit could be segmented properly. But in case of crow image, a portion of the background has been classified as foreground and hence, PME is 11.60. These results improved substantially when PGA based segmentation scheme has been applied for segmenting different windows. As observed from row 3 of Fig. 6.20, the hexagon image has been segmented properly with a minimum PME of 1.533. The improvement of PGA based method over allothers is evident in case of crow image, where background has been classified properly. The corresponding PME is as low as 1.48. Similarly the rabbit and rice grains have been classified properly. The PMEs for rabbit and rice grain are 1.328 and 1.915 respectively, which is found to be minimum in case of all the window merging approaches. As we moved to MMSE method, the result is satisfactory but not as good as PGA based method. It may be observed from row 4 of Fig. 6.20 that there are few misclassified pixels are observed in all images and this has been reflected in PME. As observed from Fig 6.20, PGA based method produced best result among Huang *et al.*'s, Otsu's, MMSE based methods. Thus, entropy based criterion with PGA based thresholding proved to be the best among all.

6.9.2 Window growing

It has been found in window merging that the accuracy of segmentation greatly depends upon the proper choice of initial window size. The initial window sizes in case of the previous approaches have been selected on trial and error basis. Thus, the window growing approach is adopted. In this case, a small window of (50x10) is selected and incremented by (5x1) till the window satisfies the entropy based criterion given in (6.10). The different windows that satisfied the criterion are tabulated in Table 6.6 and the thresholds corresponding to each window are given in Table 6.6. The overall segmentation is the union of segmentation over all the windows. Results obtained by Otsu's method is shown in row 2 of Fig. 6.21, where it may be observed that the hexagon image could be segmented properly but there are misclassified background pixels in crow image. There are few misclassified pixels in rabbit and rice grain image. The result improved when we moved to PGA based approach. The results obtained by PGA based approach are presented in row 3 of Fig. 6.21, where it may be observed that the hexagon image has been segmented properly and a few background pixels have been misclassified in case of crow image. As observed, very few misclassified pixels are there in case of rabbit and rice grain image. The result deteriorated when MMSE based method has been applied for segmentation. This is evident from the results presented in row 4 of Fig. 6.21, where there are many misclassified pixels in case of rabbit image. The PME is minimum in case of PGA based approach. The PME for hexagon, crow, rabbit and rice grain are 1.58, 2.98, 1.03, and 0.75 respectively. There are substantial improvement visibly and quantitatively over Huang's approach. Thus, in window growing approach also, the PGA based scheme performed best among all other method.

In both window merging and window growing approaches, the PGA based scheme proved to be the most effective scheme.

Table 6.1: Threshold values for Huang's Approach (Hexagon Image:400x400, initial window size 100x100)

Window SL No	Starting point	End point	Huang's Approach T
1 (2nd W)	(1,101)	(100,200)	46
2 (3rd W)	(1,201)	(100,300)	67
3 (4th W)	(1,301)	(100,400)	84
4 (8th W)	(101,301)	(200,400)	89
5 (12th W)	(201,301)	(300,400)	90
6 (14th W)	(301,101)	(400,200)	47
7 (15th W)	(301,201)	(400,300)	66
8 (16th W)	(301,301)	(400,400)	82
9 (3+4+7+8th W)	(1,201)	(200,400)	77
10 (11+12+15+16th W)	(201,201)	(400,400)	78
12 (all windows)	(1,1)	(400,400)	60

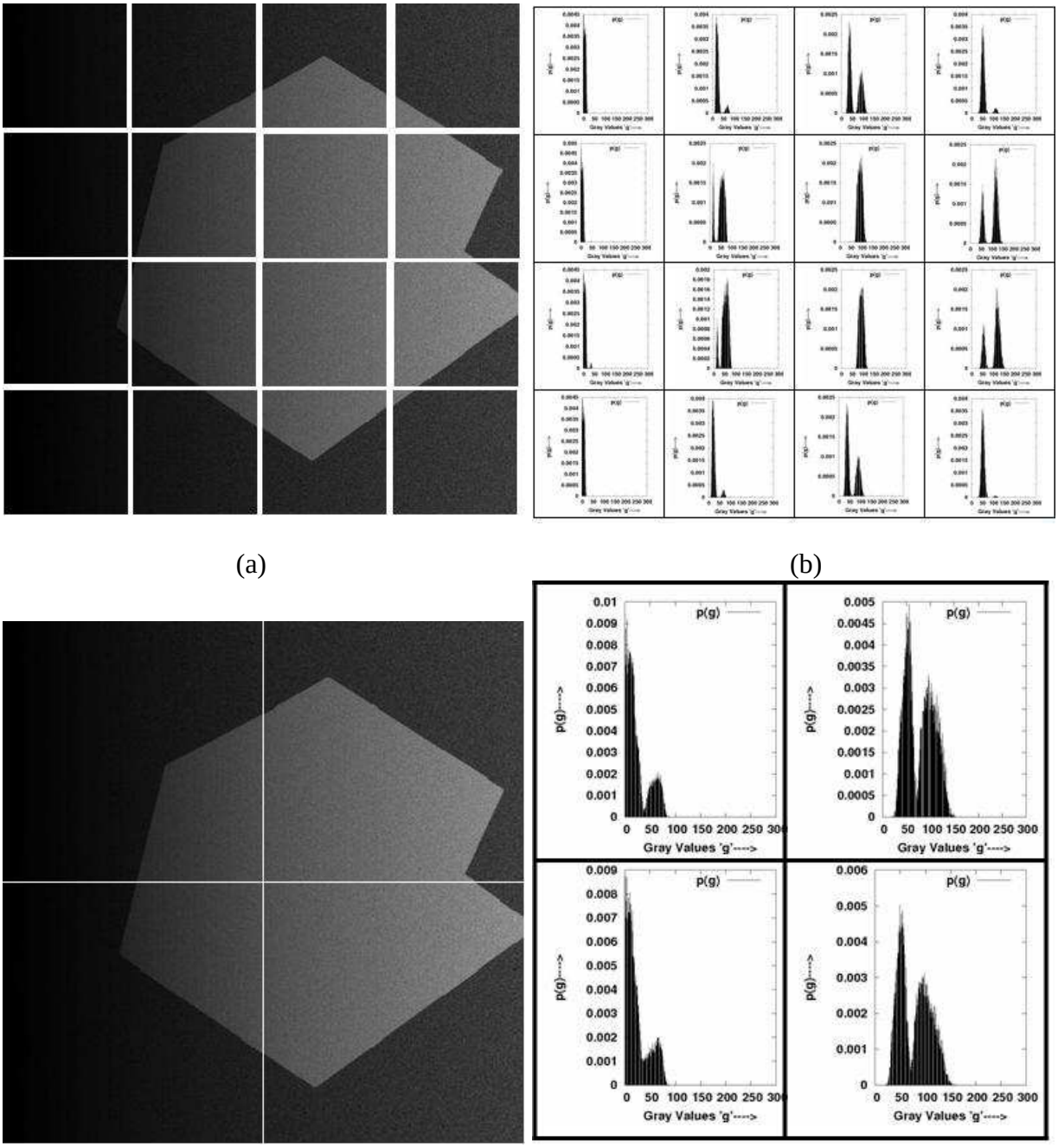

Figure 6.6: Pyramid structure Window Merging Concept: (a) Image is partitioned into 16 sub-images (windows); (b) corresponding histograms of the sub-images; (c) 4 sub-images after window merging; (d) corresponding histograms of the sub-images.

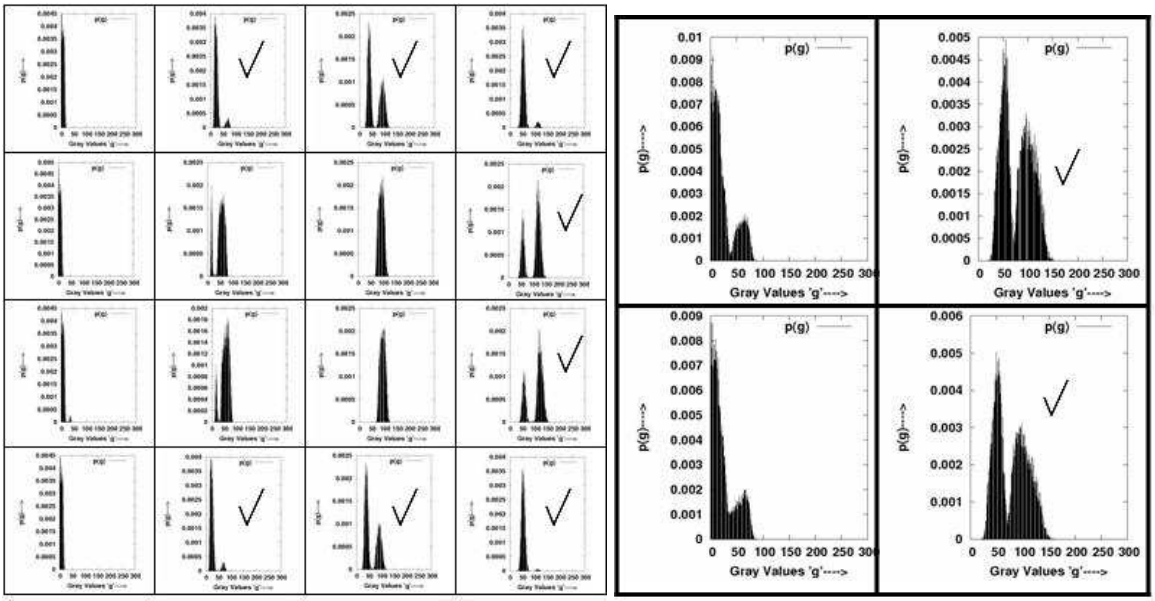

(a) (b)

Figure 6.7: Pyramid structure Window Merging Concept with Huang's criterion:(a) Histograms of the subimages with the selected windows are tick marked for segmentation, (b) histograms of the subimages after merging and the selected windows are tick marked for segmentation.

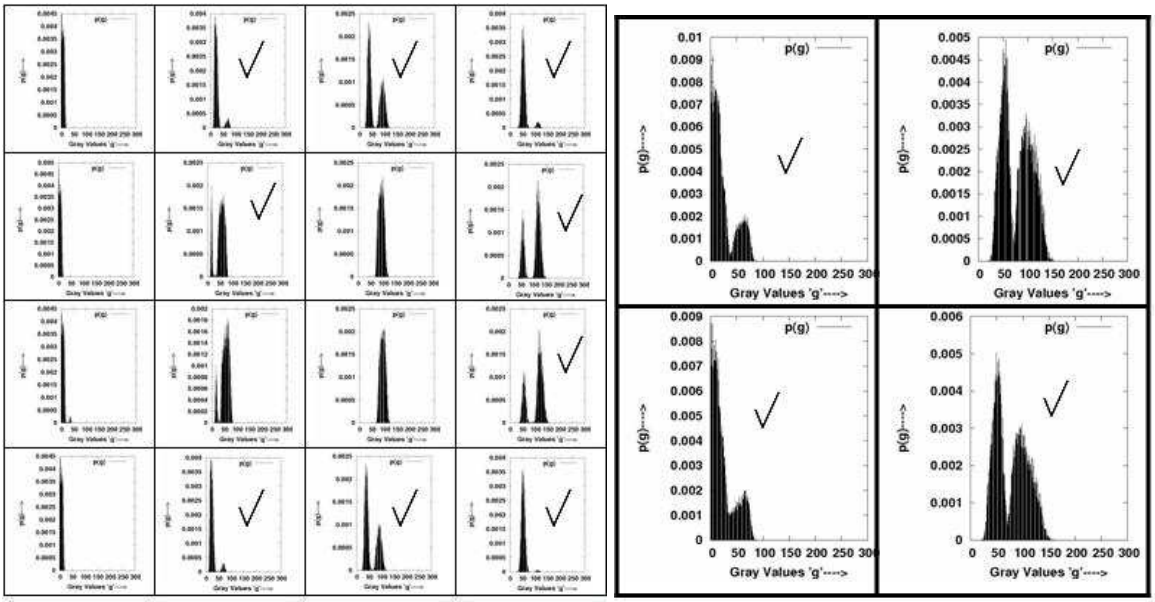

(a) (b)

Figure 6.8: Pyramid structure Window Merging Concept with biased LIM: (a) Histograms of the sub-images with the selected windows are tick marked for segmentation; (b) histograms of the sub-images after merging and the selected windows are tick marked for segmentation.

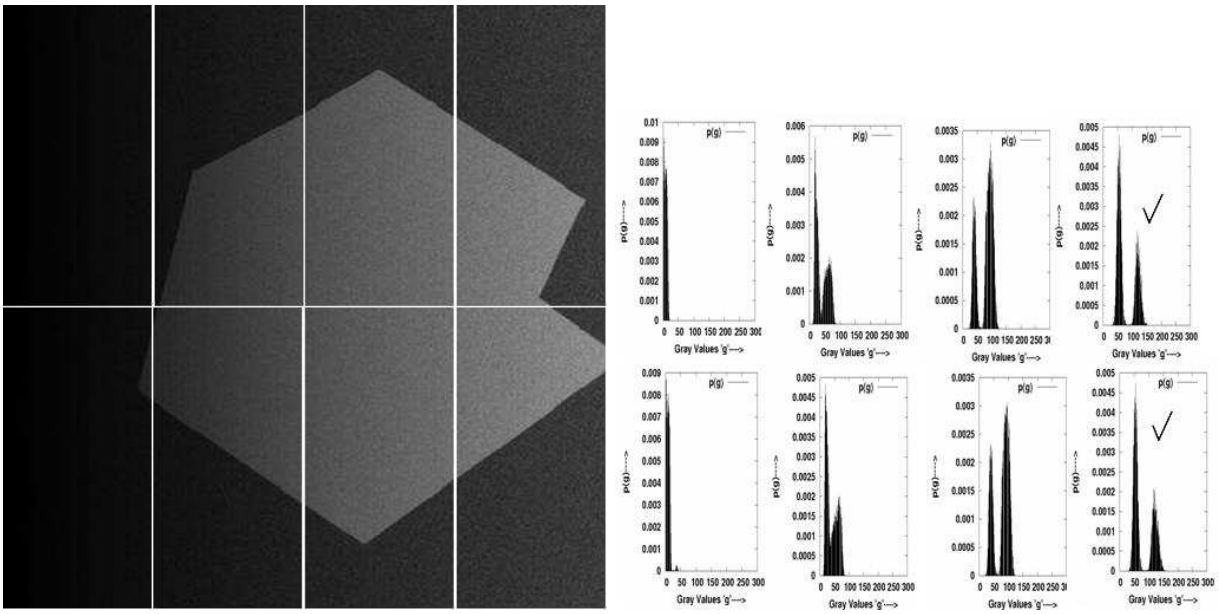

(a) (b)

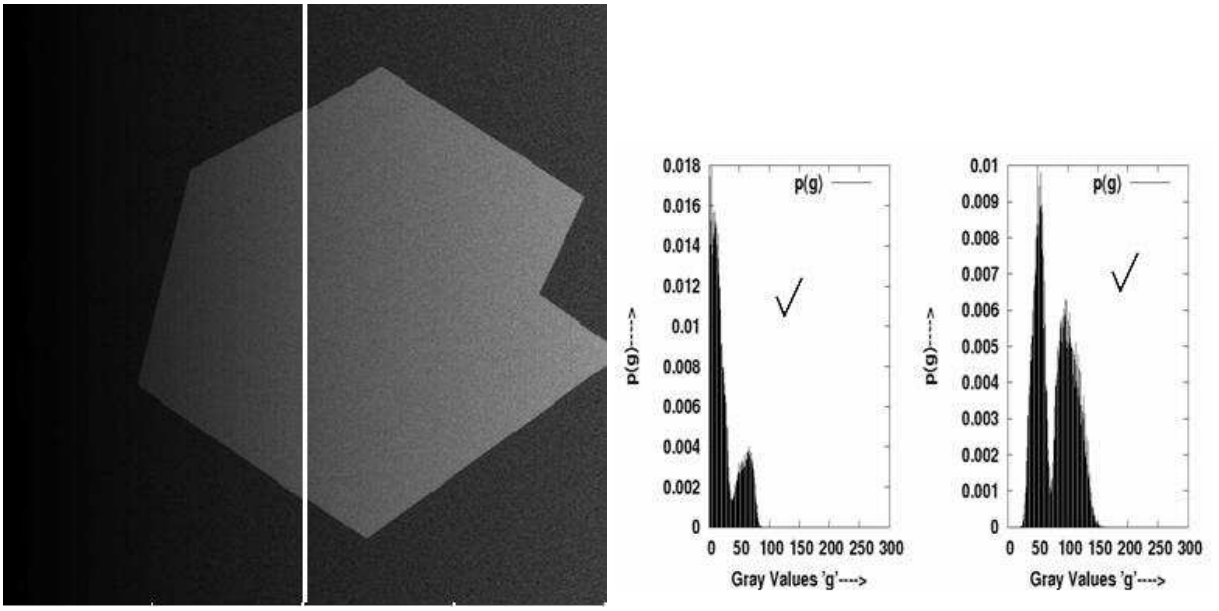

(c) (d)

Figure 6.9: Window overlapping concept with LIM criterion: (a) Image is divided into 8 sub-images (Windows); (b) corresponding histograms with tick marked windows are satisfied the criterion for segmentation; (c) Window 1 is overlapped with window 2, 5, & 6 and window 3 is overlapped with window 4, 7 & 8; (d) corresponding histograms with tick marked windows are satisfied the criterion

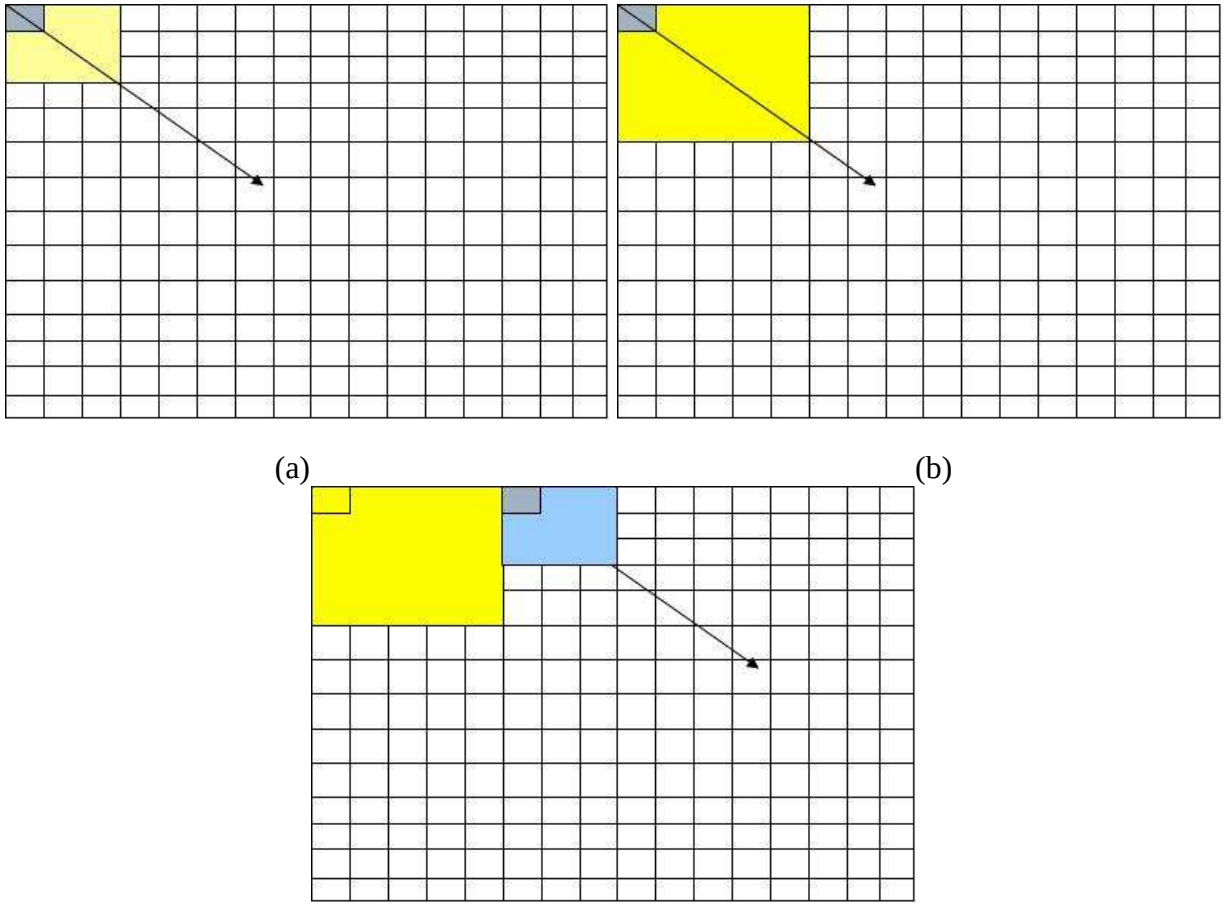

Figure 6.10: Window Growing Concept

Table 6.2: Pyramid structure window merging (Biased Lorentz): Selected windows and threshold values determined by different methods (for hexagon image of size 400x400, initial window size=100x100)

Window SL No	Starting point	End point	Ostu (Method1) T	PGA (Method2) T	MMSE (Method3) T
1 (2nd W)	(1,101)	(100,200)	46	46	52
2 (3rd W)	(1,201)	(100,300)	67	64	73
3 (4th W)	(1,301)	(100,400)	84	84	111
4 (6th W)	(101,101)	(200,200)	39	30	42
5 (8th W)	(101,301)	(200,400)	89	81	66
6 (12th W)	(201,301)	(300,400)	90	92	62
7 (14th W)	(301,101)	(400,200)	47	45	37
8 (15th W)	(301,201)	(400,300)	66	66	49
9 (16th W)	(301,301)	(400,400)	82	82	102
10 (1+2+5+6th W)	(1,1)	(200,200)	36	39	43
12 (3+4+7+8th W)	(1,201)	(200,400)	77	72	65
13 (9+10+13+14th W)	(201,1)	(400,200)	35	37	44
14 (11+12+15+10th W)	(201,201)	(400,400)	78	71	60

Table 6.3: Window overlapping (Biased Lorentz): Selected windows and threshold values determined by different methods (for hexagon image of size 400x400, initial window size=200x100)

Window SL No	Starting point	End point	Ostu (Method1) T	PGA (Method2) T	MMSE (Method3) T
1 (4th W)	(1,301)	(200,400)	87	88	67
2 (8th W)	(201,301)	(400,400)	88	92	65
3 (1+2+5+6th W)	(1,1)	(200,400)	36	37	40
4 (3+4+7+8th W)	(201,201)	(400,400)	37	71	62

Table 6.4: Window Merging (Local & Global biased approach): Selected windows and threshold values determined by different methods (for hexagon image of size 400x400, initial window size=200x100)

Window SL No	Starting point	End point	Ostu (Method1)	PGA (Method2)	MMSE (Method3)
			T	T	T
1 (3rd W)	(1,201)	(200,300)	67	62	71
2 (4th W)	(1,301)	(200,400)	87	81	67
3 (7th W)	(201,201)	(400,300)	67	66	72
4 (8th W)	(201,301)	(400,400)	88	92	65
5 (1st+2nd+5th+6th W)	(1,1)	(400,200)	36	37	40

Table 6.5: Window Merging (Entropy based): Selected windows and threshold values determined by different methods (for hexagon image of size 400x400, initial window size=200x80)

Window SL No	Starting point	End point	Ostu (Method1)	PGA (Method2)	MMSE (Method3)
			T	T	T
1 (2nd W)	(1,81)	(200,160)	35	36	39
2 (3rd W)	(1,161)	(200,240)	54	49	57
3 (4th W)	(1,241)	(200,320)	74	73	55
4 (5th W)	(1,321)	(200,400)	90	94	111
5 (7th W)	(201,81)	(400,160)	34	32	38
6 (8th W)	(201,161)	(400,240)	54	51	58
7 (9th W)	(201,241)	(400,320)	73	74	54
8 (10th W)	(201,321)	(400,400)	91	101	100
9 (1+2+3+4+6+7+8+9 W)	(1,1)	(400,320)	54	60	45

Table 6.6: Window growing approach: Selected windows and threshold values determined by different methods (for hexagon image of size 400x400, initial window size=50x10, row increment=5, col increment=1)

Window SL No	Starting point	End point	Ostu (Method1)	PGA (Method2)	MMSE (Method3)
			T	T	T
1	(1,1)	(400,175)	32	34	41
2	(1,175)	(295,234)	55	51	63
3	(1,234)	(335,301)	71	68	77
4	(1,301)	(150,331)	82	80	60
5	(1,331)	(155,362)	88	94	64
6	(1,362)	(250,400)	96	86	89
7	(150,301)	(360,343)	83	93	93
8	(155,343)	(300,372)	92	94	65
9	(170,356)	(400,400)	95	83	117
10	(295,175)	(400,240)	57	60	64
11	(235,330)	(400,400)	91	105	73
12	(310,235)	(400,400)	73	78	88

Table 6.7: Threshold values and misclassification error (ME) for diffrent window size using the FB approach.

Different Approach		Percentage (%) of Missclasification error of different images			
		Hexagone Image	Crow Image	Rabbit Image	Rice Image
Otsu's Approach (Global Thresholding)		10.8850	15.4229	2.9260	18.5837
Huang's Approach		8.1781	5.8403	14.7740	8.3664
Approach 1 (Biased Lorentz Pyramid approach)	Method1	2.4238	5.5278	1.5913	1.3840
	Method2	1.7706	3.9639	1.1940	1.7441
	Method3	3.6331	10.4976	1.1830	3.1250
Approach 2 (Biased Lorentz Overlapping approach)	Method1	2.6519	11.3550	1.8793	1.6479
	Method2	1.84	1.8394	1.48	2.4
	Method3	2.9838	4.7505	2.9293	2.6382
Approach 3 (Weighted Local & Global approach)	Method1	2.5769	12.5830	1.4320	1.5808
	Method2	1.8863	4.9326	1.1847	1.5701
	Method3	4.9069	13.4087	1.5727	6.7154
Approach 4 (Entropy based approach)	Method1	1.5619	11.6099	1.5033	1.3443
	Method2	**1.5337**	**1.4819**	**1.3280**	**1.9150**
	Method3	2.3444	2.1016	1.9033	2.6430
Approach 5 (Window Growing approach)	Method1	1.5776	10.6323	2.4767	1.4252
	Method2	**1.5844**	**2.9880**	**1.0360**	**0.75**
	Method3	2.5062	3.9395	2.4333	5.2017

(a) (b) (c) (d)

Figure 6.11: Nonuniform lighting images (a) Hexagon (400x400); (b) Crow (400x512); (c) Rabbit (300x500); (d) Rice (256x256)

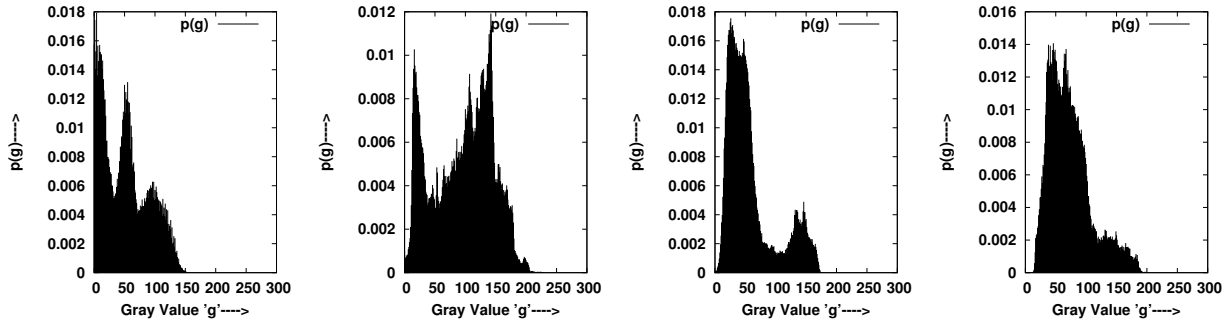

(a) (b) (c) (d)

Figure 6.12: Corresponding histogram of the (a) Hexagon; (b) Crow; (c) Rabbit; (d) Rice

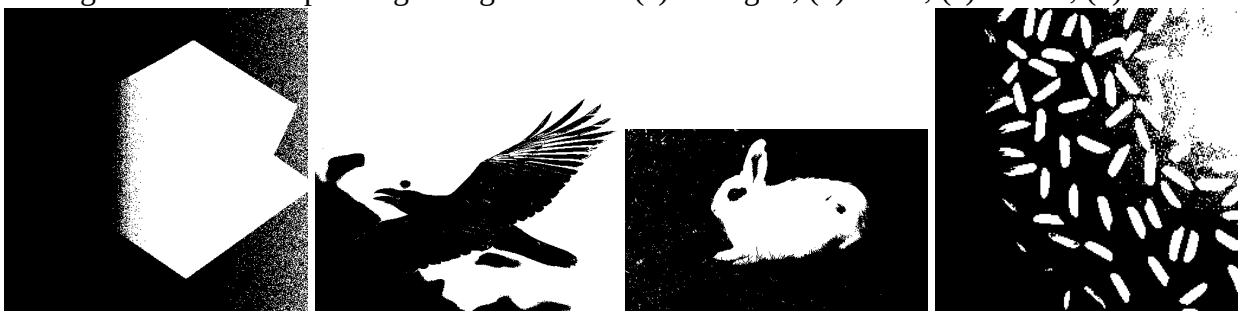

Figure 6.13: Segmented images using Ostu's Global Thresholding approach

Figure 6.14: Corresponding ground truth images manually constructed

(a) (b) (c) (d)

Figure 6.15: Nonuniform lighting images (a) Hexagon; (b) Crow; (c) Rabbit; and (d) Rice

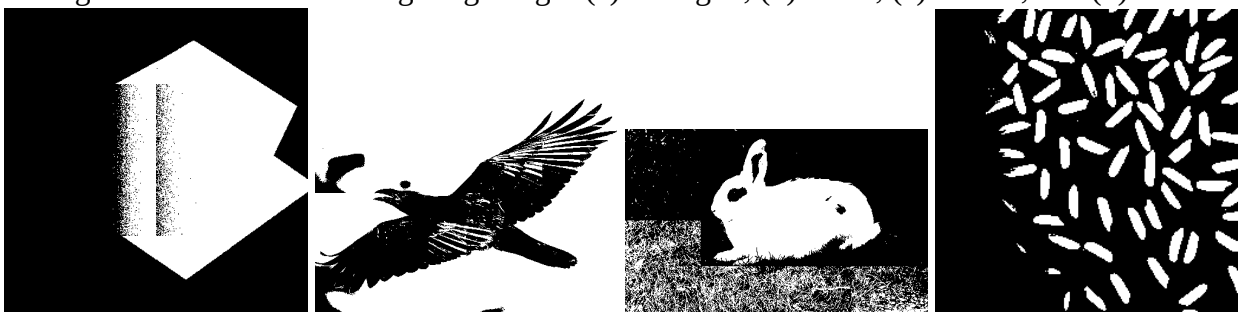

(a) (b) (c) (d)

Figure 6.16: Segmented images using Huang's Approach with Pyramid window merging. Initial window size: (a) 100x100; (b) 50x64; (c) 75x125; and (d) 32x32

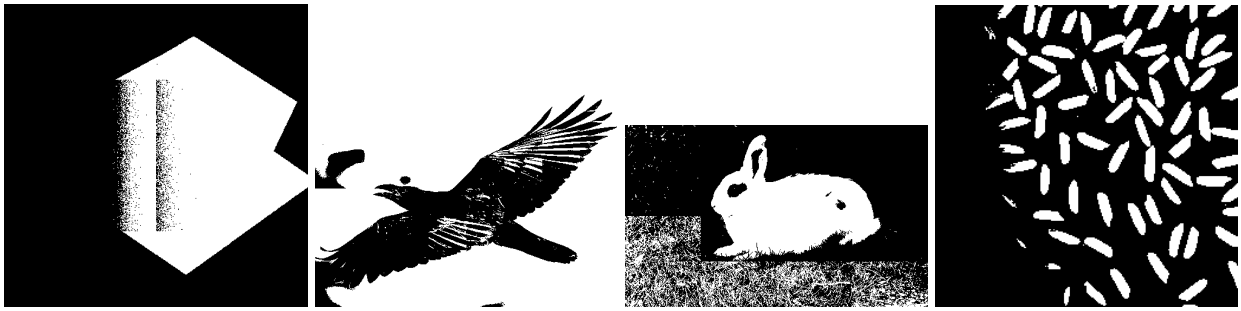

Row 1: Segmented images using Huang's Adaptive thresholding Approach.

Row 2: Segmented images using proposed Biased Lorentz Information and method 1 (Otsu).

Row 3: Segmented images using proposed Biased Lorentz Information and method 2 (PGA).

Row 4: Segmented images using proposed Biased Lorentz Information and method 3 (MMSE).

Figure 6.17: Adaptive window merging with Biased Lorentz Pyramid structre and segmentaion of windows using Otsu's and proposed method1, method2, and method 3

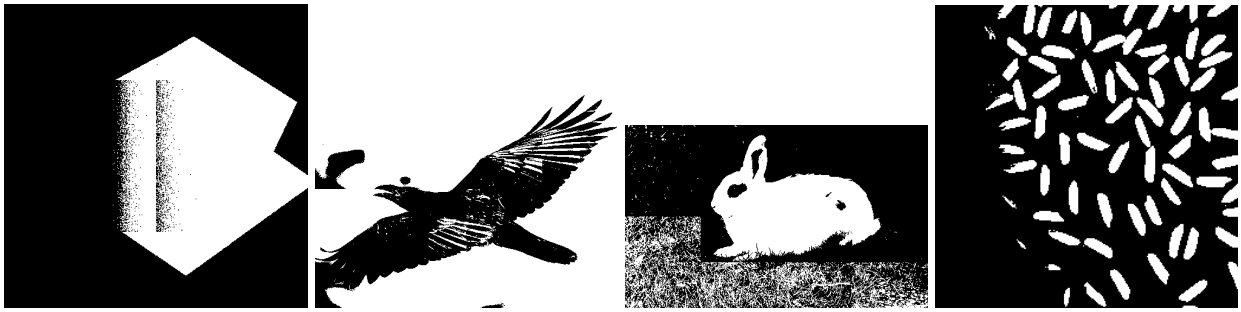

Row 1: Segmented images using Huang's Adaptive thresholding Approach.

Row 2: Segmented images using proposed Biased Lorentz Information and method 1 (Otsu).

Row 3: Segmented images using proposed Biased Lorentz Information and method 2 (PGA).

Row 4: Segmented images using proposed Biased Lorentz Information and method 3 (MMSE).

Figure 6.18: Adaptive thresholded images using Biased Lorentz Window Overlapping approach

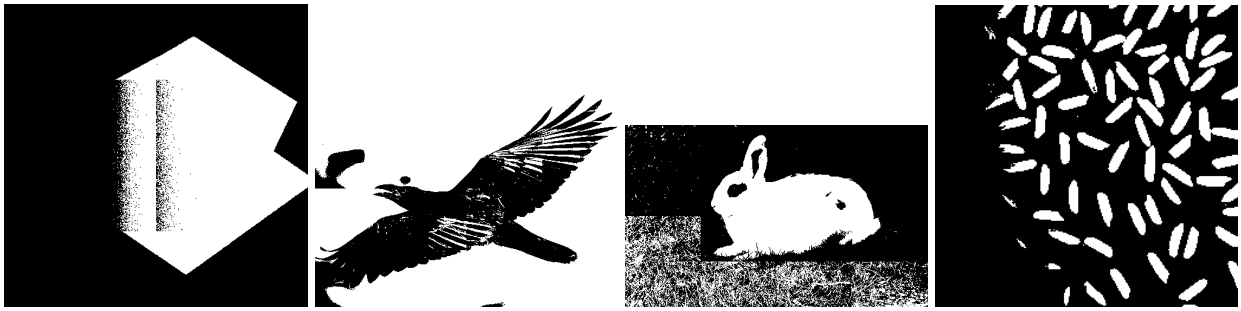

Row 1: Segmented images using Huang's Adaptive thresholding Approach.

Row 2: Segmented images using proposed local global Information and method 1 (Otsu).

Row 3: Segmented images using proposed local global Information and method 2 (PGA).

Row 4: Segmented images using proposed local global Information and method 3 (MMSE).

Figure 6.19: Adaptive window merging in pyramid structure using the local global information and segmentaion of windows using Otsu's and proposed method1, method2, and method 3

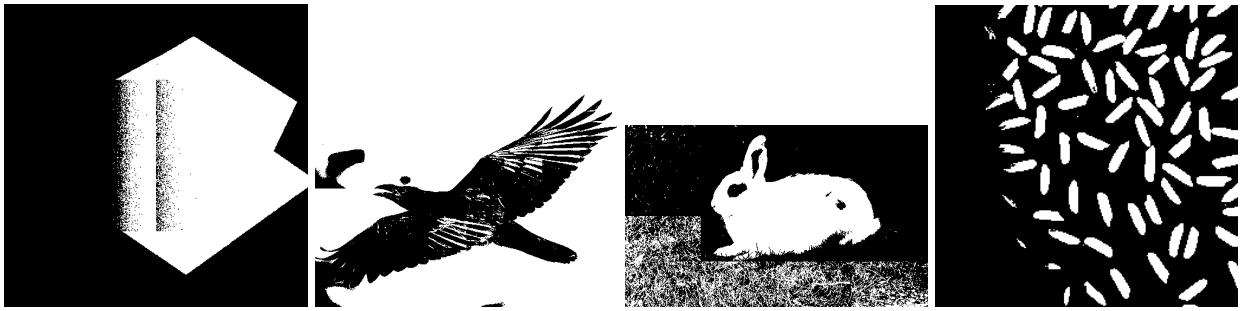

Row 1: Segmented images using Huang's Adaptive thresholding Approach.

Row 2: Segmented images using proposed entropy based criterion and method 1 (Otsu).

Row 3: Segmented images using proposed entropy based criterion and method 2 (PGA).

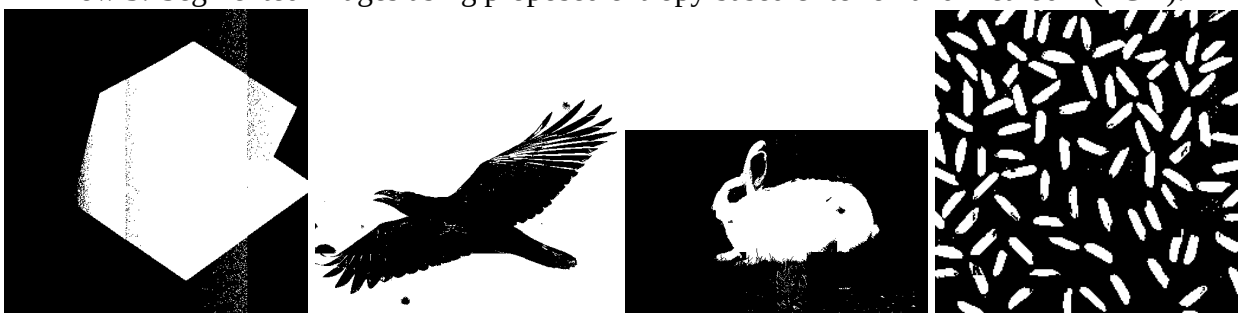

Row 4: Segmented images using proposed entropy based criterion and method 3 (MMSE).

Figure 6.20: Adaptive window growing method (Window overlapping) with entropy based criterion and segmentaion of windows using Otsu's and proposed method1, method2, and method 3

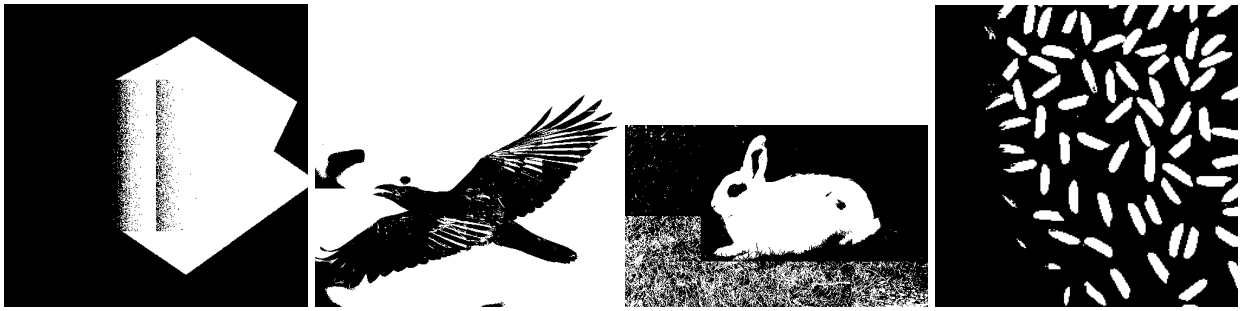

Row 1: Segmented images using Huang's Adaptive thresholding Approach.

Row 2: Segmented images using proposed window growing criterion and method 1 (Otsu).

Row 3: Segmented images using proposed window growing criterion and method 2 (PGA).

Row 4: Segmented images using proposed window growing criterion and method 3 (MMSE).

Figure 6.21: Adaptive window growing with entropy based criterion and segmentaion of windows using Otsu's and proposed method1, method2, and method 3

6.10 Conclusions

In this chapter, segmentation of images acquired under uneven lighting condition has been carried out. It has been observed that global thresholding approach failed to segment these images and hence, adaptive thresholding methods are necessary. The adaptive thresholding approaches are based on window merging and window growing notions. Three new criteria have been proposed for window merging. It has been observed that with window merging, segmentation of the proper portion of the image could be selected. The window overlapping approach is based on the notion of adding neighbourhood information in the image and hence, the adjacency is maintained for accurate segmentation. The methods, when compared with Huang's approach showed improved performance. However, it has been observed that the segmentation accuracy greatly depends upon the proper choice of size of the initial windows. This has been achieved by trial and error approach. In order to overcome this problem, a window growing approach has been proposed based on the notion of entropy and feature entropy. The accuracy of segmentation in window growing approach is found to be better than that of window merging approaches and Huang's method.

Chapter 7

Conclusions and Future Work

The problem of image segmentation has been addressed using thresholding based techniques. Often, in practice, it is necessary to separate object from the background and hence, viewed as a classification problem. If there are multiple objects in a scene, the problem boils down to a multiclass problem. Specifically, for fault detection, it has been necessary to separate faulty region from the healthy region and hence a classification problem.

Since, this thesis aimed at developing schemes suitable from real-time standpoint, the focus has been on devising novel strategies and algorithms exploiting the notion of thresholding. In this thesis, GA and PGA based schemes have been proposed to obtain optimal threshold. By and large, most of the thresholding techniques are based on the histogram of the original image.

A new notion of GA and PGA based clustering has been proposed to devise thresholding based schemes. The histogram of images are by and large, multimodal and nonlinear in nature. Therefore, the problem is viewed as handling nonlinear multimodal function. Each mode in a multimodal histogram corresponds to a class and there would be as many mode as there are classes. Each mode can be viewed to represent a class and hence, detection of class distributions of a histogram has been viewed as detecting the peaks of the histogram. If the histogram can be viewed as a nonlinear multimodal function, then determination of the classes reduce to the problem of detection of all the peaks. In nonlinear multimodal function frameworks, that is in an optimization framework, these peaks correspond to all possible solutions that is global and local optima of the nonlinear functions. Therefore, initially attempts have been made to develop schemes that would detect all the niches or peaks of a multimodal function. In such cases, basic GA (BGA) that has been widely used as function optimization problem would have reproduced one optimal solution. Therefore, it could be conceived that BGA will fail to detect all the peaks

and hence, the focus changed to devise schemes that would detect all peaks.

It has been known that GA based crowding maintains stable sub-populations at different niches of multimodal function. GA based crowding algorithm when tested on multimodal function could maintain stable sub-population at the respective niches and hence, all solutions or classes could be determined. The major bottleneck of this scheme was found to be computational burden. In order to make this scheme a viable one, the focus shifted to devise PGA based scheme. PGA based clustering algorithm has been proposed and the iterations taken was much less (some times 40 times less) than that of GA based schemes. Furthermore, PGA based schemes could detect all the peaks and hence, classes accurately. The effect of the network topology, migration policy, rate of migration, and type of migration on the rate convergence has been studied and it was observed that the migration policy and rate of migration, greatly influence the convergence rate. In order to accelerate the convergence of the PGA based schemes, a new interconnection model has been proposed based on a new notion of intra-deme migration besides the existing inter-deme migration.

This scheme accelerated the convergence to some extent even though not radically. It was also found out that the computational burden increases with increase in the neighbourhood structure of the net-topology and improvement on the result was not substantial. Hence, the first order net-topology with intra-deme migration was considered. The proposed PGA with this interconnection model converged faster than the without self-loop model. The convergence analysis of the proposed algorithm has been carried out and the algorithm has been shown to converge with a bound. The proposed PGA based algorithm could successfully be tested for two, four, and eight class nonlinear multimodal functions. In all these cases, the number of demes chosen is four. Even with decaying sinusoids, the algorithm could detect all the peaks and hence, all the classes. The only bottleneck of this scheme is that the parameters of PGA has been chosen on trial and error basis. The PGA based scheme has been found to converge within few tens of iterations.

The same notion has been used to develop thresholding based schemes of chapter 4. In this case, the shape information of the histogram has been used to device the thresholding based schemes. Besides, the threshold has also been obtained in a feature plane as opposed to original histogram. The feature pixels have been generated and the feature histogram has been constructed. Threshold is obtained from the feature histogram as opposed to the original histogram. The histogram distribution consists of modes corresponding to a class and the over-

lapping of the class distribution occurs either due to noise or typical nature of the image. It has been observed that the degree of overlapping reduces substantially in case of feature histogram thus paving the way for determination of correct threshold. PGA based clustering schemes have been used to determine the peaks followed by PGA based scheme to determine the valley. It has been found that the Feature based (FB) scheme produced satisfactory results as compared to Otsu's and Kwon's and FL approach.

In order to deal specifically with faults in a scene such as earth surface cracks, MMSE based schemes have been developed. The cracks could be of big or small size and the corresponding histogram looses bi-modality or tends to become unimodal. In such situations the FL, FB, Otsu, and Kwon's method produced poor results where as the MMSE based scheme produced satisfactory results. MMSE based schemes have been found to produce vary satisfactory results in case of image for colour blindness and earth surface cracks. The only bottleneck of the MMSE scheme is that the accuracy depends upon the assumption of the peak as the mean of the class. It is considerable that for large uneven distributions, the detected means may not correspond to the actual mean and hence, the detected threshold may yield more classification error.

It has been observed that the proposed scheme, Otsu and Kwon method produced poor results for images acquired under uneven lighting conditions. Therefore, adaptive thresholding methods have been proposed to obtain local thresholds. In window merging approach, the window selection criterion depends on the three proposed criterion. Based on this criterion, either the image is merged or unmerged. It has been found out that the results obtained by the proposed methods are superior to that of Huang's approach but the shortcoming of Huang's approach, that is the accuracy of segmentation depends upon the proper choice of window size, still persists with our proposed window merging schemes. This has been overcome by the proposed window growing approach. The proposed scheme could produce satisfactory results for different images acquired under different uneven lighting condition.

7.1 Future work

PGA based scheme has been proposed to deal with discrete histograms. The peaks and valleys have been detected by PGA based search algorithm. The results obtained are based on the serial implementation of the parallel algorithm. Hence, parallel implementation of the algorithm is

worth pursuing.

The feature based schemes have been developed to minimize the overlapping class distribution error. This can be extended to handle noisy images and images with overlapping distributions. MMSE based schemes have been developed to detect faults in a given image. Although MMSE based algorithm produced promising results, the schemes can be modified to parametrize the class distribution as opposed to assuming the peak at the mean of the classes. Robust MMSE based schemes shall be modified for multiclass problems. The scheme also can be modified to detect other type of faults.

Adaptive thresholding methods have been proposed based on adaptively selecting windows based criteria. Two dimensional entropy based criteria can be defined to handle window selection. Adaptive thresholding strategies may be devised on the feature plane. The adaptive window merging schemes have been implemented serially and its parallel implementation is worth pursuing. Multi-resolution based adaptive thresholding scheme may be designed to handle images under uneven lighting condition and noisy conditions.

Bibliography

[1] J. S. Weszka. A survey of threshold selection techniques. *Comp. Graphics and Image processing*, 7:259–265, 1978.

[2] K. S. Fu and J. K. Mui. A survey on image segmentation. *Pattern recognition*, 13:3–16, 1981.

[3] P. K. Sahoo, S. Soltani, and A. K. C. Wong. A survey of thrsholding technique. *Computer Vision, Graphics, and Image Processing*, 41:233–260, 1988.

[4] M. Sezgin and B. Sankur. Survey over image thresholding techniques and quantitative performance evaluation. *Journal of Electronic Imaging*, 13(1):146–165, 2004.

[5] N. Otsu. A threshold selection method from gray-level histograms. *IEEE Trans. Syst., Man, Cybern.*, SMC-9(1):62–66, 1979.

[6] S.S. Reddi, S. F. Rudin, and H. R. Keshavan. An optimal multiple threshold scheme for image segmentation. *IEEE Trans. on Systems, Man and Cybernetics*, 14(4):661–671, August 1984.

[7] Han Lee and Rae-Hong Park. Comments on “an optimal multiple threshold scheme for image segmentation”. *IEEE Trans. on Systems, Man, and Cybernetics*, 20(3):741–742, May/June 1990.

[8] S. Boukharouba, J. M. Rebordao, and P. L. Wendel. An amplitude segmentation method based on the distribution function of an image. *Computer Vision, Graphics, and Image Processing*, 29:47–59, 1985.

[9] A. D. Brink. Gray-level thresholding of images using a correlation criterion. *Pattern Recognition Letters*, 9:335–341, June 1989.

[10] I. Cseke and Z. Fazekas. Comments on gray-level thresholding of images using a correlation criterion. *Pattern Recognition Letters*, 11:709–710, October 1990.

[11] L. Dong and G. Yu. Fast search for thresholds from 1d and 2d histogram by an iterative algorithm for image segmentation. In *Proceedings of the IEEE International Conference on Systems, Man and Cybernetics*, volume 4, pages 3057–3062. IEEE, 10-13 Oct. 2004.

[12] Z. Hou, Q. Hu, and W. L. Nowinski. On minimum variance thresholding. *Pattern Recognition Letters*, 27:1732–1743, 2006.

[13] D. Liu and J. Yu. Otsu method and k-means. In *Ninth International Conference on Hybrid Intelligent System*, volume 1, pages 344–349. IEEE, 12-14 Aug. 2009.

[14] Punam K. Saha and Jayaram K. Udupa. Optimum image thresholding via class uncertainty and region homogeneity. *IEEE Trans. On Pattern Analysis and Machine Intelligence*, 23(7):689–706, July 2001.

[15] S. Belkasim, A. Ghazal, and O. A. Basir. Phase-based optimal image thresholding. *Digital signal processing*, 13:636–655, 2003.

[16] S. H. Kwon. Threshold selection based on cluster analysis. *Pattern Recognition Letters*, 25:1045–1050, 2004.

[17] Y. Qiao, Q. Hu, G. Qian, S. Luo, and W. L. Nowinski. Thresholding based on variance and intencity contrast. *Pattern Recognition*, 40:596–608, 2007.

[18] H Zhang, W. Gao, X. Chen, and D. Zhao. Object detection using spatial histogram features. *Image and Vision Computing*, 24:327–341, 2006.

[19] S. Chen and D. Li. Image binarization focusing on objects. *Neurocomputing*, 69:2411–2415, 2006.

[20] Qingmao Hu, Zujun Hou, and Wieslaw. L. Nowinski. Supervised range-constrained thresholding. *IEEE Transactions on Image Processing*, 15(1):228–240, January 2006.

[21] S. Wang, F. Chung, and F. Xiong. A novel image thrsholding method based on parzen window estimate. *Pattern Recognition*, 41(1):117–129, Jan 2008.

[22] D. Sen and S. K. Pal. Histogram thresholding using beam theory and ambiguity measures. *Fundamenta Informaticae*, 75(1-4):483–504, January 2007.

[23] L. Dong, G. Yu, P. Ogunbona, and W. Li. An efficient iterative algorithm for image thresholding. *Pattern Recognition Letter*, 29(9):1311–1316, 1 July 2008.

[24] R. M. Carnicer and F. J. M. Cuevas. Unimodal thresholding for edge detection. *Pattern Recognition*, 41:2337–2346, 2008.

[25] Qingmao Hu, Suhuai Luo, Yu Qiao, and Guoyu Qian. Supervised grayscale thresholding based on transition regions. *Image and Vision Computing*, 26:1677–1684, 2008.

[26] Zikuan Chen. Histogram partition and interval thresholding for volumetric breast tissue segmentation. *Computerized Medical Imaging and Graphics*, 32:1–10, 2008.

[27] Z. Li and C. Liu. An image thresholding method based on standard deviation. In *International Joint Conference on Computational Sciences and Optimization.*, pages 835–838. IEEE, 24-26 April 2009.

[28] A. Nakib, H. Oulhadj, and P Siarry. A thresholding method based on two-dimensional fractional differentiation. *Image and Vision Computing*, 27:1343–1357, 2009.

[29] E. A. A. De Maria, E. Gho, C. E. Maidana, C. A. Rodriguez, F. I. Szklanny, and H. R. Tantignone. Real time fpga based thresholding segmentation in a multi touch system. In *4th Southern Conference on Programmable Logic*, pages 237–240. IEEE, 26-28 March 2008.

[30] W. Jianlai, Y. Chunling, Z. Min, and W. Changhui. Implementation of oysu's thresholding process based on fpga. In *4th IEEE Conference on Industrial Electronics and Applications*, pages 479–483. IEEE, 25-27 May 2009.

[31] A. Cristo, A. Plaza, and D. Valencia. A novel thresholding method for automatically detecting stars in astronomical images. In *IEEE International Symposium on Signal Processing and Information Technology*, pages 180–185. IEEE, 16-19 Dec. 2008.

[32] Wen-Nung Lie. An efficient threshold-evaluation algorithm for image segmentation based on spatial graylevel co-occurances. *Signal Processing*, 31:121–126, 1993.

[33] Y. J. Jhang. A survey on evaluation methods for image segmentation. *Pattern Recognition*, 29(8):1335–1346, 1996.

[34] Y. J. Zhang. A review of recent evaluation methods for image segmentation. In *Proceedings of the International Symposium on Siganal Processing and Applications*, pages 148–151, Kuala Lumpur, Malaysia, 13-16 August 2001. IEEE.

[35] J. Kittler and J. Illingwoth. Minimum error thresholding. *Pattern Recognition*, 19(1):41–47, 1986.

[36] K. V. Mardia and T. J. Hainsworth. A spatial thresholding method for image segmentation. *IEEE Trans. on Pattern Analysis and Machine Intelligence*, 10(6):919–927, November 1988.

[37] C. K. Chow and T. Kaneko. Automatic boundary detection of the left ventricle from cineangiograms. *Computers and Biomedical Research*, 5:388–410, 1972.

[38] C. A. Glasbey. An analysis of histogram-based thresholding algorithms. *CVGIP: Graphical Models And Image Processing*, 55(6):532–537, November 1993.

[39] N. Ramesh, J.-H. Yoo, and I. K. Sethi. Thresholding based on histogram approximation. *IEE Proc.-Vis. Image Processing*, 142(5):271–279, October 1995.

[40] Vincenzo Caglioti and Vittorio Maniezzo. Mode determination in noisy bimodal images by histogram comparison. *Pattern Recognition Letters*, 16:1237–1248, 1995.

[41] Yui Man Lui and Heng-Da Cheng. A new peak selection criterion based on minimizing the classification error. *Information Sciences*, 94:213–233, 1996.

[42] J. Cai and Z. Q. Liu. A new thresholding algorithm based on all pole model. In *Proceedings of the Fourteenth International Conference on Pattern Recognition*, pages 34–36, Brisbane, Qld, Australia, 1998. IEEE.

[43] T. Pun. A new method for gray-level picture thresholding using the entropy of the histogram. *Signal Processing*, 2:223–237, 1980.

[44] T. Pun. Entropic thresholding, a new approach. *Computer Graphics and Image Processing*, 16:210–239, 1981.

[45] J. N. Kapur, P. K. Sahoo, and A. K. C. Wong. A new method for gray-level picture thresholding. *Computer Vision, Graphics, and Image Processing*, 29:273–285, 1985.

[46] N. R. Pal and S. K. Pal. Entropy: A new defination and its application. *IEEE Trans. on Systems, Man, and cybernetics*, 21(5):1260–1270, 1991.

[47] C. H. Li and C. K. Lee. Minimum cross entropy thresholding. *Pattern Recognition*, 26(4):617–625, 1993.

[48] A. D. Brink and N. E. Pendoc. Minimum cross entropy threshold selection. *Pattern Recognition*, 29(1):179–188, January 1996.

[49] N. R. Pal. On minimum cross entropy thresholding. *Pattern Recognition*, 29(4):575–580, 1996.

[50] C. I. Chang, Wang J. Chen, K., and M. L. G. Althouse. A relative entropy-based approach to image thresholding. *Pattern Recognition*, 27(9):1275–1289, 1994.

[51] Mark L. G. Althouse. Image segmentation by local entropy methods. In *International Conference on Image Processing*, volume 3, pages 61–64. IEEE, 23-26 Oct. 1995.

[52] C. H. Li and P. K. S. Tam. An iterative algorithm for minimum cross entropy thresholding. *Pattern Recognition Letters*, 19:771–776, 1998.

[53] P. Sahoo, C. Wilkins, and J. Yeager. Threshold selection using renyi's entropy. *Pattern Recognition*, 30(1):71–84, 1997.

[54] A. D. Brink. Using spatial information as an aid to maximum entropy image threshold selection. *Pattern Recognition Letters*, 17(1):29–36, January 1996.

[55] Chong Jinsong and Wang Hongqi. Entropic thresholding method using genetic algorithm. In *Proceedings of International Symposium on Geoscience and Remote Sensing*, pages 1247–1249, Hamburg,Germany, 28 June- 02 July 1999. IEEE.

[56] Nikola Pavesic. Gray level thresholding using the havrda and charvat entropy. In *Proceedings of 10th Mediterranean Electrotechnical Conference, MEleCon 2000*, volume 2, pages 631–634. IEEE, 2000.

[57] Peng-Yeng Yin. Maximum entropy based optimal threshold selection using deterministic reinforcement learning with control randomization. *Signal Processing*, 82:993–1006, 2002.

[58] M. Portes de Albuquerque, I. A. Esquef, A. R. G Mello, W. B. , and M. Portes de Albuquerque. Image thresholding using tsallis entropy. *Pattern Recognition Letters*, 25:1059–1065, 2004.

[59] Chengxin Yan, Nong Sang, and Tianxu Zhang. Local entropy-based transition region extraction and thresholding. *Pattern Recognition Letters*, 24:2935–2941, 2003.

[60] T. Chanwimaluang and G. Fan. An efficient blood vessel detection algorithm for retinal images using local entropy thresholding. In *International Symposium on Circuits and Systems (ISCAS)*, volume 5, pages v21–v24. IEEE, 25-28 May 2003.

[61] Hui Zhu, Zhizhong Fu, and Zaiming Li. A new image thresholding method based on relative entropy. In *International Conference on Communications, Circuits and Systems and West Sino Exposition*, volume 1, pages 634–638. IEEE, 29 June-1 July 2002.

[62] Shu Yang, Ying Han, Cai-Rong Wang, and Xiao-Wei Wang. Fast selecting threshold algorithm based on one-dimensional entropy. In *Proceedings of the Fourth International Conference on Machine Learning and Cybernetics*, pages 4554–4557, Guangzhou, 18-21 August 2005. IEEE.

[63] A. A. A. Shareha, M. Rajeswari, and D. Ramachandram. Textured renyi entropy for image thresholding. In *Proc. of the Fifth International Conference on Computer Graphics, Imaging and Visualisation*, pages 185–192. IEEE, 26-28 Aug. 2008.

[64] G. Al-Osaimi and Ali El-Zaart. Minimum cross entropy thresholding for sar images. In *3rd International Conference on Information and Communication Technologies: From Theory to Applications*, pages 1–6. IEEE, 7-11 April 2008.

[65] M. P. de Albuquerque, I. A. Esquef, and e M. P. de Albuquerque. Image segmentation using nonextensive relative entropy. *IEEE Trans. on Latin America*, 6(5):477–483, September 2008.

[66] Yasser Ebrahim. Entropy based thresholding of cross-dissolved ultrasound images. In *Canadian Conference on Electrical and computer Engineering*, volume 3, pages 1477–1480, Montreal, 4-7 May 2003. IEEE.

[67] Ahmed S. Abutaleb. Automatic thresholding of gray-level picture using two-dimensional entropy. *Computer Vision, Graphics, and Image Processing*, 47:22–32, 1989.

[68] W. T. Chen, C. H. Wen, and C. W. Yang. A fast two dimensional entropic thresholding algorithm. *Pattern Recognition*, 27(7):885–893, 1994.

[69] Qing Wang, Qiurang Wang, David Dagan Feng, Rongchun Zhao, and Zheru Chi. A fast 2d entropic thresholding method by wavelet decomposition. In *Proceedings of International Conference on Image Processing*, volume 3, pages III 265–III 268. IEEE, 24-28 June 2002.

[70] Y. Zimmer, R.P. Tepper, and S. Akselrod. A two dimensional extention of minimum cross entropy thresholding for the segmentation of ultrasound images. *Ultrasound in Med. and Biol.*, 22(9):1183–1190, 1996.

[71] P. K. Sahoo and G. Arora. Image thresholding using two-dimensional tsallis-havrda-charvat entropy. *Pattern Recognition Letters*, 27:520–528, 2006.

[72] X. Zhang and H. Zhang. Improved image thresholding based on 2-d tsallis entropy. In *International Conference on Environmental Science and Information Application Technology*, volume 1, pages 363–366. IEEE, 4-5 July 2009.

[73] X. Tian and X. Hou. A tsallis-entropy image thresholding method based on two-dimensional histogram obique segmentation. In *WASE International Conference on Information Engineering*, volume 1, pages 164–168. IEEE, 10-11 July 2009.

[74] Shyuan Wang and Robert M. Haralick. Automatic multithreshold selection. *Computer Vision, Graphics, and Image processing*, 25:46–67, 1984.

[75] N. Papamarkos and B. Gatos. A new approach for multilevel threshold selection. *CVGIP: Graphical Models and Image Processing*, 56(5):357–370, September 1994.

[76] Du-Ming Tsai. A fast thresholding selection procedure for multimodal and unimodal histograms. *Pattern recognition letters*, 16:653–666, 1995.

[77] Peng-Yeng Yin and Ling-Hwei Chen. A fast iterative scheme for multilevel thresholding methods. *Signal Processing*, 60:305–313, 1997.

[78] Peng-Yeng Yin. A fast scheme for optimal thresholding using genetic algorithms. *Signal Processing*, 72:85–95, 1999.

[79] L Cao, Z. K. Shi, and E. K. W. Cheng. Fast automatic multilevel thresholding method. *Electronics Letters*, 38(16):868–870, August 2002.

[80] N. Papamarkos, C. Strouthopoulos, and I. Andreadis. Multithresholding of color and gray-level images through a neural network technique. *Image and Vision Computing*, 18:213–222, 2000.

[81] Songcan Chen and Min Wang. Seeking multi-thresholds directly from support vectors for image segmentation. *Neurocomputing*, 67:335–344, March 2005.

[82] Mehmet Sezgin and Ramazan Tasaltin. A new dichotomization technique to multilevel thresholding devoted to inspection applications. *Pattern Recognition Letters*, 21:151–161, 2000.

[83] Erwie Zahara, Shu-Kai S. Fan, and Du-Ming Tsai. Optimal multi-thresholding using a hybrid optimization approach. *Pattern Recognition Letters*, 26:1082–1095, 2005.

[84] S. Arora, J. Acharya, A. Verma, and P. K. Panigrahi. Multilevel thresholding for image segmentation through a fast statistical recursive algorithm. *Pattern Recognition Letters*, 29:119–125, 2008.

[85] M. Maitra and A. Chatterjee. A hybrid cooperative-comprehensive learning based pso algorithm for image segmentation using multilevel thresholding. *Expert Systems with Applications*, 34:1341–1350, 2008.

[86] Li Cao, Paul Bao, and Zhongke Shi. The strongest schema learning ga and its application to multilevel thresholding. *Image and Vision Computing*, 26:716–724, 2008.

[87] Ren-Jean Liou, Ming-Huwi Horng, and Ting-Wei Jiang. Multi-level thresholding selection by using the honey bee mating. In *Ninth International Conference on Hybrid Intelligent System*, volume 1, pages 147–151. IEEE, 12-14 Aug. 2009.

[88] D.-Y. Haung and C.-H. Wang. Optimal multi-level thresholding using a two stage otsu optimization approach. *Pattern recognition Letters*, 30:275–284, 2009.

[89] M. Sezgin and B. Sankur. Selection of thresholding methods for non-destructive testing applications. In *Proceedings of the International Conference on Image Processing*, volume 3, pages 764–767, Thessaloniki, Greece, July 2001. IEEE.

[90] M. H. F. Wilkinson, T. Wijbenga, G. de Vries, and M. A. Westenberg. Blod vessel segmentation using moving-window robust automatic threshold selection. In *Proc. of the International Coference on Image Processing*, volume 2, pages II–1093– II–1096. IEEE, 14-17 Sept. 2003.

[91] Hui-Fuang Ng. Automatic thresholding for defect detection. *Proc. of Sixth International Conference on Information Technology, Bhubaneswar*, 27:1644–1649, 2006.

[92] W. B. Lievers and A. K. Pilkey. An evaluation of global thresholding techniques for the automatic image segmentation of automotive aluminum sheet alloys. *Material Science and Engineering A*, 381:134–142, 2004.

[93] A. Mahmoudi and F. Regragui. Welding defect detection by segmentation of radiographic images. In *World Congress on Computer Science and Information Engineering*, volume 7, pages 111–115. IEEE, 31 March- 2 April 2009.

[94] B. Dizdaroglu. Detection of painting cracks using optimal thresholding. In *IEEE 17th Signal Processing and Communications Application Conference*, pages 981–984. IEEE, 9-11 April 2009.

[95] Y. Nakagawa and A. Rosenfels. Some experiments on variable thresholding. *Pattern Recognition*, 11:191–2004, 2001.

[96] Jeng-Daw Yang, Yung-Sheng Chen, and Wen-Hsing Hsu. Adaptive thresholding algorithm and its hardware implementation. *Pattern Recognition Letter*, 15:141–150, 1994.

[97] Slobodan Ribaric, Sinisa Segvic, and Vladmir Spisic. Locally adaptive thresholding of the sequence of image frame. In *Proceedings of 10th Mediterranean Electrotechnical Conference*, volume 2, pages 673–676. IEEE, 2000.

[98] X. P. Zhang and M. D. Desai. Segmentation of bright targets using wavelets and adaptive thresholding. *IEEE Trans. on Image Processing*, 10(7):1020–1030, July 2001.

[99] B. G. Kim, D. J. Kim, and D. J. Park. Novel precision target detection with adaptive thresholding for dynamic image segmentation. *Machine Vision and Applications*, 12:259–270, 2001.

[100] J. B. Kim, H. S. Park, M. H. Park, and H. J. Kim. A real-time region-based motion segmentation using adaptive thresholding and k-means clustering. In *Proceedings of the 14th International Conference on Advances in Artificial Intelligence*, pages 213–224, Adelaide, Australia, 10-14 Dec. 2001. IEEE.

[101] S. Haker, G. Sapiro, A. Tannenbaum, and D. Washburn. Missile tracking using knowledge-based adaptive thresholding. In *Proc. of the International Conference on Image Processing*, volume 1, pages 786–789, Thessaloniki, Greece, 2001. IEEE.

[102] S. Herman and E. Bellers. Locally-adaptive processing of television images based on real-time image segmentation. In *Proceedings of the International Conference on Consumer Electronics*, pages 66–67. IEEE, 2002.

[103] M. Feigin and N. Sochen. Segmentation and denoising via an adaptive threshold mumford-shah-like functional. In *Proceedings of the 17th International Conference on Pattern Recognition*, volume 2, pages 98–101, Cambridge UK, 23-26 Aug. 2002. IEEE Computer Society.

[104] Qingming Huang, Wen Gao, and Wenjian Cai. Thresholding technique with adaptive window selection for uneven lighting image. *Pattern Recognition Letters*, 26(6):801–808, May 2005.

[105] Xiaoyi Jiang and Daniel Mojon. Adaptive local thresholding by verification-based multithreshold probing with application to vessel detection in retinal images. *IEEE Trans. on Pattern Analysis and Machine Intelligence*, 25(1):131–137, 1995.

[106] E. dos S. Filho, Y. Saijo, and T. Yambe. Segmentation of classification regions in intravascular ultrasound images by adaptive thresholding. In *Proceedings of the IEEE Symposium on Computer-Based Medical Systems*, page 785, Salt Lake City, Utah, 22-23 June 2006. IEEE Comuter Society.

[107] E. Espinoza and G. Martinez. Cell cluster segmentation based on global and local thresholding for in-situ microscopy. In *Proceedings of the IEEE International Symposium on Biomedical Imaging: from Nano to Macro*, pages 542–545, Arlington, Virginia, USA, 6-9 April. 2006. IEEE.

[108] N. Sang, H. Li, W. Peng, and T. Zhang. Knowledge-based adaptive thresholding segmentation of digital subtraction angiography images. *Image and Vision Computing*, 25:1263–1270, 2007.

[109] Joe-Air Jiang, H. Y. Chang, K. H. Wu, C. S. Ouyang, M. M. Yang, E. C. Yang, T. W. Chen, and T. T. Lin. An adaptive image segmentation algorithm for x-ray quarantine inspection of selected fruits. *Computers and Electronics in Agriculture*, 60:190–200, 2008.

[110] M. H. Pi and H. Zhang. Two-stage image segmentation by adaptive thresholding and gradient watershed. In *Proceedings of the Second Canadian Conference on Computer and Robot Vision*, pages 57–64. IEEE, 09-11 May 2005.

[111] M. M. Mokji and S. A. R. Abu Bakar. Adaptive thresholding based on co-occurrence matrix edge information. *Journal of Computers*, 2(8):44–52, 2007.

[112] B. N. Saha and N. Ray. Image thresholding by variational minmax optimization. *Pattern Recognition*, 42:843–856, 2009.

[113] Yao-Hong Tsai. A new approach for image thresholding under uneven lighting conditions. In *6th IEEE/ACIS International Conference on Computer and information Science*, pages 123–127. IEEE, 11-13 July 2007.

[114] F. Shafait, D. Keysers, and T. M. Breuel. Efficient implementation of local adaptive thresholding techniques using integral images. In *Proceedings of the XV Conference on Document Recognition and Retrival*, volume 6815. SPIE Digital Library, 28 January 2008.

[115] K. J. Batenburg and J. Sijbers. Adaptive thresholding of tomograms by projection distance minimization. *Pattern Recognition*, 42:2297–2305, 2009.

[116] D. E. Goldberg. *Genetic algorithm in search optimization machine learning*. Adiison Wesley, 1989.

[117] M. Srinivas and L. M. Patnaik. Genetic algorithms: A survey. *IEEE Magazine, Computer*, 27(6):17–26, June 1994.

[118] D. E. Goldberg. Genetic algorithm in search optimization machine learning. *Calculateurs Parallels*, 5(2):141–171, 1998.

[119] T. Back. *Evolutionary algorithms in theory and practice: Evolution strategies, Evolutionary programming, Genetic algorithms*. Oxford University Press, USA, Dec 1995.

[120] T. Back, D. B. Fogel, and T Michalewicz. *Evolutionary Computation 1; Basic Algorithms and operators*. Institute of Physics Publishing, Bristol and Philadelphia, 2000.

[121] K. A. De Jong. *Analysis of the behavior of a class of genetic adaptive systems*. PhD thesis, University of Michigan, 1975.

[122] R. Tansese. Distributed genetic algorithms. In *Proc. of the 3rd International Conference on Genetic Algorithms*, pages 434–439, George Mason University, USA, 1989.

[123] M. K. Muhlenbein. Parallel genetic algorithms, population genetics and combinational optimization. In *Proc. of the 3rd International Conference on Genetic Algorithms*, pages 416–421, George Mason University, USA, 1989. Morgan Kaufmann (San MAteo).

[124] E. Cantu-Paz. A survey of parallel genetic algorithms. *Calculateurs Parallels*, 5(2):141–171, 1998.

[125] R. Tansese. Parallel genetic algorithm for a hypercube. In *Proc. of the 2nd International Conference on Genetic Algorithms and Their Applications*, pages 177–183, Cambridge, Boston, MA, 1987.

[126] J. P. Cohoon, W. N. Martin, and D. S. Richards. A multipopulation genetic algorithm for solving the k-partition problem on hyper-cubes. In *Proc. of the 4th International Conference on Genetic Algorithms*, pages 244–248, Cambridge, Boston, MA, 1991. Morgan Kaufmann.

[127] J. P. Cohoon, S. U. Hegde, W. N. Martin, and D. S. Richards. Punctuated equilibria: A parallel genetic algorithm. In *Proc. of the 2nd International Conference on Genetic Algorithms*, pages 148–154, Cambridge, MA, 1987.

[128] J. P. Cohoon, S. U. Hegde, W. N. Martin, and D. S. Richards. Distributed genetic algorithms for the floorplan design problem. *IEEE Trans. on Computer Aided Design*, 10(4):483–492, April 1991.

[129] M. Gorges-Schleuter and M. K. Muhlenbein. Asparagos: an asynchronous parallel genetic optimization strategy. In *Proc. of the 3rd International Conference on Genetic Algorithms*, pages 422–427, George Mason University, USA, 1989. Morgan Kaufmann (San MAteo).

[130] S. W. Mahfoud. Simple analytical models of genetic algorithms for multimodal function optimization. In *In Proc. 5th International Conference on Genetic Algorithm*, page 643, 1993.

[131] S. W. Mahfoud. Crossover interaction among niches. In *Proc. of 1st IEEE Conference on Evolutionary Computation, world Congress on Computation Intelligence*, pages 188–193, 1994.

[132] S. W. Mahfoud. Crowding and preselection revisited. In *Parallel Problem Solving from Nature 2*, pages 27–36, Brussels, Belgium, 1992.

[133] Gulshan Singh and Kalyanmoy Deb. Comparision of multi-modal optimization algorithms based on evolutionary algorithms. In *Proceedings of 8th Annual Conference on Genetic and Evolutionary Computation*, pages 1305–1312, Seattle, Washington, USA, 2006. ACM, New York, USA.

[134] Rafal Drezewski and Marek Kisiel-Dorohinicki. Maintaining diversity in agent-based evolutionary computation. *Lecture Notes in Computer Science, Springer Berlin/Heidelberg*, 3999/2006:908–911, 10 May 2006.

[135] A. D. Cioppa, C. D. Stefano, and A. Marcelli. Where are the niches? dynamic fitness sharing. *IEEE Trans. on Evolutionary Computation*, 11(4):453–465, August 2007.

[136] S. W. Mahfoud. A comparision of parallel and sequential niching methods. In *In Proc. International Conference on Genetic Algorithm*, pages 136–143, 1995.

[137] S. W Mahfoud. *Niching methods for genetic algorithm*. PhD thesis, University of Illinois at Urbana-Champaign, 1995.

[138] Grant Dick. A comparision of localized and global niching methods. In *17th Annual Colloquium of Spatial Information Research Center*, pages 91–101, Dunedin, New Zealand, 24-25 November 2005.

[139] P. K. Nanda, B Ghose, and T. N. Swain. Parallel genetic algorithm based unsupervised scheme for extraction of power frequency signals in the steel industry. In *IEE Proceedings of Vision, Image and Signal Processing*, pages 204–210, August 2002.

[140] Erick Cantu-Paz. A summary of research on parallel genetic algorithm. *University of Illinois, IlliGAL Report No. 95007*, July 1995.

[141] E. C. Paz and D. E. Goldberg. Parallel genetic algorithm with distributed panmictic population. Technical Report 99006, Illinois Genetic Algorithms Laboratory, University of Illinois at Urbana-Champaign, 104 S Mathews Avenue Urbana, IL 61801, January 1999.

[142] N. R. Pal and S. K. Pal. A review on image segmentation techniques. *Pattern Recognition*, 26(9):1277–1294, 1993.

[143] S. H. Kwon. Cluster validity index for fuzzy clustering. *Electronics Letters*, 34(22):2176–2177, 21-25 June 1998.

[144] P. Kanungo, P. K. Nanda, and A. Ghosh. Classification of objects and background using parallel genetic algorithm based clustering. *Electronic Letters on Computer Vision and Image Analysis*, 6(3):42–53, October 2007.

Dissemination of work

1. P. Kanungo , P. K. Nanda and A. Ghosh , “Classication of Objects and Background Using Parallel Genetic Algorithm Based Clustering,” *Electronics Letters On Computer Vision and Image Analysis*, Vol.6, No.3, pp. 42-53 , 2007.

2. P. Kanungo , P. K. Nanda and A. Ghosh , “Parallel Genetic Algorithm Based Clustering for Object background Classification,” *to be published in Pattern Recognition and Image Processing*, World of Scientific Press.

3. P. Kanungo , P. K. Nanda and A. Ghosh , “Detection of earth surface cracks using parallel genetic algorithm based clustering algorithm,” *Communicated to Pattern Recognition Letters*, Elsevier.

4. P. Kanungo, P. K. Nanda, A. Ghosh and U. C. Samal, “Classification of objects and background using Parallel Genetic Algorithm based Clustering,” *Proc. of the IEEE-International Conference on Signal and Image Processing*, BCET, Hubli, 7-9 Dec., 2006.

5. P. Kanungo and P. K. Nanda,“Parallel genetic algorithm based thresholding for image segmentation,” *Proc. of the National Seminar on IT and Softcomputing (ITSC-06)*, IMT, Nagpur, 17-18 Nov., 2004

6. P. Kanungo, P. K. Nanda and U. C. Samal, “Image segmentation using thresholding and genetic algorithm,” *Proc. of the Conference on Soft Computing Technique for Engineering Applications (SCT 2006)*, NIT, Rourkela, 24-26 March, 2006

7. P.K.Nanda,Sucheta Panda,P.Kanungo, “Parallel Genetic Algorithm Based Textured Image Segmentation using Markov Random Field Models”, *Proc. of National Conference on recent Advances in Power Signal Processing and Control*, N.I.T,Rourkela, 16-17 Nov. 2004.

8. P. Kanungo , P. K. Nanda and A. Ghosh , “Detection of earth surface cracks using parallel genetic algorithm based thresholding,” *Accepted for the International conference on Advances in Computing, Control and Telecommunication Technology, ACT-2009*, India.

Acknowledgments

I have been very fortunate to have Prof. Pradipta Kumar Nanda as my thesis supervisor. He introduced me to the field of Image Processing and Computer Vision, educated me with the methods and principles of research and guided me patiently throughout this thesis work. He is the whole Philosopher and Guide behind this thesis. I am highly indebted and express my deep sense of gratitude to him for his invaluable guidance, constant inspiration and motivation with enormous moral support during my difficult phase to complete this work. I am extremely thankful to him for his incredible contribution in writing the manuscript despite of his busy schedule. Working with him, a person with commitment and positive attitude is highly a rewarding experience.

I record my sincere thanks and gratitude to Prof. S. K. Sarangi, Director, N.I.T., Rourkela, for his support and extended facilities to all the research scholars of NIT Rourkela.

I record my sincere thanks and gratitude to Prof. A. Behera, Dean, Academic, N.I.T., Rourkela, for his encouragement and support during my final manuscript submision.

I take this opportunity to express my deep sense of gratitude to the memebers of my Doctoral Scrutiny Committee Prof. B. D. Subudhi (HOD), Prof. J. K. Satpathy, Prof. D. Patra of Electrical Engineering Department and Prof B. D. Majhi of Computer Sc. Department for their thoughtful advice during discussion sessions. I am also thankful to my teachers Prof. P. C. Panda, Prof. K. B. Mohanty, Prof. S. Das and Prof. S. Mohanty for constant encouragement and good wishes throughout the current work.

I take this opportunity to express my gratitude and sincere thanks to Prof. S. Ghosh for his support, encouragement and inspiration throughout the years. Special thanks are due to his encouragement and support during my last phase of this work.

I record my sincere thanks to Prof. S. K. Pal (PI, SCC), Prof. A. Ghosh (Co-PI, SCC) , *Center for soft Computing Research: A National Facility (SCC)*, ISI., Kolkata for their valuable suggestions and discussions during the progress of the work.

It is my pleasure to thank Mr. Sanjeeb Rout, Chairman, C.V.Raman Group of Institutions, for his motivation for higher study and allowing me to pursue Ph.D at NIT, Rourkela with study leave.

It is my pleasure to thank Prof. B. K. Rath, Principal, Cdr. P. K. Routray, Registrar, C.V.Raman College of Engineering, Bhubaneswar for their motivation, inspiration and extended support to complete the thesis.

I would like to thank and appreciate the IPCV lab members like: Prof. D. Patra, Mrs. S. Panda, Mr. A. Pradhan, Mr. U. C. Samal, Mr. P. J. Mohapatra, Mr. R. Dev, Mr. S. Dutta and Mr. B. Subudhi for their cooperation and coordination to maintain a conducive research environment in the laboratory. Probably, as per my name I am lucky enough to get all these people during the years. The time I spent with them in the IPCV Lab, NIT Rourkela was one of the best time of my research life. Thank you all.

My special thanks to Mr. P. J. Mohapatra for his helps during the discussion of subjects, programming, information gathering and working with me in the lab at night. In his busy schedule as a research scholar at I.I.Sc., Bangalore, he has extended his support in draft correction.

My special thanks to Mr. P. K. Pattnaik for his service, above and beyond call of duty and all the staffs of the Electrical Engineering department for their regular and very professional assistance. I express my special thanks to my friends Mrs/Mr. J. R. Mohanty, Mrs/Mr. Y. S. Rao, Mr. M. Madhan, and Mr. H. M. Jena for their readiness to help for anything and everything during the years.

I am thankful to Prof. D. K. Nayak and Mr. P. Dash for helping me in draft reading, Miss S. Mohapatra and Mr. R. Nanda for their support during my thesis compilation and submission, and all the staffs of the department and my colleagues in Image Analysis and Computer Vision Laboratory, C. V. Raman College of Engineering, Bhubaneswar, for their motivation, encouragement and support.

My parent call me LUCKY and I am, really lucky to get such parent. Today, what I am is only due to the blessings and constant motivation of my mother Mrs. Ashalata Kanungo and father Dr. Rabinarayan Kanungo. They tried their best to keep me away from the problems outside my research domain. I would like to take this opportunity to thank them for the pain they have taken for me and for their selfless inspiration and motivation in my life. My special thanks to my father inlaw and mother inlaw Dr. Srikant Mohanty and Mrs. Kunjalata Mohanty for understanding, motivating and encourageing me during the years.

I Owe a lot to my wife Mrs. Leena Kanungo and my son YASH for their sacrifice and tolerating my negligence towards them during the years. In spite of financial problems and with a small kid, my wife supported me morally to survive in this period. Without any demand selflessly she has taken care of me and my son. Though, I was disturbed due to the financial problem but she managed the toughest time with a smile and courage. Thank you Leena for your sacrifice and unforgettable support during the years.

I thank the many people who have done lots of nice things for me.

Date: _____ Priyadarshi Kanungo